بسم الله الرحمن الرحيم

Palestine Polytechnic University
Deanship of Graduate Studies and Scientific Research
Master Of Civil Engineering

Response Modification Factor In Intermediate Moment-Resisting Reinforced Concrete Frame System

Name of student

Moath Baher Qasem Qubajeh

Supervisor

Dr. Haitham Ayyad

Thesis submitted in partial fulfillment of the requirements of the degree of Master of Science in civil engineering to the faculty of Graduate Studies at Palestine Polytechnic University

June, 2026

The undersigned hereby certify that they have read, examined, and recommended to the Deanship of Graduate Studies and Scientific Research at Palestine Polytechnic University

Response Modification Factor in Intermediate Moment- Resisting Reinforced Concrete Frame System

Moath Baher Qasem Qubajeh

In partial fulfillment of the requirements for the degree of Master in Structural and Earthquake Engineering.

Graduate Advisory Committee:

Prof./Dr. /Dr. Haitham Ayyad, (Supervisor), University. PPU

Signature: ______________ Date: 01-09-2026

Prof./Dr. ...., (Co-supervisor), University. ______

Signature: ______________ Date: ______________

Prof./Dr. Belal Almassri, (Internal committee member), University. PPU

signature: ______________ Date: 01-09-2026

Prof./Dr. Ibrahim Hashlamon, (External committee member), University. ______

Signature ______________

Date: ______________

Thesis Approved by:

Name: ______________________________

Dean of Graduate Studies & Scientific Research

Palestine Polytechnic University

Signature: ______________ Date: ______________

DECLARATION

I declare that the Master Thesis entitled" Response Modification Factor in Intermediate Moment Resisting Reinforced Concrete Frame System" is my own original work, and herby certify that unless stated, all work contained within this thesis is my own independent research and has not been submitted for the award of any other degree at any institution, except where due acknowledgement is made in the text.

Student Name : Moath Baher Qasem Qubajeh

Signature: ——————   Date:——————

DEDICATION

أهدي هذا الإنجاز العلمي، ثمرة سنوات من الجهد والمثابرة

- إلى من ربّياني على القيم، وغرسا فيّ حبّ العلم والسعي الدائم للمعرفة،...والدي العزيزين

- وإلى شريكة الدرب من كانت الداعم الأول، والسند الصادق، ومصدر الإلهام في أصعب اللحظات ... زوجتي الغالية

- وإلى منبع الدعم العلمي والتوجيه الحصين ، الذي كان لإرشاده وأفكاره الأثر العميق في توجيه هذا العمل وبلوغه غياته ... د.هيثم عياد

- والى طفلاي العزيزان , أنتما النور الذي يضيء طريقي وسبب إصراري ... عمر وسيما الحبيبان

- لكل من كان له الأثر الطيب في مسيرتنا , ولكل من أحاطنا بالدعاء الصادق والكلمة الطيبة...الاخوة والاصدقاء

ACKNOWLEDGEMENT

First, I would like to thank Allah, for allowing me to overcome all difficulties.

I would like to extend my sincere thanks to my supervisor (Dr. Haitham Ayyad) who made this work possible. His guidance and advice guided me through all stages of writing my project. I would also like to thank the Head of the Civil Engineering Department and the Master of Civil Engineering Program Supervisor, Dr. Bilal Al-Masry and the faculty members for making me able to turn knowledge into an enjoyable moment, and for your wonderful comments and suggestions, thank you.

I would also like to extend a special thanks to my wife Raghad and my family as a whole for their continuous support and understanding while conducting my research and writing my project.

ABBREVIATIONS

bc and dc = core dimension to the centerline of perimeter hoop in x and y direction

d_s = diameter of spiral

S_{aM} = the site-specific MCE spectral response acceleration at any period

$\mathcal{E}_{50u}$ = the strain corresponding to the stress equal to 50% of the maximum concrete strength for unconfined concrete.

$\mathcal{E}cc$= strain at the maximum compressive strength of confined concrete $f'cc$

$\mathcal{E}_m$ =Tensile Stiffness Coefficient

$\mathcal{E}_u$ =Ultimate Compressive Strength

$f'cc$= compressive strength of confined concrete

ρs = ratio of volume of transverse confining steel to the volume of confined concrete core

fyh= yield strength of transverse reinforcement

ke = confinement coefficient

ρcc = ratio of area of longitudinal reinforcement to area of core of the section

s' = clear spacing between spiral or hoop bars

ke = confinement effective coefficient, ke is given in Eq. 5.19.

Ae = area of effectively confined concrete core

Ac = area of core of section enclosed by the center lines of the perimeter spiral or hoop

Asx and Asy = the total area of transverse bars running in the x and y direction, respectively.

fl = lateral pressure from the transverse reinforcement, assumed to be uniformly distributed over the surface of the concrete core.

Δ_y =idealized yielding point

Δ_d =idealized design point

Δ_{max} =maximum structural drift

T = fundamental period

R_a= Response Modification Coefficient

R_μ = ductility reduction factor

μ= displacement ductility factor

R_0=over-strength related force modification factor

Φ =strength reduction factor

V_d =design base shear force

Ω =Over Strength Code Factor

Ω_1=first-yield over-strength factor

Ω_2=second kind of over-strength

V_{fy} =first-yield lateral strength.

V_{ult} =ultimate lateral strength

OP =Operational Performance Level

IO =Immediate Occupancy Performance Level

LS =Life Safety Performance Level

CP =Collapse Prevention Performance Level

I_i = importance factor for ice thickness

I_w = importance factor for concurrent wind pressure

Strength reduction factor, ϕ.

Ct = building period coefficient

C_{vx} = vertical distribution factor

F_a = short-period site coefficient (at 0.2-s period).

F_v = long-period site coefficient (at 1.0-s period).

C_d = deflection amplification factor

C_s = seismic response coefficient

f'_c = specified compressive strength of concrete used in design

f'_s = ultimate tensile strength [psi (MPa)] of the bolt, stud, or insert leg wires. For ASTM A307 bolts or ASTM A108 studs, it is permitted to be assumed to be 60,000 psi (415 MPa)

f_y = specified yield strength of reinforcement [psi (MPa)]

I_e = the Importance Seismic Factor

S_{DS} = design, 5% damped, spectral response acceleration parameter at short periods

S_{D1} = design, 5% damped, spectral response acceleration parameter at a period of 1 s

S_{M1} = the MCER, 5% damped, spectral response acceleration parameter at a period of 1 s adjusted for site class effects

S_{MS} = the MCER, 5% damped, spectral response acceleration parameter at short periods adjusted for site class effects.

S_S = mapped MCER, 5% damped, spectral response acceleration parameter at short periods.

T = the fundamental period of the building $T_0 = 0.2S_{D1}=S_{DS}$

T_a = approximate fundamental period of the building

T_L = long-period transition period

$T_S = S_{D1}=S_{DS}$

$T_0 = 0.2S_{D1}/S_{DS}$

$\bar{v}_s$ = average shear wave velocity at small shear strains in top 100 ft (30 m).

S_a =the design spectral response acceleration

S_1 = mapped MCER, 5% damped, spectral response acceleration parameter at a period of 1 s

$\bar{s}_u$ = average undrained shear strength in top 100 ft (30 m).

$\bar{N}$ = average field standard penetration resistance for the top 100 ft (30 m).

$\bar{N}_{ch}$ = average standard penetration resistance for cohesionless soil layers for the top 100 ft (30 m).

C_{dc} =Deflection Amplification Factor

Ω_{0b} =Overstrength Factor,

ά =Tensile Stiffness Coefficient

ν= Poisson's ratio

f't =Ultimate Tensile Strength

f'c =Ultimate Compressive Strength,

E =Young's Modulus of Elasticity,

θ =Angle with x-axis

TABLE OF CONTENTS

LIST OF FIGURES

LIST OF TABLES

ABSTRACT

The Response Modification Factor (R) is a critical parameter in seismic design, reflecting a structure's ability to withstand earthquake-induced forces through controlled inelastic behavior, including ductility, stiffness degradation, and energy dissipation, rather than relying solely on elastic response. Given that R is governed by a complex interaction between structural configuration, material properties, and detailing, its accurate determination is essential for achieving reliable and realistic seismic performance assessments.This study examines the response modification factor (R) of Intermediate Moment Resisting Concrete Frame Systems (IMRCFS) through a comprehensive nonlinear analytical framework. Four three-dimensional reinforced concrete frame models, comprising 1, 3, 6, and 9 stories, were developed with consistent geometric and material properties, while varying in height and stiffness distribution. Each model incorporates four bays in the transverse direction and three bays in the longitudinal direction, enabling a systematic evaluation of height-dependent seismic behavior.

The structural systems were initially designed using ETABS in accordance with ACI 318-19, with seismic design parameters defined based on ASCE 7-16 provisions. Subsequently, nonlinear static pushover analyses, incorporating gravity loading and P–Δ effects, were conducted using SAP2000 and ABAQUS to capture the full nonlinear response of the structures. The base shear–displacement capacity curves were obtained from pushover analysis, and the response modification factor (R) was subsequently determined using the Equal Energy Method according to ATC-19 procedures.. The results demonstrate that the base shear corresponding to the yield point provides a consistent and realistic basis for estimating the response modification factor across all investigated configurations. Although R-values exhibit an overall increasing trend with building height, the findings highlight a pronounced sensitivity of R to stiffness distribution and vertical irregularities, particularly in mid- and high-rise systems. Notably, the computed R-values are consistently lower than those prescribed by design codes, indicating that reliance on generalized code values may lead to unconservative estimations. Overall, the study confirms that accurate evaluation of the response modification factor necessitates explicit consideration of nonlinear structural behavior, stiffness irregularities, and system configuration. Furthermore, it validates nonlinear pushover analysis as a robust and reliable approach for assessing the seismic performance of IMRCFS.

Keywords: IMRCFS, Response Modification Factor, Nonlinear Pushover Analysis, Vertical Irregularity, Soft Story, SAP2000, ABAQUS, Parametric Study.

الملخص

يُعد معامل تعديل الاستجابة الزلزالية (R) من أهم المعاملات المستخدمة في التصميم الزلزالي، إذ يعكس قدرة المنشأ على مقاومة التأثيرات الناتجة عن الزلازل من خلال الاستفادة من السلوك غير الخطي، بما يشمله من المطيلية، وتبديد الطاقة، وتدهور الصلابة، بدلًا من الاعتماد على الاستجابة المرنة فقط. ونظرًا لتأثر معامل (R) بعدد من العوامل، مثل النظام الإنشائي، وخصائص المواد، وتوزيع الصلابة، والتفاصيل الإنشائية، فإن تحديده بدقة يُعد أمرًا أساسيًا لتحقيق تقييم واقعي وموثوق للأداء الزلزالي للمنشآت.

تهدف هذه الدراسة إلى تقييم معامل تعديل الاستجابة (R) لأنظمة الإطارات الخرسانية المسلحة المقاومة للعزوم المتوسطة(IMRCFS) ، وذلك من خلال منهجية تحليلية غير خطية شاملة. ولتحقيق ذلك، تم تطوير أربعة نماذج ثلاثية الأبعاد لمبانٍ خرسانية مسلحة مكونة من طابق واحد، و٣ طوابق، و٦ طوابق، و٩ طوابق، مع الحفاظ على الخصائص الهندسية والمادية الأساسية وتغيير ارتفاع المبنى وتوزيع الصلابة رأسيًا، بما يسمح بدراسة تأثير ارتفاع المبنى وعدم انتظام الصلابة على السلوك الزلزالي. وقد اشتملت النماذج على أربعة بحور في الاتجاه العرضي وثلاثة بحور في الاتجاه الطولي.

تم تصميم النماذج الإنشائية باستخدام برنامج ETABS وفق متطلبات الكود ACI 318-19 ، مع اعتماد المعايير الزلزالية وفق متطلبات الكود ASCE 7-16 بعد ذلك، أُجريت تحليلات الدفع غير الخطي (Nonlinear Pushover Analysis) باستخدام برنامجي SAP2000وABAQUS، مع الأخذ في الاعتبار تأثير الأحمال الجاذبية وتأثيرات P–Δ ، بهدف تحديد السلوك غير الخطي وقدرة المنشآت على مقاومة الأحمال الزلزالية. ومن خلال نتائج التحليل، تم استخراج منحنيات العلاقة بين قوة القص القاعدية والإزاحة، ومن ثم تحديد نقطة الخضوع واستخدام طريقة تساوي الطاقة (Equal Energy Method) وفق منهجية ATC-19 لحساب معامل تعديل الاستجابة.(R).

أظهرت النتائج أن قوة القص القاعدية المقابلة لنقطة الخضوع توفر أساسًا واقعيًا ومتسقًا لتقدير معامل تعديل الاستجابة لمختلف النماذج المدروسة. كما أظهرت النتائج وجود اتجاه عام لزيادة قيم (R) مع زيادة ارتفاع المبنى، إلا أن هذه الزيادة تأثرت بصورة واضحة بتوزيع الصلابة وعدم الانتظام الرأسي، وخاصة في المباني متوسطة وعالية الارتفاع. ومن أبرز النتائج التي توصلت إليها الدراسة أن القيم المحسوبة لمعامل (R) كانت أقل بصورة مستمرة من القيم المحددة في أكواد التصميم الزلزالي، مما يشير إلى أن الاعتماد المباشر على القيم العامة المعتمدة في الأكواد قد يؤدي في بعض الحالات إلى تقديرات غير محافظة للقوى الزلزالية التصميمية.

وتؤكد الدراسة أن التقييم الدقيق لمعامل تعديل الاستجابة (R) يتطلب الأخذ في الاعتبار السلوك غير الخطي الفعلي للمنشأ، وتوزيع الصلابة، وعدم الانتظام الرأسي، وخصائص النظام الإنشائي، وارتفاع المبنى، بدلًا من الاعتماد على قيمة موحدة لمعامل .(R) كما تؤكد النتائج فعالية تحليل الدفع غير الخطي (Nonlinear Pushover Analysis) كأداة موثوقة لتقييم الأداء الزلزالي للإطارات الخرسانية المسلحة المقاومة للعزوم المتوسطة، وتوفر الدراسة أساسًا يمكن الاستناد إليه لتحسين واقعية معاملات التصميم الزلزالي وتعزيز موثوقية وسلامة التصميم الإنشائي.

CHAPTER 1 INTRODUCTION

1.1 Background

Over the past decade, the frequency and impact of earthquakes and natural hazards on structural systems have increased significantly, intensifying the need for advanced research to better understand the mechanisms governing structural failure, as well as to enhance prediction, resistance, and mitigation strategies. Unlike conventional loads, which are typically defined in terms of force, seismic actions are characterized by ground motion, introducing highly dynamic and time-dependent effects. In contrast to static loads, earthquake-induced forces vary rapidly over short durations, imposing complex demands on structural systems.

Moment-resisting concrete frame systems (MRFS) are widely employed as primary components of seismic force-resisting systems (SFRS) due to their inherent capacity for energy dissipation and superior deformation performance. According to the American Concrete Institute (ACI 318-2002), MRFS are classified into three categories: Ordinary (OMRCF), Intermediate (IMRCF), and Special (SMRCF) moment-resisting concrete frames. In this study, the focus is placed on Intermediate Moment-Resisting Concrete Frame Systems (IMRCFS), analyzed using advanced nonlinear procedures implemented in ETABS, SAP2000, and ABAQUS.

Seismic design incorporates the Response Modification Factor (R) to account for the structure's ability to dissipate energy through inelastic behavior, thereby reducing the design seismic forces. Introduced in ATC 3-06 (1982), the concept of response modification includes both the strength reduction factor (R) and the deflection amplification factor (Cd), each reflecting different aspects of structural performance. The magnitude of R is not constant, but depends on the structural system, detailing quality, and targeted performance level, making its accurate evaluation essential for reliable seismic design.

The selection of appropriate R-values is influenced by observed system performance during past earthquakes, as well as by structural durability and damping characteristics. To estimate yield strength and displacement, bilinear idealization techniques are commonly adopted. The first approach is based on the force–displacement relationship, where the elastic stiffness is derived from the secant stiffness of the response curve ,and was not utilized in this study. The second, and more representative approach, is the isoenergetic (equal energy) method, which assumes equivalence between the areas above and below the actual response curve. This method is adopted in the present study to ensure a realistic representation of inelastic structural behavior.

Beyond conventional seismic design, enhancing structural resilience requires the integration of additional strategies such as redundancy, base isolation, and supplemental damping systems. These measures improve the ability of structures to maintain stability and limit damage under extreme seismic events by redistributing forces and reducing seismic energy transmission. The importance of implementing such strategies becomes particularly evident in regions with high seismic hazard, where strong earthquakes pose a continuous threat to the built environment. One of the most seismically active regions in the Middle East is the area influenced by the Dead Sea Transform fault system, which represents one of the most significant tectonic boundaries in the region. This fault zone has generated numerous earthquakes throughout history, resulting in substantial infrastructure damage and loss of life. A summary of recent seismic events in the Dead Sea region, based on USGS data and regional seismic records, is presented in Table 1.1 and Figures 1.1 and 1.2..

Table 1.1 : Earthquakes in the Dead Sea region (from 2000 to the present).

Date	Magnitude	Location	Report Damage/Impact
11 Feb 2004	ML 5.2	Northern Dead Sea Basin	**Minor structural damage** (cracks in buildings), felt widely in nearby cities; no fatalities reported.
Oct 2013	Mw ~4.5	Northern segment of the Dead Sea Transform	**no structural damage**.
16 May 2016	Mw ~4.9	Southern Dead Sea / transform extension	**no structural damage**.
5 Jul 2018	Mw ~4.7	Northern Dead Sea Transform	**no structural damage**.
15 May 2019	Mw ~4.5	Northern Dead Sea Transform	**no structural damage**.
17 Jun 2021	Mw ~4.2	Dead Sea region	Felt event; **no injuries or damage** reported.
2023	Mw ~4.0+	Dead Sea Basin	**no structural damage**.
2024	Mw ~4.0+	Dead Sea Basin	Recent seismicity indicating ongoing activity, without reported damage

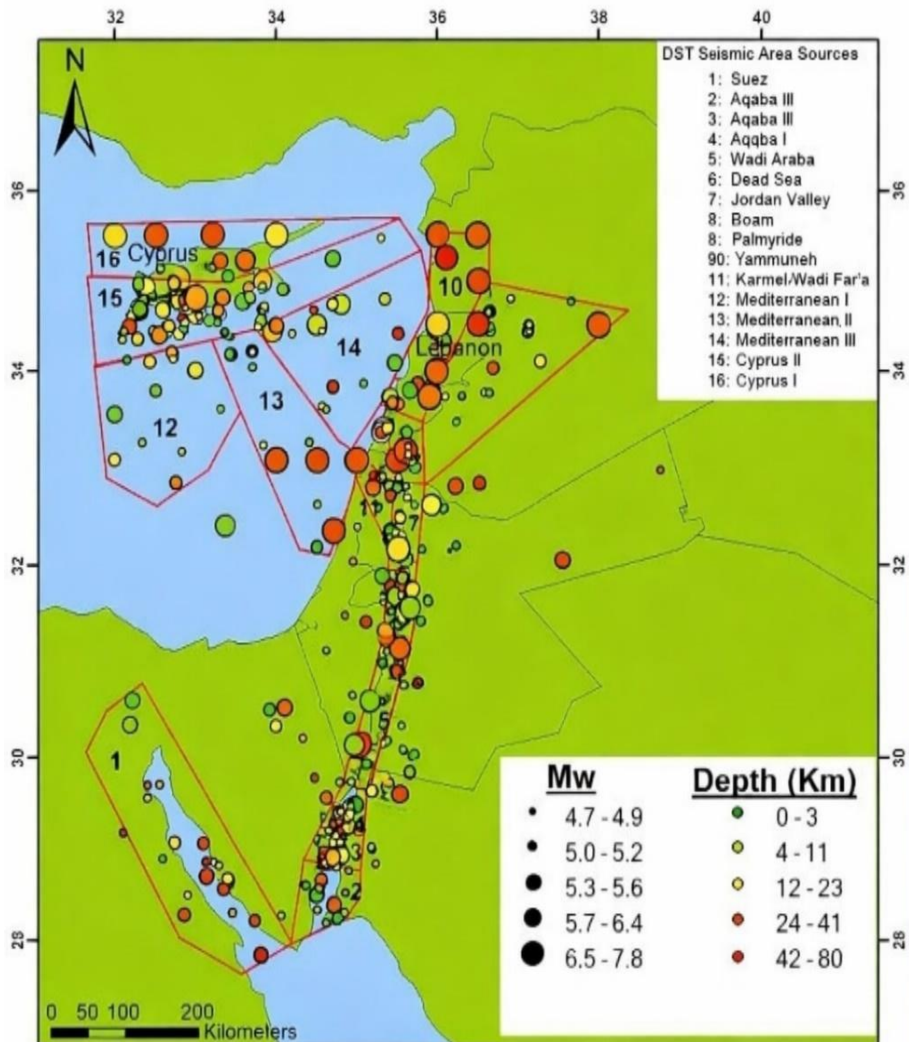

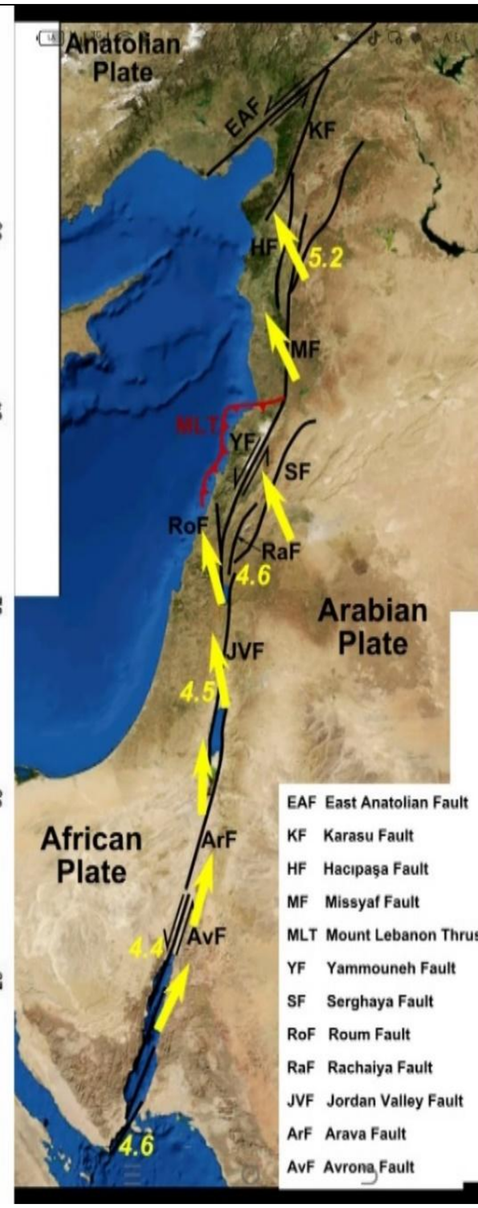

Figure 1.1 :Spatial distribution of earthquake epicenters(Mw>4)in the Dead Sea Basin from 2000 to the present.

Figure 1.2 :The Dead Sea Transform Fault system showing the main strike-slip fault segments that form the tectonic boundary between the Arabian and African plates.

1.2 Problem Statement

Seismic design is fundamental to ensuring the safety and structural integrity of buildings subjected to earthquake loading, as it governs and predicts their behavior under seismic excitation. Consequently, the continuous development and refinement of seismic design codes remain essential to enhance the resilience of structures in earthquake-prone regions.

The Response Modification Factor (R) enables engineers to achieve economically efficient designs while satisfying life-safety performance objectives by accounting for key structural attributes such as overstrength, ductility, and redundancy.

Beam–column connections represent critical components in reinforced concrete systems, as they facilitate force transfer between structural members and significantly influence global behavior under lateral loading. In non-ductile reinforced concrete frames, these connections often constitute the most vulnerable regions, where failure is likely to initiate due to inadequate detailing and limited deformation capacity.

Modern seismic design philosophies emphasize both strength capacity and displacement ductility in the design of beam–column joints. Premature degradation of the joint panel zone, caused by cracking, bond failure, or reinforcement slip, can significantly reduce structural ductility and disrupt the intended force transfer mechanism within the system. Such deficiencies may ultimately compromise the overall seismic performance of the structure.

With advancements in analytical techniques and computational tools, researchers are now able to achieve a more refined understanding of structural response and collapse mechanisms under seismic loading. In this context, the geometry and detailing of connections between beams, columns, and shear walls play a decisive role in governing stability, energy dissipation, and overall system performance during earthquakes

1.3 Research Objectives

This study aims to investigate the actual seismic behavior of Intermediate Moment Resisting Reinforced Concrete Frames (IMRCFs) and to evaluate the corresponding response modification factor (R) for structures of varying heights, specifically 1, 3, 6, and 9 stories. Given that the response modification factor is influenced by a complex interaction of structural configuration and material characteristics, the study seeks to quantify realistic and system-specific R-values that accurately reflect the inelastic performance of IMRCFs.

To achieve this objective, comprehensive three-dimensional numerical models were developed using SAP2000 and ABAQUS, enabling detailed nonlinear analysis of the structural response under seismic loading. Based on the results of these analyses, base shear–displacement capacity curves were extracted and utilized to evaluate the response modification factor (R) for each structural configuration using the equal energy method.

Subsequently, the derived R-values were employed as a basis for a critical assessment of the structural designs, allowing for a comparative evaluation of their adequacy and seismic performance. This integrated approach ensures a consistent linkage between modeling, analysis, and performance evaluation, thereby providing a more reliable representation of the seismic behavior of IMRCFs.

1.4 Research Methodology

This study adopts a comprehensive numerical approach to evaluate the seismic behavior of multi-story buildings constructed using Intermediate Moment Resisting Concrete Frame (IMRCF) systems. Advanced computational tools, including SAP2000 and ABAQUS, are employed to develop detailed structural models and perform nonlinear analyses under seismic loading conditions.

The analytical procedure focuses on extracting and evaluating base shear–displacement response curves, which serve as the primary basis for assessing the structural characteristics summarized in Table 3.9, as will be presented later in this Resarch. All models are subjected to unidirectional seismic loading to ensure consistency in evaluating the influence of structural height and system behavior.

To capture the inelastic response of the structures, nonlinear static pushover analysis is conducted, where seismic loads are applied incrementally until significant structural response is achieved. This approach enables a realistic representation of structural performance by monitoring the evolution of base shear and displacement throughout the loading process. The resulting capacity curves provide a reliable framework for interpreting the global behavior of the structures during earthquake excitation. Subsequently, the Equal Energy Method, as proposed by the Applied Technology Council (ATC), is utilized to determine the response modification factor (R). This method is based on the fundamental assumption that the energy dissipated by the structure beyond the yield point is equivalent to the energy absorbed within the elastic range. Accordingly, the bilinear idealization of the capacity curve is used to establish the relationship between base shear and displacement, forming the basis for calculating R-values.

Finally, the obtained results are systematically analyzed and compared with the reference values presented in Table 3.9 to evaluate their consistency and accuracy. Through this integrated methodology, the study provides a clear and reliable assessment of the seismic performance of IMRCF systems, offering valuable insights for improving design parameters in terms of safety, structural performance, and cost efficiency in seismic design practice..

1.5 Scope of Research

This study evaluates the response modification factor (R) of Intermediate Moment Resisting Reinforced Concrete Frame (IMRCF) buildings with 1, 3, 6, and 9 stories under seismic loading. The Equal Energy Method is used to estimate R based on base shear–displacement relationships obtained from nonlinear analysis. Structural models are developed in SAP2000 with automatic plastic hinge implementation to capture inelastic behavior. In selected cases, ABAQUS is employed to enhance the accuracy of nonlinear response predictions. The resulting R-values are then compared with code-prescribed values to assess their validity and reliability.

1.6 Research Significance

The Response Modification Factor (R) is a key parameter in seismic design, representing a structure's ability to dissipate energy through ductility, overstrength, and redundancy. Although design codes provide standard R-values, they are often based on idealized assumptions that may not reflect actual structural behavior. This study aims to provide a more realistic evaluation of R using nonlinear analysis, contributing to improved seismic performance, more efficient design, and better alignment with performance-based design principles.

CHAPTER 2 LITERATURE REVIEW

2.1 LITERATURE REVIEW AND BACKGROUND

Prior to the introduction of the response modification factor (R), seismic design codes—particularly before the 1970s—were based on full elastic force assumptions, requiring structures to resist earthquake loads without significant cracking or inelastic deformation. Early contributions by George W. Housner emphasized elastic design principles, where structures were expected to remain within the elastic range under seismic excitation. However, subsequent studies demonstrated that purely elastic analysis often results in excessively high stress demands, leading to uneconomical and impractical designs.

The advancement of dynamic analysis methods, particularly through the work of Nathan M. Newmark, marked a significant shift in seismic engineering. The development of the Newmark-beta method enabled efficient numerical solutions for structural response under dynamic loading, forming the basis for modern seismic analysis. The structural response is generally governed by the equation of motion:

$$\boldsymbol{M}\,\ddot{\boldsymbol{u}}(\boldsymbol{t}) + \boldsymbol{C}\,\dot{\boldsymbol{u}}(\boldsymbol{t}) + \boldsymbol{K}\,\boldsymbol{u}(\boldsymbol{t}) = \boldsymbol{F}(\boldsymbol{t})$$

where M, C, and K represent the mass, damping, and stiffness matrices, respectively, and $F(t)$ denotes the applied seismic force.

By the 1970s, research led by Nathan M. Newmark and William J. Hall established that structures possess significant inelastic deformation capacity, allowing them to dissipate energy without immediate collapse. This realization led to a fundamental shift in design philosophy, moving away from purely elastic design toward controlled inelastic behavior.

As a result, the concept of reducing seismic design forces emerged, incorporating key parameters such as ductility (μ) and overstrength (Ω), which together form the basis of the response modification factor:

$$\boldsymbol{R} \approx \boldsymbol{\mu} \cdot \boldsymbol{\Omega}$$

This concept was further formalized by the Applied Technology Council, established in 1973, which played a pivotal role in developing methodologies for seismic design. Early reports introduced the use of R to reduce design forces, acknowledging that well-detailed reinforced concrete and steel structures can sustain seismic demands exceeding their elastic limits. Later developments, particularly in ATC-19 (1995), refined R-values based on ductility, overstrength, and redundancy considerations.

Mortezaei and Ronagh (2013) investigated the evaluation of the response modification factor (R) for buildings subjected to long-period near-fault ground motions. The study addressed the critical challenge of structural response in regions located close to seismic fault zones, where ground motions are typically characterized by short-duration pulses capable of transferring large amounts of energy to buildings. Such motions have been identified as a major cause of severe damage during destructive earthquakes.

The authors observed that structures located near faults often exhibit significant contributions from higher vibration modes, which alter the distribution of dynamic demands and shift story drifts from lower to upper floors. Consequently, conventional nonlinear static pushover analysis, which commonly applies a lateral load pattern proportional to the fundamental mode shape, may not provide reliable results for buildings exposed to near-fault ground motions.

To improve analytical accuracy, the study proposed a modified pushover analysis procedure incorporating a special load pattern tailored to near-fault conditions. Several pushover analyses were conducted on six existing reinforced concrete buildings constructed in different periods. The results, obtained using four additional load patterns, were then compared with the FEMA-356 procedure and validated against nonlinear dynamic time-history analysis.

The study also highlighted the difficulty of directly defining the ground motion function for structural analysis. To address this, the researchers discussed linking the motion function to stiffness rather than damping through convolution integration, thereby transforming the differential equation into an integral form that is easier to solve. In this context, the load–time curve **P(t)** was divided into smaller pulse components to simplify the analysis. Based on this formulation, the impulse was expressed as the product of load and displacement over time, as presented by Mortezaei and Ronagh (2013).

G. E. Thermou et al. proposed a seismic upgrading approach for existing reinforced concrete (RC) buildings that focuses on modifying the structural response to achieve a more uniform distribution of interstorey drift along the building height. Their methodology is based on evaluating the structural response through analytical and numerical methods, assessing element capacities, identifying critical weaknesses, and implementing targeted strengthening strategies. The primary objective of this approach is to reduce damage concentration by ensuring a balanced distribution of deformation demands.

Hanan Yurizka and Anis Rosyidah (2020) investigated the seismic performance of high-rise reinforced concrete buildings exhibiting setback and soft-story irregularities, which are among the most critical forms of vertical irregularity due to their tendency to amplify inter-story drift and shear demands during seismic events. Recognizing the limitations of conventional elastic analysis in representing post-yield structural behavior, the authors employed nonlinear static pushover analysis to evaluate the response modification factor (R) for two ten-story building models with setback-area ratios of 0.3 and 0.6. The study aimed to quantify the influence of setback severity on key seismic response parameters, including lateral displacement, inter-story drift, base shear capacity, and overall structural performance, in accordance with ATC-40 and FEMA-356 performance-based assessment procedures. The results demonstrated that increasing setback irregularity led to a significant increase in seismic demand, as evidenced by higher lateral displacements, larger inter-story drifts, and greater base shear requirements. Despite these adverse effects, both structural configurations satisfied the Damage Control performance level, indicating limited structural damage under design-level earthquake loading. The study provided valuable insight into the relationship between geometric irregularity and seismic performance and established a robust analytical framework for assessing the influence of setback intensity on the global capacity and response characteristics of vertically irregular moment-resisting reinforced concrete frames.

Al-Shroof (2025) investigated the seismic performance of multi-story reinforced concrete Intermediate Moment Resisting Frame (IMRCF) buildings using nonlinear pushover analysis in SAP2000. The study focused on the influence of column reinforcement ratios and structural stiffness while maintaining fixed column cross-sectional dimensions. The results demonstrated that the Response Modification Factor (R) is strongly influenced by column dimensions, reinforcement ratio, and overall structural stiffness. However, the study was limited to SAP2000 and did not investigate the independent effects of column width and depth or validate the numerical results using advanced finite element analysis. Building upon this work, the present study extends the investigation by incorporating ABAQUS for numerical validation and performing a broader parametric study that evaluates the independent influence of column dimensions, beam dimensions, confinement reinforcement, structural stiffness, and building height on the Response Modification Factor (R).

Abu Azzanid (2023) investigated the influence of building height on the Response Modification Factor (R) of Intermediate Moment Resisting Reinforced Concrete Frame (IMRCF) systems using nonlinear pushover analysis. The study evaluated the seismic performance of buildings with different heights and demonstrated that building height has a significant influence on the estimated R-factor and overall structural response. However, the investigation was primarily limited to the effect of building height without considering other influential structural parameters such as column dimensions, beam geometry, confinement reinforcement, and structural stiffness. Building upon this work, the present study extends the investigation through a comprehensive parametric analysis that evaluates the combined influence of building height, member dimensions, reinforcement detailing, structural stiffness, and numerical validation using both SAP2000 and ABAQUS.

In a broader analytical context, **Mehmed Causevic** conducted a comparative study between nonlinear static and dynamic seismic analysis methods in accordance with European and U.S. design provisions. His work reviewed key procedures, including nonlinear dynamic time-history analysis, the N2 method (Eurocode 8), the nonlinear static procedure (FEMA 356), and the capacity spectrum method (FEMA 440). The study demonstrated that these methods provide effective alternatives to linear analysis by integrating performance-based design concepts, with a particular focus on damage control. An application example involving an eight-story reinforced concrete frame building was presented to illustrate the practical implementation and effectiveness of these approaches.

Hussein, Gamal, and Attia (2021) investigated the response modification factor (R) for reinforced concrete buildings with span and height irregularities, and evaluated the adequacy of code-prescribed values. The study examined three structural configurations: regular buildings, buildings with irregular spans, and buildings with irregular heights.

To achieve this, a total of 30 reinforced concrete models were designed and analyzed using nonlinear static (pushover) analysis in SAP2000, following the provisions of FEMA-356 for R-factor estimation. The results revealed that the response modification factor is highly sensitive to structural irregularities, with span irregularity having a particularly significant impact. Additionally, R-values were found to decrease with increasing building height.

The study further concluded that code-specified R-values may be overly conservative and potentially uneconomical when applied to irregular reinforced concrete structures. Accordingly, the authors emphasized the importance of explicitly accounting for both span and height irregularities to obtain more realistic and reliable estimates of the response modification factor in seismic design.

Anurag Sharma et al. conducted a comparative study to evaluate the performance of reinforced concrete frame structures designed using Direct Displacement-Based Design (DDBD) and Force-Based Design (FBD) methods. The structural models were developed in accordance with the Indian seismic code IS 1893 (Part 1): 2016, and assessed using nonlinear analysis techniques. The results indicated that the DDBD approach provides superior seismic performance, particularly under high seismic demand, as reflected in improved response parameters such as base shear, maximum displacement, and inter-storey drift ratio (IDR). This highlights the effectiveness of displacement-based methodologies in achieving more reliable seismic design outcomes.

Nassar (2023) investigated the influence of building aspect ratio on the response modification factor (R) of reinforced concrete Intermediate Moment-Resisting Frame (IMRF) systems through nonlinear pushover analysis. A comprehensive parametric study was conducted on thirty three-dimensional building models with varying aspect ratios, seismic zone factors, and site classes. The results demonstrated that the response modification factor is not a fixed structural parameter but is significantly affected by geometric and seismic characteristics. In particular, variations in aspect ratio produced noticeable changes in the calculated R-values, indicating a direct relationship between structural configuration and seismic energy dissipation capacity. Furthermore, the computed R-values were generally equal to or greater than those prescribed by IBC 2016, suggesting that code-based values may be conservative for certain building configurations. Based on the analytical results, the study proposed a predictive equation relating the response modification factor to building aspect ratio and regional seismicity, providing a more rational basis for performance-based seismic design.

In a related analytical context, **Mehmed Causevic and Mitrovic (2011)** compared nonlinear dynamic time-history analysis with nonlinear static (pushover) analysis for structures designed according to European and U.S. seismic provisions using SAP2000. Their results showed that pushover analysis can provide reasonable estimates of global structural response for regular systems. However, significant discrepancies were observed in cases involving higher-mode effects and structural irregularities. The study highlighted the limitations of static nonlinear procedures when applied beyond their valid range, emphasizing the importance of selecting appropriate analysis methods based on structural characteristics..

Bhende and Mistry (2021) evaluated the seismic performance of reinforced concrete moment-resisting frames using nonlinear static pushover analysis implemented in SAP2000. Their study focused on key response parameters, including base shear capacity, displacement demand, and plastic hinge formation under increasing lateral loads. The results demonstrated that pushover analysis is an effective tool for identifying performance levels and critical structural weaknesses, while confirming the capability of SAP2000 to reliably capture global nonlinear behavior. The study also highlighted the influence of structural configuration on seismic response, supporting the practical application of pushover analysis in performance-based seismic assessment.

In the context of strength-based considerations, **J. L. Humar et al.** emphasized the importance of overstrength in seismic design, highlighting the role of reserve capacity in enhancing structural resilience. Their work demonstrated that accounting for all potential sources of strength enables the development of more robust and efficient structural systems capable of withstanding severe seismic demands while minimizing damage.

Further advancing analytical procedures, **Craig D. Comartin et al**. identified several critical areas for improving inelastic analysis methods, including displacement modification procedures, equivalent linearization techniques, multi-degree-of-freedom (MDOF) effects, and soil–structure interaction. Their work aimed to enhance the accuracy and efficiency of seismic evaluation and design methodologies, providing engineers with more reliable tools for assessing and rehabilitating structures in seismic regions.

From a displacement-based perspective, **B. Borzi et al.** introduced an advanced approach to inelastic displacement spectra and displacement reduction factors. Their study established a relationship between elastic and inelastic systems based on vibration period and energy dissipation capacity, and proposed a displacement modification factor (h) that accounts for plastic behavior without requiring explicit identification of ductility capacity..

Finally, R. A. **Hakim et al.** evaluated seismic assessment procedures based on ATC-40, FEMA 356, and FEMA 440, demonstrating the advantages of pushover analysis over conventional force-based design methods. Their study showed that pushover analysis provides detailed insight into structural behavior by capturing nonlinear response, enabling the identification of potential failure mechanisms and assessment of capacity, stiffness, and deformation characteristics under progressively increasing lateral loads.

2.2 Pushover Analysis Method:

Pushover analysis is a nonlinear static procedure used to evaluate the extent to which a structure can sustain inelastic deformation before reaching partial or total collapse. This is achieved by applying incrementally increasing lateral loads that simulate seismic effects and monitoring the resulting structural response in terms of displacement and internal forces.

The method is widely utilized for both existing and newly designed structures to assess structural performance and the effectiveness of strengthening strategies. It enables the evaluation of global and local performance levels—such as Immediate Occupancy (IO), Life Safety (LS), and Collapse Prevention (CP)—in accordance with performance-based seismic design principles, as highlighted by Karanja Kuria and Katalin Kegyes-Brassai (2023).

By capturing the nonlinear behavior of structural components, pushover analysis provides valuable insight into key parameters such as ductility, reserve strength, and the influence of structural imperfections, which are often neglected in linear elastic analysis, as discussed by Golestani et al. (2023). In addition, the method allows for tracking the progressive development of damage through plastic hinge formation, enabling the identification of potential weak zones and the prediction of failure mechanisms.

Overall, pushover analysis offers a practical and efficient tool for understanding structural behavior under seismic loading, supporting performance evaluation and enhancing the reliability of seismic design.

2.2.1 Pushover Analysis Process -Equal Displacement Method-

This method is based on the principle that the maximum displacement a structure reaches after reaching nonlinear behavior is equal to the maximum displacement resulting from elastic linear analysis.
This applies when the structure experiences a medium to long period of vibration. In other words, during earthquakes, the stiffness decreases and the structure enters a yielding phase, but the displacement does not reach the elastic displacement. Therefore, the displacement itself, not the energy or forces acting on it, is the determining factor. (Newmark, N. M., & Hall, W. J. (1982)).
Assuming that Up ≈ Ue, we express the degree of nonlinearity using the displacement Ductility
$\mu\delta$ =Up/ Uy, where:
Up: Maximum displacement after yielding
Uy: Effective yielding displacement (derived from the amplitude curve).

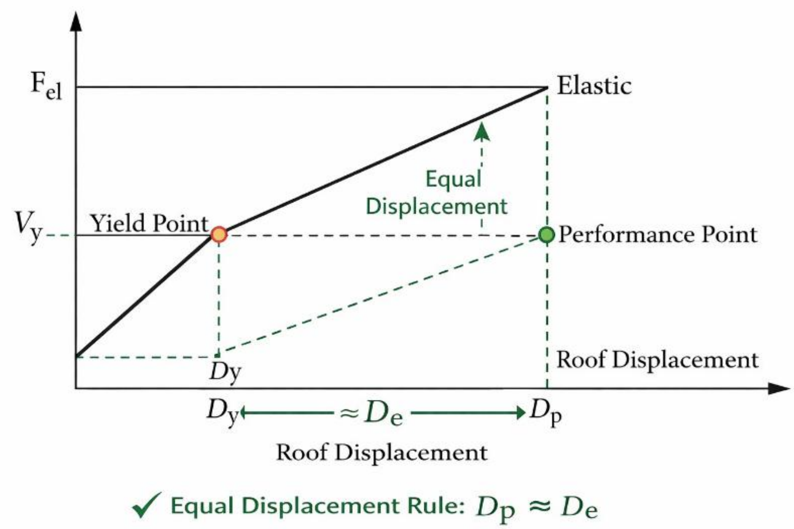

Figure 2.1 Equal Displacement Method (Force–Displacement) Diagram.

2.2.2 Pushover Analysis Process -Energy Balance Method-

This type represents a qualitative leap in the world of conventional seismic design, as it makes the seismic performance of the structure the starting point of the design process itself.
From the outset, it defines and determines the required seismic behavior and the resulting expected level

of damage, without relying on the base shear values and force distributions stipulated by codes. This method is based on the principle of energy balance, meaning that the external force required to gradually push the building towards the target drift equals the seismic energy entering the system.

The structure is represented as an equivalent system with one degree of freedom of the elastic-perfectly plastic (SDOF) type, at a defined seismic hazard level. The seismic energy consists of the elastic deformation energy (Ee), which is up to the yield energy, and the plastic energy dissipated due to inelastic deformations.

$Ee = \frac{1}{2} M.Sv^2$

Plastic energy is taken into account through a modification factor γ

γ, which reflects the proportion of plastic energy involved in energy dissipation.

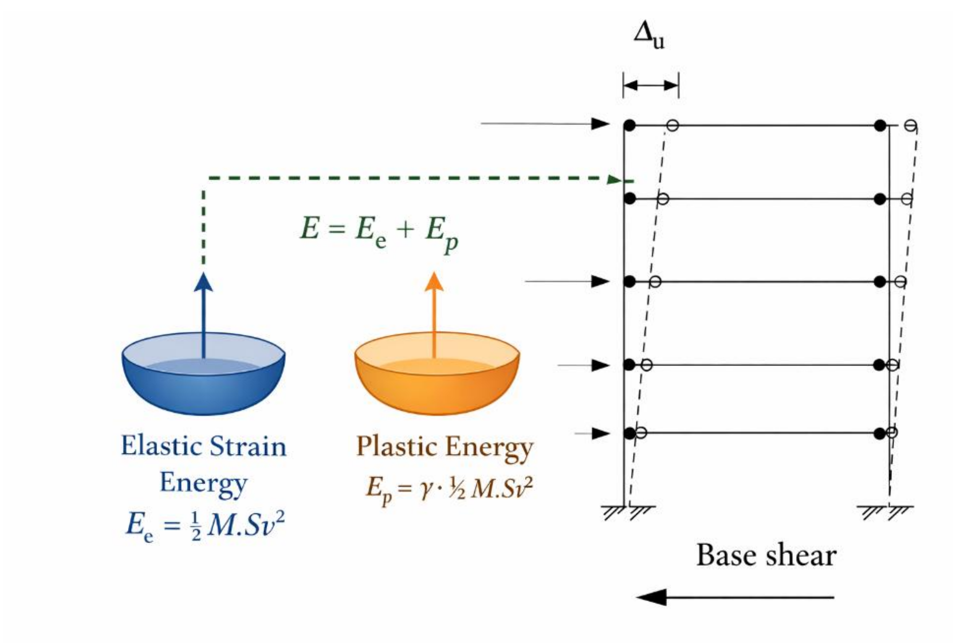

Figure 2.2 Energy Balance Representation in Performance-Based Plastic Design (PBPD).

2.2.3 Pushover Analysis Process -In-elastic Spectrum Method-

This method relies on combining static nonlinear analysis with modified seismic response spectra that take into account the nonlinear behavior of the structure. It determines the seismic response of the building by identifying stiffness loss, Ductility loss, and energy dissipation after yielding.

This is achieved by applying lateral forces to the structure until advanced stages of deformation are reached. An Capacity curve representing the basal shear and displacement is then plotted. This curve is then converted into a spectral acceleration versus spectral displacement. From the Capacity curve, the yield displacement, displacement ductility, and the plastic properties necessary to modify the elastic spectrum and convert it into a nonlinear spectrum are extracted.

The performance point is determined by the intersection of the transformed capacity curve with the nonlinear demand spectrum.

This point represents the state where seismic demand is balanced with the structural capacity of the building, thus determining the building's resistance and safety capabilities. This method is one of the most important nonlinear structural analysis techniques because it links the nonlinear capacity of the structure with seismic demand.

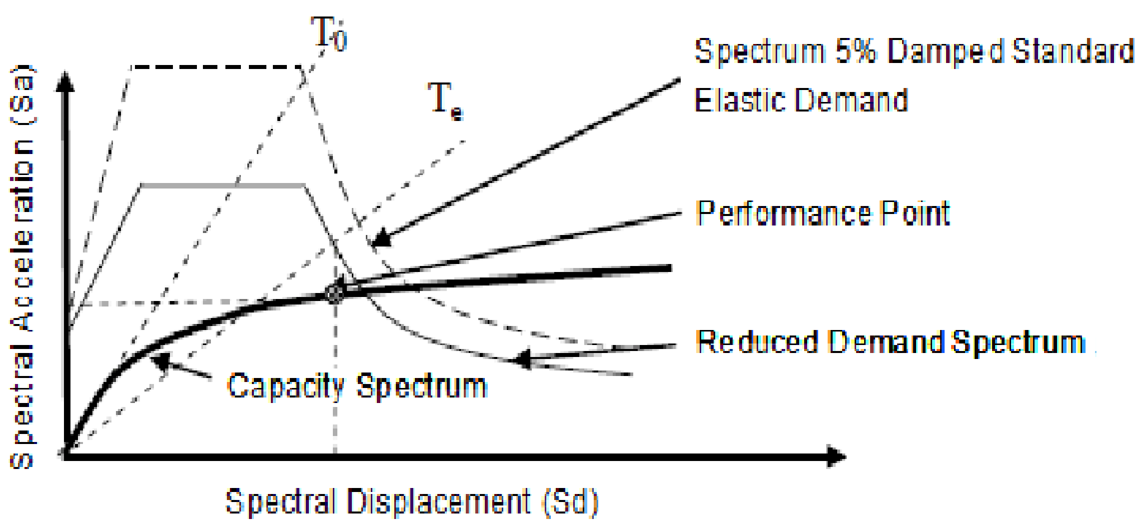

Figure 2.3 Determining the performance point according to the Capacity spectrum method.

2.2.4 Pushover Analysis Process -Rµ-T Relations Method-

The displacements of elastic and inelastic structural systems were originally found to be approximately equivalent for medium- to long-period structures. This experimental observation, commonly referred to as the Equal Displacement Principle or Equal Displacement Rule (EDR), has since become a cornerstone in earthquake-resistant structural design. The EDR states that the maximum inelastic displacement of a structure is essentially equal to its maximum elastic displacement, regardless of the selected yield strength. Accordingly, the peak inelastic displacement is independent of the yield force or yield displacement, where the yield strength and yield displacement may be expressed as

$F_y = F_{el}/R$ and $\Delta_y = \Delta_{el}/R$, respectively

Fy = Yield Strength

Fel = Elastic Strength Demand

R = Response Modification Factor

Δy = Yield Displacement

Δel = Elastic Displacement

When structural stiffness is assumed to be independent of strength, the equal displacement rule leads to the conclusion that the strength reduction factor (R) is equal to the total displacement ductility of the system (Newmark & Hall, 1982).

2.2.5 Time History Analysis Method

The nonlinear dynamic analysis, when properly implemented, provides a more accurate representation of structural response to strong ground motions compared to nonlinear static procedures. This method explicitly models inelastic behavior of structural members under earthquake excitation, allowing direct simulation of hysteretic energy dissipation. The seismic response is obtained through time-history records of displacement, velocity, acceleration, and internal forces for specified ground motions, such as those illustrated in Figure 2.4. Due to the inherent variability of earthquake records, multiple ground motions are required to achieve statistically reliable response estimates. The accuracy of nonlinear dynamic analysis depends on the fidelity of the analytical model and its ability to capture key nonlinear effects. Gravity loads, defined according to ASCE 7-16, must be applied prior to and maintained during seismic excitation to account for P–Δ effects. Time history analysis solves the governing equations of motion using numerical integration schemes such as Newmark-β or Wilson-θ. This approach enables direct evaluation of ductility demand and overstrength. Consequently, the response modification factor (R), defined as the product of ductility and overstrength reduction factors, can be reliably quantified. Overall, time history analysis represents the most comprehensive and physically realistic method for seismic performance assessment and R-factor evaluation.

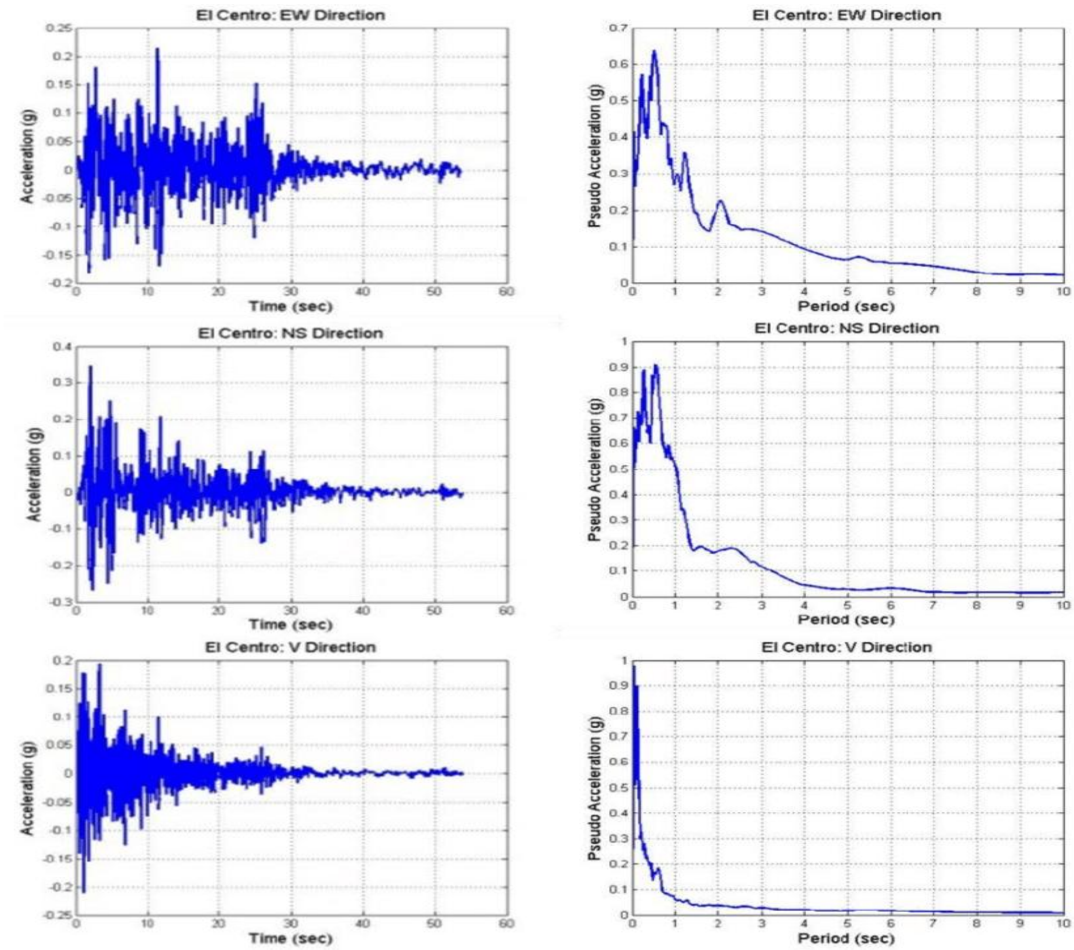

Figure 2.4 Ground-time-histories-and-response-spectra-of-El-Centro-earthquake-in-three-directions.

2.2.6 Pushover Analysis Process -Equal Energy Method-

This process is done in a number of steps:

2.2.6.1 : Create the computational model

Initially, the structure nonlinear is designed taking into account its characteristics and the materials used.

2.2.6.2 Load distribution:

Lateral loads are applied to the structure, such as earthquakes, and then these loads gradually increase until we reach the point of collapse. Lateral loads are applied to determine the effects of earthquakes on structures, determine their ability to withstand these earthquakes, and help engineers understand how the structure behaves under these forces.

2.2.6.3 *Nonlinear analysis*

At each load step, a nonlinear analysis is performed to determine the structural response. This analysis considers the nonlinear behavior of materials, such as yielding, plastic deformation.

2.2.6.4 Estimation of structural response:

The structural response parameters, including displacements, inter-story drifts, and base shear, are evaluated at each load step. These parameters help identify the weak links and the overall behavior of the structure.

2.2.6.5 Iterative process:

Based on the results of the analysis, the model is revised to incorporate the changes in the structure caused by yielding or failure of components. The analysis is repeated iteratively until a yield pattern for the entire structure is identified.

By performing pushover analysis, engineers can assess the seismic performance of existing structures, evaluate the need for retrofitting or strengthening measures, and guide the design of new buildings with desired performance objectives.In the pushover analysis method, the structure is subjected to a sequence of increasing lateral loads applied at different levels. The analysis accounts for the nonlinear behavior of the structure, including plastic deformations and the redistribution of forces, which are important factors during seismic events.

The pushover analysis typically involves the following steps:

Model Creation: Structural models can be developed using ETABS, SAP2000, or Abaqus to represent geometry, loading, boundary conditions, and nonlinear material behavior. Nonlinearity is modeled through plastic hinges in ETABS and SAP2000, while Abaqus enables detailed finite element simulation of material damage and inelastic response.

Load Patterns: The lateral load patterns that simulate the seismic forces are applied to the structure. These load patterns can be based on design response spectra or earthquake time-history records.

Load incrementation: The lateral loads are incrementally increased, typically until a predefined performance level or limit state is reached. The analysis tracks the structural response at each load increment.

Capacity Curves: The analysis generates capacity curves, also known as pushover curves, which plot the structural capacity (such as base shear or interstorey drift) against the applied load. These curves provide valuable information about the structure's strength and deformation capacities.

Performance Assessment: The capacity curves are compared with predefined performance objectives or acceptance criteria to assess the structure's seismic performance. This evaluation can include criteria related to maximum displacements, interstorey drifts, and member forces.

The pushover analysis method allows engineers to assess the behavior and performance of a structure under different load levels. It helps identify potential weak points, determine the distribution of forces, and evaluate the effectiveness of structural elements and systems in resisting seismic forces. The results of the pushover analysis can inform design decisions, retrofit strategies, and structural modifications to enhance the seismic performance of buildings.

2.2.7 When and why we use pushover analysis of a structure?

Pushover analysis is typically used in structural engineering for the following purposes:

2.2.7.1 Seismic Design

Pushover analysis is commonly employed for the seismic design of buildings and structures. It allows engineers to evaluate the behavior and performance of the structure under seismic loads, considering the nonlinear behavior and plastic deformations. By performing pushover analysis, engineers can determine the capacity of the structure, assess its ductility, and identify potential failure modes.

2.2.7.2 Performance-Based Design

Pushover analysis is a key component of performance-based design approaches. It helps engineers assess the expected response of the structure under different levels of seismic loading and evaluate its performance in meeting specific performance objectives or criteria. Performance-based design allows for a more tailored and efficient design process by focusing on desired performance levels rather than relying solely on prescriptive code provisions.

2.2.7.3 Retrofitting and Rehabilitation

Pushover analysis is utilized in the evaluation and retrofitting of existing structures to improve their seismic performance. By analyzing the structure's response and capacity through pushover analysis, engineers can identify weaknesses, determine the retrofit requirements, and develop effective retrofit strategies to enhance the structure's resistance to seismic forces.

2.2.7.4 Comparative Analysis

Pushover analysis is often used for comparative studies between different design options or structural systems. By subjecting different design alternatives to pushover analysis, engineers can compare their response, capacity, and performance, allowing for informed decision-making and optimization of the structural design.

2.2.7.5 Code Development and Validation

Pushover analysis plays a significant role in the development and validation of seismic design codes and guidelines. The analysis results can be used to refine design provisions, assess the adequacy of code provisions, and validate the performance of different structural systems and design methodologies.

Pushover analysis provides valuable insights into the behavior and performance of structures under seismic loading. It allows engineers to evaluate the structure's capacity, assess its response characteristics, and make informed design decisions to ensure adequate seismic resistance and safety.

2.2.8 Performance level of structures against earthquakes

Fully Operational performance level: No damage (The structure of building is safe).

Immediate occupancy performance level: Slight damage (shear cracks in nonstructural elements).

Life safety performance level: Moderate damage (Shear cracks in main structural elements).

Collapse prevention performance level: Very heavy damage (Collapse of parts or total of building).

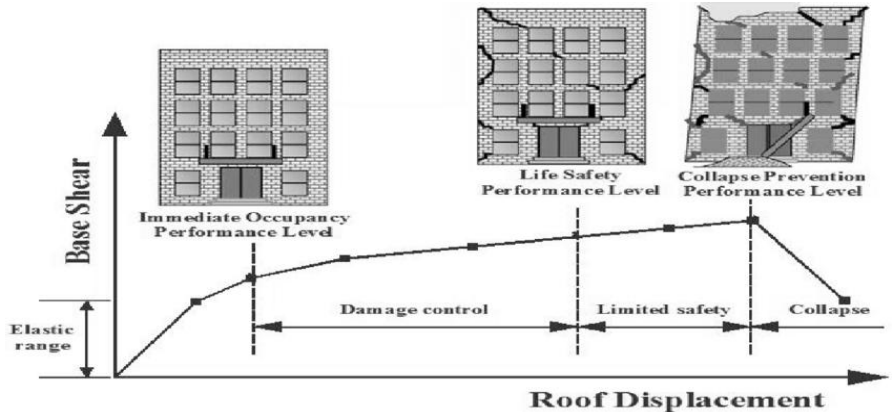

Figure 2.5: Capacity curve of structures with illustration of building performance levels and damage states.

2.3 Research Gap

A close look at past research and technical studies on nonlinear pushover analysis and how to estimate the seismic response modification factor (R) shows there is a big missing piece in current work. Many studies have used pushover analysis to find rough estimates of R-values, but most of them depend on general ideas, standard ways of applying forces, or rules of thumb that aren't really suited to specific buildings or local earthquake risks. Also, there isn't much work that connects the evaluation of R-values for a specific structure with the actual response spectrum that depends on the site, especially for reinforced concrete (RC) buildings made with modern earthquake design rules. This means the R-values people usually use might not show the real way a building behaves when it bends and twists during an earthquake. To fix this, this thesis presents a new system that uses advanced pushover methods along with better ways to adjust response spectra. The research mainly looks at mid-rise concrete buildings and focuses on making the models more accurate for how buildings act when they bend. It also links the final response spectra directly to real site conditions and design rules. This method is a big step forward in how we design buildings to be safe and cost-effective during earthquakes.

CHAPTER 3 STUDY DESCRIPTION

3.1 Introduction

This chapter presents the methodology adopted to evaluate the influence of the response modification factor (R) on the seismic performance of Intermediate Moment Resisting Concrete Frame Systems (IMRCFS). The proposed framework integrates advanced numerical modeling with nonlinear analytical techniques to quantify the effect of varying R-values on structural response under seismic loading.

In this context, high-fidelity three-dimensional models of reinforced concrete moment-resisting frames are developed and analyzed using advanced structural analysis platforms, including SAP2000, ETABS, and ABAQUS. These models are carefully configured to simulate realistic earthquake loading conditions, allowing for a consistent and reliable evaluation of structural behavior.

Accordingly, the analysis focuses on key performance indicators, including load-carrying capacity, ductility demand, and energy dissipation mechanisms. Through this integrated approach, the chapter establishes a clear foundation for assessing the seismic response of IMRCFS and the role of the response modification factor in influencing overall structural performance.

3.2 Prototype Structure Description

The structural prototype adopted in this study consists of reinforced concrete multi-story building configurations with heights of 1, 3, 6, and 9 stories. All models share a consistent structural layout, comprising four bays in the x-direction and three bays in the y-direction, and are supported by a 250 mm thick two-way solid slab system. At each story level, the structural system includes 20 columns and 9 primary beams, ensuring uniformity in geometry across all configurations.

All gravity and seismic loads, along with the governing design parameters, are defined in accordance with ASCE 7-16 provisions. The buildings are designed and detailed as Intermediate Moment-Resisting Reinforced Concrete Frame Systems (IMRCFS), with material properties corresponding to normal-strength concrete with a compressive strength of f_c' =25 MPa and high-yield deformed steel reinforcement with a yield strength of f_y =420 MPa.

To realistically capture the inelastic behavior under seismic loading, beam–column joints in all models are assigned automatic plastic hinge properties. The analytical investigation begins with a three-story building, which serves as the reference model for the study. Subsequently, the same modeling framework is extended to include one-, six-, and nine-story configurations while maintaining identical geometric and material characteristics to ensure a consistent basis for comparison.

In the later stages, variations in cross-sectional dimensions and reinforcement areas of structural members are introduced in accordance with design requirements, allowing for a systematic evaluation of their influence on nonlinear seismic response. The analysis focuses on key performance parameters, including lateral displacement demand, ductility capacity, and energy dissipation behavior.

For the reference case, the three-story structure consists of columns with cross-sectional dimensions of 40 × 40 cm and beams measuring 30 × 35 cm, as illustrated in Figure 3.2. The overall geometric configurations of the one-story and multi-story models are presented in Figures 3.1 and 3.2, respectively. Figures 3.1 and 3.2 illustrate the geometric configurations of the one-story and multi-story structural models, respectively.

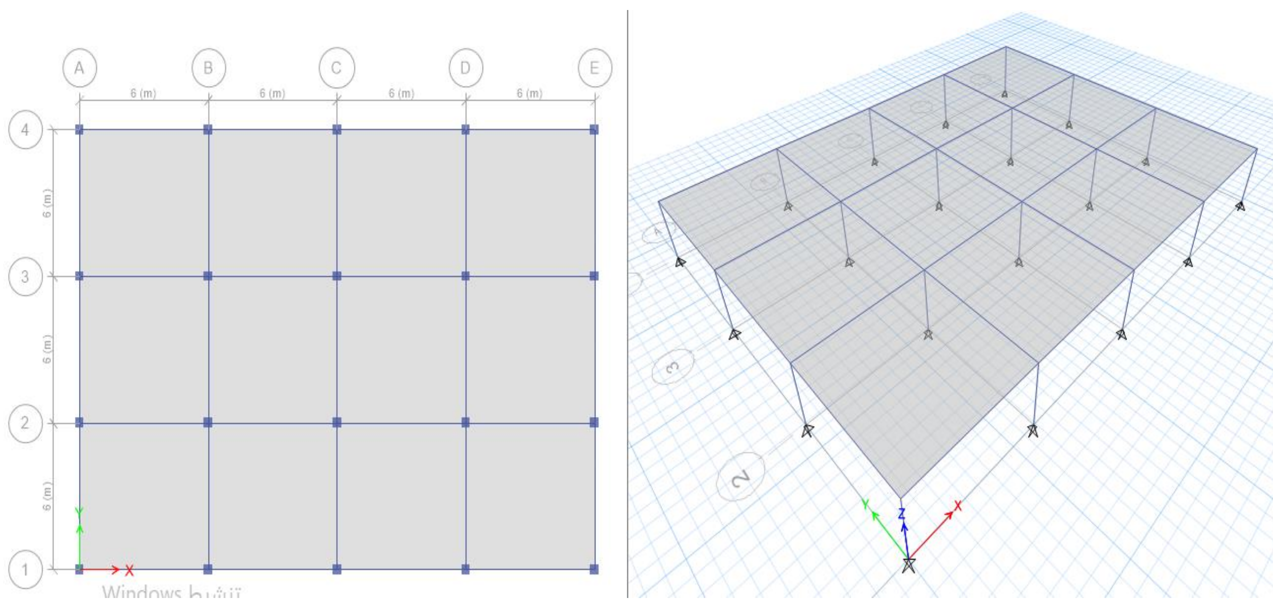

Figure 3.1 The Dimension and The Layout of the One - Story Structure Building (Frames).

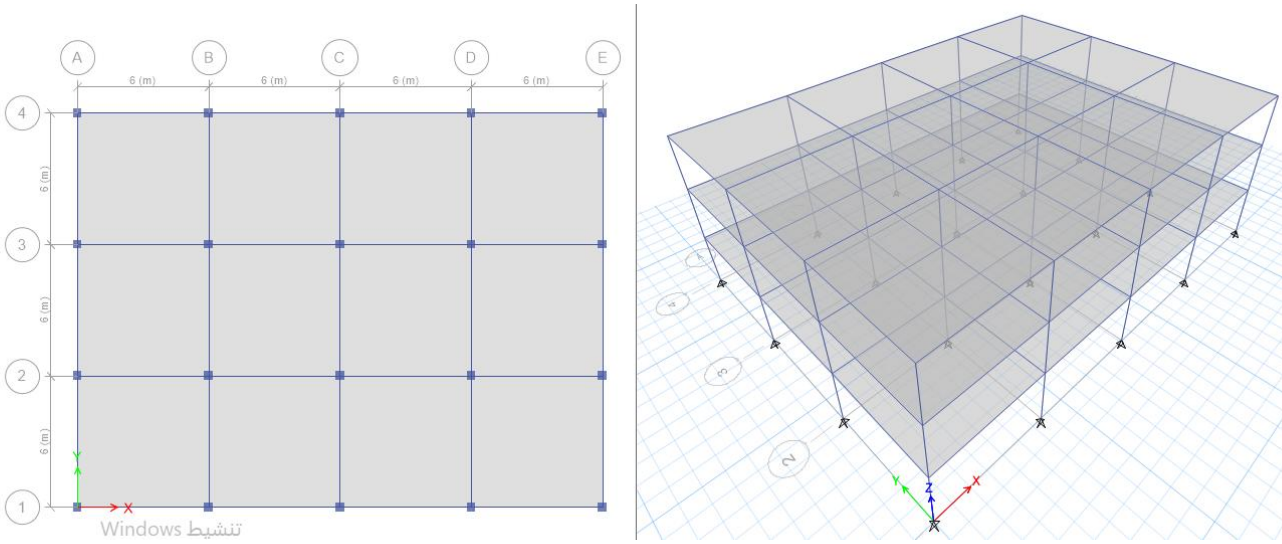

Figure 3.2 The Dimension and The Layout of the Three - Story Structure Building (Frames).

The building is subjected to a uniformly distributed dead load of 5 kN/m², excluding self-weight, and a live load of 3 kN/m². The structure is assumed to be located within a Middle seismic design category. All design assumptions and loading criteria are established in accordance with the provisions of Minimum Design Loads and Associated Criteria for Buildings and Other Structures (ASCE 7-16). The reinforcement ratios adopted for all beams and columns comply with the limits specified by the relevant design codes. The self-weight of the structural system is automatically computed and assigned by the structural analysis software SAP2000. The procedures employed for the evaluation of seismic design forces and the execution of nonlinear static (pushover) analysis are based on established seismic performance assessment guidelines, namely FEMA 356 and ATC-40. These criteria are utilized to ensure reliable estimation of the structure's strength capacity, ductility demand, and overall seismic performance under earthquake-induced loading conditions (FEMA 356, 2000; ATC-40, 1996).Classification Of Buildings and Other Structures.

3.3 Seismic Importance Factor and Occupancy-Based Classification

Table 3.1, developed in accordance with the American Society of Civil Engineers Standard ASCE 7-16 (2016), presents the seismic coefficients required for the evaluation of lateral seismic forces acting on structures. The parameters and values listed in this table are governed by several key criteria, most notably the building importance level and occupancy classification. Accurate assignment of the seismic importance factor (I) represents a fundamental step in seismic design, as it directly influences the magnitude of seismic forces incorporated in structural analysis. This approach ensures that structures—particularly those classified as essential facilities or those exhibiting elevated collapse risk—are designed with enhanced reliability to withstand earthquake-induced demands while safeguarding human life and critical assets (FEMA 356, 2000). Seismic design regulations and standards, including the Uniform Building Code (UBC), the International Building Code (IBC), and ASCE 7: Minimum Design Loads and Associated Criteria for Buildings and Other Structures, classify structures based on occupancy type and corresponding risk category, commonly referred to as Seismic Design Categories (SDCs), as summarized in Table 3.2. Accordingly, each category is assigned a specific seismic importance factor that either amplifies or reduces the design seismic forces in proportion to the criticality of the structure's intended function during and after a seismic event (ASCE, 2022; UBC, 1997; International Code Council, 2021).

Table 3.1 Occupancy Category (1997 UNIFORM BUILDING CODE - UBC)].

OCCUPANCY CATEGORY	OCCUPANCY OR FUNCTIONS OF STRUCTURE	SEISMIC IMPORTANCE FACTOR, I	SEISMIC IMPORTANC E1FACTOR, I_p	WIND IMPORTANCE FACTOR, I_w
1. Essential facilities[2]	Group I, Division 1 Occupancies having surgery and emergency treatment areas Fire and police stations Garages and shelters for emergency vehicles and emergency aircraft Structures and shelters in emergency-preparedness centers Aviation control towers Structures and equipment in government communication centers and other facilities required for emergency response Standby power-generating equipment for Category 1 facilities Tanks or other structures containing housing or supporting water or other fire-suppression material or equipment required for the protection of Category 1, 2 or 3 structures	1.25	1.50	1.15

2. Hazardous facilities	Group H, Divisions 1, 2, 6 and 7 Occupancies and structures therein housing or supporting toxic or explosive chemicals or substances Nonbuilding structures housing, supporting or containing quantities of toxic or explosive substances that, if contained within a building, would cause that building to be classified as a Group H, Division 1, 2 or 7 Occupancy	1.25	1.50	1.15

3. Special occupancy structures [3]	Group A, Divisions 1, 2 and 2.1 Occupancies Buildings housing Group E, Divisions 1 and 3 Occupancies with a capacity greater than 300 students Buildings housing Group B Occupancies used for college or adult education with a capacity greater than 500 students Group I, Divisions 1 and 2 Occupancies with 50 or more resident incapacitated patients, but not included in Category 1 Group I, Division 3 Occupancies All structures with an occupancy greater than 5,000 persons Structures and equipment in power-generating stations, and other public utility facilities not included in Category 1 or Category 2 above, and required for continued operation	1.00	1.00	1.00
4. Standard occupancy structures	All structures housing occupancies or having functions not listed in Category 1, 2 or 3 and Group U Occupancy towers	1.00	1.00	1.00
5. Miscellaneous structures	Group U Occupancies except for towers	1.00	1.00	1.00

Table 3.2 Risk Category of Buildings and Other Structures for Flood, Wind, Snow, Earthquake, and Ice Loads.

Use or Occupancy of Buildings and Structures	Risk Category
Buildings and other structures that represent low risk to human life in the event of failure	I
All buildings and other structures except those listed in Risk Categories I, III, and IV	II
Buildings and other structures, the failure of which could pose a substantial risk to human life	III
Buildings and other structures, not included in Risk Category IV, with potential to cause a substantial economic impact and/or mass disruption of day-to-day civilian life in the event of failure Buildings and other structures not included in Risk Category IV (including, but not limited to, facilities that manufacture, process, handle, store, use, or dispose of such substances as hazardous fuels, hazardous chemicals, hazardous waste, or explosives) containing toxic or explosive substances where the quantity of the material exceeds a threshold quantity established by the Authority Having Jurisdiction and is sufficient to pose a threat to the public if released[a]	
Buildings and other structures designated as essential facilities Buildings and other structures, the failure of which could pose a substantial hazard to the community Buildings and other structures (including, but not limited to, facilities that manufacture, process, handle, store, use, or dispose of such substances as hazardous fuels, hazardous chemicals, or hazardous waste) containing sufficient quantities of highly toxic substances where the quantity of the material exceeds a threshold quantity established by the Authority Having Jurisdiction and is sufficient to pose a threat to the public if released[a] Buildings and other structures required to maintain the functionality of other Risk Category IV structures	IV

Table 3.3 Importance Factors by Risk Category of Buildings and Other Structures for Snow, Ice, and Earthquake Loads.

Risk Category	Snow Importance Factor, Is	Ice Importance Factor-Thickness, Ii	Ice Importance Factor-Wind,Iw	Seismic Importance Factor, I e
I	0.80	0.80	1.00	1.00
II	1.00	1.00	1.00	1.00
III	1.10	1.15	1.00	1.25
IV	1.20	1.25	1.00	1.50

Table 3.4 Site Classification.

Site Class	$\bar{v}_s$	$\bar{N}$ or $\bar{N}_{ch}$	$\bar{s}_u$
A. Hard rock	>5,000 ft /s	NA	NA
B. Rock	2,500 to 5,000 ft /s 762 to 1524 m /s	NA	NA
C. Very dense soil and soft rock	1,200 to 2,500 ft /s	>50 blows /ft	>2,000 lb /ft^2
D. Stiff soil	600 to 1,200 ft /s	15 to 50 blows /ft	1,000 to 2,000 lb /ft^2
E. Soft clay soil	<600 ft /s	<15 blows /ft	<1,000 lb /ft^2
	Any profile with more than 10 ft of soil that has the following characteristics: —Plasticity index PI > 20, —Moisture content w ≥ 40%, —Undrained shear strength $\bar{s}_u$ < 500 lb /ft^2		
F. Soils requiring site response analysis in accordance with Section 21.1	See Section 20.3.1		

Note: For SI: 1 ft = 0.3048 m; 1 ft /s = 0.3048 m /s; 1 lb /ft2 = 0.0479 kN /m2

Table 3.5 Site Coefficient, F_a.

Site Class	Mapped Maximum Considered Earthquake Spectral Response Acceleration Parameter at 1-s Period				
	$S_S \leq 0.25$	$S_S = 0.5$	$S_S = 0.75$	$S_S = 1.0$	$S_S \geq 1.25$
A	0.8	0.8	0.8	0.8	0.8
B	1.0	1.0	1.0	1.0	1.0
C	1.2	1.2	1.1	1.0	1.0
D	1.6	1.4	1.2	1.1	1.0
E	2.5	1.7	1.2	0.9	0.9
F	See Section 11.4.7				

NOTE: Use straight-line interpolation for intermediate values of S_S.

Table 3.6 Site Coefficient, F_v.

Site Class	Mapped Maximum Considered Earthquake Spectral Response Acceleration Parameter at 1-s Period				
	$S_1 \leq 0.1$	$S_1 = 0.2$	$S_1 = 0.3$	$S_1 = 0.4$	$S_1 \geq 0.5$
A	0.8	0.8	0.8	0.8	0.8
B	1.0	1.0	1.0	1.0	1.0
C	1.7	1.6	1.5	1.4	1.3
D	2.4	2.0	1.8	1.6	1.5
E	3.5	3.2	2.8	2.4	2.4

NOTE: Use straight-line interpolation for intermediate values of S_1.

Table 3.7 Importance Factors.

Occupancy Category	I
I or II	1
III	1.25
IV	1.5

Table 3.8 Values of Approximate Period Parameters Ct and x.

Structure Type	C_t	x
Moment-resisting frame systems in which the frames resist 100% of the required seismic force and are not enclosed or adjoined by components that are more rigid and will prevent the frames from deflecting where subjected to seismic forces:		
Steel moment-resisting frames	0.028 (0.0724)[a]	0.8
Concrete moment-resisting frames	0.016 (0.0466)[a]	0.9
Eccentrically braced steel frames	0.03 (0.0731)[a]	0.75
All other structural systems	0.02 (0.0488)[a]	0.75

[a] Metric equivalents are shown in parentheses.

Table 3.9 Design Coefficients and Factors for Seismic Force–Resisting Systems (ASCE 17-6).

Seismic Force–Resisting System	**ASCE 7 Section where Detailing Requirements are Specified**	**Response Modification Coefficient, *Ra***	**System Overstrength Factor, *Ω0g***	**Deflection Amplification Factor, *Cdb***	**Structural System Limitations and Building Height (ft) Limit*c*Seismic Design CategoryB C D*d* E*d* F**				
C. MOMENT-RESISTING FRAME SYSTEMS									
1. Steel special moment frames	14.1 and 12.2.5.5	8	3	5.5	NL	NL	NL	NL	NL
2. Steel special truss moment frames	14.1	7	3	5.5	NL	NL	160	100	NP
3. Steel intermediate moment frames	12.2.5.7 and 14.1	4.5	3	4	NL	NL	35k	NPk	NPk
					NL	NL		NPl	

4. Steel ordinary moment frames	12.2.5.6 and 14.1	3.5	3	3			NPl		NPl
5. Special reinforced concrete moment frames	12.2.5.5 and 14.2	8	3	5.5	NL	NL	NL	NL	NL
6. Intermediate reinforced concrete moment frames	14.2	5	3	4.5	NL	NL	NP	NP	NP
7. Ordinary reinforced concrete moment frames	14.2	3	3	2.5	NL	NP	NP	NP	NP
8. Steel and concrete composite special moment frames	12.2.5.5 and 14.3	8	3	5.5	NL	NL	NL	NL	NL
9. Steel and concrete composite intermediate moment frames	14.3	5	3	4.5	160	160	NP	NP	NP
10. Steel and concrete composite partially restrained moment frames	14.3	6	3	5.5	NL	NL	100	NP	NP
11. Steel and concrete composite ordinary moment frames	14.3	3	3	2.5	35	35	NP	NP	NP
12. Cold-formed steel—special bolted moment framen	14.1	3.5	3º	3.5	NL		35	35	35
								12.2.5.1	

W: Seismic Load Calculation at X-X Direction. Area of Floor = 24*18 = 432 m²

One Story Loads Frame:

Depth of Slab = 25 cm, Dead Load = 5 KN/m²

Beams Weight = 25*0.30*0.35*(24*4+18*5) = 488/432=1.13 KN/m2

Column Self weight/ Stories = 0.4*0.4*3*25*20 = 240/432 = 0.56 KN/m2

Total Dead Load at Typical Stories = 5 + 1.13 + 0.56 =6.69 KN/m2

Weight of one-story = 6.69 * 432 = 2890.08 KN

3 Stories Loads: 2890.08*3=8670.24KN

Table 3.10 Design Conditions and Site Class Specific Factors, per ASCE 7-16

Design Code	ASCE 7-16
Ss=2.50 * Z	0.75
S1=1.25 * Z	0.375
Soil Site Class	A Hard Rock
Fa	0.8
Fv	0.8
Sms = Fa*Ss	0.6
Sm1 = Fv*S1	0.3
SDs = 2/3 Sms	0.4
SD1 = 2/3 Sm1	0.2
Intermediate Reinforced Concrete Moment Frames	R =5, Ω =3, Cd = 4.5
Seismic Design Category	D
Occupancy Category	III (Ie = 1.25)
To = 0.2 SD1/SDS	0.10 Sec
Ts = SD1/SDS	0.50 Sec

Ta = C h x = 0.0466*(3*3)0.9 = 0.337 sec, (From 3-Storey Frame System). (ASCE 7-16, 2016)

T = 0.073 H 3/4 = 0.073 * 9 3/4= 0.38 sec, (For Concrete Structures) General Relation

Sa= SD1/ T = 0.53 g T0=0.1 ≤ T=0.38s ≤ TS=0.50, (This curve equation). (ASCE 7-16, 2016)

Sa= SD1*TL/T2= 0.50 g, (TL= 4 sec – For Site Class A Soil, From (ASCE 7-16, 2016, p. 85))

Response spectra are curves plotted between maximum response of SDOF system subjected to specified earthquake ground motion and its time period (or frequency). Response spectrum can be interpreted as the locus of maximum response of a SDOF system for given damping ratio. Response spectra thus helps in obtaining the peak structural responses under linear range, which can be used for obtaining lateral forces developed in structure due to earthquake thus facilitates in earthquake-resistant design of structures. Usually response of a SDOF system is determined by time domain or frequency domain analysis, and for a given time period of system, maximum response is picked. This process is continued for all range of possible time periods of SDOF system. Final plot with system time period on x-axis and response quantity on y-axis is the required response spectra pertaining to specified damping ratio and input ground motion. Same process is carried out with different damping ratios to obtain overall response spectra.

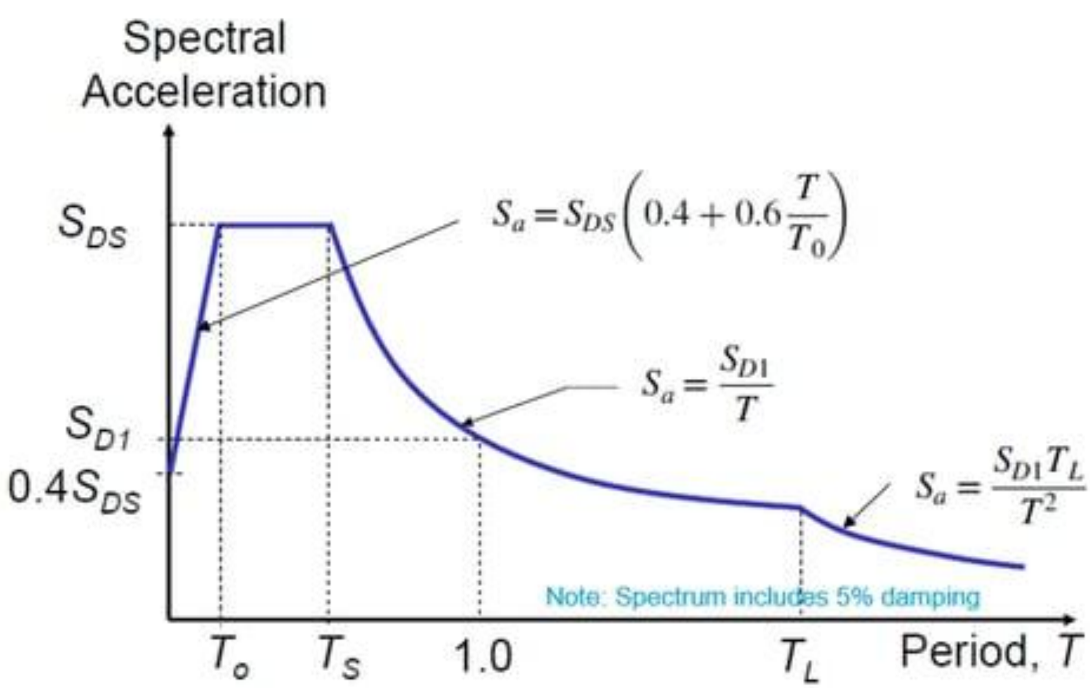

Figure 3.3 Response Spectrum Curve.

CHAPTER 4 VEREFICATION AND NUMIRICAL

APPLICATIONS

4.1 Chapter Layout

In this chapter, the nonlinear static analysis methodology is rigorously validated through high-fidelity numerical simulations applied to reinforced concrete systems with well-documented experimental behavior. The validation process relies on benchmark models that have been extensively studied in the literature, ensuring a reliable basis for comparison.

The first benchmark consists of a single-span beam with end continuity, originally tested by Duddeck et al. (1976) and later reported by Mueller. This specimen exhibits predominantly linear behavior up to the onset of concrete crushing and reinforcement yielding, making it an efficient and reliable reference case for evaluating the accuracy of nonlinear numerical modeling procedures.

The second benchmark involves a single-story reinforced concrete frame experimentally investigated by Xiao et al. (2006). This model provides a more representative structural system for assessing global response characteristics under seismic loading conditions.

The experimental data obtained from both benchmarks are utilized as authoritative references to verify the accuracy and robustness of the adopted modeling approach. The validation is conducted using SAP2000, with particular emphasis on advanced nonlinear modeling techniques and their ability to accurately reproduce observed structural behavior.

4.2 Analysis Parameters, Material Properties, and Load–Displacement Curve Comparison.

In nonlinear structural analysis, the accuracy of the results is highly dependent on the definition of modeling assumptions and solution strategies. When using advanced analysis platforms such as SAP2000, it is essential to define appropriate material constitutive models, particularly for the nonlinear behavior of concrete under tension and compression, in addition to selecting suitable analysis options such as large-displacement effects and joint displacement formulations.

Within this framework, nonlinear static pushover analysis is widely used to evaluate the inelastic behavior and seismic performance of structures due to its computational efficiency and ability to capture the progression of structural response from the elastic range to yielding and ultimate capacity. The method provides valuable insight into strength, stiffness degradation, ductility, and potential failure mechanisms, making it a practical and reliable tool for performance-based seismic assessment.

In light of these limitations, alternative approaches have been explored, most notably the force-based formulation, as advocated by Hu and Thomson (1996), Kaljević et al. (1996), and Spacone et al. (1996). In this approach, internal forces are treated as the primary unknowns rather than nodal displacements, allowing for a more accurate representation of inelastic structural behavior. Accordingly, the force-based formulation provides improved capability in capturing the elastic–plastic response of structural elements, particularly under large deformation demands. In this study, the adopted material model incorporates a complete elastic–plastic stress–strain relationship, defined using tangent stiffness values derived from experimental data, as illustrated in Figure 4-1.

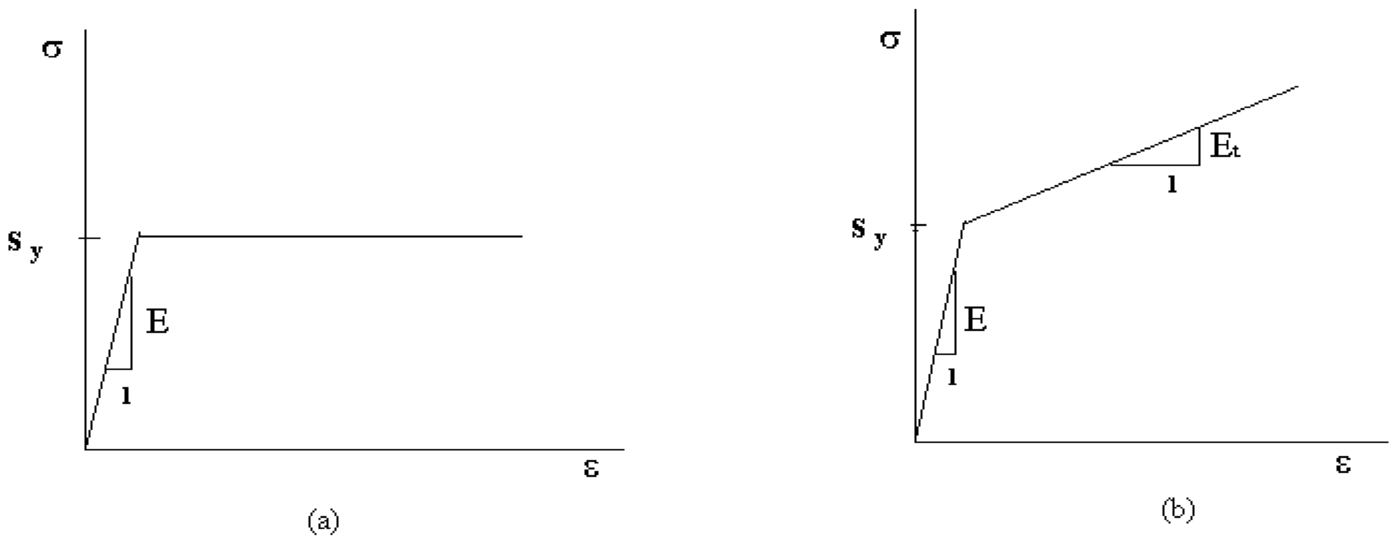

Figure 4.1 a. Elastic-Perfectly Plastic Stress-Strain Curve. b. Elasto-Plastic With Linear Hardening Stress-Strain Curve.

4.2.1 Single Span Beam

single span reinforced concrete beam with (60x80) mm2 cross section area that had a (2Φ4 and 2Φ4) longitudinal reinforcement for compression and tension regions respectively. The elevation, cross section and reinforcement details of the beam are illustrated in (Figure 4.2), where a concentrated vertical force of 20 KN was applied. And the material properties of the single span beam are specified in (Table 4.1). It presents identical steel properties and slightly different properties for concrete. The material parameters for concrete are given in (Bresler, B & Scordelis, A. C, 1963).

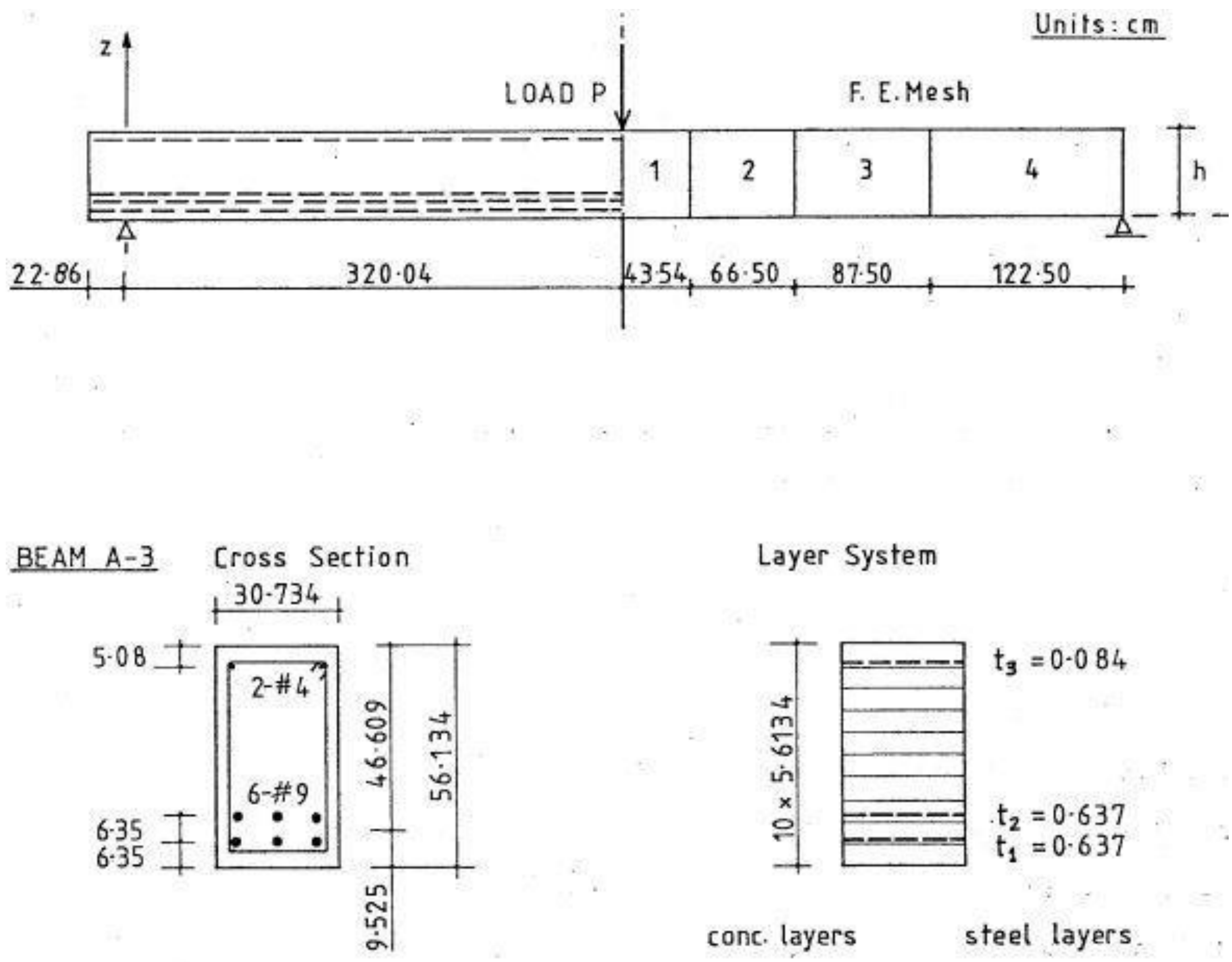

Figure 4.2 Geometry and Finite Element Idealization for Single Span Beam.

Table 4.1 Problem Parameters for Single Span Beam, Figure 4.2

Material Properties (kN, cm)		
Concrete	Steel	
Young's Modulus, E_c=2980	Young′s Modulus, E_s = 2053	#9
Poisson′s Ratio, V = 0.15	Young′s Modulus, E_s' = 8150	
Ult. Comp. St., f′c = 3.50	Yield Stress, fy = 55.2	
Ult. Tens. St., ft′ = 0.43	Angle with x-axis, ⊖ =0.0	
Ult. Comp. St n., $\in$=0.003	Young′s Modulus, E_s = 20120	#4
Tens. Stiff. Coefficient, a = 0.6 (*)	Young′s Modulus, E_s' = 0	
Tens. Stiff. Coefficient, $\in_m$= 0.0015 (*)	Yield Stress, fy = 34.52	
(*) Only considered in the four bottom layers	Angle with x-axis, ⊖ =0.0	

Figure 4.3 presents the relationship between mid-span deflection and the applied load, where the experimental results are compared with the corresponding numerical predictions obtained from SAP2000. Overall, the comparison indicates good agreement between the experimental data and the numerical model.

However, the numerical results exhibit a slightly higher collapse load, reaching approximately 480 kN, along with a stiffer response at higher load levels. This is reflected in the load–deflection curve, which shows increased stiffness compared to the experimental behavior. Such differences can be attributed to the initial stiffness assumptions adopted in the SAP2000 modeling procedure, which tend to produce a relatively stiffer structural response.

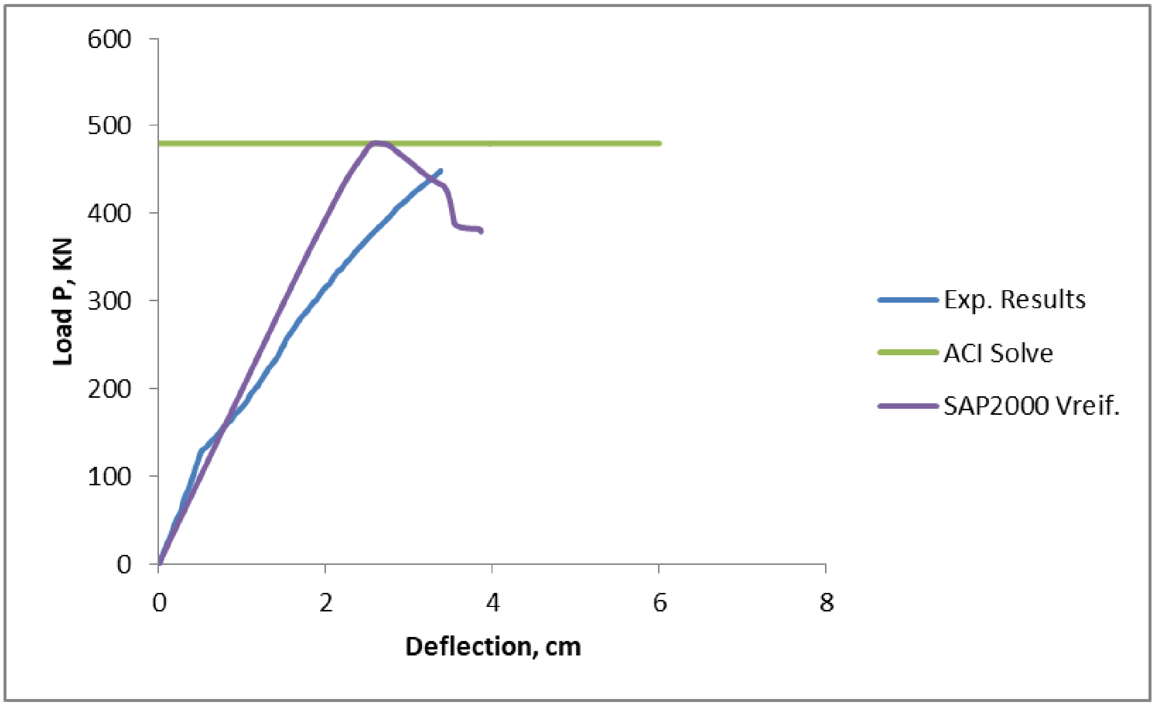

Figure 4.3: Load-Deflection Curve for Single Span Beam.

4.2.2 Two Span Beam

two-span reinforced concrete beam with (60x80) mm2 cross section area which has a (8Φ4) longitudinal reinforcement for compression and tension regions. The analysis of geometry and loading of the reinforced concrete beam (micro-concrete) is illustrated in Figure 4.3 (a). Only one half of the beam is taken into consideration in the investigation due to symmetry,where a concentrated vertical force of 20 KN was applied. The same figure also includes the assumed loading and boundary conditions. The material properties of the beam are specified in (Table 4.2), with identical steel properties and slightly different properties for concrete.

The Young's modulus, Ec, the ultimate compressive stress, fc' and the compressive strain at peak stress (€C=0.0027) were experimentally obtained. The other concrete properties have been assumed for the analysis.

Table 4.2: Problem Parameters for Two Span Beam

Material Properties (kN, cm)	
Concrete	Steel
Young's Modulus, Ec=1666	Young’s Modulus, Es = 19600
Poisson’s Ratio, V = 0.0	Young’s Modulus, Es' = 2800
Ult. Comp. St., f’c = 3.2	Young’s Modulus, Es' '= 500
Ult. Tens. St., ft’ = 0.32	Yield Stress, fy = 49.0
Ult. Comp. St n., Є=0.004	Yield Stress, fy ' = 57.4
Tens.Stiff.Coefficient, a= 0.5	Angle with x-axis, Ө =0.0
Tens.Stiff.Coefficient,Єm=0.0015	

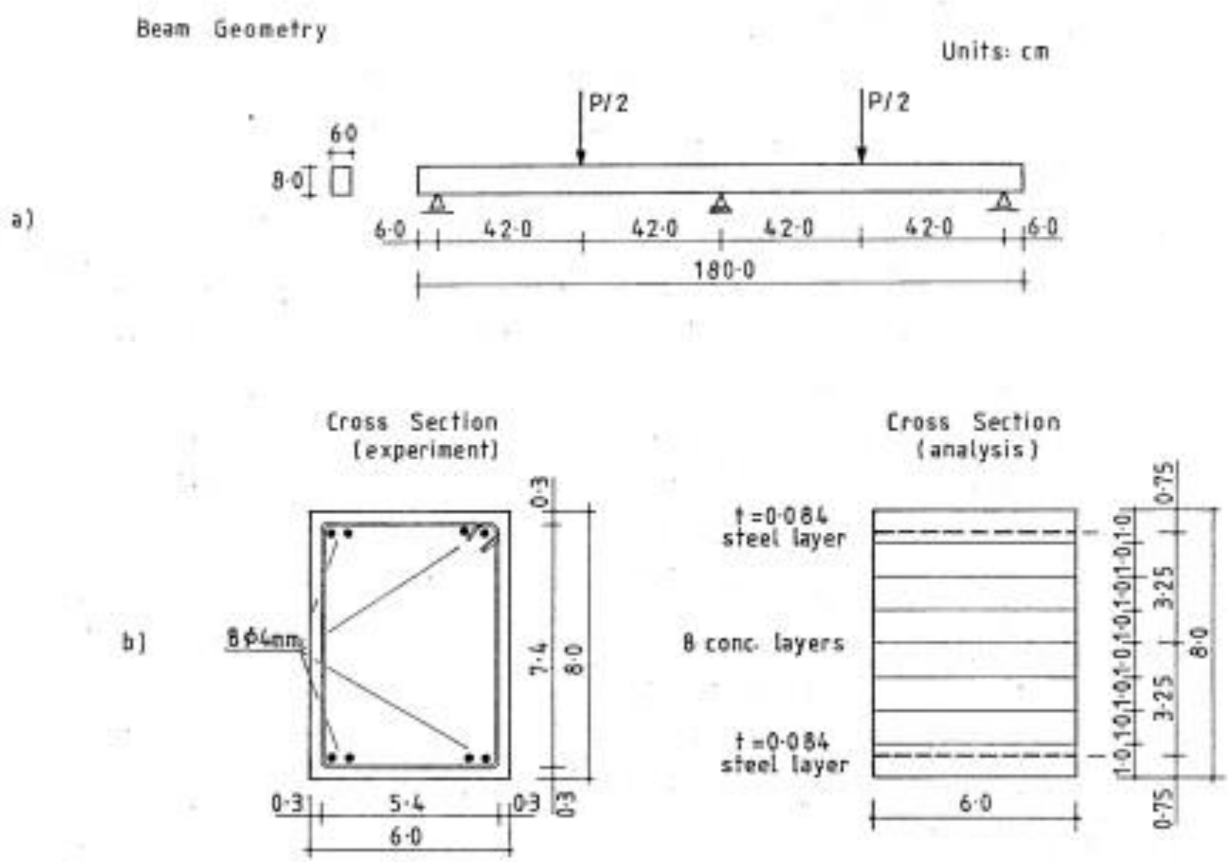

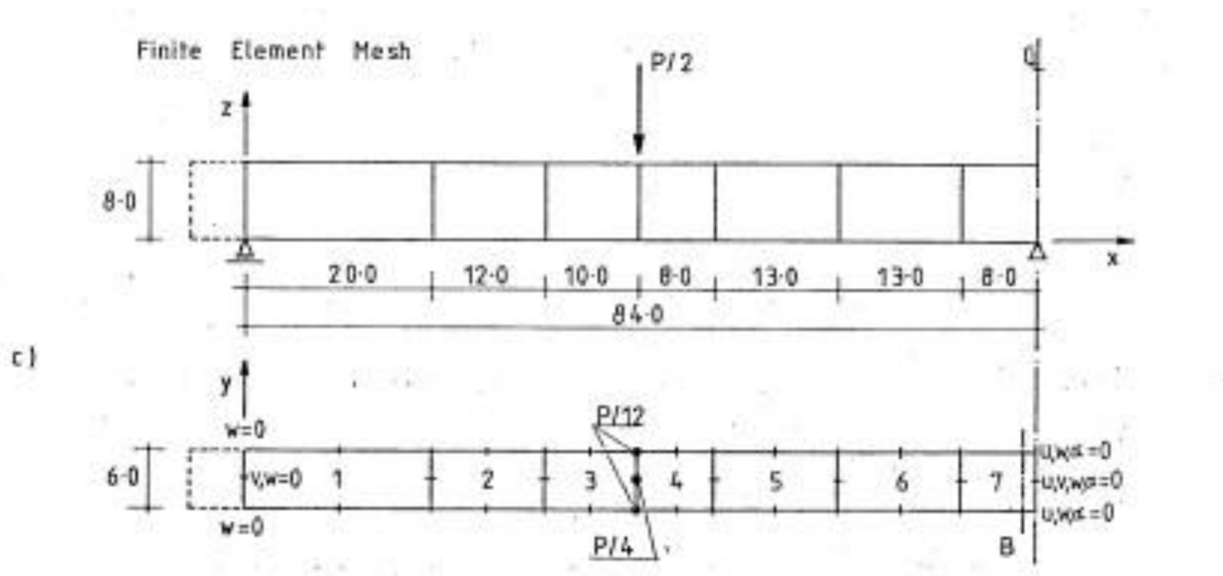

Figure 4.4 (a) Geometry, (b) Loading and Finite Element Idealization for Two Span Beam,
(c) discretized 7 finite elements of the beam.

Figure 4.5 illustrates the relationship between point-load deflection and the total applied force, where the experimental results are compared with the numerical predictions obtained using SAP2000 under identical material properties and concrete strength. The comparison demonstrates good agreement between the numerical and experimental responses.

The numerical model predicts an ultimate load of approximately 32.4 kN, which exceeds the limit load obtained from the plastic hinge formulation (31.3 kN) and shows close agreement with the experimentally observed capacity. This indicates that the numerical model is capable of capturing the overall structural behavior with reasonable accuracy.

However, the load–deflection response derived from the numerical analysis exhibits a relatively stiffer behavior, particularly in the initial stages. This can be attributed to the initial stiffness assumptions inherent in the SAP2000 modeling approach, which influence the nonlinear response and lead to an overestimation of stiffness.

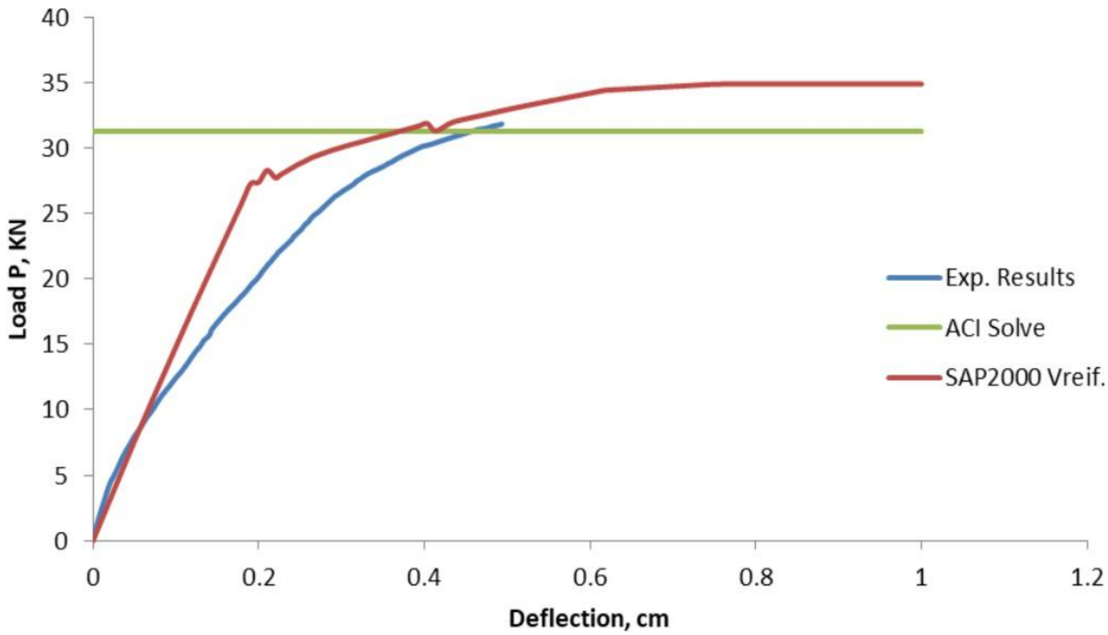

Figure 4.5 Load-Deflection Curve for Two Span Beam.

The ultimate strength for the numerical and the experimental results are close to the section analysis method according to the ACI code.

4.2.3 One-Story Frame Building

One-story reinforced concrete frame which consist of two columns and a beam with a (250x150) mm2 cross-section area, it has a (4Φ14) longitudinal reinforcement for both compression and tension regions. The geometry and loading of the reinforced concrete frame under analysis are illustrated in Figure 4.6. The material properties of the beam are specified in Table 4.3, with identical steel properties and slightly different properties for concrete. The 28-day compressive strength and the elastic modulus of the concrete were 27 MPa and 33 GPa, respectively. The longitudinal and stirrups bars have yield stresses of 448 and 433 MPa, respectively. The steel reinforcements' elastic modulus was 200 GPa. The distance between the clear concrete cover and the longitudinal bars was 20 mm. On the tops of the two columns, vertical point loads of 150 kN were applied. At one-third and two-thirds from the beam's left end, point loads of 12 kN were applied.

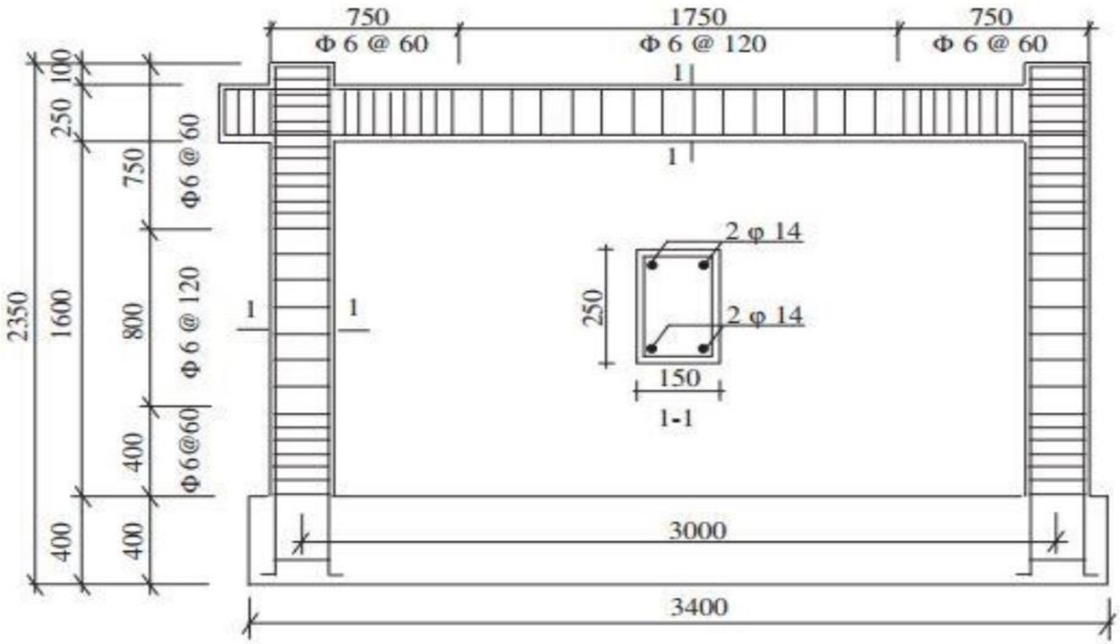

Figure 4.6 Details of The One-Story Frame.

Table 4.3 Parameters for One Story Frame, Figure 4.6.

Material Properties (N, mm)	
Concrete	Steel
Young's Modulus, Ec=33000	Young’s Modulus, Es = 200000
Ult. Comp. Strength, f'c =27	Yield Stress for Longitudinal, fy = 448
	Yield Stress for Stirrups, fy = 433

Figure 4.7 (**Abu Azzanid (2023)** presents a comparative evaluation between the experimental results and the roof-level lateral load–displacement response predicted through nonlinear finite element analysis conducted using SAP2000 and Abaqus. The figure demonstrates a strong correlation between the numerical simulations and the experimental observations. the analytical predictions closely replicate the experimental response, indicating the reliability of the adopted modeling approach in capturing the initial nonlinear behavior of the frame The stiffened behavior of the frame could be attributed to the initial stiffness method adopted by SAP2000 And Abaqus.

Furthermore, the structural model illustrated in Figure 4.6 was retained for additional parametric investigations. A series of analyses were performed by varying the number of transverse stirrups in order to assess their influence on the structural response. The outcomes of these investigations are presented and discussed in a subsequent section.

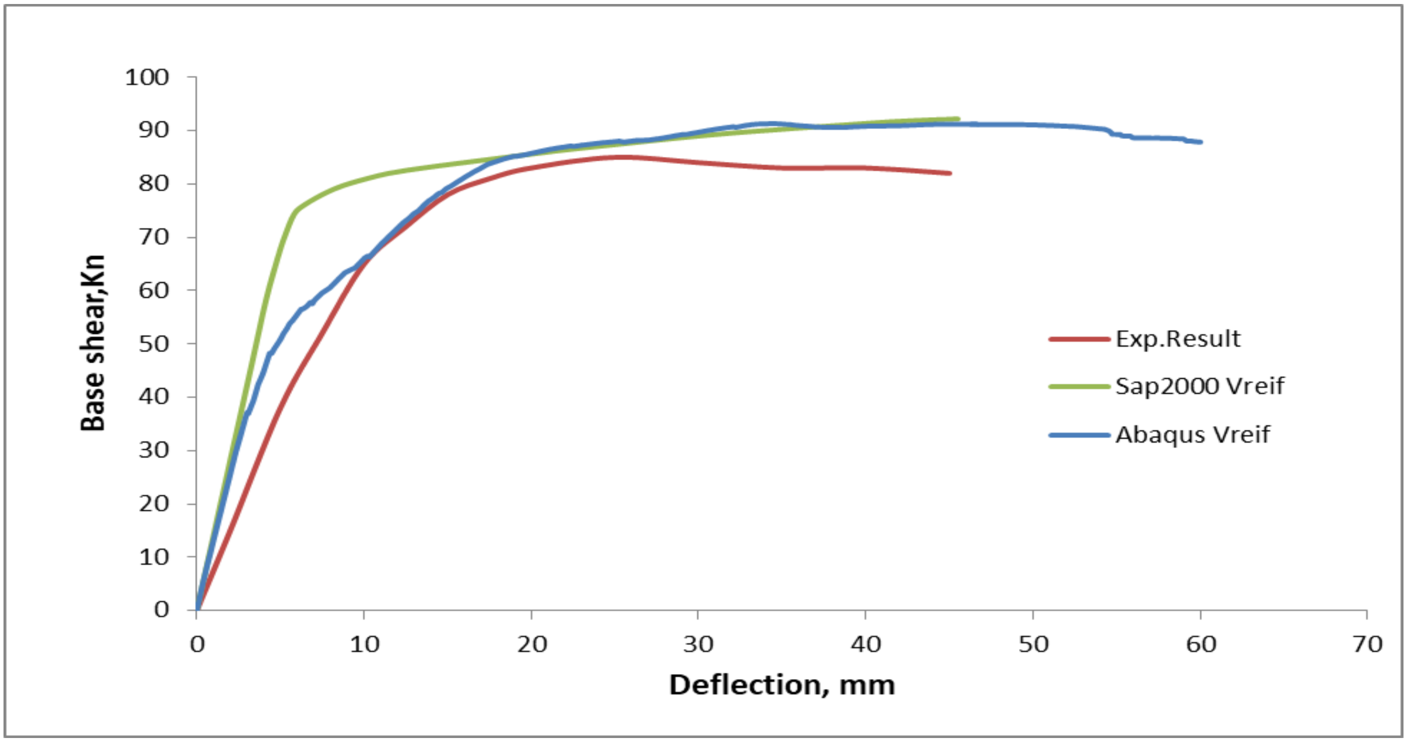

Figure 4.7 Load-Deflection Curve for One Story Frame.

The pushover curve obtained from ABAQUS is considered more accurate than that derived from SAP2000 due to fundamental differences in the treatment of structural nonlinearity and stiffness degradation. ABAQUS adopts an updated tangent stiffness formulation, in which the stiffness matrix is continuously modified throughout the analysis to reflect the actual material behavior, including cracking, yielding, and damage evolution. This approach allows for a realistic representation of the gradual transition from elastic to inelastic behavior and provides a smooth and physically consistent load–displacement response. In contrast, SAP2000 primarily relies on the initial stiffness of structural elements, with nonlinear behavior idealized through predefined concentrated plastic hinges. The post-yield stiffness degradation in SAP2000 is therefore governed by assumed hinge properties rather than by the intrinsic material response, which may lead to a simplified or less realistic representation of stiffness deterioration and post-elastic behavior.

CHAPTER 5 INTERMEDIATE MOMENT RESISTING FRAME

MODELING AND CALIBRATION

5.1 Chapter Layout

In this study, an analytical and parametric investigation is carried out using the finite element modeling software SAP2000, while selected models are additionally analyzed using Abaqus for verification and comparative purposes. To realistically represent the expected structural behavior of reinforced concrete building frames—comprising beams, columns, and shear walls in the X-direction—models with varying numbers of stories (1, 3, 6, and 9) were developed under idealized boundary conditions within the SAP2000 environment.This chapter focuses on evaluating the structural performance of the frame elements through the nonlinear auto P.H hinge analysis approach. It further examines key response characteristics directly related to the response modification factor, including ductility, overstrength, maximum lateral displacement, and performance point levels. In addition, the influence of Mander's confined concrete model on the stress–strain behavior of concrete is investigated. This constitutive model is inherently implemented within SAP2000 and is utilized to capture realistic nonlinear material behavior. All analyses explicitly consider material nonlinearity and incorporate second-order (P–Δ) effects beyond the elastic design stage, enabling a more accurate prediction of post-yield structural response and overall seismic performance.

5.2 Mander's Model

The Mander Model, developed by Mander et al. (1988), is one of the most widely used constitutive models for representing the nonlinear stress–strain behavior of concrete under compression. The model provides separate stress–strain relationships for confined and unconfined concrete and is particularly suitable for seismic performance assessment of reinforced concrete structures. Unlike simplified material models, the Mander Model accounts for the beneficial effect of transverse reinforcement (stirrups or ties) on the compressive strength and ductility of concrete. When concrete is confined by closely spaced transverse reinforcement, lateral expansion is restrained, resulting in increased compressive strength, larger ultimate strain, and enhanced energy dissipation capacity.

Unconfined concrete exhibits a relatively brittle response after reaching its peak compressive strength, followed by a rapid reduction in stress. In contrast, confined concrete demonstrates a more ductile behavior, maintaining its load-carrying capacity over a wider strain range and showing a gradual descending branch after the peak stress. Consequently, confined concrete can sustain significantly larger deformations before failure, making it highly desirable in seismic-resistant design.

In this study, the Mander Model was employed to evaluate the effect of confinement on the concrete stress–strain relationship. The confinement level was controlled by modifying the spacing of transverse reinforcement. Reducing the stirrup spacing increases the lateral confining pressure, which in turn increases the effective compressive strength of concrete ((f'c)) and alters the shape of the stress–strain curve by increasing both the peak stress and the ultimate strain. The modified confined concrete properties obtained from the Mander Model were subsequently used to define the concrete material in SAP2000, where the updated (f'c) value and corresponding stress–strain relationship were assigned to the material model for nonlinear analysis.

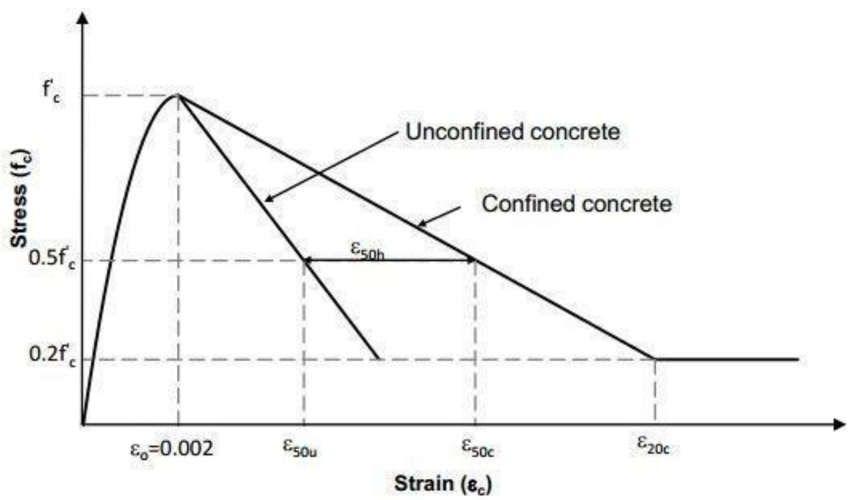

Figure 5.1 Proposed Stress-Strain Model for Confined and Unconfined Concrete – Kent And Park (1971) Model.

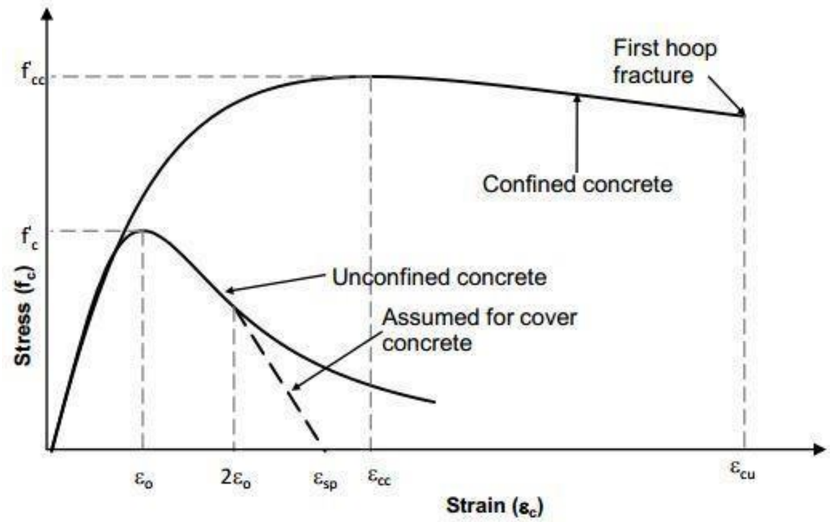

Figure 5.2 Stress-Strain Relation for Monotonic Loading of Confined and Unconfined Concrete - Mander Et Al. (1988b).

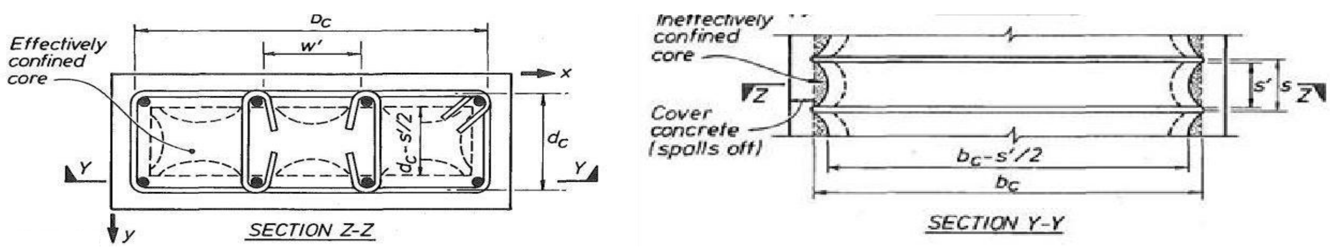

Figure 5.3 Effectively Confined Core for Rectangular Hoop Reinforcement.

Figures 5.1–5.3 illustrate the fundamental concepts of concrete confinement according to the Mander Model and the influence of transverse reinforcement on the stress–strain behavior of reinforced concrete members. Figures 5.1 and 5.2 compare the response of confined and unconfined concrete under compression. The results indicate that unconfined concrete reaches its peak compressive strength and subsequently experiences a rapid loss of strength, reflecting a relatively brittle behavior. In contrast, confined concrete exhibits increased compressive strength, greater ultimate strain capacity, and a more gradual post-peak response due to the lateral restraint provided by transverse reinforcement. This confinement delays crushing and enhances ductility, allowing the concrete core to sustain larger deformations while maintaining its load-carrying capacity.

5.3 Ductility Factor (μ)

The ductility factor (μ) is one of the most important parameters in earthquake engineering, as it quantifies the ability of a structure to undergo inelastic deformations beyond the yield point without experiencing significant loss of strength or collapse. It is defined as the ratio of the maximum displacement attained by the structure to its yield displacement, expressed as:

$\mu = \Delta u / \Delta y$

where Δu is the ultimate displacement and Δy is the yield displacement. A higher ductility factor indicates a greater capacity of the structure to dissipate seismic energy through controlled inelastic behavior. Ductility plays a fundamental role in the evaluation of seismic performance and is directly related to the response modification factor (R), since structures with higher ductility can be designed for lower seismic forces while maintaining adequate safety and stability during strong earthquake events.

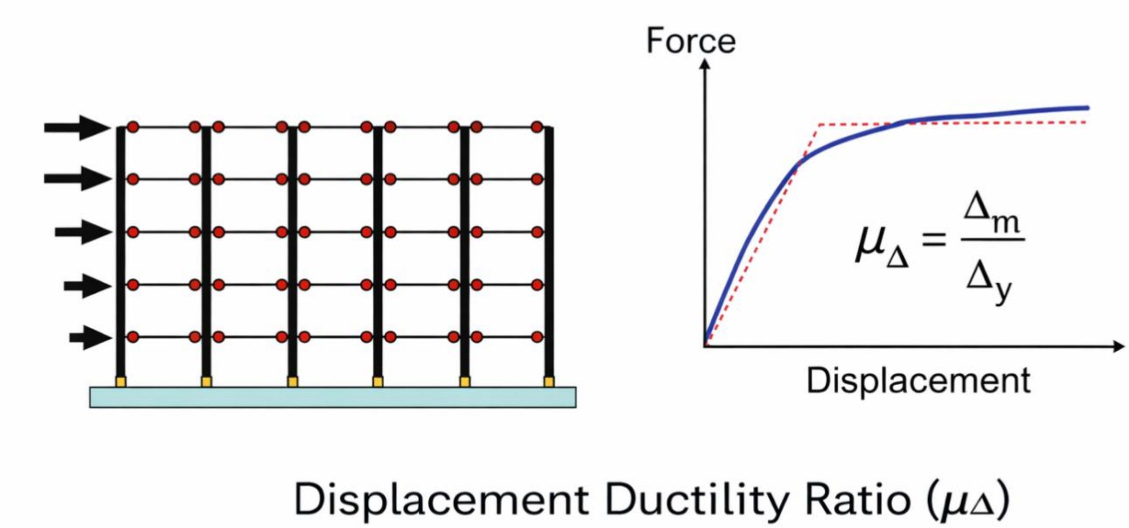

Figure 5.4 Displacement Ductility Ratio (μΔ).

The hysteretic energy-induced nonlinear response of a structure was calculated using the reduction factor given to R. (R) is dependent on the parameters of the ground motion during an earthquake as well as structural qualities including damping, ductility, and the basic period of vibration. The idealized yielding point (Δ_y), created by (Newmark and Hall, 1982), corresponds to the maximum structural drift (Δ_{max}), which is how R is expressed in Equations:

$R_\mu = \mu$ if $T > 0.5$ sec 5.1

$R_\mu = \sqrt{(2\mu - 1)}$ if $0.1 < T < 0.5$ sec 5.2

$R_\mu = 1$ if $T < 0.03$ sec 5.3

Throughout this study, the system proposed by Paulayin addition to Priestley (1992) is utilized.

$R_\mu = 1.0$, for zero-period structures 5.4.

$R_\mu = \sqrt{(2\mu-1)}$, for short-period structure 5.5

$R_\mu = \mu$ for long-period structure, 5.6

$R_\mu = 1 + (\mu-1)\, T/0.70$, $(0.70 < T < 0.30)$ 5.7

Where R_μ is the ductility reduction factor and μ is the displacement ductility. T is the fundamental period and μ is the displacement ductility factor defined as the following:

$\mu = \Delta_{max}/\Delta_y$ 5.8

Where Δ_{max} is the maximum displacement (displacement corresponding to the limit state), and Δ_y is the yield displacement of the structure.

Note: For safe design --------- Ductility Demand < Ductility Capacity

5.4 Over Strength Code Factor (Ω)

Structures are typically designed from the outset using equivalent static forces defined by building codes. These static forces are mainly divided based on basic elastic vibration patterns, so current structural design codes take into account the probability of an earthquake (ATC3-06, 1978). However, by using an inelastic energy dissipation system, a number of structural and nonstructural damages can be analyzed to economically attain a high level of safety in structural design. The majority of seismic codes allow a decrease in design loads by stating that structures have a sizable amount of reserve strength (overstrength Ω) and the ability to disperse energy (ductility $R\mu$). When designing for lateral strength, lateral strength is often less than what seismic standards specify is necessary for structures to remain elastic.Calculating the actual forces acting on a structural element designed to remain elastic involves taking into account an over-strength factor in seismic design. For tall buildings, the sources that contribute to this over-strength have not yet been extensively quantified (Khy K et.al., 2019). Even if the earthquake's actual seismic demands exceeding their design values, most of buildings with shear wall structures perform well and appear to sustain little to no damage (L. M. Massone et.al. 2012 and D. Ugalde and D. Lopez-Garcia, 2017). This is because the design's essential reserve strength or over-strength, which keeps structures from collapsing. The ratio of actual ultimate lateral strength to code-based design lateral force is known as the over-strength factor (**Ω**). The provisions of (ASCE 7- 16, 2016 and NBCC, 2010) acknowledge the existence of a building's significant overstrength.

While the over-strength factor is implicitly taken into account in (ASCE 7-16, 2016) with the usage of response modification factor (R), which represents both ductility and overstrength factors, the over strength component is explicitly shown in (NBCC, 2010) as an over-strength related force modification factor (R_0). When designing critical structural members that must remain essentially elastic, such as collectors in a diaphragm, transfer beams, discontinuous systems, and elements supporting discontinuous frames or walls. the over-strength factor plays a key role in amplifying seismic forces (ASCE 7-16, 2016). Because it can enhance the shear forces of RC shear walls, the over-strength factor is also connected to the shear-amplification issue in shear walls (K. Khy et.al., 2019 and K. Leng et.al., 2014). To calculate the design forces of certain structural elements, it is crucial to estimate the over-strength factor accurately. A building over strength can be attributed to a variety of factors that have all been extensively discussed in several earlier research (C. M. Uang, 1991and A. S. Elnashai and A. M. Mwafy, 2002). Two categories can be used to categorize various factors that contribute to the over strength factor (ASCE 7-16, 2016 and C. M. Uang, 1991and). Material over-strength (actual material strengths are higher than nominal strengths specified in design), strength reduction factor (Φ), multiple load cases and load combinations, conservative design selection (selecting sections or specifying reinforcements that exceed the required design), design controlled by code minimum requirement, and design controlled by drift rather than strength are among the factors in the first group that contribute to the design process. The second group has to do with redundancy (the redistribution of internal forces among structural parts following the occurrence of yielding) and steel strain-hardening.

According to Figure 5.6, the whole over-strength factor (**Ω**) is divided into two categories. The first type is the so-called first-yield over-strength factor (**Ω**1), which is the relationship between the design base shear force (V_d) and the first-yield lateral strength (Vf_y), as indicated in Eq. 5.9. The second kind of over-strength results from internal force redistribution and steel strain hardening (Ω2), which is the ratio between ultimate lateral strength (V_{ult}) and first-yield lateral strength, as indicated in Eq. 5.9. According to Eq. 5.10, the ratio between the ultimate lateral strength and the design base shear force is the total over-strength factor.

$\Omega_1 = V_{fy}/V_d$ 5.9

$\Omega_2 = V_{ult}/V_{fy}$ 5.10

$\Omega = \Omega_1 x\ \Omega_2 = V_{ult}/V_{d\ 5.37}$ 5.11

$\Omega = V_y/V_d$ 5.12

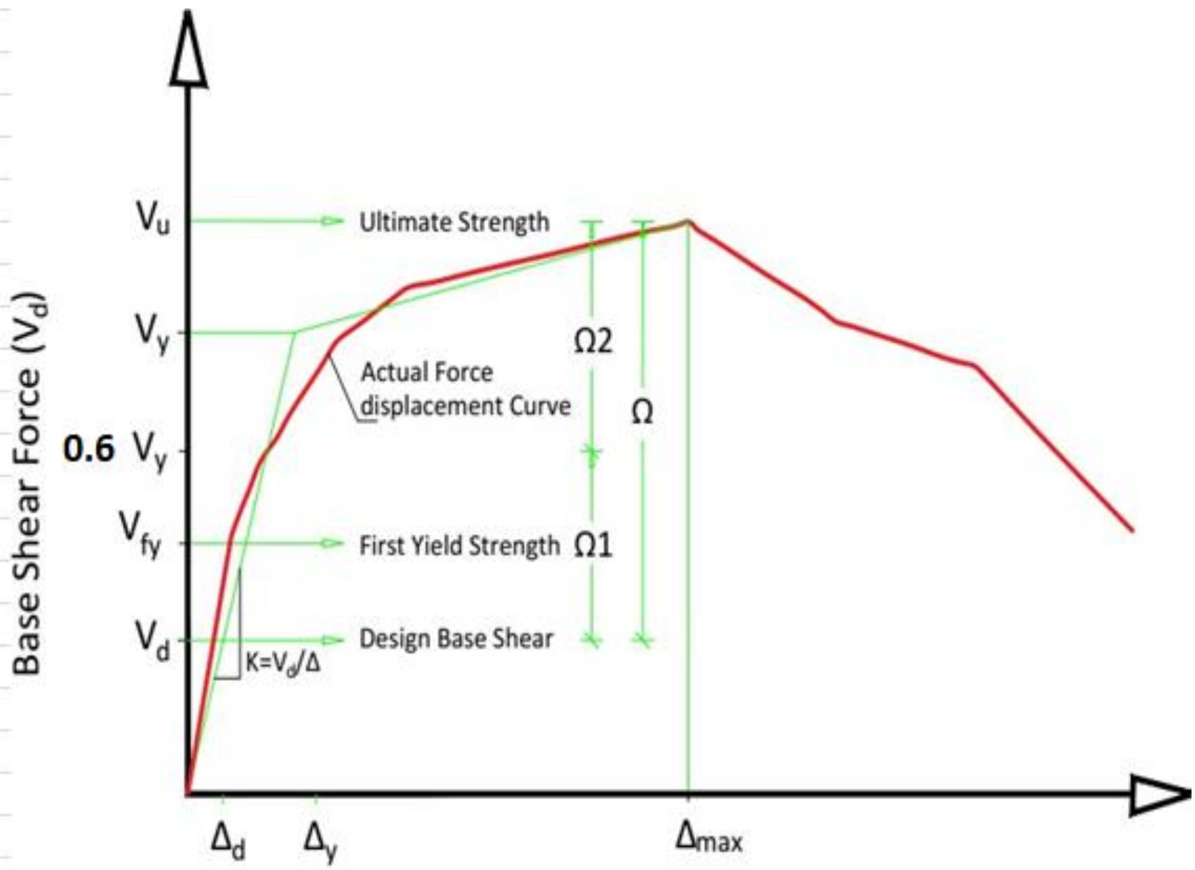

Figure 5.5 Lateral Load Capacity Curve and Over-Strength Factor of The Building.

5.5 Performance Point and Performance Level of Structures Against Earthquakes

The performance point is the point on the pushover curve with the greatest seismic displacement. Utilizing data obtained from the pushover analysis, engineers can assess the structural condition aligned with the displacement of this performance point. This assessment aids in locating plastic hinges, gauging their limit states, and determining interstory drifts. In other words, it signifies the point of physical equilibrium between structural capacity and seismic demand. The pushover curve, or capacity curve, represents the structural capacity, while the acceleration response spectrum of ground motions, or demand curve, signifies seismic demand, as shown in Figure 5.6. In theory, the performance point is the point at which the capacity and demand curves intersect. However, the capacity curve is represented as force versus displacement, while the demand curve is expressed as spectral acceleration versus period. To establish a common performance point, these two curves must initially be standardized to the same reference frame (Pednekar SC et al., 2015).

The Acceleration Displacement Response Spectra (ADRS) is a standardized reference that illustrates the relationship between spectral acceleration and spectral displacement. The spectral accelerations and displacements corresponding to the base shear forces and control node displacements of the capacity curve are calculated utilizing structural modal traits (i.e., modal mass and modal participation factor), and the capacity spectrum in the ADRS form is obtained. The equivalent spectral displacements can be calculated using the spectral accelerations and associated periods of the demand curve, and the demand spectrum in the ADRS form can be generated. Finding the performance point is not an easy task once the capacity and demand curves are given in the ADRS form. In fact, the first acceleration response spectrum (demand curve) corresponds to an elastic structure with a damping factor of about 5%. While plastic deformations occur in the structure, hysteretic damping is generated, increasing the overall damping of the structure.

To calculate the performance point ATC 40 method is adopted. Advance Design can now determine the performance point using either method (Dal Lago B and Molina FJ, 2018).

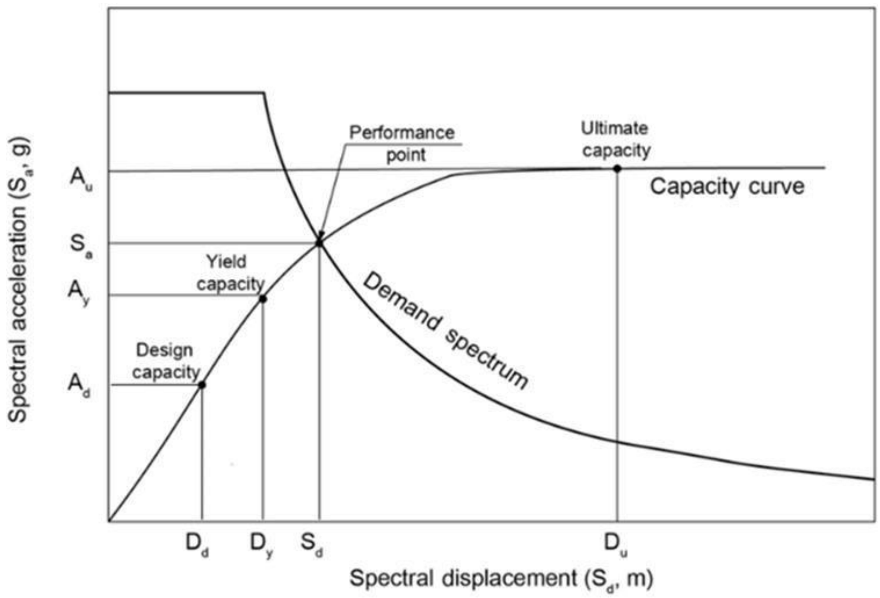

Figure 5.6 Performance Point Curve.

Upon determining the performance point, the structure's performance is evaluated to four levels of earthquake resistance: Operational Performance Level (OP), Immediate Occupancy Performance Level (IO), Life Safety Performance Level (LS), and Collapse Prevention Performance Level (CP). **Immediate Occupancy** Performance Level (IO) signifies a scenario where the structure sustains minor damage. There's no significant permanent drift, maintaining the original strength and stiffness. Minor cracking might occur in facades, partitions, ceilings, and structural elements, with the building's space and systems generally being fairly usable. Equipment and contents are generally secure, although they may not function due to mechanical failure or utility disruptions. Concrete frames experience minor hairline cracking, limited yielding in a few locations, and no excessive deformation (strain of concrete less than 0.003). Steel moment frames exhibit minor local yielding in specific locations, with no buckling, fractures, or noticeable distortions of members. In braced steel frame structures, minor yielding or distortion of braces might occur.

Life Safety Performance Level (LS) aims to achieve a damage condition with a low probability of endangering life safety. Moderate overall damage is evident, yet all stories retain residual strength and stiffness. No out-of-plane wall failures or parapet tipping occurs. However, permanent drift is present, and partitions suffer damage. The building may be beyond economical repair, and while falling hazards are mitigated, numerous architectural, mechanical, and electrical systems sustain damage. Concrete frame beams suffer extensive damage, exhibiting shear cracking and spalling of cover in ductile columns, along with minor cracking in nonductile columns. Hinges form in steel moment frames, accompanied by local buckling of some beams, significant joint distortion, and isolated moment connection fractures. Despite this, shear connections remain sound, and few elements may partially fracture. In braced frames, most braces yield or buckle to some extent, and certain connections might fail.

Collapse Prevention Performance Level (CP) mainly concerns the vertical load-carrying system, requiring the structure to remain stable under vertical loads only. Typically, building damage is severe, and residual stiffness and strength are minimal. While loadbearing columns and walls continue to function, substantial permanent drifts occur, some exits might be blocked, and infills and unbraced parapets either fail or are on the verge of failure. The building nears collapse, nonstructural components suffer extensive damage, hinges and extensive cracking arise in ductile elements of concrete frames, nonductile columns experience splice failure and limited cracking, and short columns are significantly damaged. In steel frames, beams and columns undergo pronounced distortion, while several moment connections fracture, and shear connections stay intact. In braced frames, numerous braces yield and buckle extensively, with many of them, along with their connections, facing potential failure, as shown in Figure 5.7.

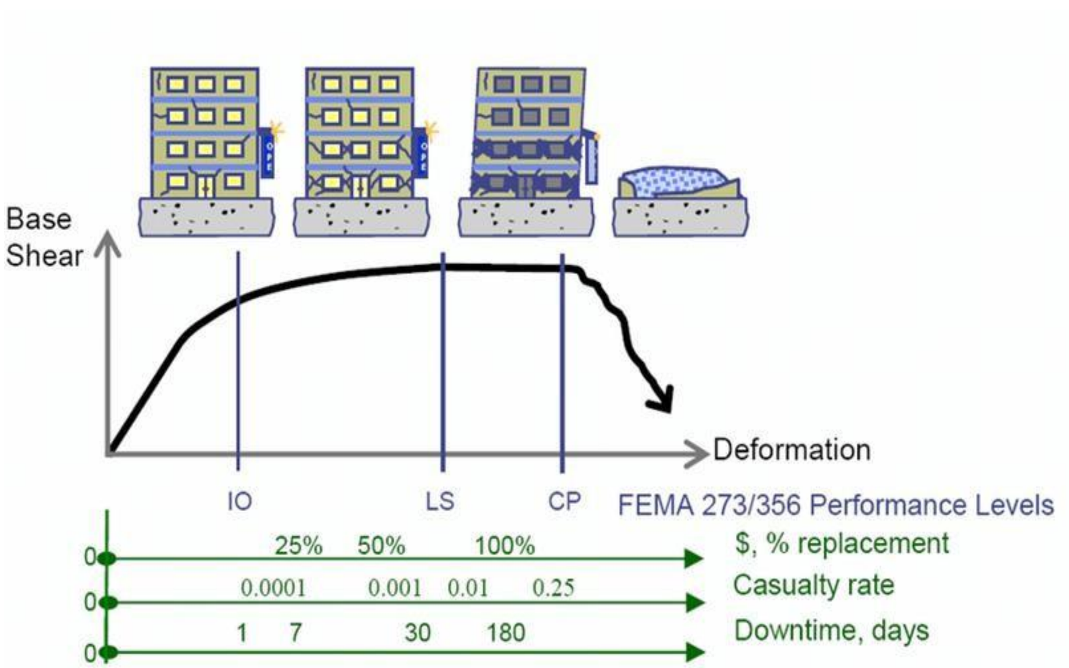

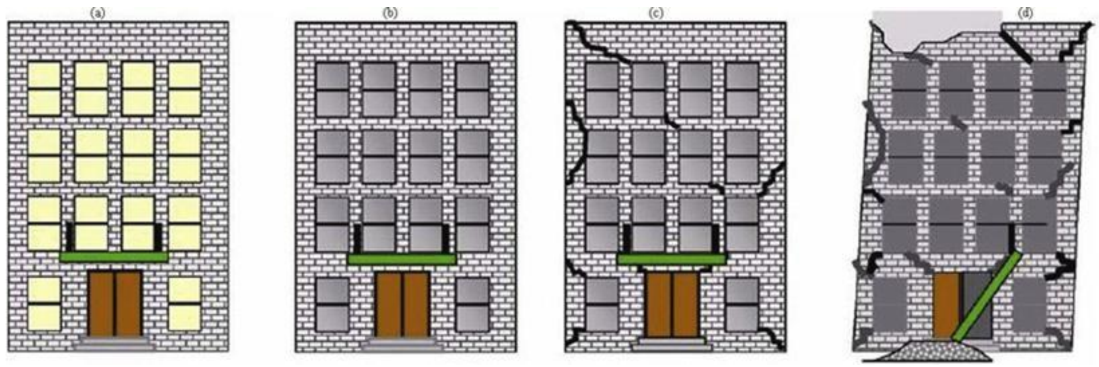

Figure 5.7 Levels of Building Performance: (A) Operational, (B) Immediate Occupancy, (C) Life-Safety, And (D) Collapse Prevention.

5.6 Equal Energy Method

Figure 5.8 illustrates a representative force–displacement response of an intermediate moment-resisting concrete frame (IMRCF), where the structural behavior becomes distinctly nonlinear as lateral displacement increases due to the development of inelastic deformations within the structural components. This response, commonly obtained from nonlinear static pushover analysis, is characterized by an initial linear elastic phase, followed by yielding and subsequent strain hardening or softening, depending on the ductility capacity of the system.

For the purposes of seismic performance evaluation and design, the inherently complex nonlinear response is typically idealized using a bilinear force–displacement relationship. This simplification provides a rational and practical basis for estimating key response parameters, including yield force and yield displacement. Among the available idealization techniques, the Equal Energy Method is widely recognized and adopted, particularly for intermediate moment-resisting frames exhibiting sufficient ductility, in accordance with the recommendations of ATC-19 (1995) and FEMA-440 (2005).

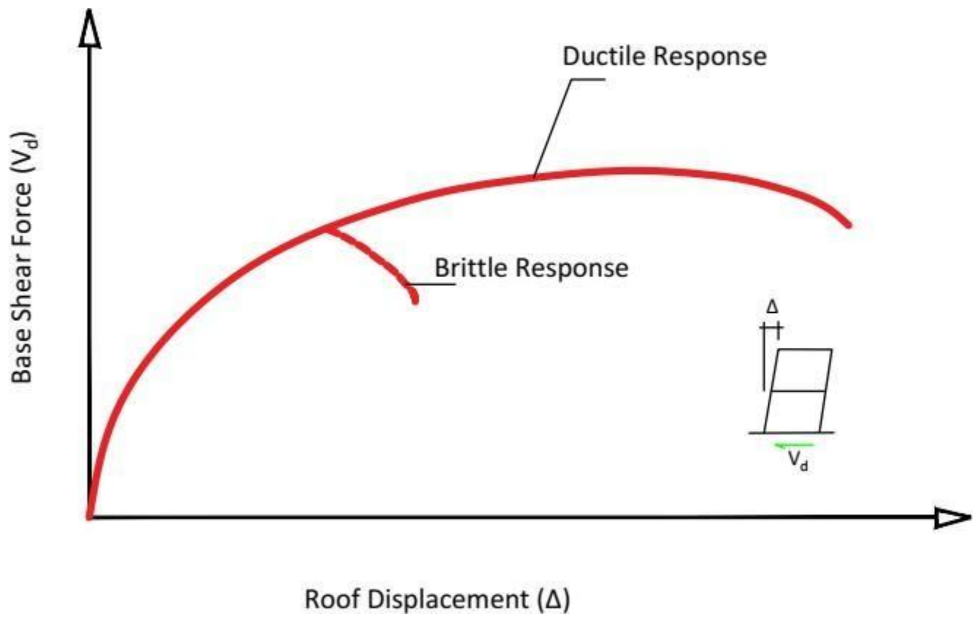

Figure 5.8 Sample base shear force versus roof displacement relationship.

Figure 5.9 illustrates the initial idealization employed to establish the load–displacement relationship of reinforced concrete elements, as proposed by Paulay and Priestley (1992). This first approximation is defined on the basis of the frame yield strength (Vy). The elastic stiffness of the system is evaluated using the secant stiffness at the intersection point extracted from the force–displacement curve corresponding to 0.6Vy. Accordingly, the elastic stiffness (K) is calculated as the ratio of the base shear to the associated lateral displacement, in accordance with the provisions of ATC-19 (1995).

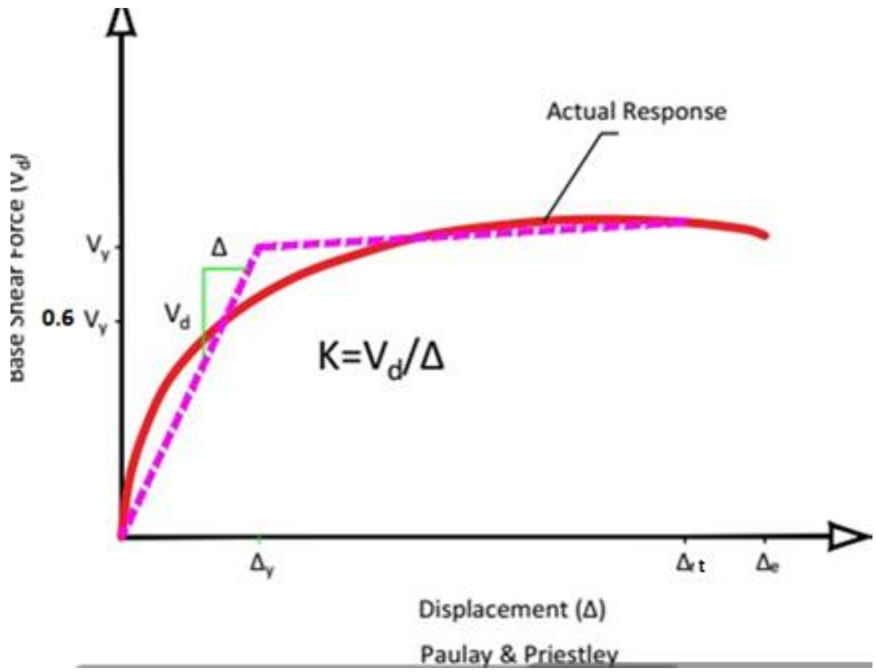

Figure 5.9 Bilinear approximations to fore-displacement relationship Pauly and Priestley.

Figure 5.10 illustrates the second approach employed to idealize the force–displacement relationship of the structural frame, commonly referred to as the ***Equal Energy Method***. This method is based on the assumption that the area enclosed by the actual nonlinear response curve above the bilinear idealization is equal to the area enclosed below it, thereby ensuring energy equivalence between the real and idealized structural responses, as recommended by ATC-19 (1995).

In the present study, this approach is adopted to determine the response modification factor (R), owing to its suitability for representing the nonlinear behavior of frames with adequate ductility.

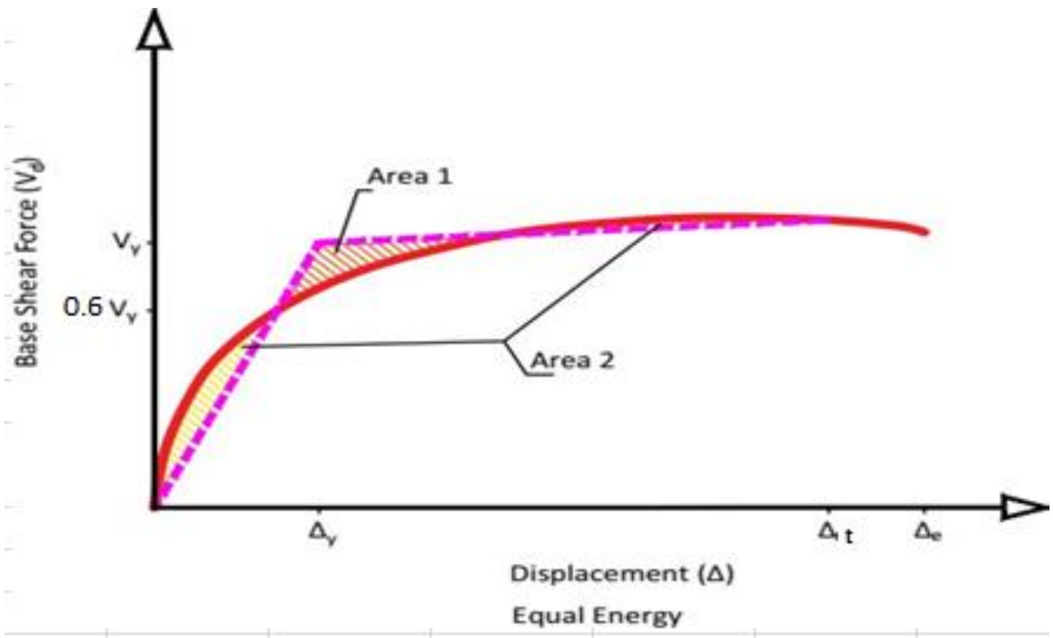

Figure 5.10 Bilinear approximations to fore-displacement relationship equal energy.

The nonlinear relationships are described by the yield force (V_y), yield displacement (Δ_y), maximum force (V_e), displacement corresponding to a limit state (Δ_t), and the displacement immediately prior to failure (Δ_e). Displacement Δ_t and Δ_e far exceed the yield displacement of a ductile framing system. The ability of a building frame to displace beyond its elastic limit, while resisting significant force and absorbing energy through inelastic behavior, is called ductility. Displacement ductility is defined as the difference between Δ_t and Δ_y. The maximum displacement ductility is the difference between Δ_e and Δ_y. The displacement ductility ratio is generally defined as the ratio of Δ_t to Δ_y and is:

$$\mu_\Delta=\Delta_t/\Delta_y \quad 5.13$$

Where Δ_t is always greater than Δ_y. Brittle failures are characterized by negligible ductility. Brittle failures of this type are common in older structures built before the advent of ductile details in the mid-1960s.

The relationship between force and displacement of a building can be determined either experimentally or analytically. Experimental evaluation is difficult, very expensive, and therefore rare. Pseudo-dynamic tests of small- to medium-scale building models have provided force-displacement relationships for buildings of various scales.

According to FEMA-356 (2000), the Equal Energy Method requires idealizing the actual pushover response using a bilinear force–displacement curve such that the strain energy—represented by the area under the curve—remains equivalent to that of the original nonlinear response up to a specified target displacement, typically taken as the maximum displacement demand. This energy equivalence ensures that the bilinear idealized system possesses the same energy absorption capacity as the real nonlinear system, thereby providing a physically meaningful representation of inelastic structural behavior.

Consequently, the Equal Energy Method serves as an effective framework for calibrating the yield point of intermediate moment-resisting concrete frames (IMRCFs), allowing the idealized response to realistically capture energy dissipation characteristics up to the anticipated displacement level. This coordination enhances the reliability of performance predictions, particularly for structural systems exhibiting limited ductility capacity, such as IMRCFs, as emphasized in FEMA-440 (2005).

CHAPTER 6 DESIGN AND PARAMETERS – ETAB

In this research, four reinforced concrete buildings with identical material properties and varying numbers of stories (1, 3, 6, and 9) are investigated. The buildings were initially designed and modeled using ETABS, which enables the development of detailed structural models and supports the implementation of multiple international design codes and standards. Figures 6.1 through 6.4 illustrate the structural configurations of the four buildings as modeled in ETABS. In accordance with ASCE 7-16, all four buildings were subjected to both seismic and gravity loading conditions. This code provides comprehensive procedures for determining design loads on buildings and other structures, accounting for seismic effects as well as gravity-related actions. All reinforced concrete structural elements were designed in accordance with the requirements and detailing provisions of ACI 318-19. Following the initial code-based design, additional modifications were introduced at a later stage of the research to investigate their influence on the structural response. These modifications included adjustments to the cross-sectional dimensions of beams and columns, variations in member sizes, and changes in both horizontal and transverse structural configurations. No specific reinforcement ratio was enforced during this stage; however, all reinforcement layouts remained within the limits prescribed by the design code. All modified configurations were implemented in ETABS and will be presented and discussed in subsequent sections. After completing the modeling and modification phase, the structural design outputs—including the cross-sectional properties of beams, columns, and slabs—were extracted from ETABS and transferred to SAP2000 for nonlinear structural analysis. In addition, selected structural models were further analyzed using Abaqus to perform advanced nonlinear finite element simulations and to provide independent validation of the SAP2000 results.

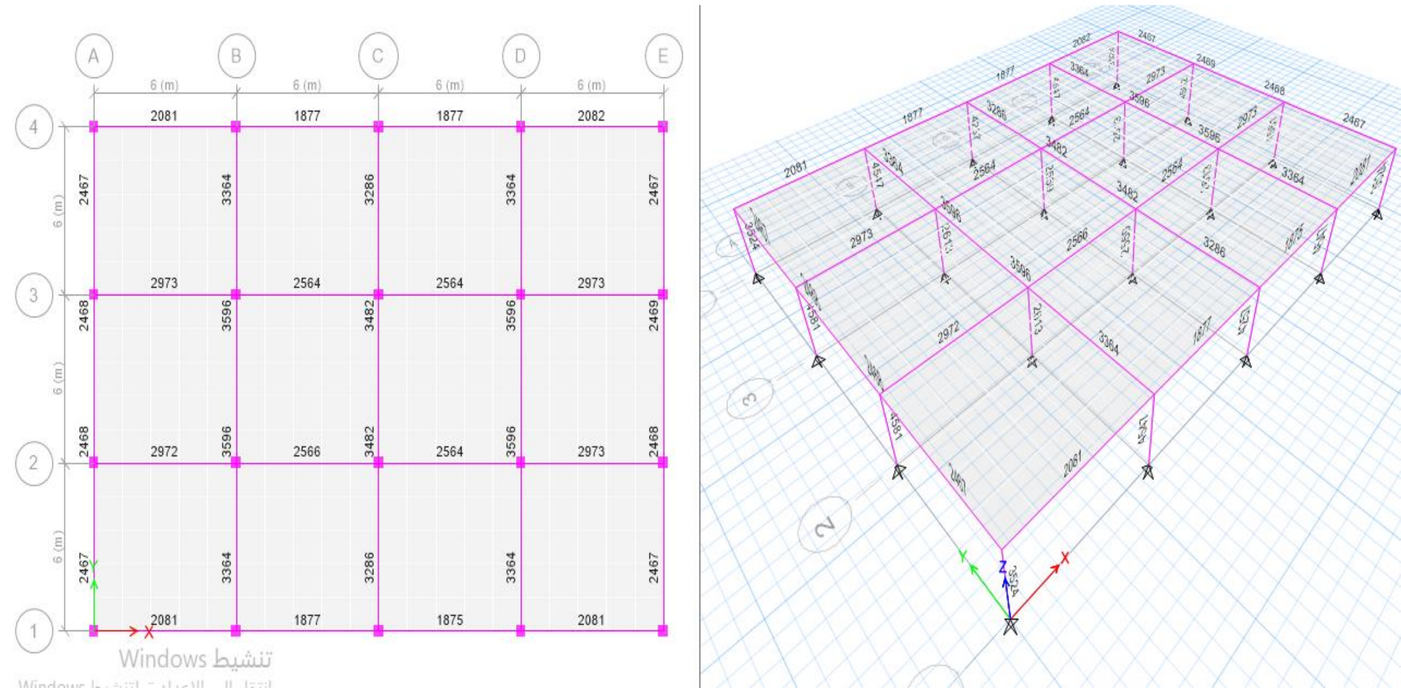

Figure 6.1: Output Design of the 1-Story Structural Building Showing the Required Reinforcement Area (mm).

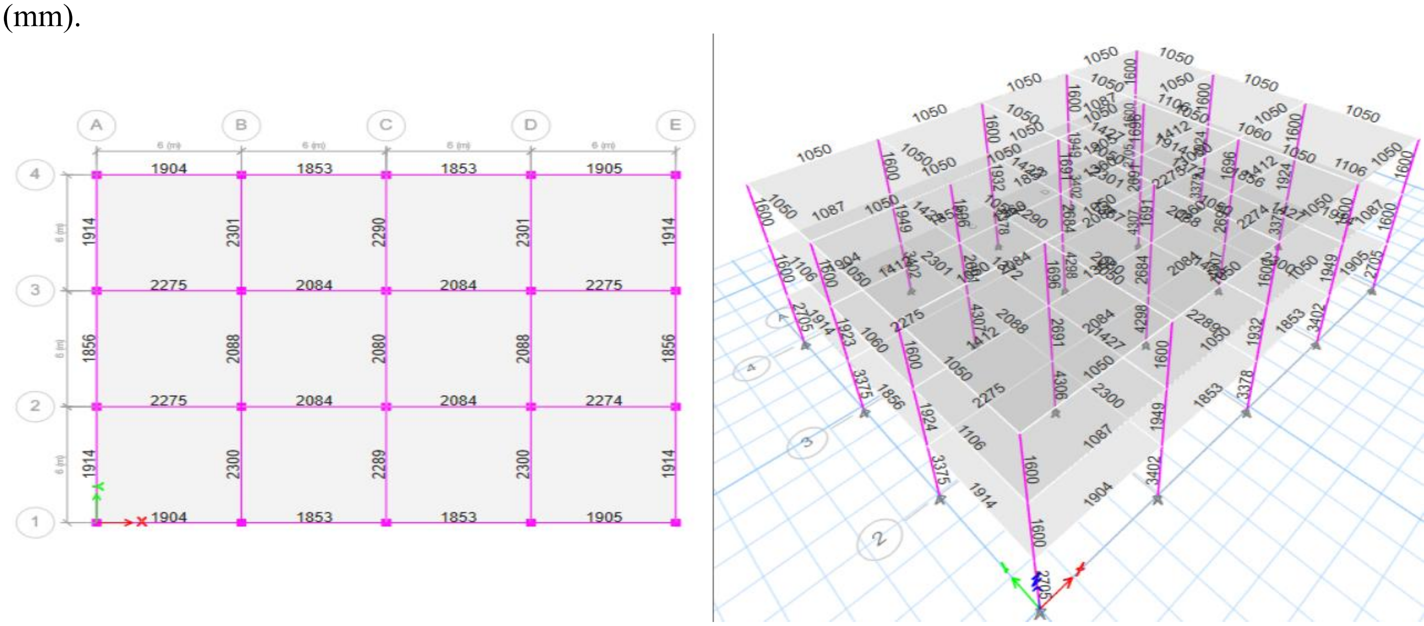

Figure 6.2 Output Design of the 3-Story Structural Building Showing the Required Reinforcement Area (mm).

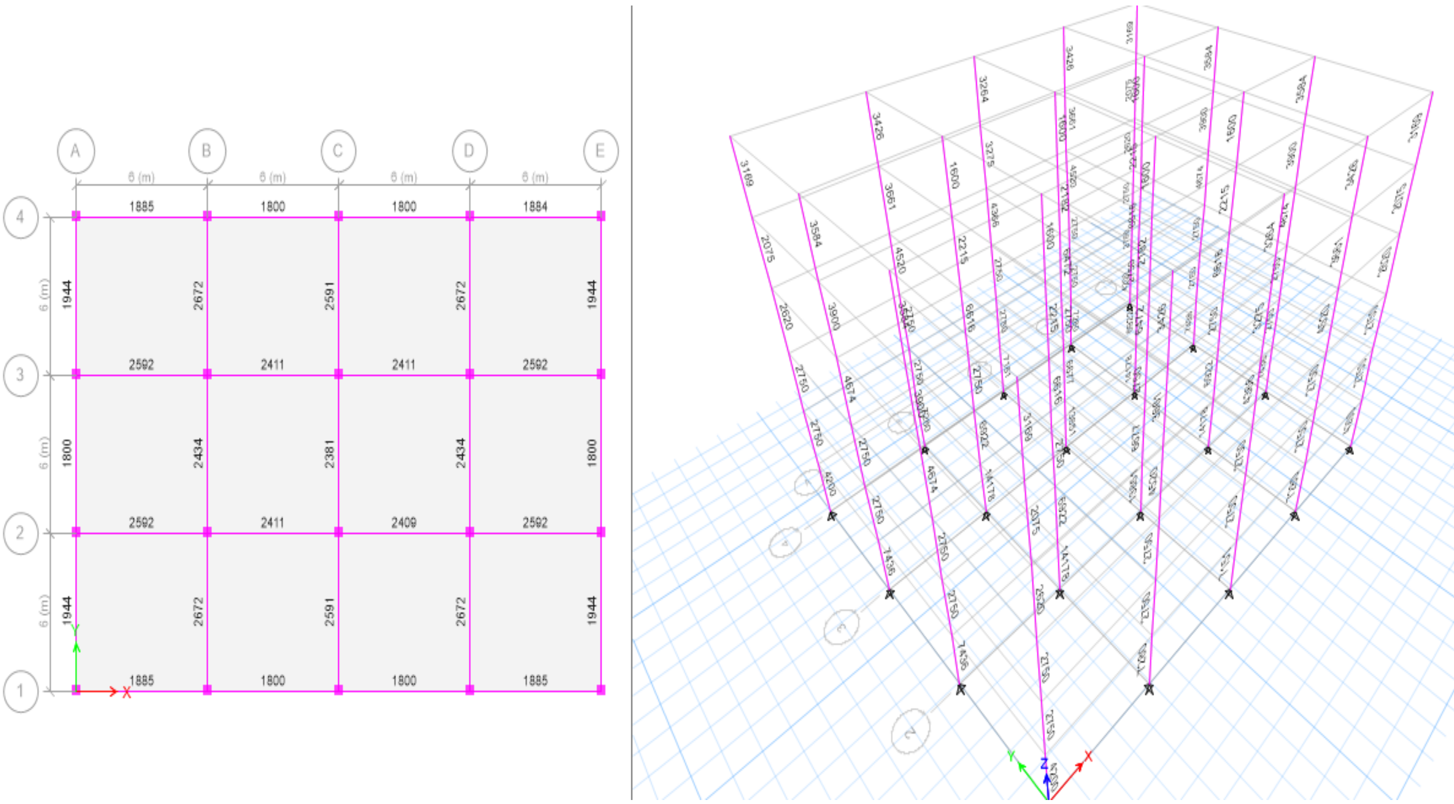

Figure 6.3 Output Design of the 6-Story Structural Building Showing the Required Reinforcement Area (mm).

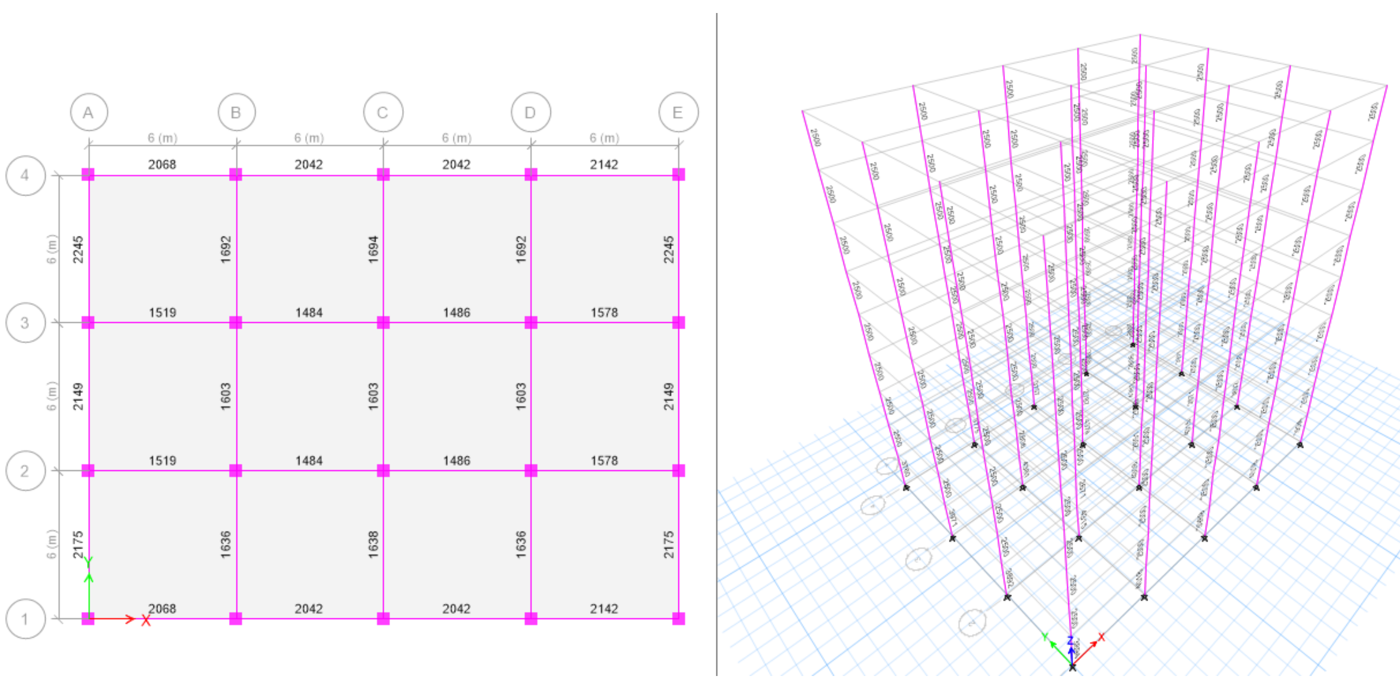

Figure 6.4 Output Design of the 9-Story Structural Building Showing the Required Reinforcement Area (mm).

Columns are among the most critical structural elements affected by seismic loading, as they play a fundamental role in maintaining both strength and overall stability of the structure. Accordingly, special attention is given during the design stage to ensure adequate ductility and flexibility, enabling columns to accommodate lateral displacements induced by earthquake actions.

This is achieved through the careful selection of cross-sectional dimensions, material properties, and reinforcement detailing , all of which contribute to enhancing the column's capacity to withstand dynamic seismic forces. Subsequently, detailed structural analysis is performed to evaluate column performance under seismic loading conditions and to verify compliance with design requirements related to strength, stability, and ductility.

The accuracy of this assessment is highly dependent on the material properties adopted in the numerical models. Table 6.1 summarizes the material parameters used in SAP2000 and ETABS. The use of reliable and representative material data ensures that the analytical results closely reflect actual structural behavior under various loading conditions.

Table 6.1 Materials properties used in design and analysis programs ETABS ,Abaqus and SAP 2000 .

concrete	Steel
Young's Modulus of Elasticity, E= 23500 MPa	Young's Modulus of Elasticity, E= 200000 MPa
Poisson's Ratio, v= 0.2	Fy=420Mpa
Ultimate Compressive Strength, f'c= 25 MPa	

CHAPTER 7 PARAMETRIC STUDY FOR RESPONSE MODIFICATION FACTOR

7.1 introduction

In this chapter, the response modification factor (R) is evaluated using the Equal Energy Method as presented in the Applied Technology Council Report ATC-19. This approach is based on the premise that the total energy absorbed by an inelastic structural system subjected to earthquake loading is approximately equal to the energy absorbed by an equivalent elastic system. To facilitate the evaluation process, the nonlinear force–displacement capacity curve is idealized using a bilinear representation, from which the yield point, ductility demand, and strength reduction characteristics are determined. The method provides an energy-consistent framework for relating structural ductility to the response modification factor and has been widely adopted in seismic performance assessment and code calibration studies.

The nonlinear static pushover curve represents the relationship between the applied base shear and the resulting structural displacement. This curve typically exhibits linear elastic behavior up to the yield point, followed by pronounced nonlinear behavior due to the development of inelastic deformations in structural components. Such nonlinear response is essential for accurately capturing the seismic performance of structural systems.

In structural engineering, ductility is defined as the capacity of a structure or material to undergo substantial deformation beyond the elastic limit without sudden failure. This property enables structures to dissipate seismic energy through controlled inelastic behavior, allowing them to sustain large displacements during extreme loading events while maintaining overall stability. Accordingly, ductile behavior is a primary objective in seismic design, as it provides warning prior to collapse and enhances occupant safety.

In contrast, brittle behavior is characterized by limited deformation capacity and abrupt failure once the ultimate strength is exceeded. Such systems exhibit minimal energy dissipation and are particularly vulnerable to collapse under seismic loading. This behavior is commonly associated with older structures lacking adequate confinement and ductile detailing, which limits their inelastic deformation capacity.

For all structural systems, the maximum displacement demand (Δ_{max}) exceeds the yield displacement (Δ_{Y}), indicating that structures are expected to undergo significant post-yield deformation prior to reaching their ultimate capacity. This design philosophy intentionally promotes ductile performance, ensuring that failure is preceded by substantial deformation rather than sudden collapse.

To facilitate seismic performance assessment, the nonlinear force–displacement relationship is commonly idealized using a bilinear representation consisting of elastic and post-yield segments. In the Equal Energy Method, the equivalent yield point is determined such that the area enclosed by the actual capacity curve is approximately equal to that of the idealized bilinear curve, thereby preserving the overall energy absorption capacity of the structure. This approach provides an energetically consistent representation of the structural response while simplifying the evaluation of ductility and response modification factors.

Once the yield point is established, the bilinear relationship is constructed by connecting the elastic and post-yield stiffness segments, providing a rational basis for evaluating seismic demand and determining the response modification factor (R).

Furthermore, this chapter presents and discusses the analytical results obtained from SAP2000 and ABAQUS for structural models with 1, 3, 6, and 9 stories. Particular emphasis is placed on identifying and comparing failure zones, displacement patterns, and overall structural response across different building heights, providing a comprehensive assessment of nonlinear behavior and seismic performance.

7.2 FRAME ANALYSIS - SAP2000

The structural design models were initially developed using ETABS and subsequently transferred to SAP2000 to enable rigorous nonlinear analysis beyond the limitations of linear elastic design procedures. Figures 7.1 through 7.4 illustrate the detailed numerical representations of the four structural models with different numbers of stories within the SAP2000 environment. For the single-story model, loading was directly applied at the beam, consistent with the adopted analytical framework, thereby eliminating the need for explicit graphical load representation.

To evaluate the inelastic seismic response, nonlinear static pushover analyses were performed for all structural models. Lateral loads were applied incrementally according to predefined load patterns to simulate seismic demand, while the structural response was continuously monitored in terms of base shear versus roof displacement. This procedure enabled the generation of capacity curves that capture the global strength, stiffness degradation, and ductility characteristics of each system. The resulting force–displacement data were subsequently extracted and processed using Microsoft Excel to facilitate accurate interpretation and further analytical evaluation.

Following the development of the capacity curves, the seismic response parameters were recalibrated using the Equal Energy Method in accordance with the Applied Technology Council (ATC-19) provisions. This approach ensures that the energy dissipated by the actual nonlinear system is consistently represented by an equivalent bilinear model. The bilinearization process, implemented within SAP2000, was critically assessed to verify compliance with the fundamental energy equivalence condition, whereby the areas above and below the idealized curve are equal ($A_1 = A_2$).

The results demonstrate a high level of consistency between the numerical outputs and the theoretical assumptions of the Equal Energy Method, confirming the validity of the adopted analytical framework. This agreement enhances the reliability of the derived seismic performance indicators and supports their application in evaluating the response modification factor (R) and overall structural efficiency under seismic loading.

Table 7.1 Calculation of Slab Loads and Corresponding Beam Line Loads Based on Tributary Width for the One-Story Building.

Item	**Unit Weight / Value**	**Thickness**	**Calculation**	**Load (kN/m²)**
Reinforced Concrete	25 kN/m³	0.25 m	25 × 0.25	6.25
Partitions	—	Assumed	—	1.25
Live Load (L.L)	—	Code-based	—	3
Total Load (Wu)	—	—	6.25 + 1.25 + 3	**10.5**

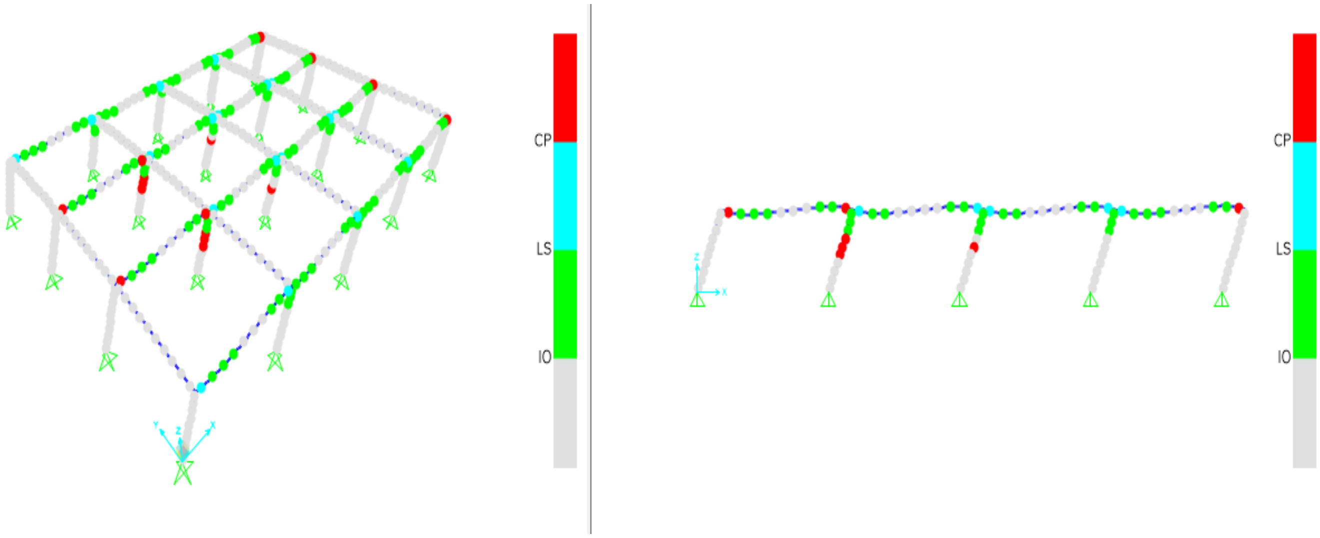

Figure 7.1 The Output Analysis of the One-Story Structure Building(Failure).

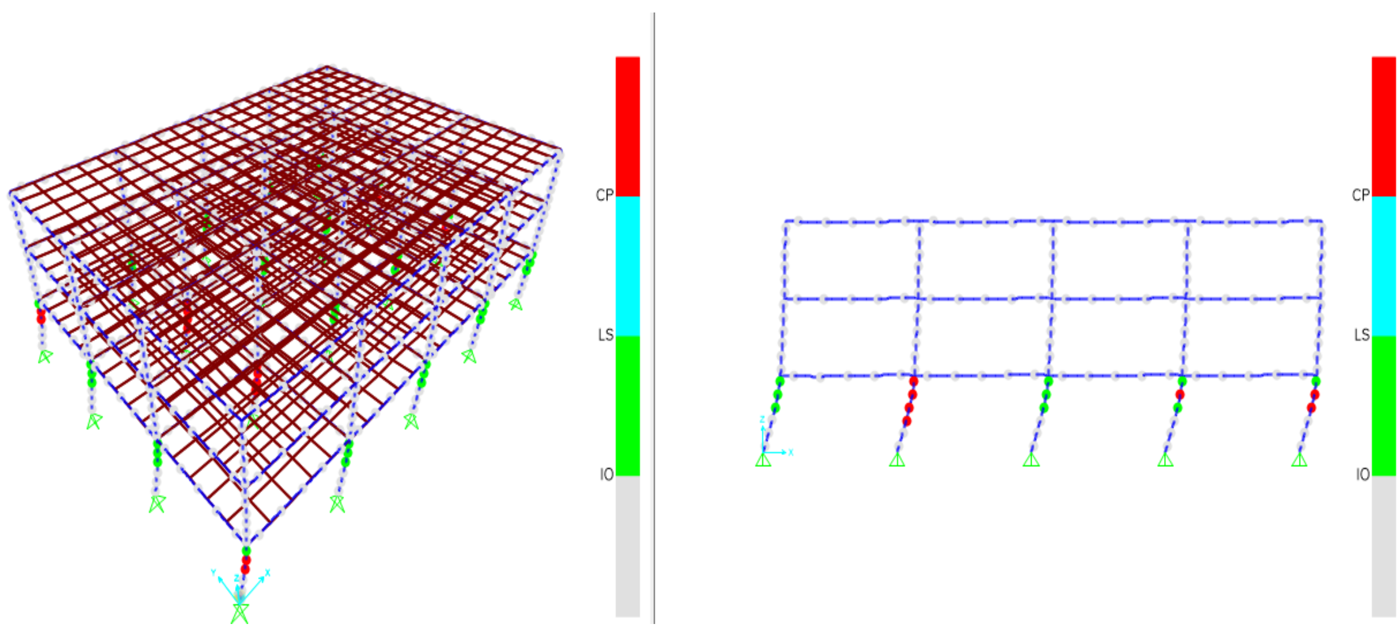

Figure 7.2 The Output Analysis of the Three-Story Structure Building(Failure).

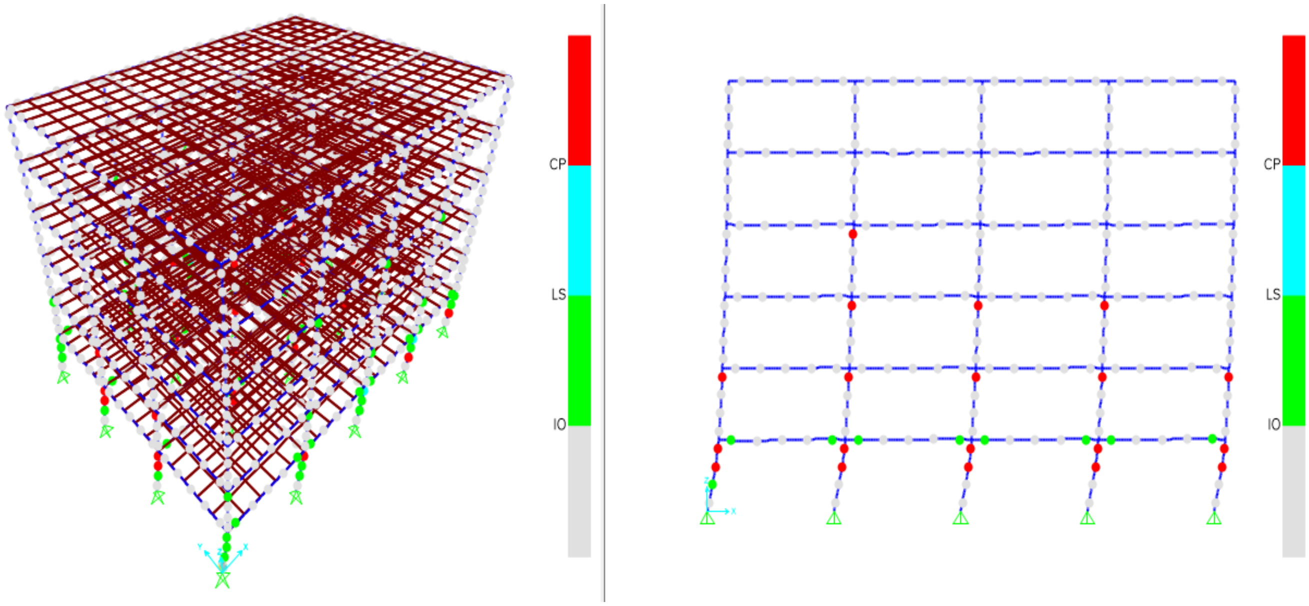

Figure 7.3 The Output Analysis of the Six-Story Structure Building(Failure).

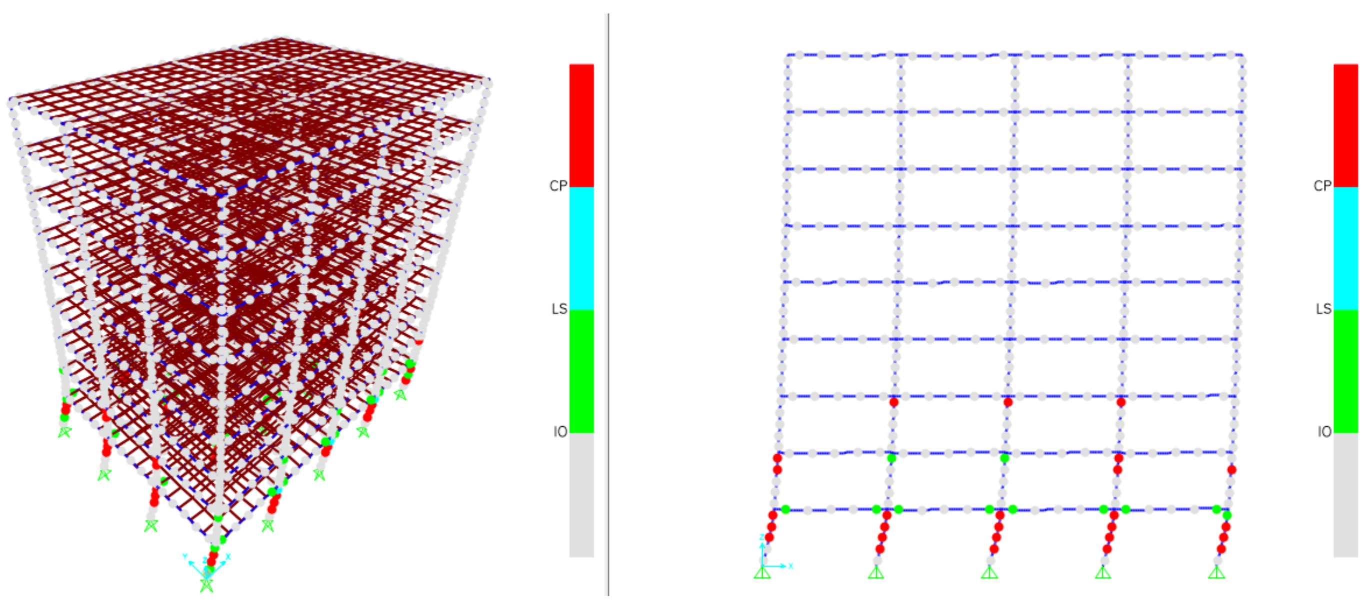

Figure 7.4 The Output Analysis of the Nine-Story Structure Building(Failure).

7.3 Moment Frame Building (IMRFS)

The seismic design parameters are defined in accordance with Table 3.9 of ASCE 7-16 for Intermediate Reinforced Concrete Moment-Resisting Frames. These parameters play a critical role in determining the seismic forces and overall structural response. The structural models are initially designed using ETABS to account for both seismic and gravity loads, generating outputs that include member dimensions, reinforcement details, and global structural response. Subsequently, the ETABS output is utilized to develop corresponding models in SAP2000 and ABAQUS, where nonlinear static pushover analyses are performed to obtain the base shear–displacement relationships. The resulting pushover curves represent the structural response under the adopted code parameters ($R = 5$, $\Omega = 3$, $Cd = 4.5$), as specified in Table 3.9 of ASCE 7-16. Based on the pushover curves, key seismic parameters—including the ductility reduction factor ($R\mu$) and the displacement ductility factor (μ)—are determined and subsequently used to evaluate the response modification factor (R), overstrength factor (Ω), and deflection amplification factor (Cd).As shown in Figure 7.5, the base shear at yielding (Vf) is identified as the yield point on the load–displacement curve. This point is selected to define the corresponding displacement (Δd). The Target displacement (Δt) is then calculated by multiplying Δd by the code-defined amplification factor Cd, in accordance with the Equal Energy Method as outlined in ATC-19:

$$\Delta t = \Delta d \times C d$$

The displacement Δt represents the endpoint of the curve and is used to establish energy equivalence between the elastic and inelastic regions. According to the Equal Energy Method, the yield base shear (Vf) is determined at the corner point of the idealized bilinear curve, located within the region above the pushover curve. This point corresponds to a specific force level on the vertical axis, from which the associated yield displacement (Δy) is obtained.

Similarly, the design displacement (Δd) is determined either by identifying the corresponding force (Vd) using code-based static equations or directly from the pushover curve. Based on these values, the seismic parameters μ, Ω, $R\mu$, R, and Ve are calculated in accordance with the formulations provided in ATC-19.

To ensure accuracy in evaluating the energy balance, the pushover curve is exported and redrawn using AutoCAD, allowing for precise calculation of the enclosed areas. The results indicate that the sum of areas A1 and A3 is approximately equal to area A2 ($A1 + A3 \approx A2$), confirming compliance with the energy equivalence condition. Accordingly, the yield base shear (Vy) is adopted directly from the SAP2000 results, as it provides a consistent and reliable representation of the structural yield point.

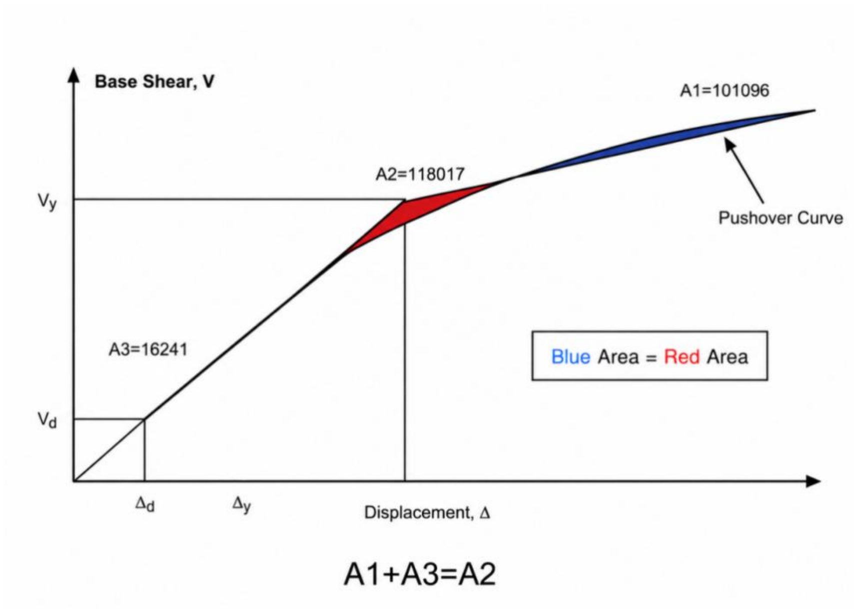

Figure 7.5 Evaluation of the Areas Above and Below the Pushover Curve Using AutoCAD

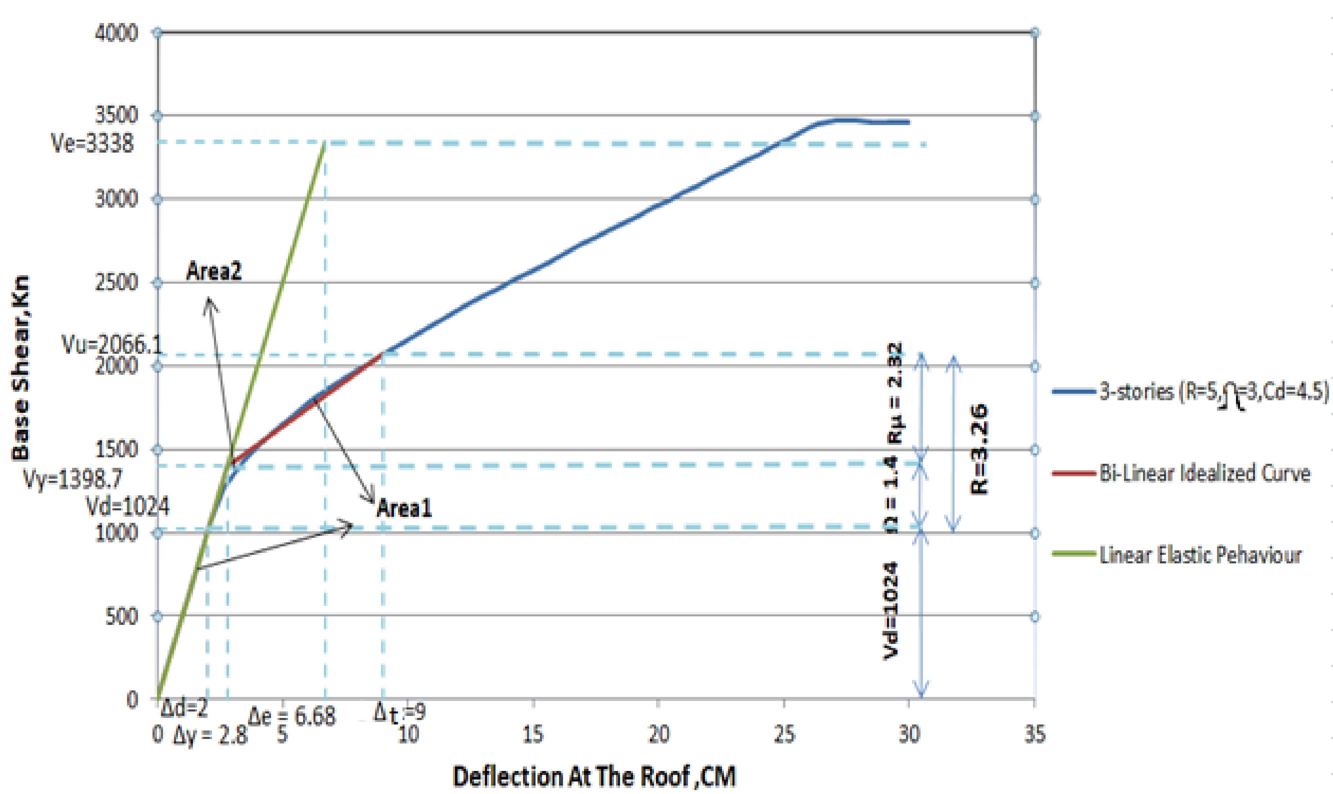

Figure 7.6 (R Factor) Calculations by Drawing Output (Vd = 1024 KN From Drawing).

$\Delta_t=\Delta_d*C_d=0.02*4.5=0.09m$

From Figure 7.6 , Vy=1398.7 Kn   Δy=2.8 cm from Sap2000

$\Omega=V_y/V_d=1398.7/1024=1.4\approx2$

$\mu=\Delta_t/\Delta_y=0.09/0.028=3.2$

$R_\mu=\sqrt{(2*\mu -1)}=\sqrt{(2*3.2-1)}=2.32$

$\mathbf{R=R_\mu*\Omega=1.4*2.32=3.26}$

$V_e= V_y *R=1024*3.26=3338KN$

R = 5, Ω = 3, Cd = 4.5 (IMRFS)

For Six Stories

Vmax=6592.02kn ,, Vy=3094.72kn,, Δy=15.3cm,Vd=2060Kn

$\Delta_t=\Delta_d*C_d=0.107*4.5=0.48m$

Ω=vy/vd=1.53

μ =Δt/Δy=3.1   , Rμ= Rμ=√(2*μ -1) =2.28

$\mathbf{R=R_\mu*\Omega=2.28*1.53=3.5}$

R = 5, Ω = 3, Cd = 4.5 (IMRFS)

For Nine Stories

Vmax=7267.4kn ,, Vy=3482.3kn,, Δy=22.1cm,Vd=2350Kn

$\Delta_t=\Delta_d*C_d=0.15*4.5=0.675m$

Ω=vy/vd=1.53

μ =Δt/Δy=3.1 , Rμ= Rμ=√(2*μ -1) =2.5

$R=R_\mu*\Omega=2.5*1.5=3.8$

R = 5, Ω = 3, Cd = 4.5 (IMRFS)

The response modification factor obtained from pushover analysis using the Equal Energy Method, in accordance with ATC-19 (1995), was found to be R=3.26, which is lower than the code-specified value of R=5 for Intermediate Moment-Resisting Frames (IMRFs) as provided in Table 3.9 of ASCE 7-16 (2016).

To further investigate this difference, the original structural model was re-analyzed using ETABS with modified lateral shear forces corresponding to the calculated yield base shear (Vy =1398.7kN), as illustrated in Figure 7.6. This step was conducted as part of a parametric sensitivity study to evaluate the influence of recalculated seismic parameters on the structural response. It is important to note that the original design configuration was preserved, and the modifications were introduced solely for analytical comparison rather than as a code-based redesign.

Subsequently, the updated structural properties were transferred to SAP2000, where nonlinear static pushover analysis was performed under incrementally applied lateral loads. This procedure enabled the development of capacity curves representing the nonlinear force–displacement behavior of the structure, from which key response parameters such as lateral displacement, story drift, and overall structural performance were obtained.

The resulting force–displacement data were exported to Microsoft Excel for further post-processing. Based on this data, seismic coefficients were recalculated using the Equal Energy Method to verify the values initially assumed during the design stage. The objective of this recalculation was to assess the realism and reliability of the adopted seismic parameters rather than to propose alternative design values.

Initially, the response modification factor was defined according to code provisions ($R=5$), and structural analysis was conducted to determine the corresponding internal forces and displacements. From the pushover curves, fundamental response parameters such as yield strength (V_y) and yield displacement (Δ_y) were determined. These values were subsequently used to evaluate additional seismic performance indicators, including Target displacement (Δ_t), displacement ductility (μ), and the ductility reduction factor (R_μ). The consistency of these parameters across different models confirms the adequacy of the adopted design approach in representing seismic behavior.

Similarly, Figure 7.7 presents an alternative analytical scenario in which the original model was re-evaluated using recalculated shear force parameters ($V_y=903.27$ kN, $V_d=513.7$kN, $\Delta_y=4.2$cm). The corresponding structural properties were again transferred to SAP2000 for nonlinear pushover analysis under incremental lateral loading. The resulting response was used to compute the response modification factor and validate the consistency of the analytical outcomes..

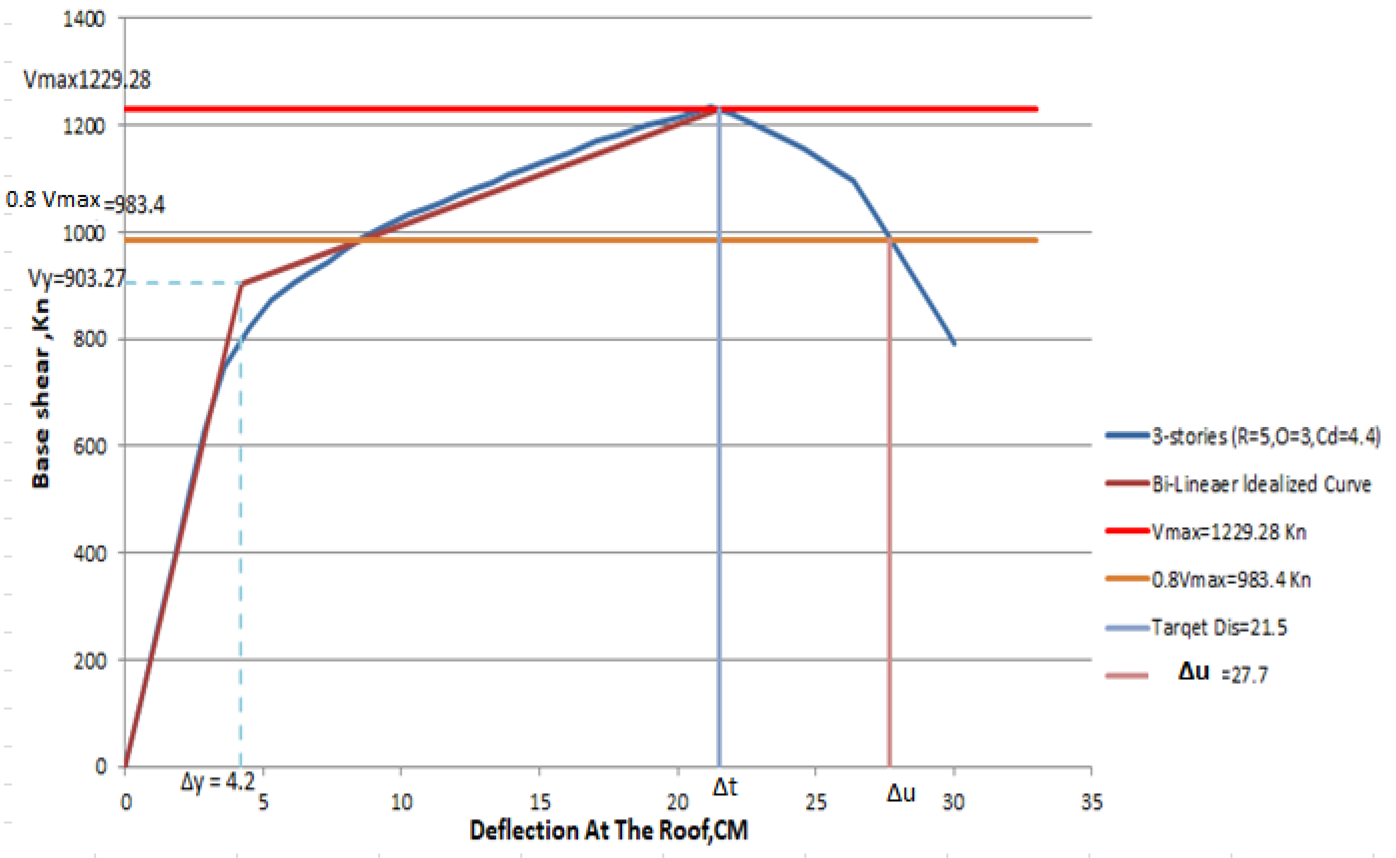

Figure 7.7 (R Factor) Calculations by Drawing Output (Vd = 513.7 KN From Drawing).

7.3.1 Calculate the R coefficient using the target displacement (Δt = 21.5).

From Figure 8.3, Vy = 903.27 KN

Ω = Vy / Vd = 903.27 / 513.7 = 1.8

μ = Δt / Δy = 0.215 / 0.042 =5

Rμ = √ (2*μ -1) = √ (2*9 -1) ≈ 3

R = Rμ * Ω = 3 * 1.8 = 5.5

Ve = Vfy * R = 531.7 * 5.5 = 2924.35 KN **R = 5, Ω = 3, Cd = 4.5 (IMRFS).**

7.3.2 Calculate the R coefficient using the maximum displacement (Δu= 27.7).

From Figure 8.3, Vy = 903.27 KN

Ω = Vy / Vd = 903.27 / 513.7 = 1.8

$\mu = \Delta max / \Delta y = 0.277 / 0.042 = 6.6$

$R\mu = \sqrt{(2*\mu - 1)} = \sqrt{(2*6.6 - 1)} \approx 4$

$R = R\mu * \Omega = 4 * 1.8 = 7.2$

Ve = Vfy * R = 531.7 * 7.2 = 3828.24 KN **R = 5, Ω = 3, Cd = 4.5 (IMRFS).**

7.3.3 Comparison between Δu and Δt .

The comparison of the response modification factor (R), as evaluated using target displacement and maximum displacement criteria, reveals notable discrepancies, highlighting the sensitivity of R to the selected displacement parameter. When the target displacement approach is adopted, the resulting value R=5.5 reflects a relatively conservative estimate, as the structural response is constrained within a predefined performance limit. This approach is consistent with performance-based seismic design principles, where structural behavior is evaluated at specific limit states—namely Immediate Occupancy (IO), Life Safety (LS), and Collapse Prevention (CP). Accordingly, the resulting R-value represents a balanced compromise between safety requirements and design efficiency.

In contrast, when the maximum displacement is considered as the governing parameter, the response modification factor increases significantly to R=7.2. This increase is attributed to the fact that maximum displacement corresponds to the peak inelastic response of the structure, which inherently exceeds the target displacement. As a result, higher ductility and greater energy dissipation capacity are reflected, leading to an overestimation of the R-value. However, despite indicating enhanced structural capacity, this approach does not necessarily satisfy performance objectives, since maximum displacement levels are often associated with severe damage and are not typically acceptable within design limits.

Based on Figure 7.7 and the calculations presented in Section 7.3 (1,2), the maximum seismic base shear was determined as Vmax =1229.3kN. Taking 80% of this value yields approximately 983.4kN, which intersects the pushover curve at a maximum displacement of $\Delta u \approx 27.7$cm. This corresponds to approximately 1.29 times the target displacement (e). These results are in strong agreement with established benchmarks reported in ASCE 41-17 (2017), and Eurocode 8 (2005), thereby confirming the validity and reliability of the adopted analytical methodology..

7.4 Moment Frame Building Results (Sap2000)

This section presents the structural response of multi-story buildings based on the from the three-story reference model developed and detailed in Chapter 3. All analyzed structures are reinforced concrete Intermediate Moment-Resisting Frames (IMRFs) designed in accordance with seismic code provisions. While the buildings share identical architectural layouts, material properties, and structural systems, they differ in column and beam cross-sectional dimensions as well as longitudinal reinforcement ratios. These variations were intentionally introduced to calibrate the response modification factor (R) and align it as closely as possible with the values specified by the governing code. Detailed design assumptions, reinforcement ratios, and structural detailing for all models are provided in Chapter 6 (pp. 60-61).

The load–displacement capacity curves presented in this section illustrate the global response of the frame systems corresponding to a constant code-based R-value, as defined in Table 3.9. These curves represent the combined analytical response of multiple structural configurations with varying building height, member dimensions, and reinforcement ratios. The maximum base shear demand is clearly identified to enable direct comparison of structural performance. In accordance with ASCE 7-16 (2016), a two-way rigid slab with a thickness of 250 mm was adopted, along with a seismic redundancy factor of ρ = 1 and an importance factor of I=1.25 for all models.

Following the establishment of the three-story reference model, the analytical framework was extended to include six- and nine-story buildings. The increase in structural height necessitated systematic adjustments to column dimensions and reinforcement ratios in order to maintain adequate lateral stiffness, strength capacity, and control of inelastic deformation under seismic loading.

Subsequently, a single-story IMRF with identical structural characteristics was developed. In this case, Acceleration were directly applied to the beams in accordance with the adopted loading scheme. The model was analyzed using ABAQUS to enable direct comparison with results obtained from SAP2000. Furthermore, the frame presented in Figure 4.6 was modeled in both software environments to facilitate cross-validation of numerical results and ensure consistency in predicting the nonlinear seismic response of IMRF systems..

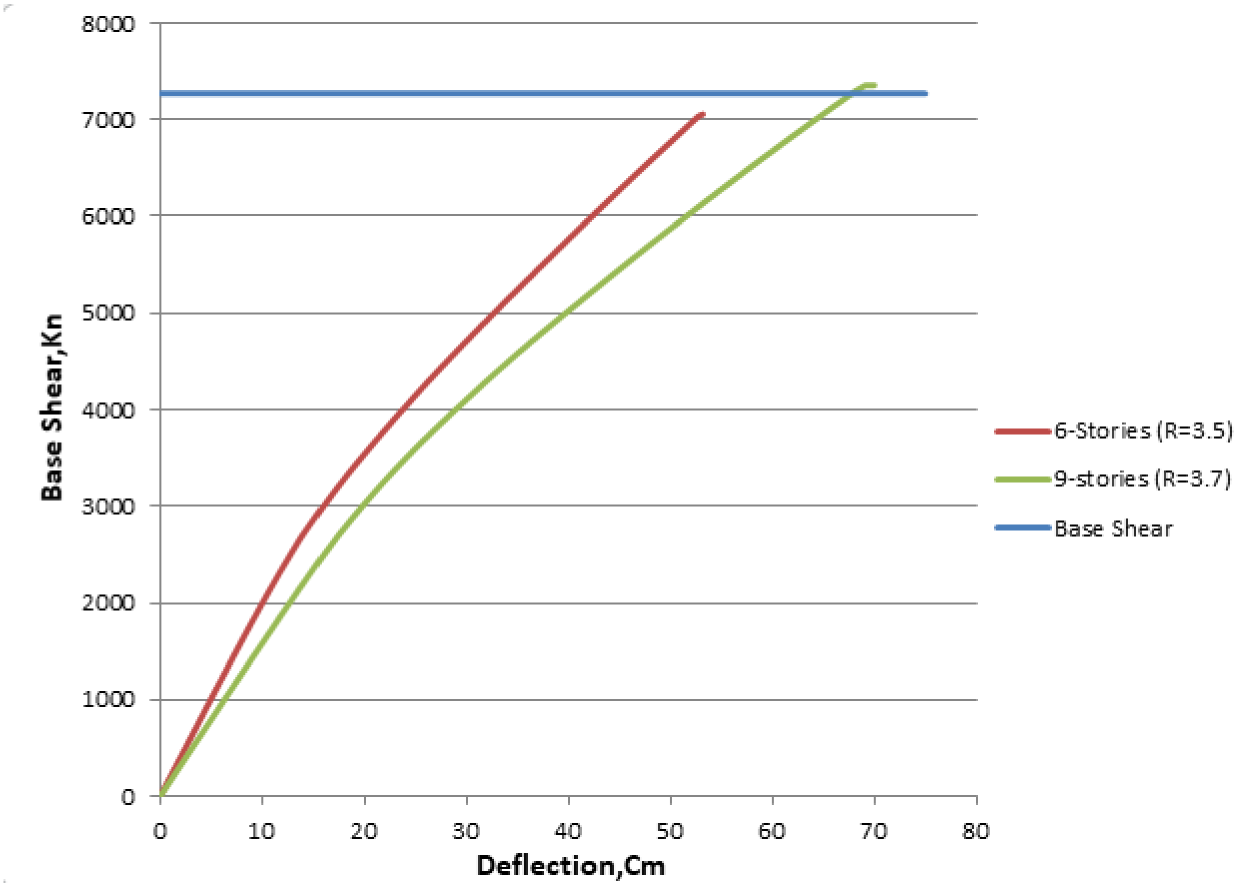

Figure 7.8 Pushover Capacity Curves of Six- and Nine-Story IMRF Buildings .

Table 7.2 Summary of Seismic Performance Results for Six- and Nine-Story IMRF Frames.

No.of Stories		Column Size	Main Reinforcement For Column	Beam Size	Main Reinforcement For Beam	Value Of Base Shear Max , Kn	Response Modification Factor (R)
6-Story	1-3 Floor	50X50	(12 Ø16)	Edge:45X40	(10 Ø16)	6492.02	3.5
	4-6 Floor	40X40	(8 Ø16)	Mid:30X40	(6 Ø12)		
9-Story	1-5 Floor	50X50	(12 Ø16)	Edge:50X40	(12 Ø16)	7267.4	3.7
	6-9 Floor	40X40	(8 Ø16)	Mid:35X40	(8 Ø12)		

Figure 7.8 illustrates the pushover capacity curves of reinforced concrete Intermediate Moment-Resisting Frame (IMRF) systems with varying connection cross-sectional configurations for Six- and Nine-story buildings. The corresponding reinforcement ratios for each model are presented in Figures 6.3 and 6.4, while Table 7.2 summarizes the cross-sectional dimensions and key structural properties, providing a consistent basis for direct comparison between the two structural configurations.

The results indicate that the response modification factor (R) is significantly influenced by the adopted cross-sectional dimensions and reinforcement ratios, highlighting the sensitivity of seismic performance to member sizing and detailing. In addition, the nine-story structure exhibits a higher base shear capacity (7267.4 kN) compared to the six-story structure (6492.02 kN), reflecting the increased strength and stiffness demands associated with greater building height.

Furthermore, the implementation of column grouping along the building height—achieved through systematic variation of column cross-sections—resulted in R-values that fall within acceptable ranges for intermediate sections. This approach provides a more realistic representation of structural behavior and enhances the accuracy of numerical predictions related to the inelastic seismic response of IMRF systems.

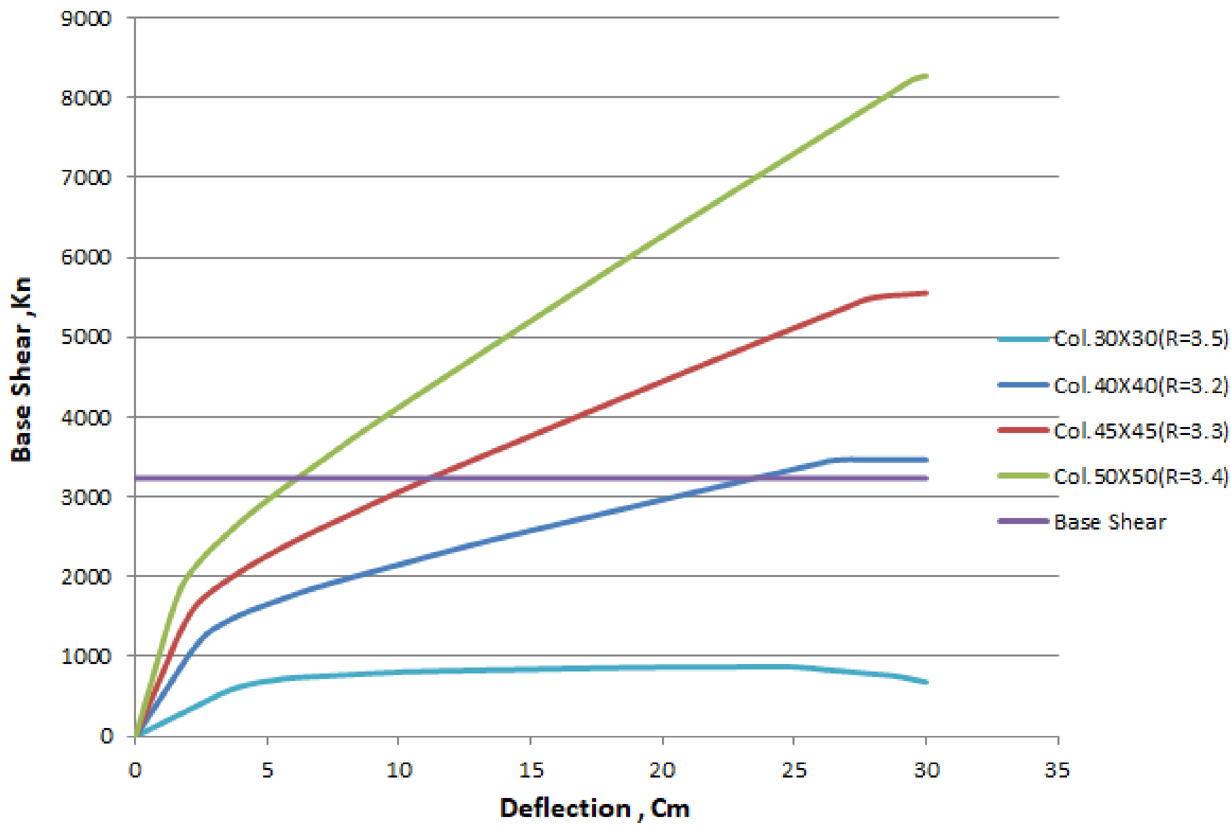

Figure 7.9 Pushover Capacity Curves of Three-Story IMRF Buildings with Varying Column Cross-Sections.

As shown in Figure 7.9, the pushover capacity curves continue to increase beyond the yielding point, reaching base shear levels of approximately 8000 kN due to post-yield stiffness and strain-hardening effects. However, for Intermediate Moment Resisting Frame (IMRF) systems, the effective base shear governing the seismic response is defined at the yielding performance level, rather than at the ultimate or peak strength. Accordingly, a constant horizontal base shear line corresponding to the yielding base shear ($V_y \approx 3229.7$ kN) is adopted in the figure to represent the governing force level used for the evaluation of the response modification factor (R).

It is important to note that, in this parametric study, only the column cross-sectional dimensions were varied, while the number of longitudinal reinforcement bars and the steel grade were kept

constant across all 3-Story models. This modeling strategy isolates the effect of column sizing on the global seismic response. The close intersection of the pushover curves with the yielding base shear level indicates that variations in column dimensions alone have a limited influence on the effective yielding strength of the three-story IMRF system. Although larger column sections lead to increased post-yield strength and overstrength capacity, the global yielding mechanism remains essentially unchanged. This behavior explains the minor variation observed in the calculated R-values, as reported in Table 7.3, and confirms that, for low-rise IMRF buildings, changes in column geometry primarily affect post-yield behavior rather than the yielding response that governs seismic design.

Table 7.3 Actual R-Values for Three-Story IMRF with Different Column Cross-Sectional Areas.

Number Of Stories	Column Section(cm)	Base Shear(Kn)	Δmax(mm)	Δy(mm)	R
3-Story	30X30	841.4	15.6	4.5	3.52
	40X40	2066.1	9	4.2	3.26
	45X45	2655.7	7.4	2.1	3.32
	50X50	3229.7	6.1	1.8	3.44

The influence of transverse reinforcement spacing (stirrups) on the seismic performance and response modification factor (R) of the reinforced concrete Intermediate Moment Resisting Frame (IMRF) system is evaluated for the three-story building model, while maintaining constant member cross-sectional dimensions for Columns(40X40). In this stage of the analysis, the stirrup spacing was varied to 5 cm, 10 cm, and 15 cm, allowing for a direct assessment of confinement effects on the global nonlinear response of the structure.Figure 7.10 presents the pushover capacity curves corresponding to the different stirrup spacings for the three-story IMRF building. The results indicate that reducing the spacing between stirrups significantly enhances structural ductility and energy dissipation capacity, which is reflected in higher estimated R-values. Improved concrete confinement and a more stable post-yield response are observed as the stirrup spacing decreases, leading to a progressive increase in the response modification factor. The smallest spacing of 5 cm yielded the highest R-value, reaching approximately R = 4, demonstrating a substantial improvement in the inelastic seismic behavior of the three-story IMRF system.

In addition, Table 7.4 summarizes the associated base shear capacities, yield parameters, and displacement demands for each stirrup configuration. The tabulated results are consistent with the trends observed in the pushover curves, confirming that tighter transverse reinforcement spacing results in increased base shear resistance, delayed yielding, and enhanced displacement capacity. These findings highlight the critical role of transverse reinforcement detailing in governing the seismic response and reliability of R-value estimation for three-story IMRF buildings.

The three-story reinforced concrete Intermediate Moment Resisting Frame (IMRF) building was adopted as the reference model to evaluate the influence of key design parameters on seismic performance and response modification factor (R). The analytical investigations conducted on this model provide a comprehensive assessment of how member geometry and reinforcement detailing govern the nonlinear seismic response of low-rise IMRF buildings.

The initial analyses demonstrated that variations in column cross-sectional dimensions, while maintaining consistent material properties and structural configuration, directly affect lateral stiffness and base shear capacity. However, for the three-story building, increasing column cross-sectional dimensions did not result in a noticeable change in the response modification factor (R). Despite the increase in strength and stiffness, the global inelastic behavior and ductility characteristics of the low-rise system remained largely unchanged, leading to relatively stable R-values across the investigated column sections. This response is attributed to the limited height and the dominance of overall frame behavior in low-rise structures.

Further refinement of the three-story model involved the implementation of column grouping along the building height, where column sections were systematically varied to better reflect realistic design practice. This modeling approach produced R-values within acceptable ranges for IMRF systems and provided a more accurate representation of actual structural behavior, improving the reliability of nonlinear response predictions.

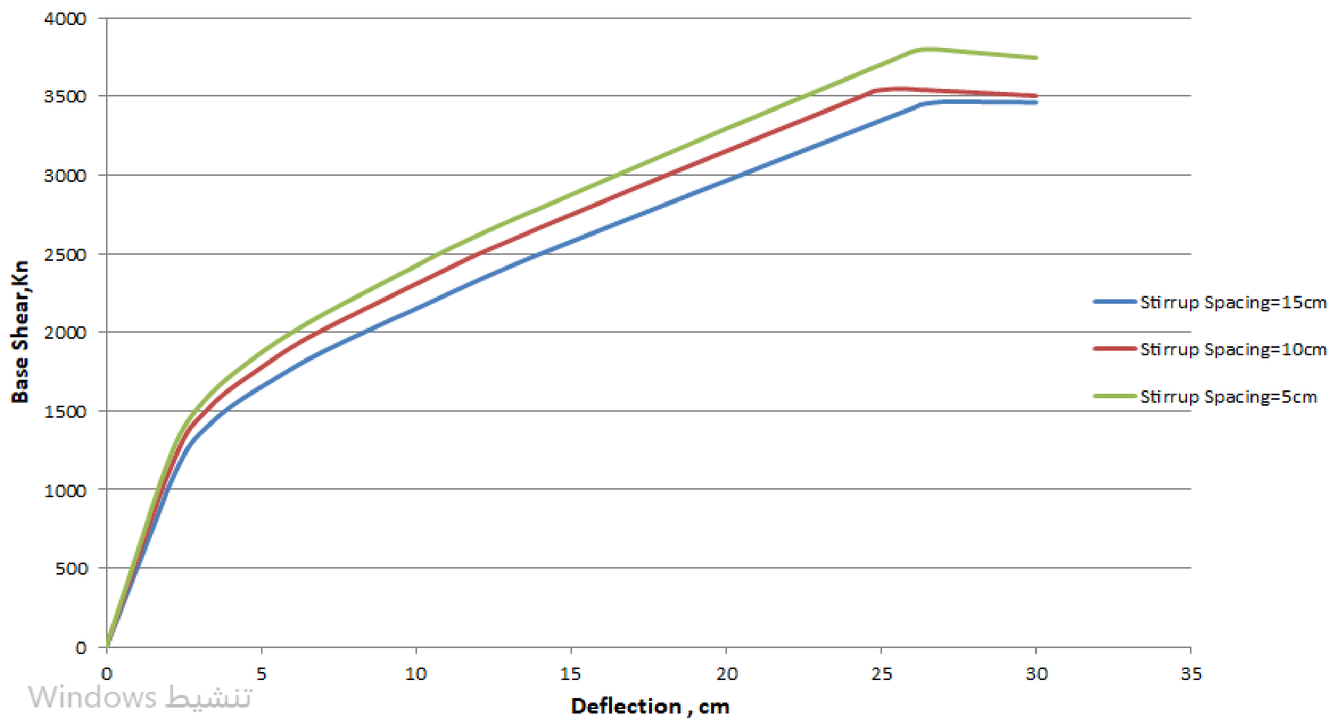

.

Figure 7.10 Pushover Capacity Curves of the Three-Story IMRF Building with Varying Stirrup Spacing.

Table 7.4 Actual R-Values for Three-Story IMRF with Varying Stirrup Spacing.

Number Of Stories	Stirrup Spacing(cm)	Base Shear(Kn)	Δmax(mm)	Δy(mm)	R
3-Story	15	2066.1	9	4.2	3.5
	10	2280.9	9.7	3.1	3.7
	5	2436.8	11.1	2.6	4

In addition, the influence of transverse reinforcement (stirrup) spacing was evaluated while keeping member cross-sections constant. Stirrup spacings of 15 cm, 10 cm, and 5 cm were examined to isolate confinement effects. The pushover capacity curves revealed that reducing stirrup spacing significantly enhances ductility, energy dissipation capacity, and post-yield stability. A clear increase in the response modification factor was observed with decreasing stirrup spacing, with the smallest spacing of 5 cm yielding an R-value approaching 4, indicating a substantial improvement in inelastic seismic performance.

The corresponding results for base shear capacity and displacement demand consistently supported the observed trends. **Notably, the displacement (Δy) was found to decrease as stirrup spacing decreased, reflecting an increase in structural stiffness and improved confinement efficiency**. This confirms that tighter transverse reinforcement not only delays yielding but also enhances deformation control and overall structural stability.

These findings underscore the critical role of confinement detailing in governing seismic response and R-value estimation for low-rise IMRF buildings. Overall, the results indicate that reinforcement detailing—particularly transverse reinforcement spacing—has a more pronounced influence on the response modification factor.

As will be shown in the subsequent sections, column sizing exerts a significantly greater influence on the seismic response and R-value estimation of the nine-story building, where increased height amplifies lateral demands and alters inelastic deformation mechanisms.

Following the evaluation of column cross-sectional variations, the study was extended to investigate the influence of beam geometry on the seismic performance of a six-story IMRF system, while maintaining constant column properties to isolate the effect on the response modification factor (R).

Two parametric scenarios were considered: increasing beam depth in successive 5 cm increments with constant width, and increasing beam width in similar increments while keeping depth unchanged. The pushover capacity curves demonstrate a clear and consistent improvement in structural performance with increasing beam depth, reflected in higher lateral stiffness and base shear capacity. This behavior is primarily attributed to the significant increase in flexural rigidity (EI), as the moment of inertia varies with the cube of the beam depth.

Additionally, models with greater beam depth exhibited enhanced post-yield behavior, including higher displacement capacity and improved energy dissipation, leading to a noticeable increase in R-values, reaching approximately 4.1.

In contrast, increasing beam width produced only marginal changes in the pushover response, with R-values remaining nearly unchanged. This limited effect is due to the linear contribution of width to the moment of inertia, which is significantly less influential than depth.

Overall, the results confirm that beam depth is the governing parameter in controlling the seismic response of IMRF systems, effectively enhancing stiffness, strength, and ductility while preserving the strong-column–weak-beam mechanism.

The following figure 7.11 to 7.15 present the design output results for all structural sections under two modification scenarios. The first scenario examines the effect of varying the section width, while the second scenario investigates the effect of varying the section depth. The corresponding design outputs obtained from ETABS are presented for comparison and evaluation.

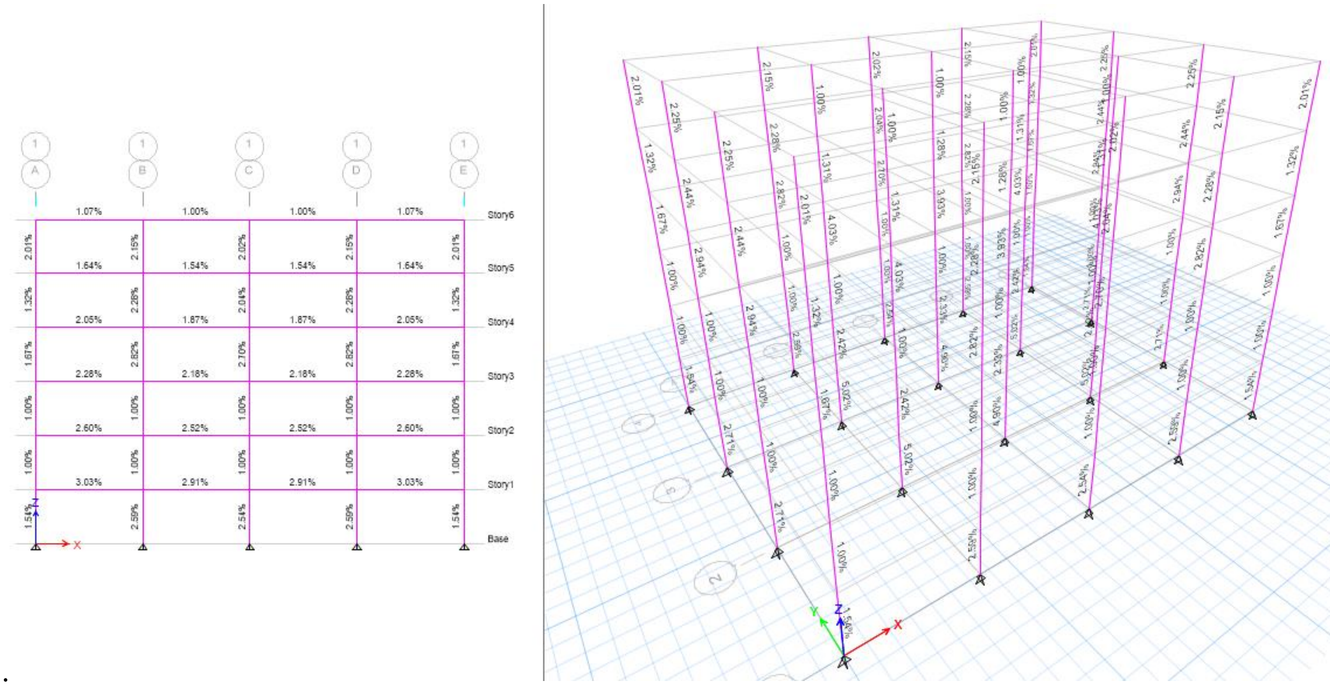

Figure 7.11 Output Design of the 6-Story Structural Building Showing the Required Reinforcement Area (mm) with Beam A (40cmX45cm),Beam B (30cmX40cm).

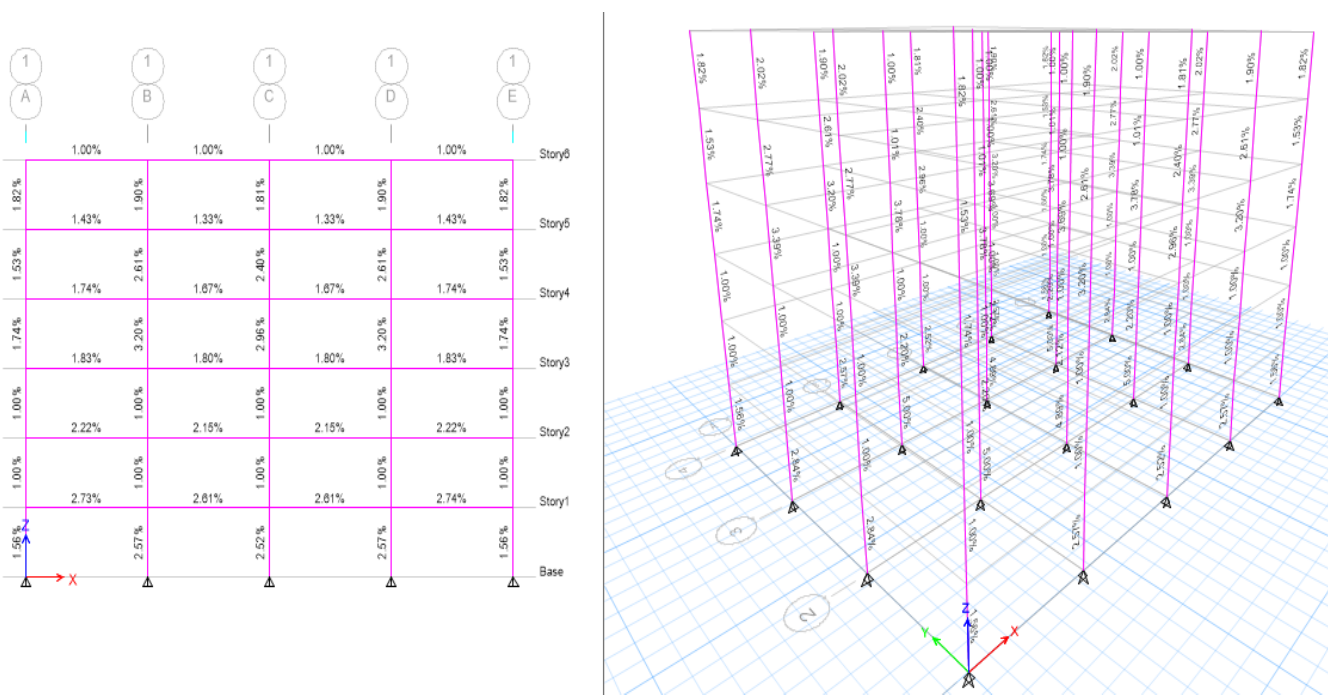

Figure 7.12 Output Design of the 6-Story Structural Building Showing the Required Reinforcement Area (mm) with Beam A (45cmX45cm),Beam B (35cmX40cm).

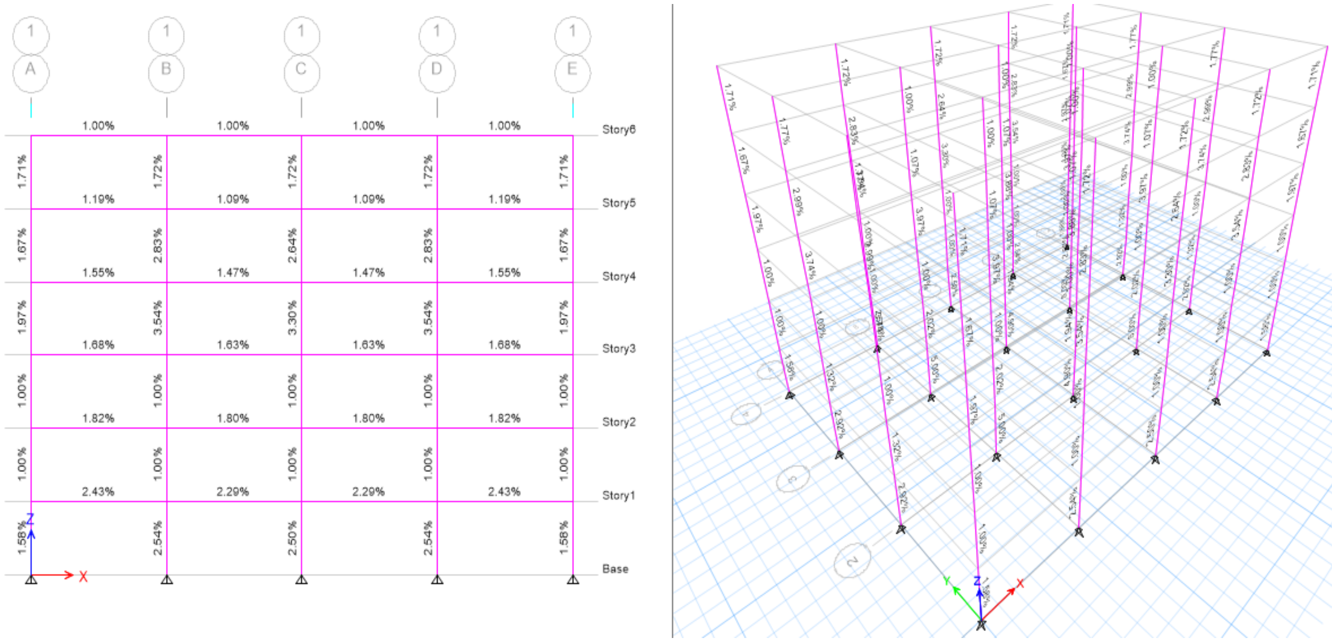

Figure 7.13 Output Design of the 6-Story Structural Building Showing the Required Reinforcement Area (mm) with Beam A (50cmX45cm),Beam B (40cmX40cm).

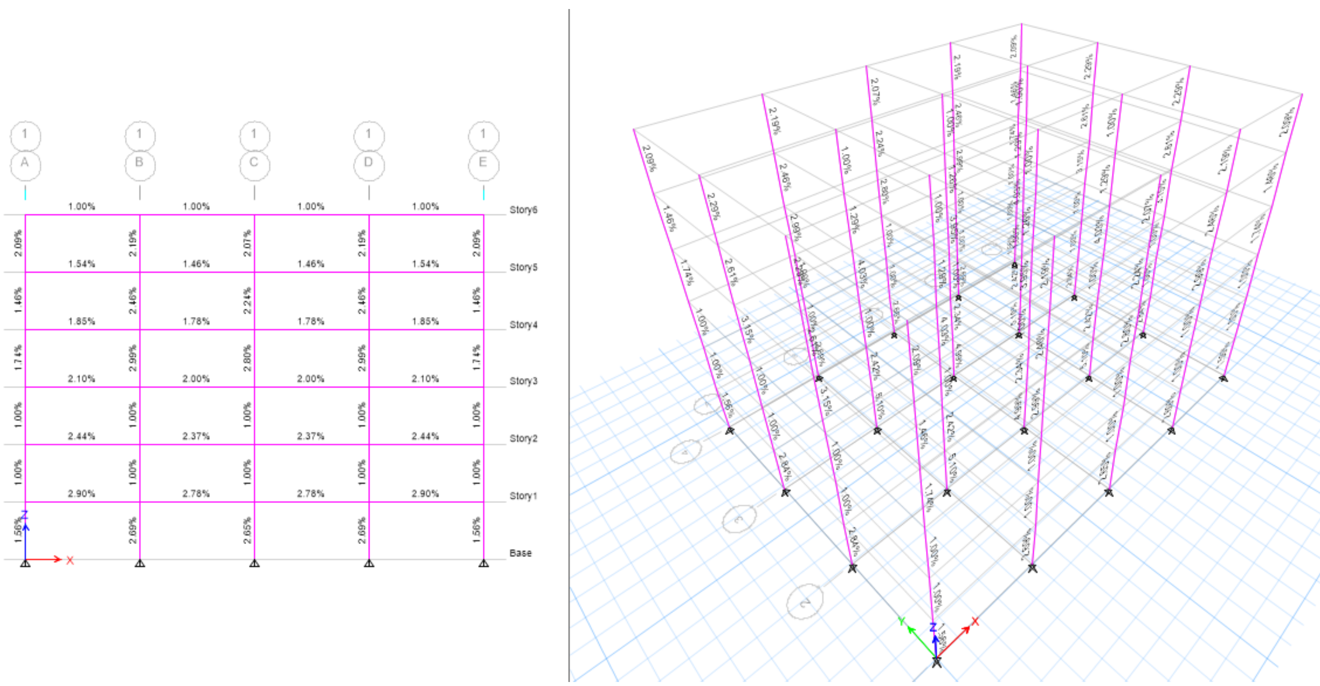

Figure 7.14 Output Design of the 6-Story Structural Building Showing the Required Reinforcement Area (mm) with Beam A (40cmX50cm),Beam B (30cmX45cm).

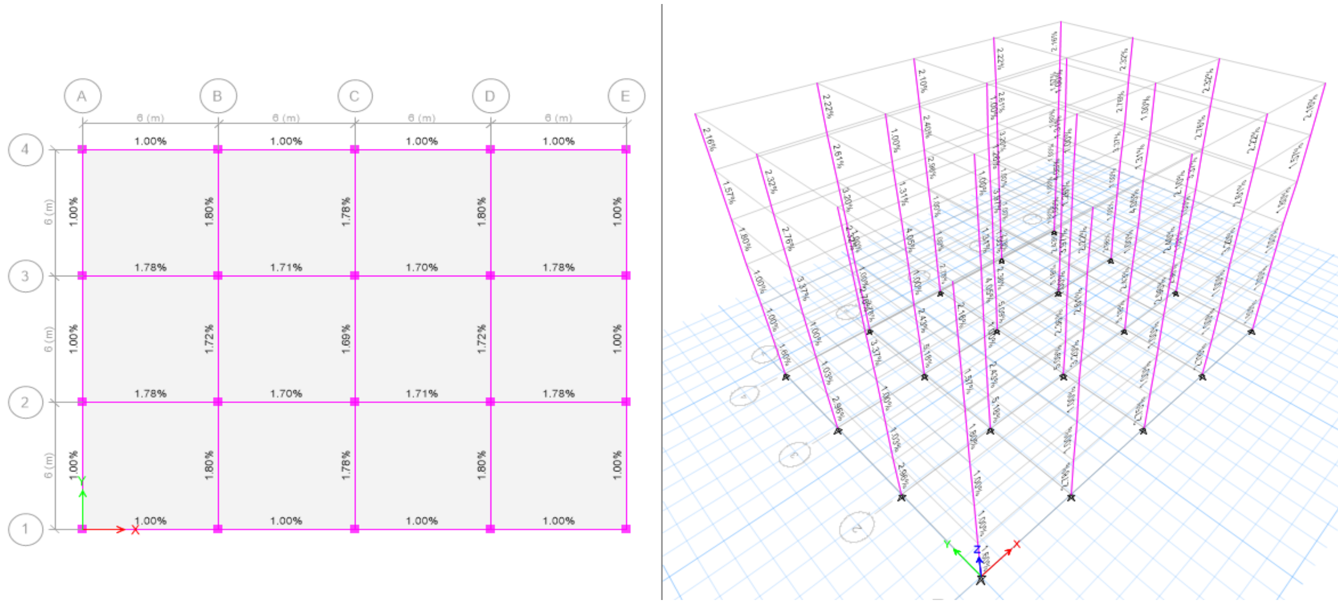

Figure 7.15 Output Design of the 6-Story Structural Building Showing the Required Reinforcement Area (mm) with Beam A (40cmX55cm),Beam B (30cmX50cm).

NOTE: Note: Beams labeled as (A) denote edge beams, whereas beams labeled as (B) denote interior beams.

Table 7.5 summarizes the geometric properties of the investigated sections together with the corresponding response modification factor (R) obtained for each case. Furthermore, Figure 7.16 illustrates the pushover curves for the three cases associated with section depth variation, highlighting their influence on the structural response. The corresponding results and performance indicators for the depth-modification cases are also presented in the accompanying table for comparison and assessment.

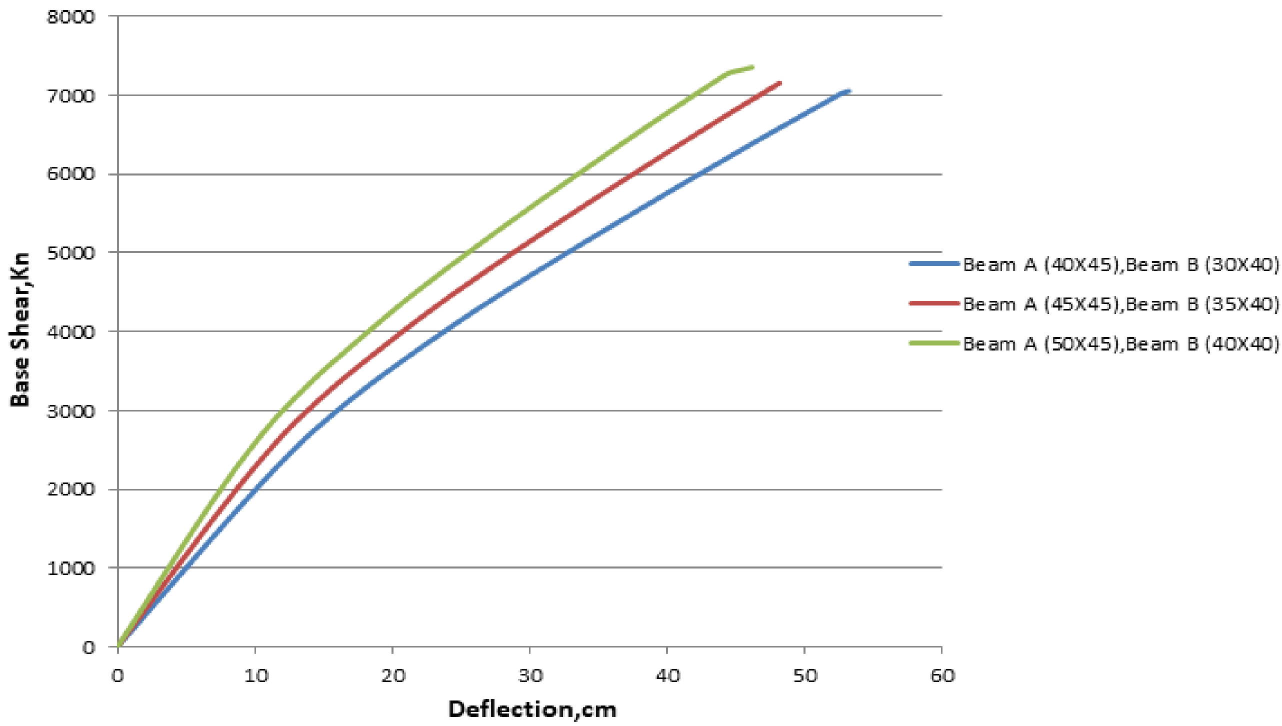

Figure 7.16 Pushover Capacity Curves of the Six-Story IMRF Building with Increasing Beam **Depths**.

Table 7.5 Seismic Response Results of the Six-Story IMRF Building with Varying Beam **Depths**.

Number Of Stories	Beam Section(cm)	Base Shear(Kn)	Δmax(mm)	Δy(mm)	R

6-Story	Beam A (40X45),Beam B (30X40)	6592.1	48.2	15.5	3.56
	Beam A (45X45),Beam B (35X40)	6862.2	45.4	14	3.8
	Beam A (50X45),Beam B (40X40)	7096.9	42.7	12.3	4.1

Table 7.6 summarizes the geometric properties of the sections considered in the width-modification study together with the corresponding response modification factor (R) values obtained for each case. In addition, Figure 7.17 presents the pushover curves for the three cases associated with section width variation, illustrating the influence of beam width on the overall structural behavior and seismic performance. The results provide a comparative assessment of the effect of width modification on strength, ductility, and response modification capacity.

Table 7.6 Seismic Response Results of the Six-Story IMRF Building with Varying Beam **Widths**.

Number Of Stories	Beam Section(cm)	Base Shear(Kn)	Δmax(mm)	Δy(mm)	R

6-Story	Beam A (40X45),Beam B (30X40)	6592.1	48.2	15.5	3.56
	Beam A (40X50),Beam B (30X45)	6743.1	47.9	16	3.54
	Beam A (40X55),Beam B (30X50)	6854.7	47.5	15	3.6

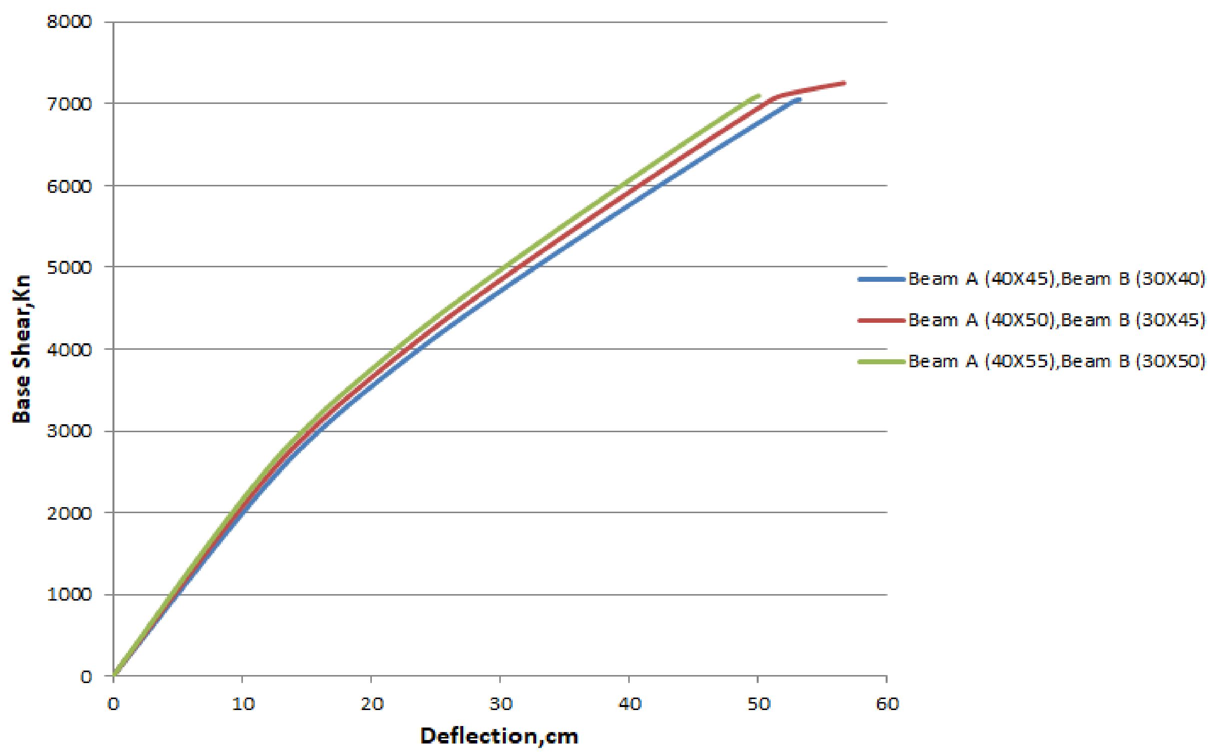

Figure 7.17 Pushover Capacity Curves of the Six-Story IMRF Building with Increasing Beam **Widths**.

The results indicate that increasing beam cross-sectional dimensions leads to a moderate increase in base shear capacity and the response modification factor (R), accompanied by a reduction in maximum displacement due to the increase in structural stiffness. Larger beam sections improve force distribution and enhance the overall seismic performance of the frame. However, the observed improvements remain relatively limited when compared to the influence of column dimensions, as columns play a more significant role in controlling global stiffness, lateral load resistance, and the overall seismic response of the structure.

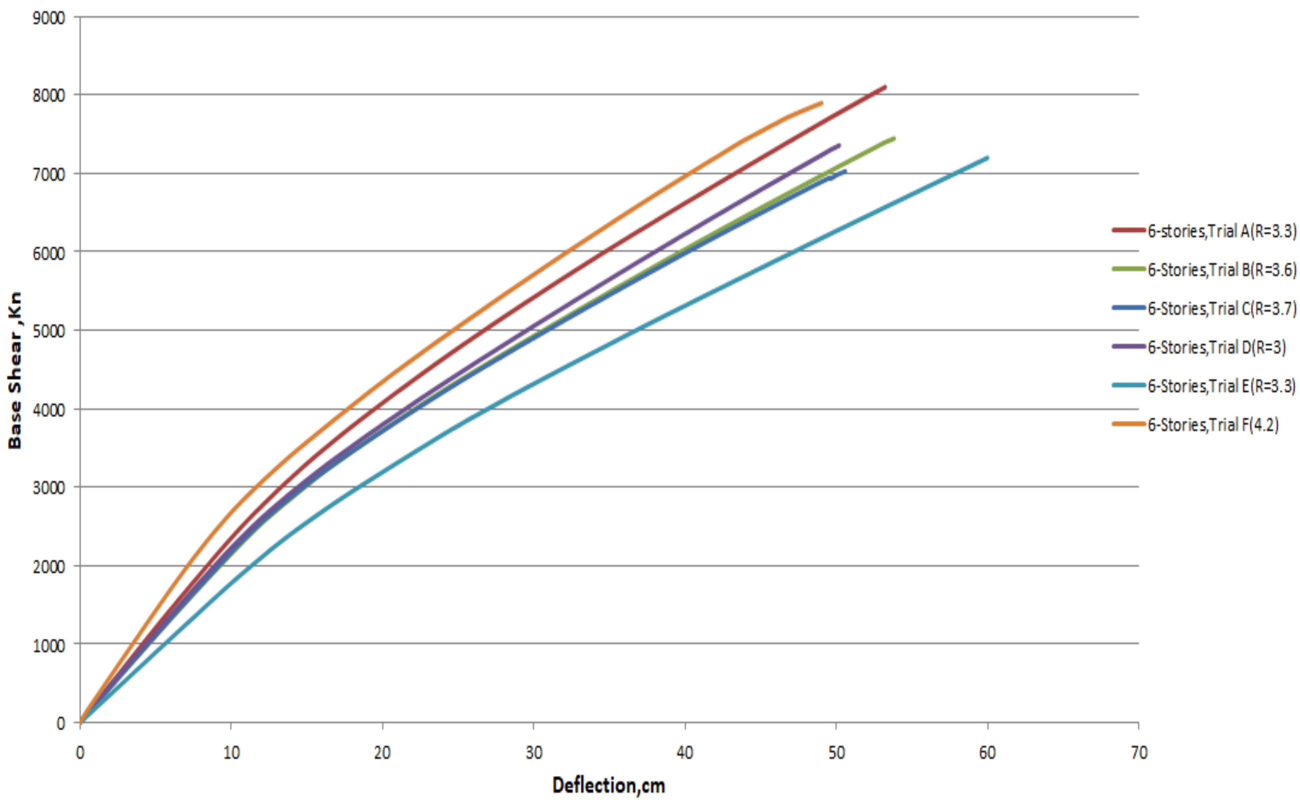

Figure 7.18 Pushover Capacity Curves of the Six-Story IMRF Building under Different Stiffness Configurations.

The seismic response and response modification factor (R) of the six-story Intermediate Moment Resisting Frame (IMRF) building were further examined through a detailed evaluation of stiffness characteristics and stiffness distribution along the building height. The adopted approach aims to clarify how variations in structural stiffness influence the global nonlinear behavior, deformation demand, and energy dissipation capacity of the frame system.

Several structural configurations were analyzed by modifying the geometric properties of the building, with particular emphasis on changes that directly affect the lateral stiffness distribution. In one configuration, the plan area of the top story was reduced, leading to a localized reduction in lateral stiffness at the upper level. This modification introduces a clear case of Vertical Stiffness Irregularity, where stiffness is no longer uniformly distributed along the height of the structure. Such irregularity alters the lateral load-resisting mechanism and significantly influences the way seismic forces and deformations are distributed among the stories.Changes in stiffness distribution play a decisive role in controlling interstory drift concentration, the onset of inelastic behavior, and the overall shape of the pushover capacity curve. When vertical stiffness irregularity is present, deformation demand tends to concentrate in stiffness-deficient regions, resulting in earlier stiffness degradation and reduced efficiency in energy dissipation. These effects directly influence the effective ductility of the structure and, consequently, the estimated response modification factor (R).

The global nonlinear seismic behavior corresponding to the different stiffness configurations is illustrated in Figure 7.18, which presents the pushover capacity curves for multiple frame trials (Trials A–F). Each curve represents a distinct stiffness condition of the six-story building, while the complete geometric, structural, and reinforcement characteristics of all frame configurations are summarized in Table 7.8. The comparison of the pushover curves highlights the sensitivity of base shear capacity, displacement demand, and post-yield behavior to variations in stiffness distribution.Frames exhibiting higher and more uniformly distributed stiffness show steeper initial slopes in the pushover curves and achieve greater base shear resistance at lower displacement levels, indicating enhanced lateral stiffness and strength. In contrast, configurations affected by reduced or uneven stiffness display a more gradual response, increased displacement demand, and earlier stiffness degradation. These differences demonstrate that stiffness distribution governs not only the elastic response but also the inelastic deformation mechanism and energy dissipation capacity of the frame system.

Overall, the results confirm that stiffness—and particularly Vertical Stiffness Irregularity—is a governing parameter in the seismic performance and R-value estimation of IMRF buildings. A balanced and continuous stiffness distribution along the building height promotes stable inelastic behavior, improved ductility, and more reliable response modification factors, whereas stiffness irregularities lead to deformation localization and reduced seismic efficiency. The trends observed in Figure 7.18, in conjunction with the frame properties summarized in Table 7.8, provide a consistent and physically sound explanation for the observed variations in seismic response and R-values.

Table 7.7 Comparison of Story Stiffness Distribution for Different Structural Models.

	Trial A	Trial B	Trial C	Trial D	Trial E	Trial F
#Of Stories	N/m	N/m	N/m	N/m	N/m	N/m

6	62470.99	84559.87	65361.96	27951.69	13182.17	48510.23
5	66814.86	89861.43	70968.86	48839.52	16507.9	57398.28
4	64676.13	87525.3	75474.25	64916.58	22656.94	72439.06
3	76990.38	103525.2	109289.1	89656.82	61061.16	95248.19
2	71714.55	94144	100666.4	84498.59	68271.61	98207.79
1	57696.27	70968.22	75059.98	65827.86	61445.32	74602.57

According to ASCE 7-16, a soft-story irregularity exists when:

{Ki}/{K{i+1}} < 0.70

where (Ki) is the stiffness of the considered story and

(K{i+1}) is the stiffness of the story immediately above.

The story stiffness values presented in Table 7.7 were evaluated according to the vertical stiffness irregularity requirements of ASCE 7-16. A soft-story irregularity is considered to exist when the stiffness of a story is less than 70% of the stiffness of the story immediately above. The calculated stiffness ratios indicate that Trials A, B, and F satisfy the code requirements and exhibit a relatively uniform stiffness distribution along the building height. However, Trials C, D, and E show localized stiffness irregularities, with Trial E exhibiting the most significant reduction in stiffness. These results demonstrate that the modification of member dimensions has a direct influence on the vertical stiffness distribution and the overall seismic performance of the structure. Therefore, maintaining a balanced stiffness distribution is essential to avoid soft-story behavior and ensure compliance with seismic design requirements.

Table 7.8 Seismic Response Parameters and Stiffness-Related Properties of the Six-Story IMRF Building.

Type Of Models	Beam Section(cm)	Col. Section(cm)	Base Shear(Kn)	Δmax(mm)	Δy(mm)	R	% Reinf. Ratio	
							Col.A	Col.B
A	Beam A (45*40),Beam B (40*40)	Col A (45*40),Col B (30*40)	6249.8	36.8	13.5	3.3	2.5	2
B	Beam A (45*40),Beam B (45*40)	Col A (50*50),Col B (40*40)	6452.5	44	14.4	3.6	2.7	2
C	Beam A (45*40),Beam B (40*40)	Col A (50*50),Col B (40*40))	6307.1	43.2	14.1	3.7	3	2.3
D	Beam A (45*40),Beam B (30*40)	Col A (50*50),Col B (40*40))	6775.3	44.9	13.5	3	3.5	2
E	Beam A (45*40),Beam B (30*40)	Col A (50*50),Col B (40*40)	5177.5	38.6	15.2	3.3	1.5	3.5
F	Beam A (50*50),Beam B (40*40)	Col A (50*50),Col B (40*40)	7534.4	45	11.4	4.2	2	2-3

Although several geometric configurations were introduced for the six-story IMRF building, the results summarized in the attached table indicate that the estimated response modification factor (R) did not vary significantly among the studied cases. This outcome suggests that the applied plan-shape modifications produced limited influence on the global inelastic response mechanism of the structure. In other words, while the geometric changes may slightly alter local stiffness distribution and displacement demand (Δmax) or yielding characteristics (Δy).

Accordingly, the attached table confirms that, within the investigated range of geometric modifications, the six-story IMRF building exhibits robust global seismic behavior, with R-values remaining within a narrow band despite changes in plan configuration.

Effects of Reinforcement Ratio.

The The longitudinal reinforcement ratio in columns plays a critical role in controlling the response modification factor (R), as it directly governs the structural ductility, failure mechanism, and energy dissipation capacity of the seismic force-resisting system. The numerical results of this study indicate that moderate reinforcement ratios lead to optimal seismic performance, whereas excessive reinforcement adversely affects the global response

. At lower reinforcement ratios, the structural system exhibits limited ductility due to early yielding of the reinforcing steel, resulting in relatively modest R-values. In the present study, the highest and most stable R-values were observed at reinforcement ratios of approximately 2%, indicating an optimal balance between strength, stiffness, and ductility.

It should be noted, however, that the objective of this study was not to identify a specific reinforcement ratio or a particular cross-sectional configuration as an optimum design solution. Rather, all investigated models were designed in accordance with the applicable code requirements and verified to satisfy structural design criteria. The purpose of varying the reinforcement ratios was to evaluate their influence on the seismic response and response modification factor (R), while maintaining structurally acceptable and code-compliant designs throughout the analysis..

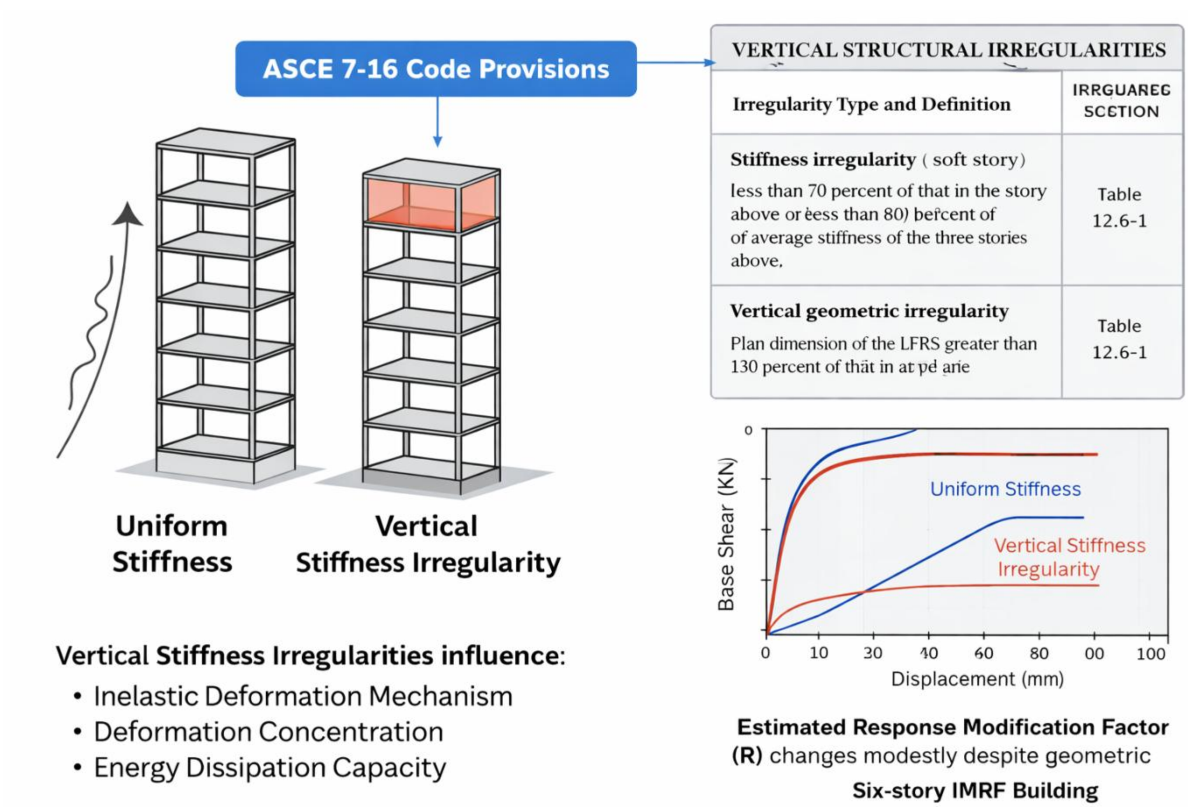

Figure 7.19 Conceptual Illustration of Vertical Stiffness Distribution and Its Influence on Seismic Response and R-Value.

After examining the effect of column dimensions on the three-story building, the analysis was extended to a nine-story building, where height-dependent stiffness effects play a dominant role in governing the global response.

The results obtained from the pushover capacity curves in figure 7.20 and summarized in the accompanying table 7.9 indicate that increasing the column cross-sectional dimensions leads to a reduction in the response modification factor (R). Specifically, R decreased from approximately 3.7 to 2.7 as the column sizes increased. This behavior is fundamentally associated with the significant increase in global lateral stiffness introduced by larger column sections in a mid structure.

For the nine-story building, enlarging column dimensions substantially increases axial and flexural stiffness, resulting in a stiffer structural system with reduced lateral deformability. Although this stiffness enhancement increases the base shear capacity, it simultaneously limits displacement ductility and reduces post-yield deformation capacity, as observed in the pushover curves. The steeper initial slopes of the capacity curves reflect higher stiffness, while the reduced curvature in the post-yield range indicates a more constrained inelastic response.

Moreover, larger column sections promote a response in which plastic deformations are suppressed or delayed, leading to a reduction in energy dissipation through hysteretic behavior. In such cases, the structure tends to resist seismic forces predominantly through elastic action rather than controlled inelastic mechanisms. This shift in response behavior directly reduces the displacement ductility ratio, which is a key parameter governing the estimation of the response modification factor (R).

In summary, the results demonstrate that for the nine-story IMRF building, increasing column cross-sectional dimensions does not enhance seismic performance in terms of R-value. Instead, excessive stiffness leads to reduced ductility and diminished energy dissipation capacity, explaining the observed reduction of R from 3.7 to 2.7. The trends observed in the pushover capacity curves and the corresponding values reported in the accompanying table confirm that optimal seismic performance in taller buildings requires a balanced stiffness distribution rather than maximum column stiffness.

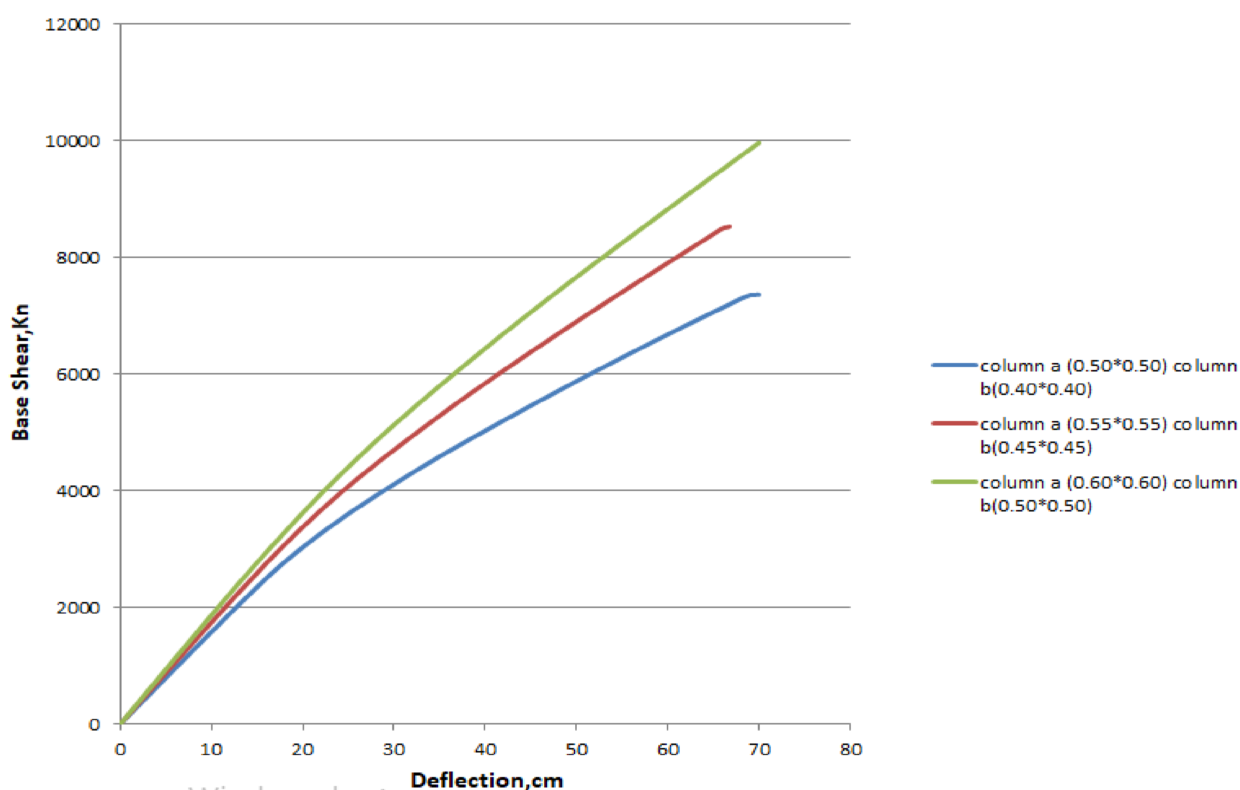

Figure 7.20 Pushover Capacity Curves of Nine-Story IMRF Buildings with Varying Column Cross-Sections.

Note: *Column A represents columns extending from Story 1 to Story 5, while Column B represents columns extending from Story 6 to Story 9.*

Table 7.9 Seismic Response Results of the Nine-Story IMRF Building with Varying Column Cross-Sections.

Number Of Stories	**Column Section(cm)**	**Base Shear(Kn)**	**Δmax(mm)**	**Δy(mm)**	**R**	**% Reinf. Ratio**	
						Col.A	**Col.A**
9-Story	column A (0.50*0.50) column B(0.40*0.40)	7267.4	67.8	22.1	3.7	2	1
	column A (0.55*0.55) column B(0.45*0.45)	7489.4	55.9	21.3	3	2	1

	column A (0.60*0.60) column B (0.50*0.50)	8219.9	54.8	22.7	2.7	1	1

For the nine-story IMRF building, an additional parametric modification was introduced by increasing the span length between two adjacent frames to 12 m, which was achieved by removing one column continuously along the full height of the building. This modification was applied to the same structural frame presented in Figure 6.4, while maintaining identical reinforcement ratios and material properties, in order to isolate the effect of span enlargement and column removal on the seismic response.

The reduction in the response modification factor (R) can be attributed to the removal of the intermediate column, which increased the beam span from 6 m to 12 m. This modification significantly reduced the lateral stiffness and strength of the structural system, resulting in larger deformation demands and a lower base shear capacity. In addition, the removal of the column altered the load-transfer mechanism and reduced the effectiveness of inelastic energy dissipation. Consequently, both the ductility and overstrength characteristics of the frame were adversely affected, leading to a decrease in the response modification factor from 3.7 to 2.5.

The observed behavior can be primarily attributed to the loss of structural redundancy and the change in force distribution caused by the removal of the intermediate column. Increasing the span length from 6 m to 12 m altered the structural response and reduced the effectiveness of the lateral load-resisting system, resulting in lower base shear capacity and a reduction in the calculated response modification factor. Furthermore, the absence of the column alters the load transfer path and reduces the number of vertical elements participating in resisting seismic forces. As a result, the structural response transitions from a ductility-controlled frame behavior toward a more flexibility-dominated and deformation-sensitive response, which directly lowers the displacement ductility ratio and, consequently, the estimated R-value. Despite the reinforcement remaining unchanged, the geometric and stiffness-related modification alone was sufficient to significantly degrade seismic performance.

Overall, this case demonstrates that in nine-story IMRF buildings, the removal of a vertical load-resisting element and the associated increase in span length can markedly reduce both strength and ductility. The reduction of R from 3.7 to 2.5, together with the drop in base shear from 7267.4 kN to 5328.3 kN, confirms that structural continuity and stiffness distribution are governing parameters in seismic performance, often outweighing the influence of reinforcement ratios when major geometric modifications are introduced.

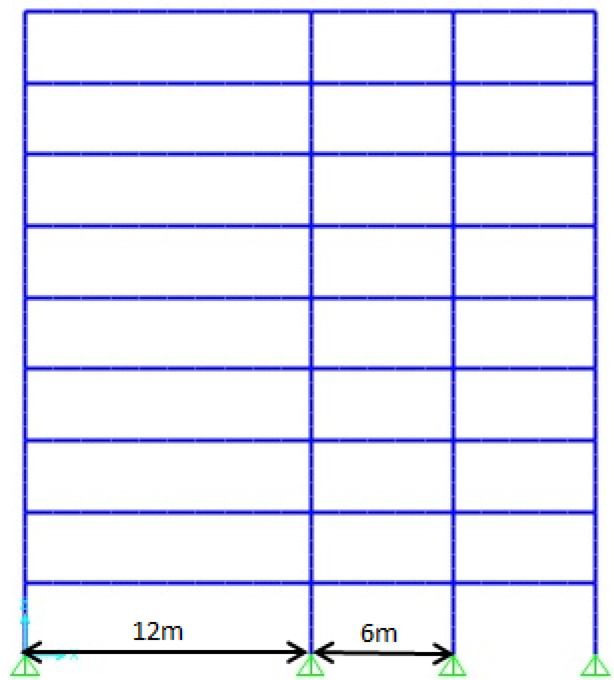

Figure 7.21 Column Removal Configuration in the Nine-Story IMRF Building

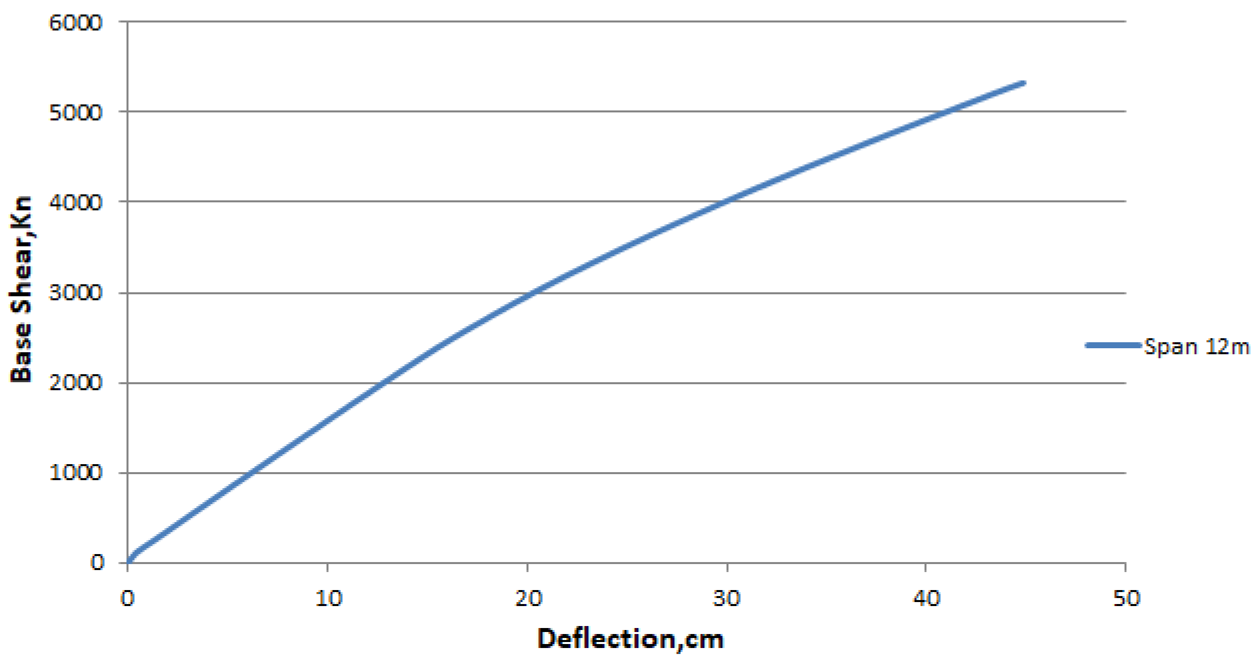

Figure 7.22 Pushover Capacity Curves of the Nine-Story IMRF Building with Column Removal (12 m Span Case).

7.5 Moment Frame Building Results (Abaqus)

ABAQUS is an advanced finite element analysis (FEA) software widely used for nonlinear structural analysis and research-oriented simulations. It is particularly powerful in modeling material nonlinearity, geometric nonlinearity, and damage mechanisms, making it well suited for seismic analysis beyond the elastic range.

In reinforced concrete structures, ABAQUS allows explicit modeling of concrete cracking, crushing, stiffness degradation, and steel yielding through advanced constitutive models such as Concrete Damage Plasticity (CDP) for concrete and nonlinear plasticity models for reinforcing steel. Unlike simplified frame-based approaches, ABAQUS does not rely on predefined plastic hinges; instead, inelastic behavior develops naturally wherever stress and strain concentrations occur.

For pushover analysis, ABAQUS provides a physically realistic representation of the nonlinear response, capturing the evolution of damage and failure mechanisms at the material level. As a result, the extracted pushover capacity curves reflect the true degradation of stiffness and strength, particularly in the post-yield range. Although the analysis is computationally intensive and sensitive to modeling assumptions (mesh density, material parameters, convergence criteria), ABAQUS is considered highly reliable for research validation and detailed seismic behavior assessment.

Table 7.10 presents a comparative summary highlighting the key differences between ABAQUS and SAP2000 in the context of nonlinear pushover analysis. The table outlines the fundamental distinctions in modeling philosophy, representation of material and geometric nonlinearities, stiffness degradation mechanisms, and the extraction of pushover capacity curves. While SAP2000 employs a simplified, code-calibrated hinge-based approach that is well suited for practical structural design and parametric studies, ABAQUS provides a detailed material-level simulation capable of capturing concrete cracking, crushing, reinforcement yielding, and progressive damage. This comparison helps explain the observed variations in seismic response and response modification factors obtained from the two analysis platforms and supports the validation of the numerical results.

Table 7.10 Comparison between ABAQUS and SAP2000 for Nonlinear Pushover Analysis

Aspect	SAP2000	ABAQUS
Primary Purpose	Structural design and practical engineering analysis	Research-oriented, advanced nonlinear analysis
Modeling Approach	Frame elements (beam–column idealization)	Continuum finite elements (solid/shell elements)
Material Nonlinearity	Simplified nonlinear behavior via predefined hinges	Explicit material models (CDP for concrete, nonlinear steel)
Plasticity Representation	Plastic hinges assigned at predefined locations	Plastic zones form naturally based on stress–strain response
Cracking & Crushing	Implicitly accounted for through hinge properties	Explicitly modeled and tracked
Stiffness Degradation	Idealized and hinge-based	Naturally captured through damage evolution
Pushover Curve Shape	Smoother and more stable	Less smooth, more realistic, shows sudden degradation
Post-Yield Behavior	Controlled by hinge backbone curves	Highly sensitive to damage and failure mechanisms
Computational Demand	Low to moderate (fast and robust)	High (time-consuming, convergence-sensitive)
Numerical Stability	Generally stable and user-friendly	Sensitive to mesh, material parameters, and increments
Accuracy (Physical Realism)	Moderate (code-calibrated idealization)	Very high (material-level realism)
Best Use Case	Design studies, parametric analysis, code-based evaluation	Validation, research, detailed seismic behavior

A comparative nonlinear pushover analysis was carried out for a one-story reinforced concrete frame using SAP2000 and ABAQUS in order to examine the differences in seismic response resulting from the adopted modeling approaches. The geometric configuration and reinforcement details were maintained identical in both models to ensure a consistent basis for comparison. The beam section (30 × 35 cm) was reinforced with 6Ø12, while the column section (40 × 40 cm) was reinforced with 8Ø16.

The slab self-weight and associated gravity loads were transferred to the supporting beams using the tributary area method, whereby the slab load was distributed to each beam according to its contributing floor area. This approach ensured a realistic representation of gravity effects and mass distribution in both numerical models, allowing for a direct and meaningful comparison between the two analysis platforms.

The resulting pushover capacity curves obtained from SAP2000 and ABAQUS are presented in Figure 7.23, illustrating the similarities in overall response trends as well as the differences in stiffness evolution and post-yield behavior. These differences are primarily attributed to the distinct nonlinear modeling strategies employed by the two programs, with SAP2000 relying on predefined hinge properties and ABAQUS capturing material-level nonlinearities and stiffness degradation more explicitly.

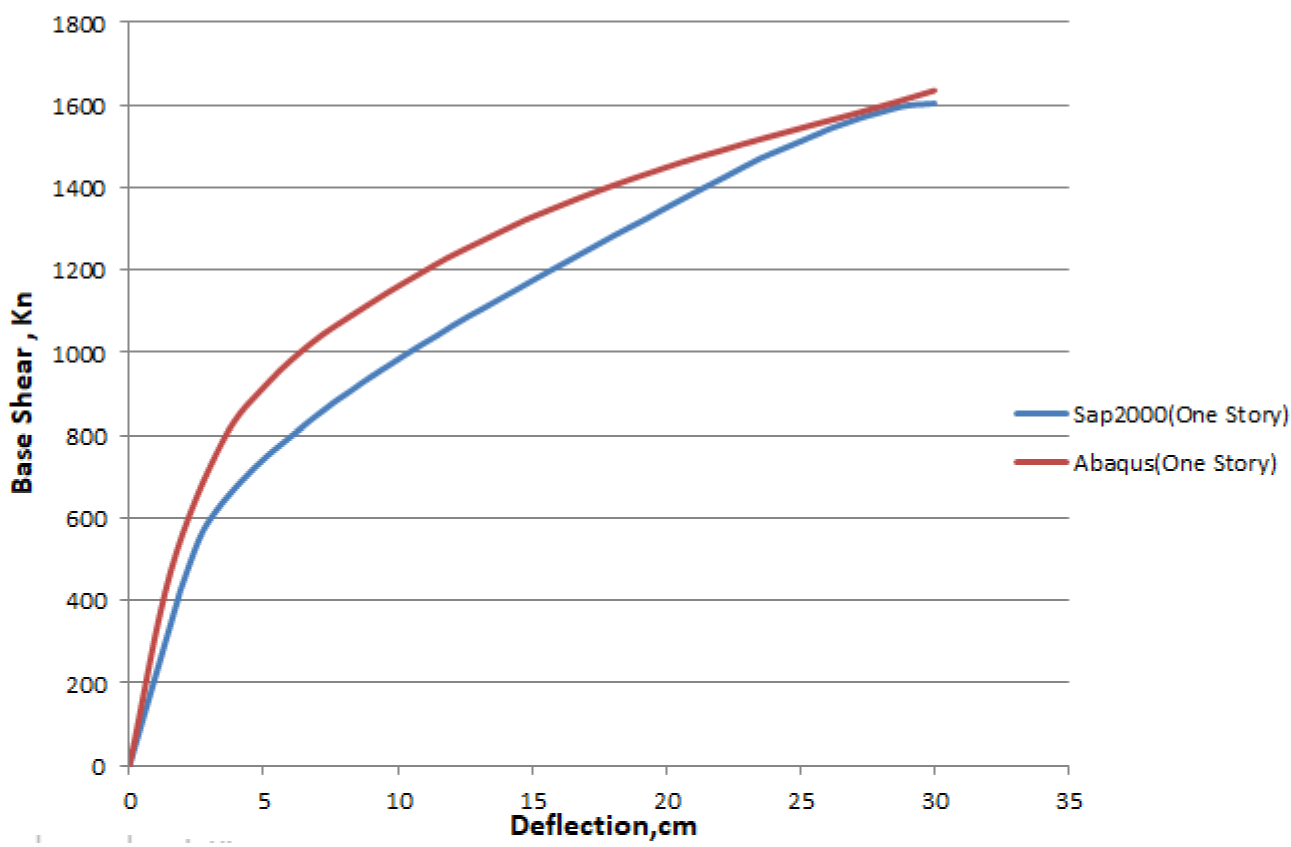

Figure 7.23 Pushover Capacity Curves for a One-Story RC Frame Using SAP2000 and ABAQUS.

At the initial loading stage, both curves exhibit comparable stiffness, indicating consistent elastic behavior. However, as lateral displacement increases, the divergence between the two curves becomes more pronounced. The SAP2000 curve maintains a steeper slope and reaches a higher ultimate base shear, whereas the ABAQUS curve shows a gradual reduction in stiffness, resulting in lower base shear values at larger displacements.

Overall, the figure demonstrates that although both analyses predict similar deformation patterns, ABAQUS provides a more conservative and realistic estimation of post-yield behavior, while SAP2000 tends to overestimate structural strength in the nonlinear range. The observed difference highlights the influence of the adopted modeling strategy on the extracted pushover response and subsequent seismic performance evaluation.

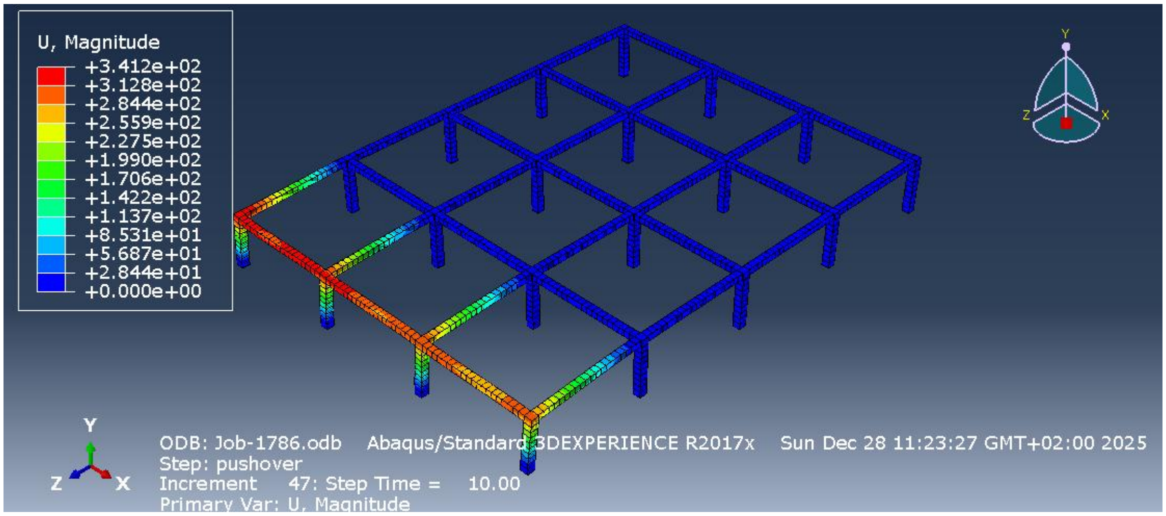

Figure 7.24 The deformed shape and displacement distribution of a one-story reinforced concrete frame.

Based on Section 4.2.3 (One-Story Frame Building), Two ABAQUS models with identical geometry, material properties, and loading conditions were analyzed, differing only in the stirrup spacing of the frame members. Stirrup spacings of 6 cm and 12 cm were adopted, and nonlinear pushover analyses were performed for both cases. The resulting capacity curves are presented in Figure 7.25.

As shown in the figure, both frames exhibit comparable elastic stiffness in the initial loading stage. However, beyond yielding, the frame with 6 cm stirrup spacing demonstrates higher base shear capacity and a more stable post-yield response compared to the frame with 12 cm spacing, which experiences earlier stiffness degradation and strength reduction. This difference directly affects the ductility capacity and energy dissipation potential of the structural system.

From a seismic performance perspective, the Response Modification Factor (R) is strongly dependent on the structure's ability to undergo inelastic deformations while maintaining adequate strength. The denser stirrup configuration (6 cm) enhances concrete confinement, delays shear-related damage, and promotes a more ductile flexural failure mechanism. Consequently, this configuration results in a higher effective R-value due to increased displacement capacity and improved post-yield behavior.

In contrast, increasing the stirrup spacing to 12 cm reduces confinement efficiency, accelerates stiffness degradation, and limits the stable inelastic deformation range. As a result, the corresponding frame exhibits a lower R-value, reflecting reduced ductility and diminished seismic energy dissipation capacity. These findings confirm that transverse reinforcement detailing plays a critical role in governing the R-factor, even for low-rise reinforced concrete frames with otherwise identical characteristics.

.

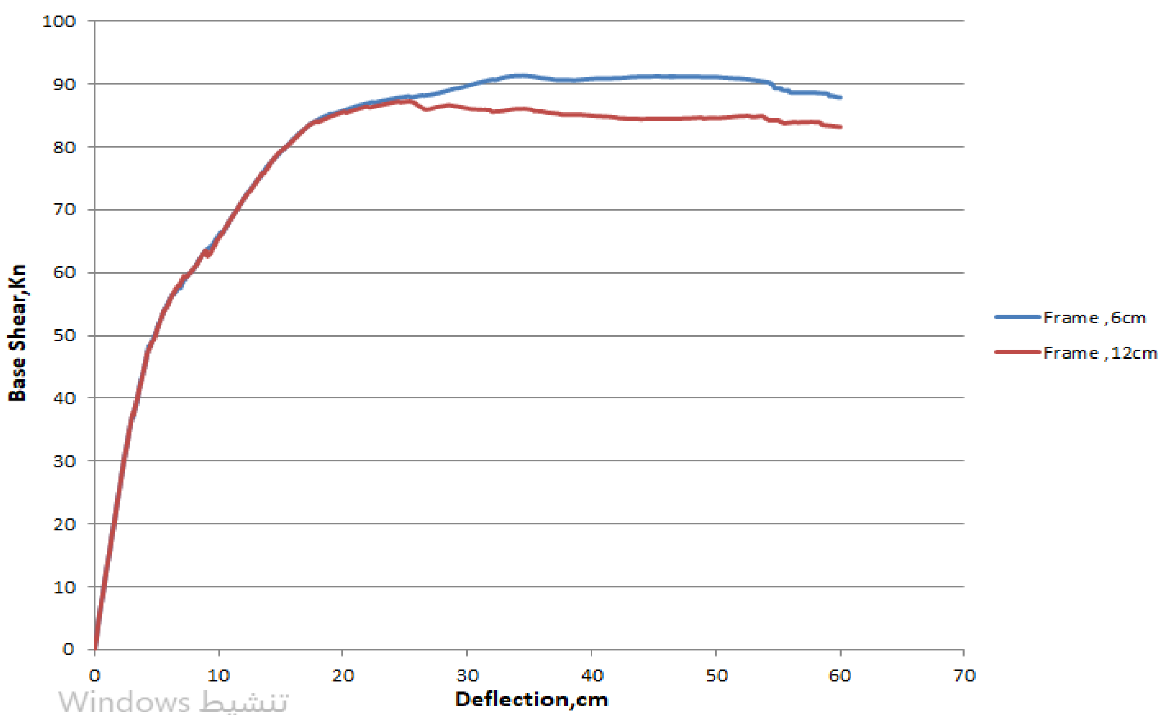

Figure 7.25 Effect of Stirrup Spacing on Pushover Capacity Curves of a One-Story RC Frame (ABAQUS).

Figures 7.26 and 7.27 present the tensile concrete damage (DAMAGET) obtained from the ABAQUS pushover analysis for stirrup spacings of 6 cm and 12 cm. In both cases, damage is concentrated primarily at the beam–column joints and beam ends, which represent the critical regions of the frame. The 6 cm spacing shows a slightly more uniform damage distribution, indicating improved confinement and ductility. However, the overall difference between the two configurations is relatively small, suggesting that the change in stirrup spacing has a limited influence on the global damage pattern and structural response of the investigated frame.

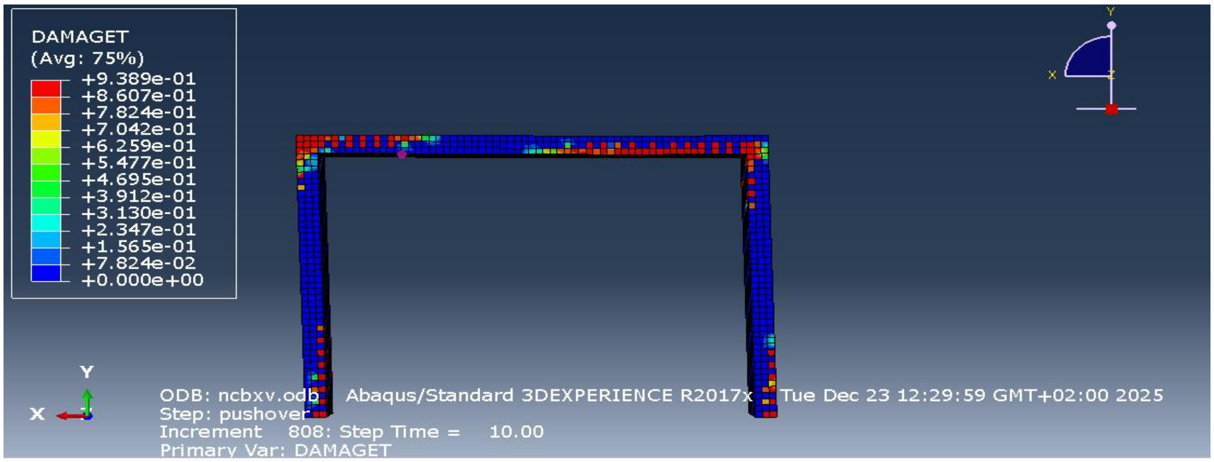

Figure 7.26 Tensile Damage Distribution of a One-Story RC Frame with 6 cm Stirrup Spacing (ABAQUS).

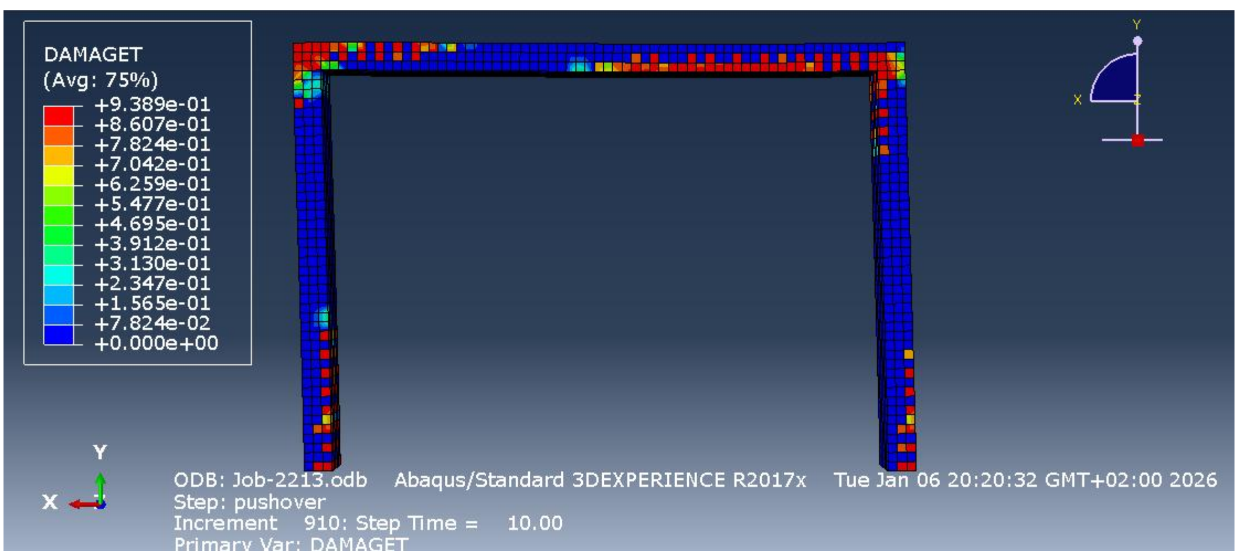

Figure 7.27 Tensile Damage Distribution of a One-Story RC Frame with 12 cm Stirrup Spacing (ABAQUS).

7.6 Performance Level of the IMRF

The performance-based table presented herein was developed through a detailed interpretation of the nonlinear static (pushover) analysis results, rather than being directly generated by the analysis software.

The identification of the performance levels—Immediate Occupancy (IO), Life Safety (LS), and Collapse Prevention (CP)—was carried out by carefully tracking the plastic hinge state transitions throughout the analysis process.

For each structural configuration, the pushover analysis was examined incrementally, and the analysis step corresponding to the first occurrence of each performance level was recorded. This approach ensures that the reported step numbers represent the onset of structural performance degradation, rather than a global or averaged response. The extracted step numbers therefore provide a consistent basis for comparing the influence of column dimensions and number of stories on the seismic performance of the frame systems.

It is important to emphasize that the step number itself is not a direct measure of structural capacity, as it is dependent on the selected load increment size and numerical convergence criteria. Instead, the step number serves as an indicator of the relative progression toward different performance limits, allowing for a clear and systematic comparison between alternative structural configurations.

Accordingly, the developed table offers a concise and effective framework for evaluating how changes in structural stiffness, member dimensions, and global configuration influence the sequence at which critical performance levels are reached. This interpretation aligns with the principles of performance-based seismic assessment, where structural behavior is evaluated based on damage progression and deformation capacity rather than solely on strength-based criteria.

Number of Stories	properties	Step Number	Performance Level
One Stories		7	IO
		15	LS
		27	CP
Three Stories	Col(40X40)	8	IO
		9	LS
		30	CP
	col(45X45)	8	IO
		11	LS
		22	CP
	col(50X50)	10	IO
		12	LS
		21	CP
	stirrups spac.=10 cm	6	IO
		16	LS
		21	CP
	stirrups spac.=5 cm	8	IO
		18	LS
		17	CP
Six Stories	Beam(40X45)	23	IO
		27	LS
		30	CP
	Beam(45X50)	18	IO
		20	LS
		29	CP
	Beam(50X55)	16	IO
		22	LS
		25	CP
	Trial 1	25	IO
		27	LS
		22	CP
	Trial 2	21	IO
		24	LS
		35	CP
	Trial 3	20	IO
		26	LS
		27	CP
	Trial 4	16	IO
		22	LS
		33	CP
	Trial 5	25	IO
		32	LS
		34	CP
	Trial 6	20	IO
		22	LS
		27	CP
Nine Stories	Col(50X50)	24	IO
		30	LS
		35	CP
	Col(55X55)	33	IO
		22	LS
		27	CP
	Col(60X60)	27	IO
		30	LS
		33	CP
	Cut-col.	21	IO
		22	LS
		9	CP

Table 7.11 Step Number and Performance Levels for all Frame Structural Building.

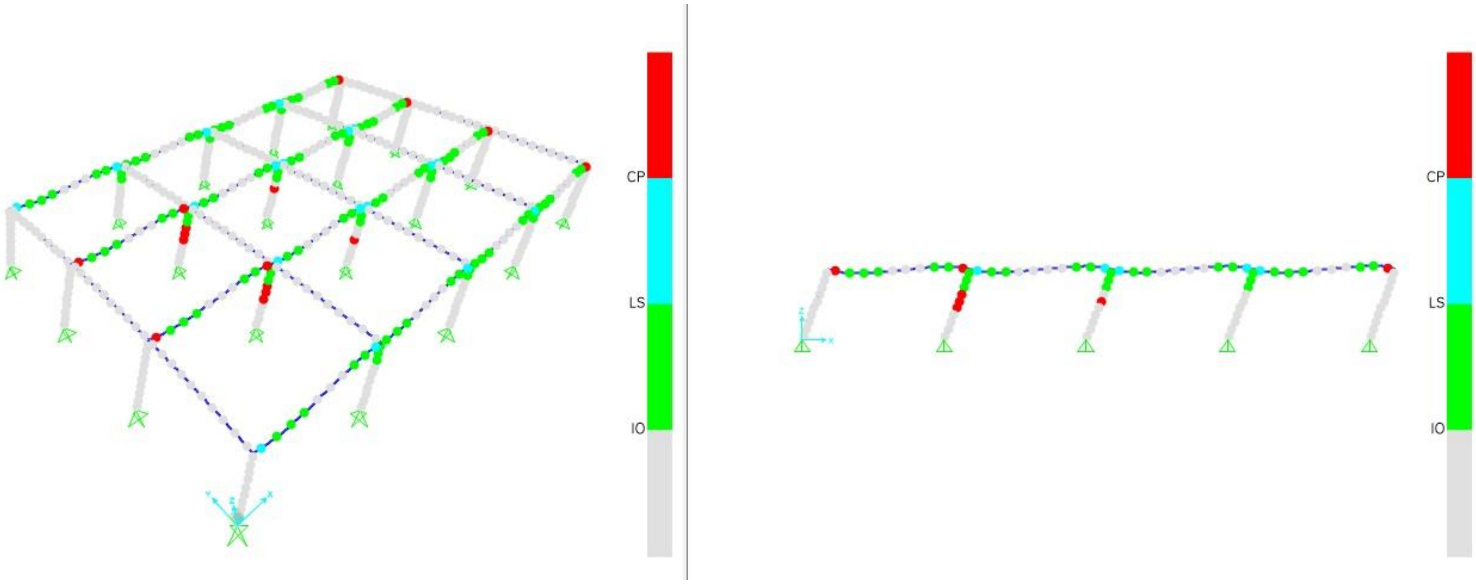

Figure 7.28 Plastic Hinge Distribution and Performance Levels of a One-Story Frame during Pushover Analysis(Failure).

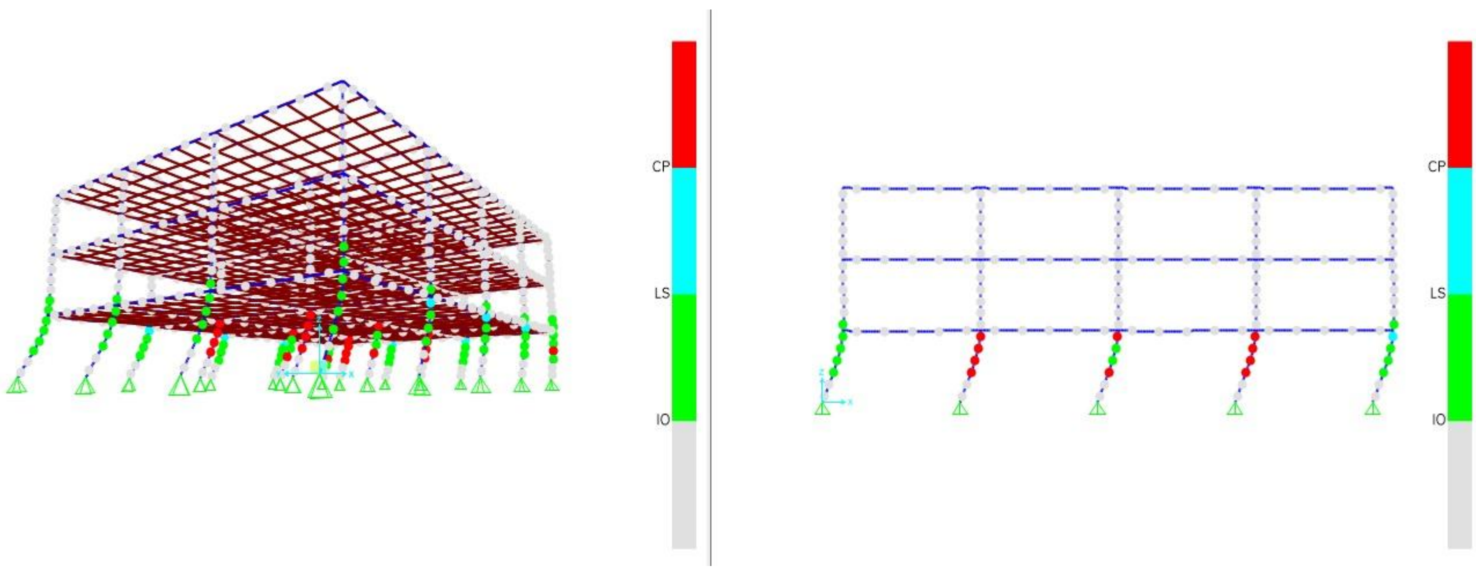

Figure 7.29 Plastic Hinge Distribution and Performance Levels of a 3-Story Frame with 40 X 40 cm Columns during Pushover Analysis(Failure).

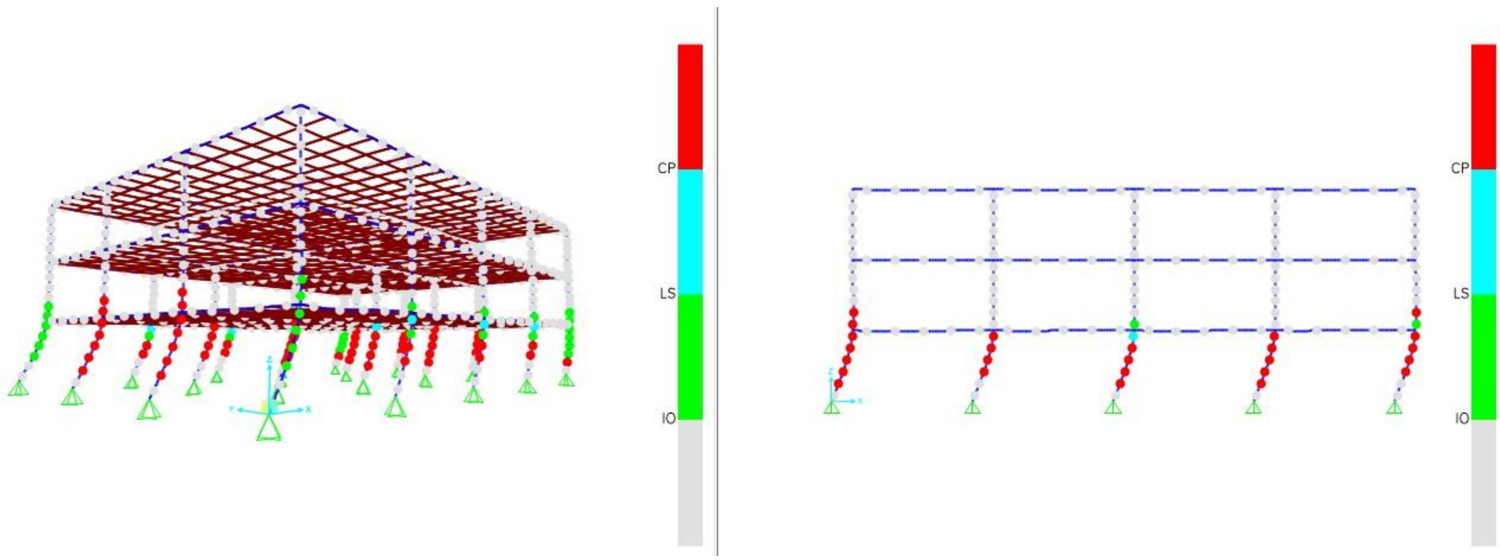

Figure 7.30 Plastic Hinge Distribution and Performance Levels of a 3-Story Frame with 45 X 45 cm Columns during Pushover Analysis(Failure).

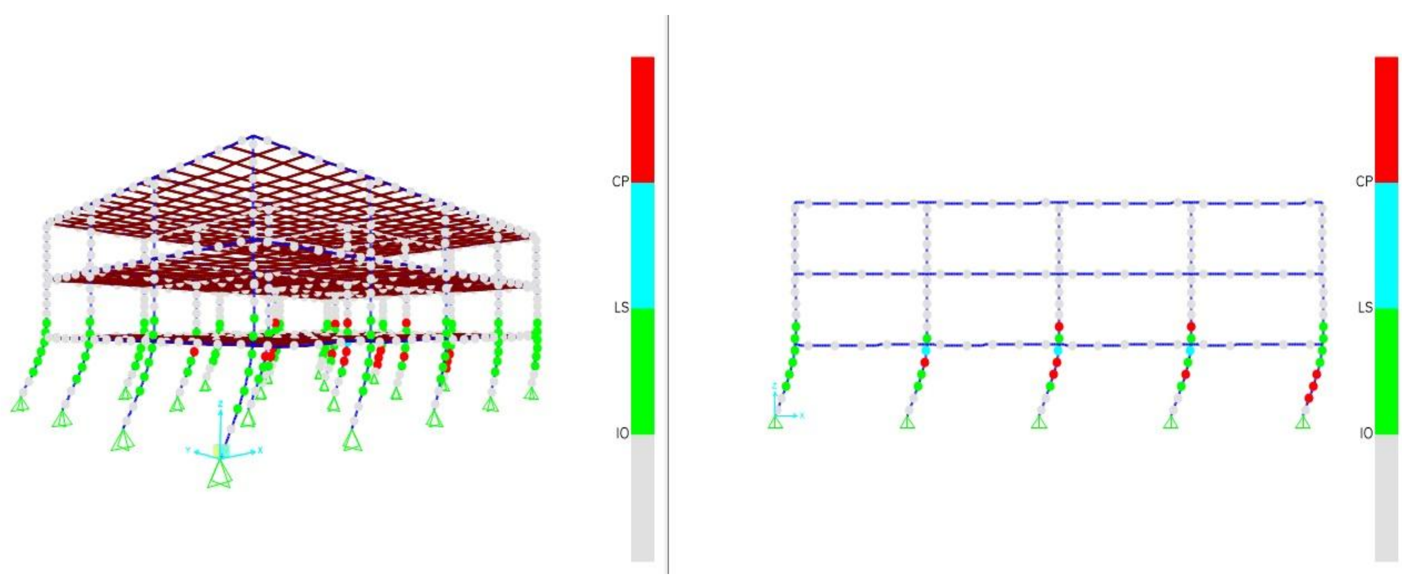

Figure 7.31 Plastic Hinge Distribution and Performance Levels of a 3-Story Frame with 50 X 50 cm Columns during Pushover Analysis(Failure).

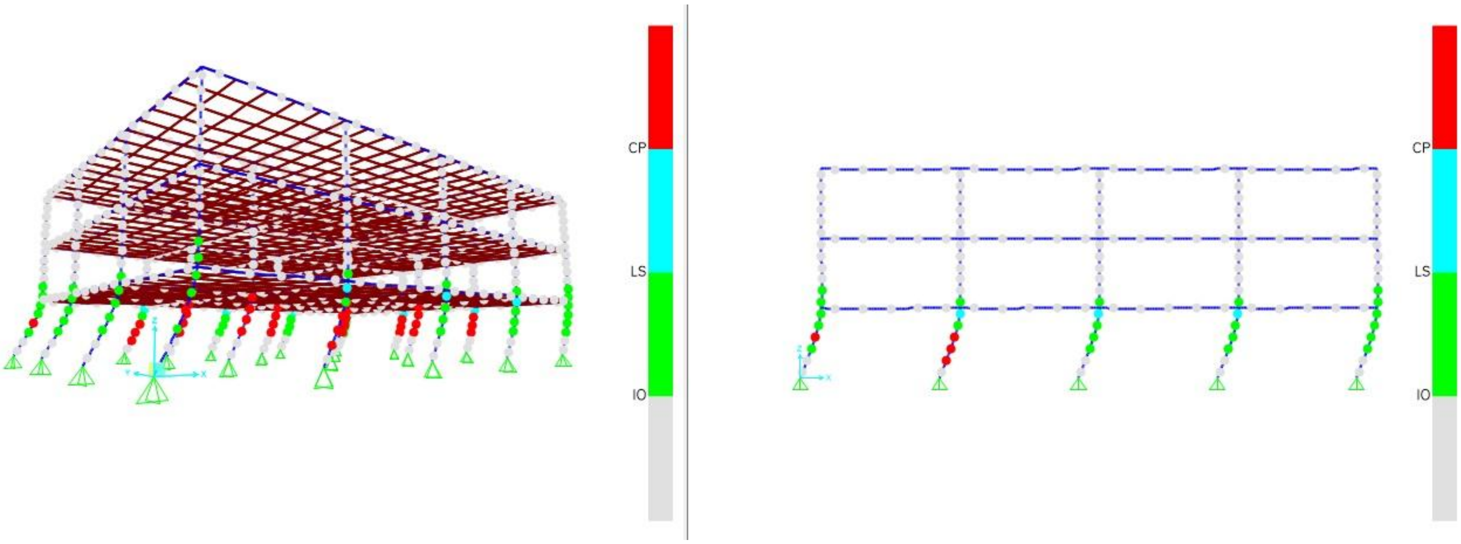

Figure 7.32 Plastic Hinge Distribution and Performance Levels of a 3-Story Frame with 10 cm Stirrup Spacing during Pushover Analysis(Failure).

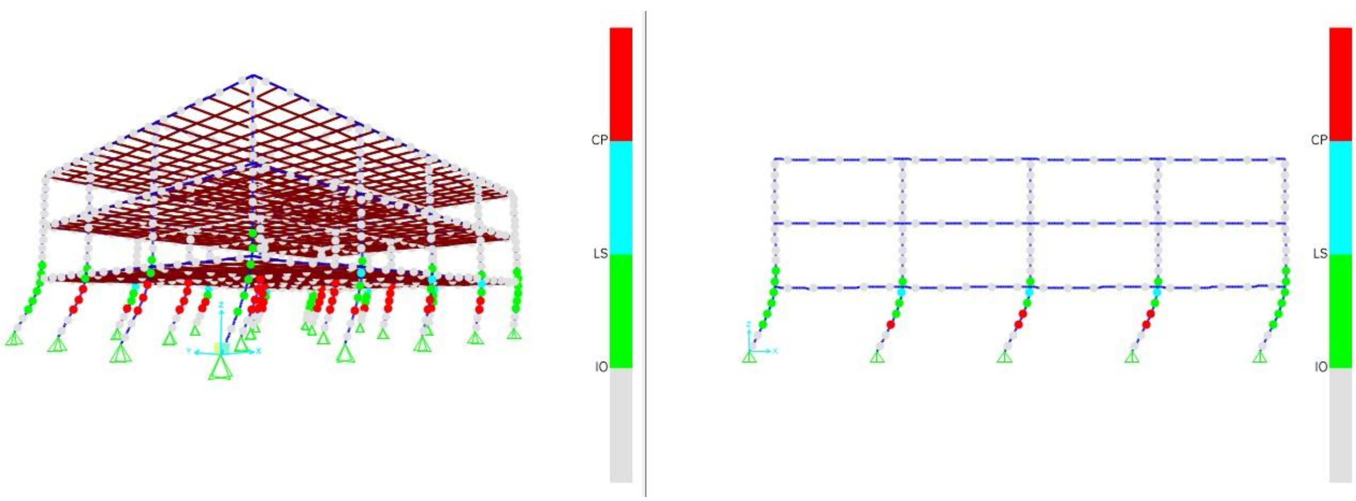

Figure 7.33 Plastic Hinge Distribution and Performance Levels of a 3-Story Frame with 5 cm Stirrup Spacing during Pushover Analysis(Failure).

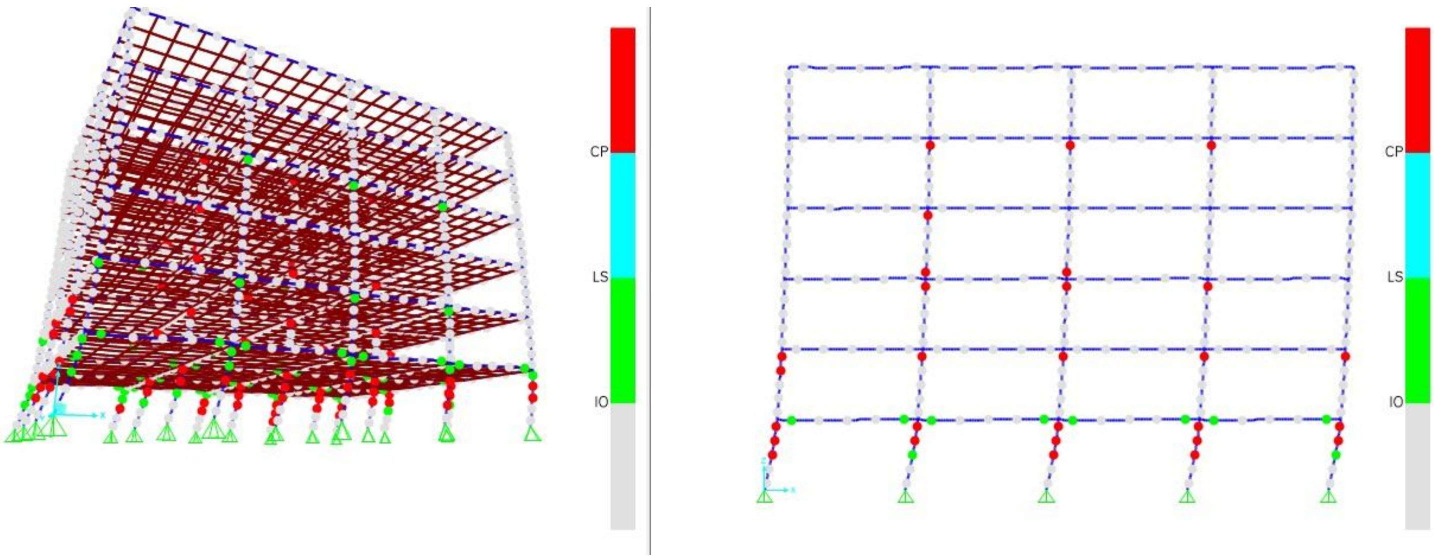

Figure 7.34 Plastic Hinge Distribution and Performance Levels of a 6-Story Frame with Beam Sections Edge (40 × 45 cm) and Mid (30 × 40 cm) during Pushover Analysis(Failure).

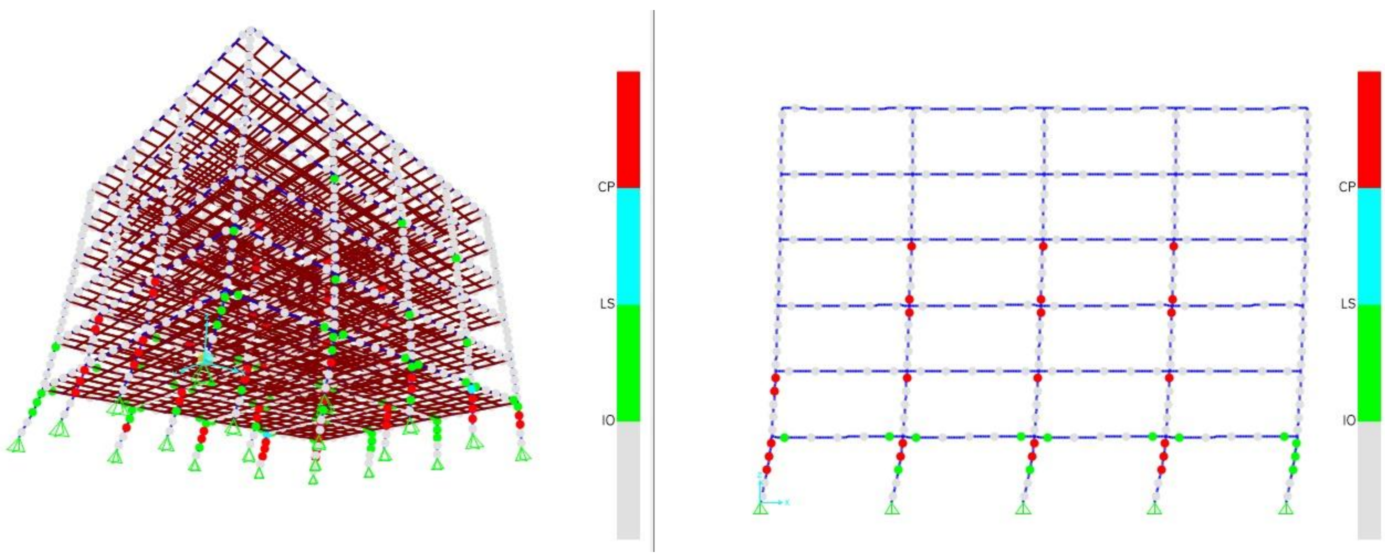

Figure 7.35 Plastic Hinge Distribution and Performance Levels of a 6-Story Frame with Beam Sections Edge (45 × 50 cm) and Mid (35 × 45 cm) during Pushover Analysis(Failure).

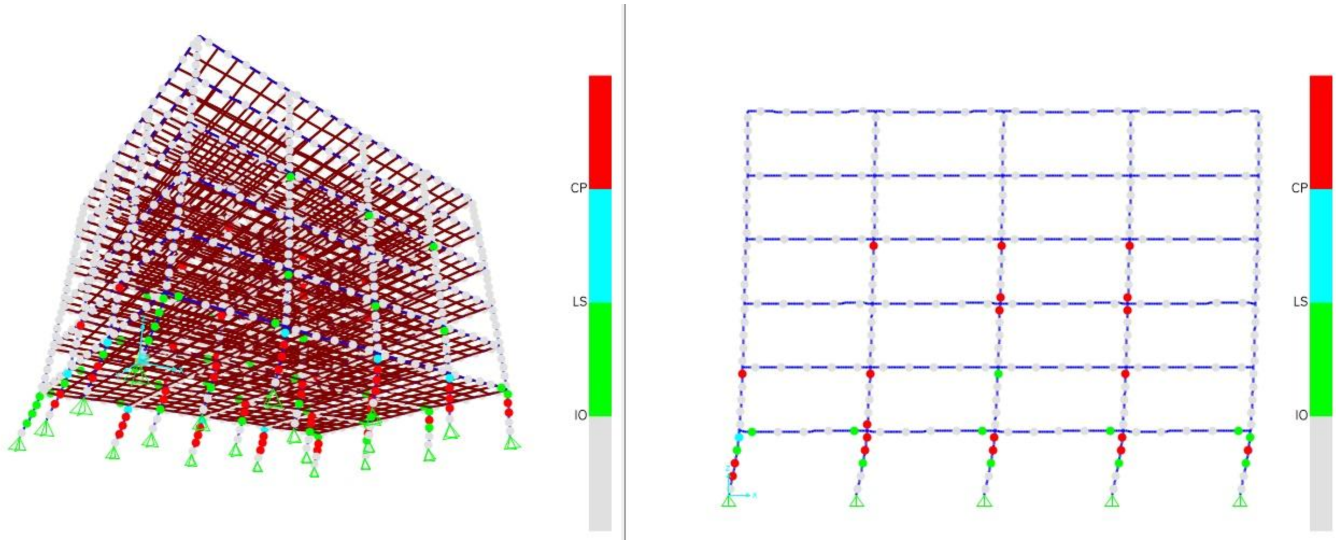

Figure 7.36 Plastic Hinge Distribution and Performance Levels of a 6-Story Frame with Beam Sections Edge (50 × 55 cm) and Mid (40 × 50 cm) during Pushover Analysis(Failure).

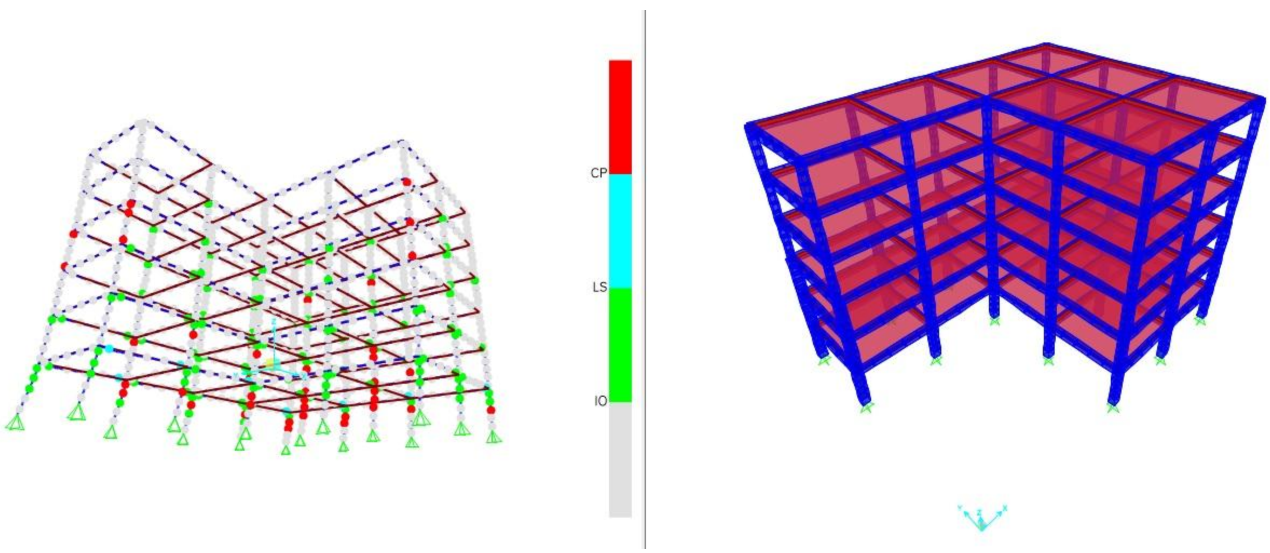

Figure 7.37 Plastic Hinge Distribution and Performance Levels of a Six-Story Frame (Trial 1) during Pushover Analysis(Failure).

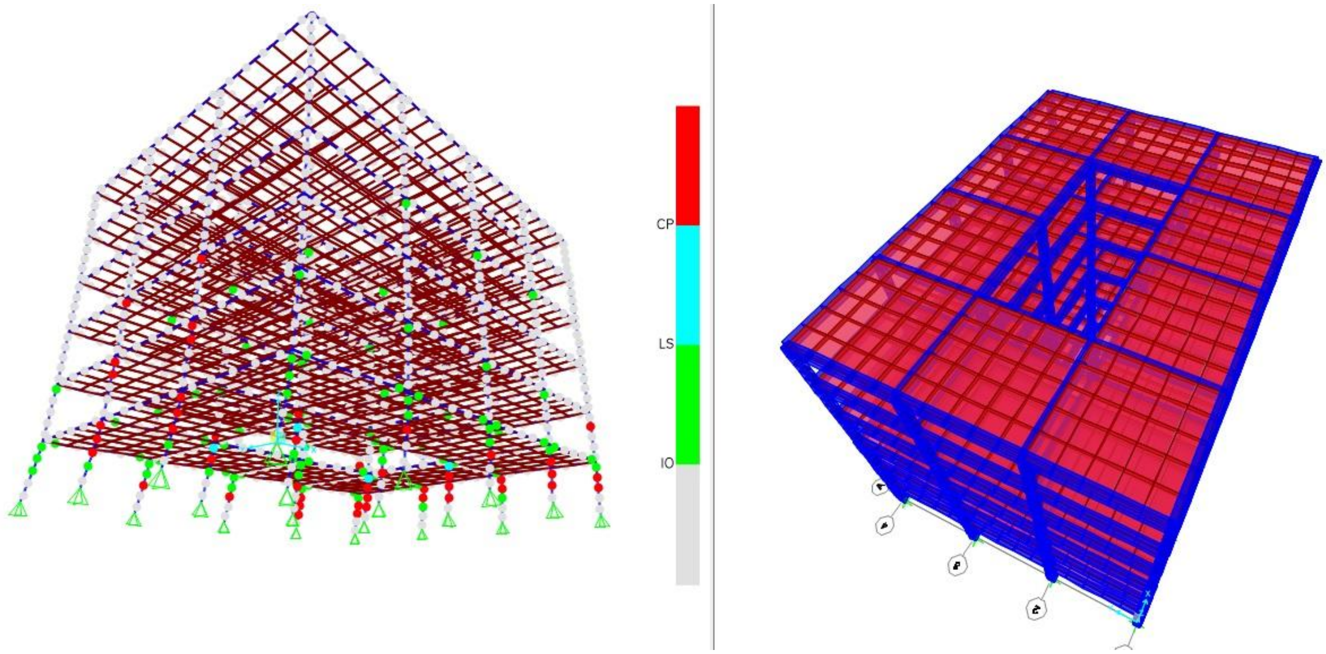

Figure 7.38 Plastic Hinge Distribution and Performance Levels of a Six-Story Frame (Trial 2) during Pushover Analysis(Failure).

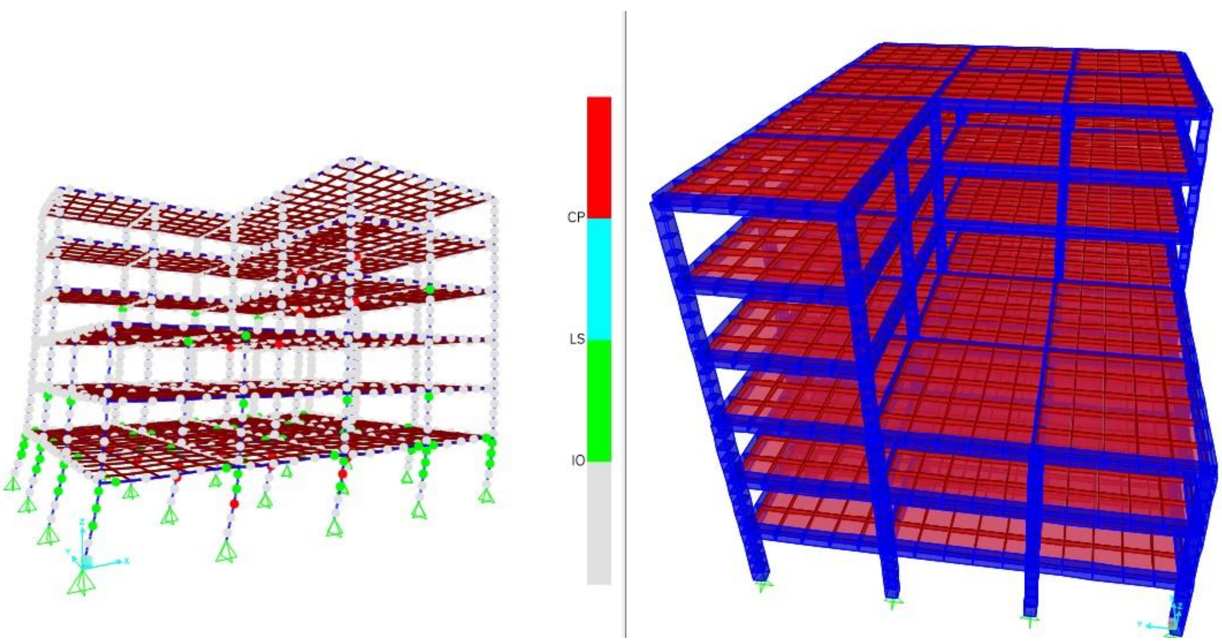

Figure 7.39 Plastic Hinge Distribution and Performance Levels of a Six-Story Frame (Trial 3) during Pushover Analysis(Failure).

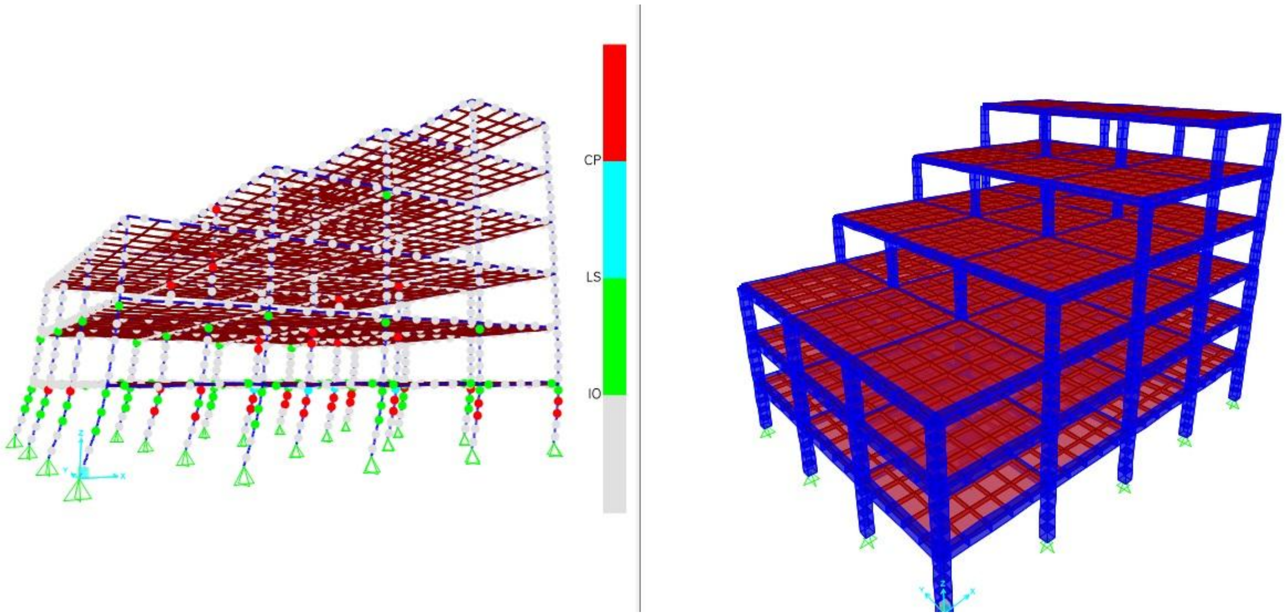

Figure 7.40 Plastic Hinge Distribution and Performance Levels of a Six-Story Frame (Trial 4) during Pushover Analysis(Failure).

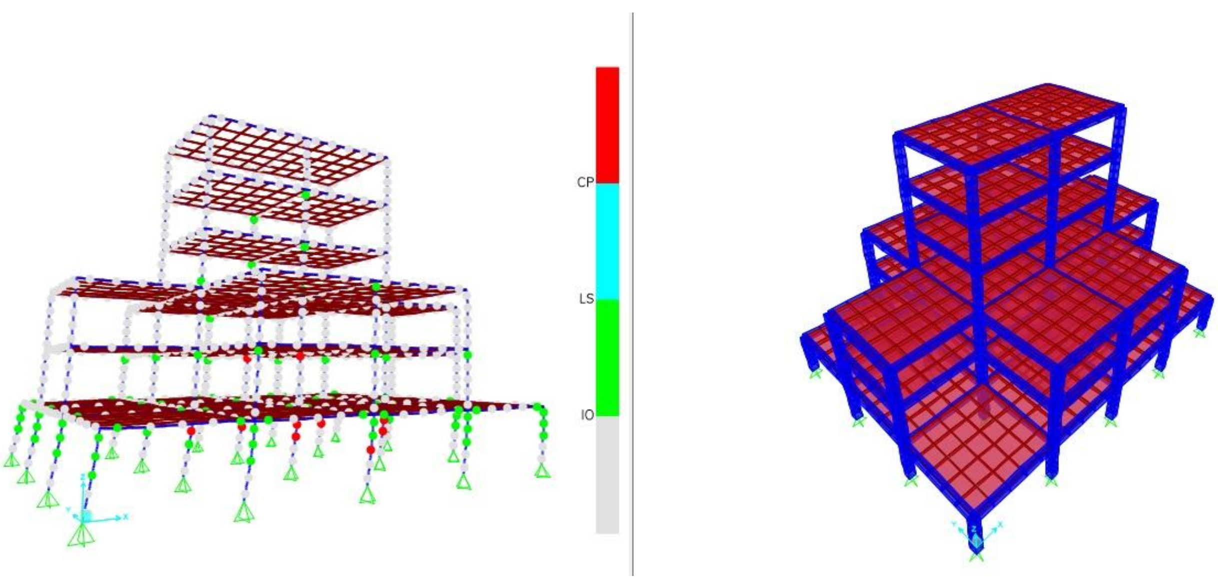

Figure 7.41 Plastic Hinge Distribution and Performance Levels of a Six-Story Frame (Trial 5) during Pushover Analysis(Failure).

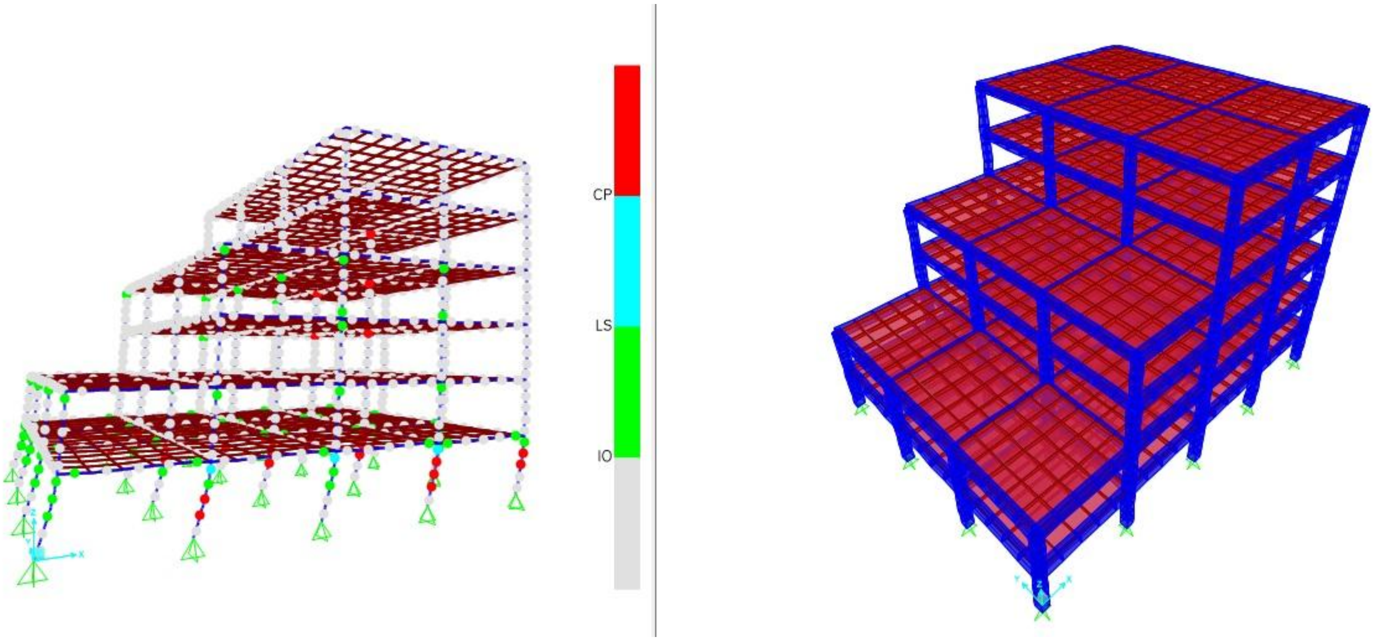

Figure 7.42 Plastic Hinge Distribution and Performance Levels of a Six-Story Frame (Trial 6) during Pushover Analysis(Failure).

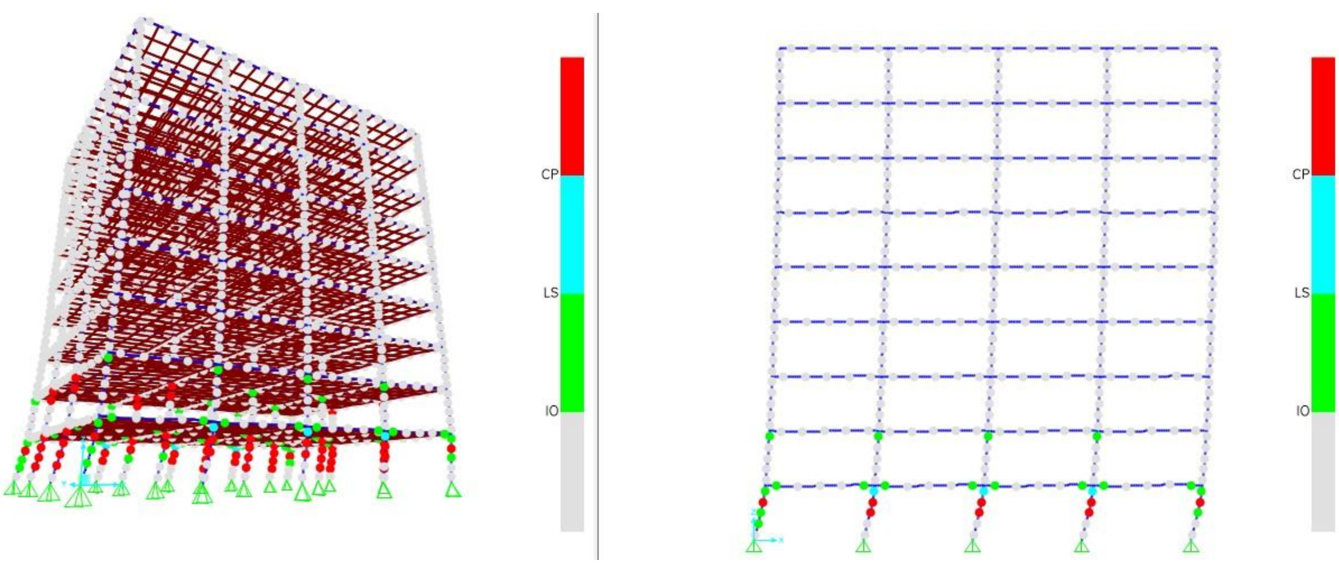

Figure 7.43 Plastic Hinge Distribution and Performance Levels of a 9-Story Frame with Column Sections 50 × 50 cm (Stories 1–5) and 40 × 40 cm (Stories 6–9) during Pushover Analysis(Failure).

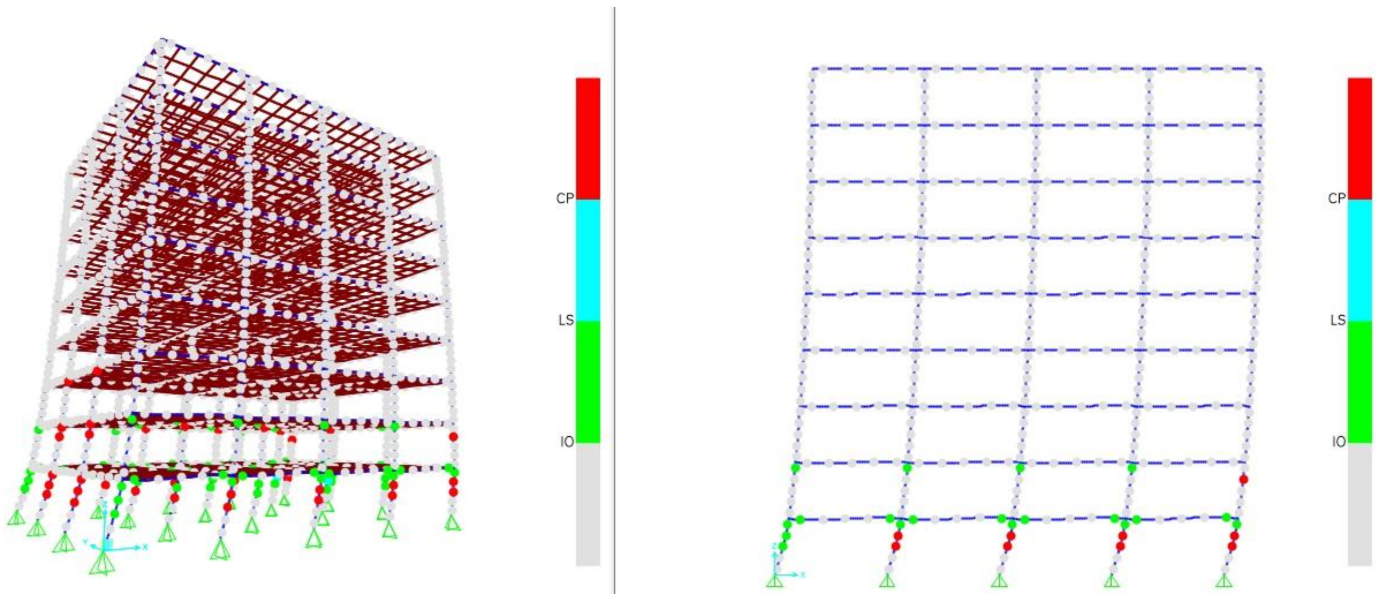

Figure 7.44 Plastic Hinge Distribution and Performance Levels of a 9-Story Frame with Column Sections 55 × 55 cm (Stories 1–5) and 45 × 45 cm (Stories 6–9) during Pushover Analysis(Failure).

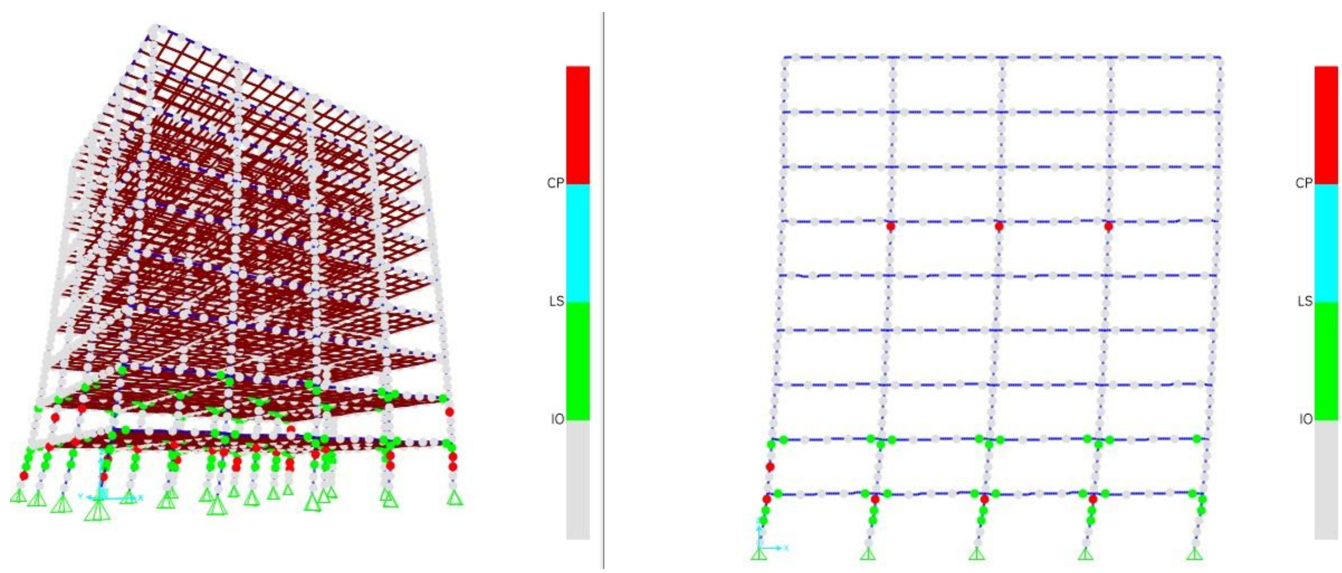

Figure 7.45 Plastic Hinge Distribution and Performance Levels of a 9-Story Frame with Column Sections 60 × 60 cm (Stories 1–5) and 50 × 50 cm (Stories 6–9) during Pushover Analysis(Failure).

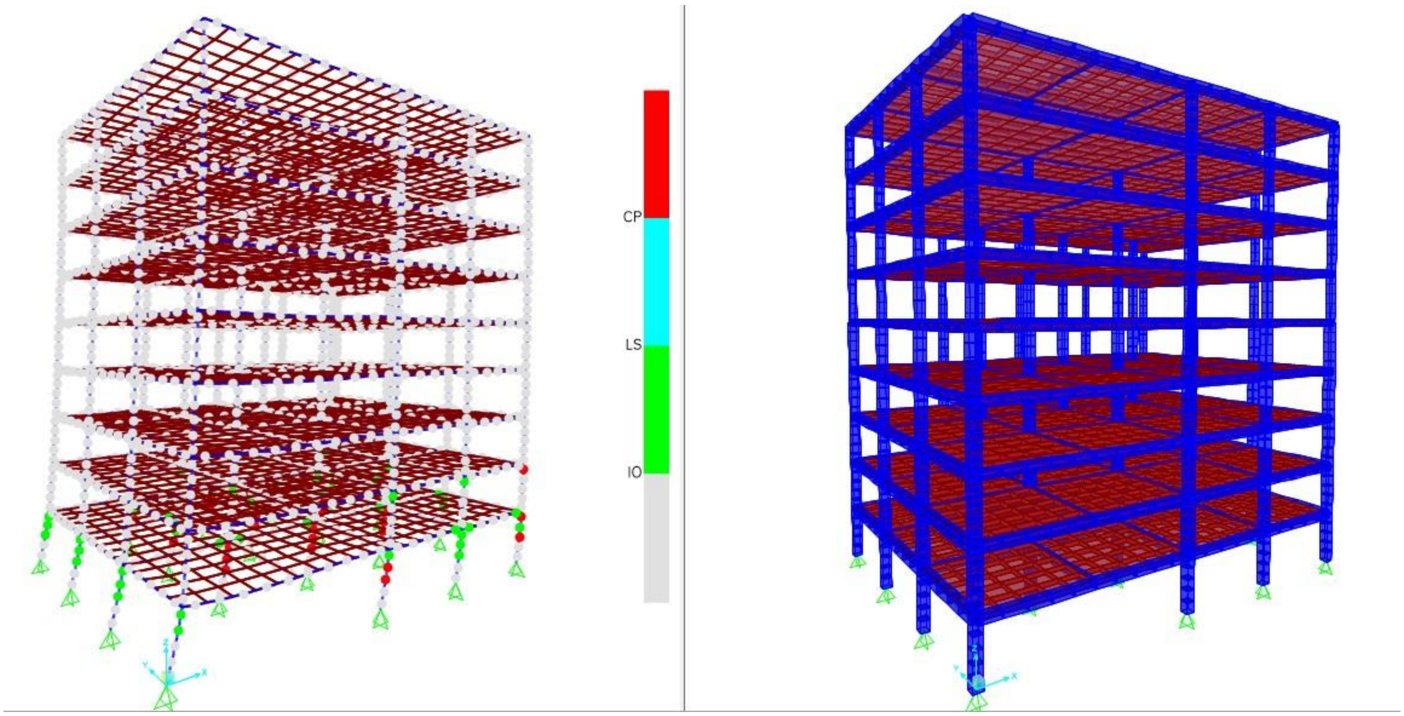

Figure 7.46 Plastic Hinge Distribution and Performance Levels of a Nine-Story Frame With Cut Column during Pushover Analysis(Failure).

CHAPTER 8 CONCLUSION

8.1 Conclusions

1. **The response modification factor (R) is not a constant property of Intermediate Moment Resisting Concrete Frames (IMRCFs)**, but rather a system-dependent parameter influenced by multiple interacting structural characteristics. The results clearly demonstrate that R is governed by the combined effects of stiffness distribution, ductility capacity, redundancy, detailing, and global structural configuration, rather than by building height alone.
2. **The pushover analysis approach proved effective in evaluating the nonlinear seismic behavior of IMRCFs**, particularly in capturing post-yield response, stiffness degradation, and energy dissipation mechanisms. The validation of SAP2000 nonlinear auto-hinge modeling against experimental results for both a two-span beam and a one-story concrete frame confirmed the reliability of SAP2000 as an analysis tool for reinforced concrete structures.
3. **Building height significantly influences seismic response**, as the estimated R-values generally increased with the number of stories (from one to nine stories). However, this trend was neither linear nor unconditional. The results indicate that increased height enhances energy dissipation capacity only when accompanied by an appropriate balance between stiffness and ductility. Excessive stiffness or poor detailing can counteract the beneficial effect of increased height.
4. **Column cross-sectional dimensions were found to have a dominant influence on global stiffness and seismic behavior**, particularly in mid- and high-rise buildings. For low-rise structures (one- and three-story frames), increasing column dimensions had a limited impact on R. In contrast, for nine-story buildings, increasing column sizes led to a noticeable reduction in R (from approximately 3.7 to 2.7), as excessive stiffness restricted inelastic deformation and reduced ductility demand.
5. **Vertical stiffness distribution plays a critical role in controlling seismic performance**, especially in taller buildings. Configurations with abrupt stiffness changes along the height—such as varying column sizes between lower and upper stories or removing a continuous column—resulted in significant reductions in both base shear capacity and R-value. The removal of a column along the full height of a nine-story building reduced R from 3.7 to 2.5 and decreased base shear from 7267.4 kN to 5328.3 kN, highlighting the importance of structural continuity and redundancy.

6. **Beam dimensions and stiffness contribution were shown to directly affect R-values when column properties were held constant**. Increasing beam cross-sections enhanced base shear capacity and improved energy dissipation, leading to higher R-values (up to approximately 4.2 in six-story buildings). This confirms that achieving a balanced beam–column stiffness ratio is essential for developing a favorable ductile mechanism.
7. **Reinforcement detailing, particularly transverse reinforcement (stirrup spacing), has a pronounced effect on ductility and R-value**. Reducing stirrup spacing from 12 cm to 6 cm significantly improved confinement, delayed stiffness degradation, and resulted in more uniform damage distribution. Consequently, frames with denser stirrup spacing exhibited higher effective R-values and more stable post-yield behavior.
8. **Longitudinal reinforcement ratios in columns exhibit an optimal range for seismic performance**. Moderate reinforcement ratios (approximately 2%) produced the highest and most stable R-values, while excessive reinforcement (around 4%) reduced R due to premature concrete crushing and limited ductility. This finding confirms that seismic efficiency is governed by ductility rather than strength alone.
9. **Comparative analysis between SAP2000 and ABAQUS highlighted the influence of modeling philosophy on pushover results**. While SAP2000 provides a code-calibrated and computationally efficient representation of nonlinear behavior, ABAQUS captures material-level nonlinearities, cracking, and stiffness degradation more realistically. ABAQUS consistently produced more conservative pushover curves and lower R-values, reinforcing its suitability for validation and detailed seismic behavior assessment.
10. **In all investigated cases (one-, three-, six-, and nine-story frames), the calculated R-values remained lower than the code-specified value of R = 5 for IMRCFs (ASCE 7-16)**. This suggests that the code value may represent an upper-bound assumption that may not be achieved in practice without optimized detailing, balanced stiffness distribution, and favorable inelastic mechanisms.
11. Overall, the findings of this study emphasize that **achieving higher R-values requires a holistic seismic design strategy**, integrating appropriate member sizing, controlled stiffness distribution, effective reinforcement detailing, and structural redundancy. Simply increasing member dimensions or strength does not guarantee improved seismic performance and may, in some cases, be detrimental.

8.2 Recommendation For Future Work

Although the present study provides valuable insight into the seismic behavior and response modification factor (R) of Intermediate Moment Resisting Concrete Frames (IMRCFs), several aspects warrant further investigation to enhance the generality and applicability of the findings.

1. **Advanced nonlinear modeling techniques** may be further explored by conducting a detailed comparison between the **auto-hinge approach based on ASCE 41 procedures in SAP2000** and the **fiber hinge modeling technique**. Such a comparison would allow for a deeper understanding of how different plasticity representations influence the load–displacement relationship, stiffness degradation, ductility demand, and the resulting R-values.
2. Future studies may extend the current modeling framework to **structures exceeding nine stories**, enabling the investigation of height-dependent effects in high-rise IMRCFs. This extension would help clarify whether the observed reduction in R-values with increasing stiffness persists in taller buildings and how optimal stiffness distribution can be achieved in high-rise applications.
3. The **influence of reinforcement ratios**, particularly longitudinal reinforcement in columns and transverse reinforcement detailing, deserves further attention. Systematic parametric studies could be conducted to identify optimal reinforcement ranges that maximize ductility and energy dissipation while avoiding over-reinforced and brittle behavior.
4. Additional research is recommended to examine the **relationship between the number of stories and the response modification factor**, with a focus on identifying critical height thresholds where the governing seismic response mechanisms shift from ductility-controlled to stiffness-dominated behavior.
5. The **effect of the number of bays and bay length in each direction** should be investigated in future work. Variations in bay configuration directly affect redundancy, stiffness distribution, and load transfer paths, all of which influence seismic performance and R-value estimation.
6. Comparative studies involving **different lateral force-resisting systems**, such as Ordinary Moment Resisting Frames (OMRFs), Special Moment Resisting Frames (SMRFs), and dual systems, are recommended. Such comparisons would provide a broader perspective on the adequacy of current code-prescribed R-values across different structural systems.

7. A **historical evaluation of moment-resisting concrete frames** may be performed by comparing the performance of existing or previously designed structures with results obtained from nonlinear pushover and advanced numerical analyses. This approach could help bridge the gap between theoretical modeling and observed structural behavior.
8. Further research should investigate **vertical and plan irregularities**, including mass irregularity, vertical geometric irregularity, in-plane discontinuity of lateral force-resisting elements, and weak-story behavior. Comprehensive numerical and experimental studies are needed to quantify their combined effects on ductility, energy dissipation capacity, and collapse probability.
9. Finally, advanced multidisciplinary studies are recommended to evaluate the **combined effects of seismic loading, wind loading, and fire exposure** on the seismic performance of high-rise IMRCFs, particularly for structures incorporating structural settlement or expansion joints. Such investigations would contribute to a more holistic understanding of structural resilience under extreme loading scenarios.

REFERENCES

- Ahmad, N., Sheheryar, K., Ali, Q., & Ashraf, M. (2021, February 15). Numerical modeling for nonlinear static pushover and response history analyses of Dhajji-Dewari structures. Journal of Earthquake Engineering, 26(10), 5338–5359. https://doi.org/10.1080/13632469.2021.1871680

- Abuznaid, H. A. (2023). Response modification factor in intermediate moment resisting frame building [Master's thesis, Palestine Polytechnic University].

- American Society of Civil Engineers. (2017). ASCE/SEI 7-16: Minimum design loads and associated criteria for buildings and other structures. ASCE.

- Applied Technology Council. (1995). Structural response modification factors. ATC.

- Athanassiadiou, C., Karakostas, C., Kappos, A. J., & Lekidis, V. (2004, August 6). Inelastic strength and displacement design spectra based on Greek earthquake records. In Proceedings of the 14th World Conference on Earthquake Engineering.

- Bathe, K. J. (1996). Finite element procedures. Prentice Hall.

- Bhende, A. G., & Mistry, K. R. (2021). Seismic performance evaluation of reinforced concrete moment resisting frames using pushover analysis. Journal of Building Engineering, 44, 102761. https://doi.org/10.1016/j.jobe.2021.102761

- Borzì, B., Calvi, G. M., Elnashai, A. S., Faccioli, E., & Bommer, J. J. (2008). Inelastic spectra for displacement-based seismic design. Engineering Structures, 30(8), 2070–2080.

-Borzì, B., & Elnashai, A. S. (2000). Inelastic displacement spectra and displacement reduction factors. In Proceedings of the 12th World Conference on Earthquake Engineering (12WCEE). Auckland, New Zealand.

- Castro, L. F., Castaño, H. A., Molina-Herrera, M., Morales, J., & Arroyo, O. (2024, July). Evaluating the response modification factor (R) for reinforced concrete and steel structures equipped with TADAS devices designed for high seismic hazard in Colombia. Structures, 65, 106748. https://doi.org/10.1016/j.istruc.2024.106748

- Causevic, M., & Mitrovic, S. (2011). Comparison between non-linear dynamic and static seismic analysis of structures according to European and US provisions. Bulletin of Earthquake Engineering, 9(2), 467–489. https://doi.org/10.1007/s10518-010-9199-1.

- Chao, S.-H., Goel, S. C., & Lee, S.-S. (2007). A seismic design lateral force distribution based on inelastic state of structures. Earthquake Spectra, 23(3), 547–569. https://doi.org/10.1193/1.2740332

- **C**hopra, A. K., & Goel, R. K. (1999). Capacity-demand-diagram methods for estimating seismic deformation of inelastic structures: SDF systems. Report No. PEER-1999/02, Pacific Earthquake Engineering Research Center, University of California, Berkeley.

- Chopra, A. K. (2004). A modal pushover analysis procedure to estimate seismic demands for unsymmetric-plan buildings: Theory and preliminary evaluation. Earthquake Engineering & Structural Dynamics, 33(7), 903–927.

- Comartin, C. D., Aschheim, M., Guyader, A., Hamburger, R., Hanson, R., Holmes, W., Iwan, W., Mahoney, M., Miranda, E., Moehle, J., Rojahn, C., & Stewart, J. (2004). A summary of FEMA 440: Improvement of nonlinear static seismic analysis procedures. Earthquake Spectra, 20(1), 241–261.

- Duddeck, H., König, G., & Müller, H. S. (1976). Experimental investigations on reinforced concrete beams with end continuity. Technical report, Institute of Concrete Structures, University of Stuttgart.

- Earthquake Engineering Research Center. (1997). The EERC–CUREe symposium in honor of Vitelmo V. Bertero. University of California, Berkeley.

https://nehrpsearch.nist.gov/static/files/NSF/PB97186795.pdf

- **E**lnashai, A. S., & Mwafy, A. M. (2002). Overstrength and force reduction factors of multistorey reinforced-concrete buildings. The Structural Design of Tall Buildings, 11(5), 329–351. https://doi.org/10.1002/tal.200

- European-Mediterranean Seismological Centre (EMSC). (n.d.). Earthquake information and monitoring. Retrieved January 2026, from https://www.emsc.eu/

- European Committee for Standardization. (2005). Eurocode 8: Design of structures for earthquake resistance—Part 1: General rules, seismic actions and rules for buildings (EN 1998-1). CEN. https://www.confinedmasonry.org/wp-content/uploads/2009/09/Eurocode-8-1-Earthquakes-general.pdf

- Federal Emergency Management Agency (FEMA). (2005). *Improvement of nonlinear static seismic analysis procedures (FEMA 440)*. https://mitigation.eeri.org/wp-content/uploads/fema-440.pdf.

- Golestani, M., Rajabi, A., & Rajabi Soheyli, A. (2023). *Seismic performance evaluation of reinforced concrete buildings using pushover analysis: Identification of failure mechanisms and mode shapes*. Journal of Structural Engineering and Mechanics, 85(4), 321–33 https://doi.org/10.12989/SEM.2023.85.4.321

- Hakim, R. A., & Al-Safi, M. (2012). Seismic performance evaluation of reinforced concrete frame buildings using pushover analysis. International Journal of Civil and Structural Engineering, 3(1), 45–60.

- Hognestad, E. (1951). A study of combined bending and axial load in reinforced concrete members. Bulletin No. 399, University of Illinois Engineering Experiment Station.

- Humar, J. L., & Rahgozar, M. A. (1996). Concept of overstrength in seismic design. Canadian Journal of Civil Engineering, 23(1), 1–15. https://doi.org/10.1139/l96-001

- Hussein, M., Gamal, M., & Attia, W. (2021). Seismic response modification factor for RC frames with non-uniform dimensions. Civil & Environmental Engineering. https://doi.org/10.1080/23311916.2021.1923363

-International Conference of Building Officials. (1997). Uniform Building Code (1997 ed.). ICBO.

- Ismail, A. (2013, July 25). Nonlinear static analysis of a retrofitted reinforced concrete building. HBRC Journal, 1(1). https:// doi:10.1016/j.hbrcj.2013.07.002

- Kent, D. C., & Park, R. (1971). Flexural members with confined concrete. Journal of the Structural Division, ASCE, 97(ST7), 1969–1990.

-Kim, J., & Choi, H. (2005). Response modification factors of steel moment-resisting frames. Journal of Constructional Steel Research, 61(12), 1658–1673. https://doi.org/10.1016/j.jcsr.2005.06.003

- Kuria, K. K., & Kegyes-Brassai, O. K. (2023). Nonlinear static analysis for seismic evaluation of existing RC hospital building. Applied Sciences, 13(21), 11626. https://doi.org/10.3390/app132111626

-Mander, J. B., Priestley, M. J. N., & Park, R. (1988a). Theoretical stress–strain model for confined concrete. Journal of Structural Engineering, ASCE, 114(8), 1804–1826.

- Massone, L. M., Orakcal, K., Wallace, J. W., & Bonelli, P. (2012). Observed seismic performance of reinforced concrete buildings with shear walls. Earthquake Spectra, 28(4), 1421–1444. https://doi.org/10.1193/1.4000084

- Massena, B., Bento, R., Degée, H., & Candeias, P. (2015). Direct displacement-based design for RC structures: Procedure, advantages and shortcomings. Engineering Structures, 98, 65–77.

- Mortezaei, A., & Ronagh, H. R. (2013). Effectiveness of modified pushover analysis procedure for the estimation of seismic demands of buildings subjected to near-fault ground motions having fling step. Natural Hazards and Earth System Sciences, 13, 1579–1593. https://doi.org/10.5194/nhess-13-1579-2013.

- Müller, H. S. (1977). Documentation and evaluation of experimental tests on continuous reinforced concrete beams. Institute of Concrete Structures, University of Stuttgart.

- Nassar, D. I. A. K. (2023). Effect of the Building Aspect Ratio on the Response Modification Factor (R) of Reinforced Concrete Buildings. Master's Thesis, An-Najah National University, Nablus, Palestine.

- National Research Council of Canada (NRC). (2010). National building code of Canada (NBCC 2010). Ottawa, ON: NRC.

- Newmark, N. M., & Hall, W. J. (1970). Earthquake spectra and design. Earthquake Engineering Research Center, University of California, Berkeley.

- Newmark, N. M., & Hall, W. J. (1982). Earthquake spectra and design. Earthquake Engineering Research Institute.

- Paulay, T., & Priestley, M. J. N. (1992). Seismic design of reinforced concrete and masonry buildings. John Wiley & Sons.

- Popovics, S. (1973). A numerical approach to the complete stress–strain curve of concrete. Cement and Concrete Research, 3(5), 583–599.

- Sharma, A., Tripathi, R. K., & Bhat, G. (2016). Comparative performance evaluation of RC frame structures using direct displacement-based design method and force-based design method. Engineering Structures, 123, 1–15.

- Sharma, A., Tripathi, R. K., & Bhat, G. (2020). Comparative performance evaluation of RC frame structures using direct displacement-based design method and force-based design method. Asian Journal of Civil Engineering, 21(3), 381–394. https://doi.org/10.1007/s42107-019-00198-y

- Sherstobitoff, J., Ventura, C. E., & Prion, H. (2008, November). Nonlinear dynamic analysis procedures for performance-based seismic design. Proceedings of a seismic engineering conference.

Shroof, M. (2025). Response modification factor in intermediate moment resisting frame building [Master's thesis, Palestine Polytechnic University].

- Thermou, G. E., & Elnashai, A. S. (2006). Seismic retrofit schemes for RC structures and local-global consequences. Progress in Structural Engineering and Materials, 8(1), 1–15. https://doi.org/10.1002/pse.208

- Uang, C. M. (1991). Establishing R (or Rw) and C_d factors for building seismic provisions. Journal of Structural Engineering, 117(1), 19–28. https://doi.org/10.1061/(ASCE)0733-9445(1991)117:1(19)

- Ugalde, D., & Lopez-Garcia, D. (2017). Seismic behavior of reinforced concrete wall buildings subjected to strong ground motions. Engineering Structures, 150, 174–189. https://doi.org/10.1016/j.engstruct.2017.07.024

- Wang, J., & Kusunoki, K. (Year). An effective beam width model of slab in thick wall–thick slab joints subjected to lateral forces. Journal Name, Volume(Issue), pages.

- Xiao, J., Sun, Y., & Falkner, H. (2006). Seismic performance of frame structures with recycled aggregate concrete. Engineering Structures, 28(1), 1–8. https://doi.org/10.1016/j.engstruct.2005.06.019

-Yurizka, H., & Rosyidah, A. (2020). The performance of irregular building structures using pushover analysis. Logic: Jurnal Rancang Bangun dan Teknologi, 20(2), 65–72. https://doi.org/10.31940/logic.v20i2.1456

APPENDIX

Table 0.1 Concrete Column Design Summary - ACI 318-14

Label	DesignSect	DimSect (mm)	ColSect (mm²)	AsMin (mm²)	As (mm²)	% As	Diameter	Area	VMajRebar(mm²/m)
Story6									
C1	COLUMN B	400X400	160000	1600	1882	1	16	201	333.33
C1	COLUMN B	400X400	160000	1600	1600	1	16	201	333.33

C1	COLUMN B	400X400	160000	1600	3169	2	16	201	333.33
C2	COLUMN B	400X400	160000	1600	2453	2	16	201	333.33
C2	COLUMN B	400X400	160000	1600	1600	1	16	201	333.33
C2	COLUMN B	400X400	160000	1600	3426	2	16	201	333.33
C3	COLUMN B	400X400	160000	1600	2389	1	16	201	333.33
C3	COLUMN B	400X400	160000	1600	1600	1	16	201	333.33
C3	COLUMN B	400X400	160000	1600	3264	2	16	201	333.33
C4	COLUMN B	400X400	160000	1600	2453	2	16	201	333.33
C4	COLUMN B	400X400	160000	1600	1600	1	16	201	333.33
C4	COLUMN B	400X400	160000	1600	3426	2	16	201	333.33
C5	COLUMN B	400X400	160000	1600	1882	1	16	201	333.33
C5	COLUMN B	400X400	160000	1600	1600	1	16	201	333.33
C5	COLUMN B	400X400	160000	1600	3169	2	16	201	333.33
C6	COLUMN B	400X400	160000	1600	2512	2	16	201	486.01
C6	COLUMN B	400X400	160000	1600	1600	1	16	201	492.82
C6	COLUMN B	400X400	160000	1600	3584	2	16	201	499.63
C8	COLUMN B	400X400	160000	1600	1882	1	16	201	333.33
C8	COLUMN B	400X400	160000	1600	1600	1	16	201	333.33
C8	COLUMN B	400X400	160000	1600	3169	2	16	201	333.33
C9	COLUMN B	400X400	160000	1600	2453	2	16	201	333.33
C9	COLUMN B	400X400	160000	1600	1600	1	16	201	333.33
C9	COLUMN B	400X400	160000	1600	3426	2	16	201	333.33
C10	COLUMN B	400X400	160000	1600	1600	1	16	201	333.33
C10	COLUMN B	400X400	160000	1600	1600	1	16	201	333.33

C10	COLUMN B	400X400	160000	1600	1600	1	16	201	333.33
C11	COLUMN B	400X400	160000	1600	1600	1	16	201	333.33
C11	COLUMN B	400X400	160000	1600	1600	1	16	201	333.33
C11	COLUMN B	400X400	160000	1600	1600	1	16	201	333.33
C12	COLUMN B	400X400	160000	1600	1600	1	16	201	333.33
C12	COLUMN B	400X400	160000	1600	1600	1	16	201	333.33
C12	COLUMN B	400X400	160000	1600	1600	1	16	201	333.33
C13	COLUMN B	400X400	160000	1600	1600	1	16	201	333.33
C13	COLUMN B	400X400	160000	1600	1600	1	16	201	333.33
C13	COLUMN B	400X400	160000	1600	1600	1	16	201	333.33
C14	COLUMN B	400X400	160000	1600	2389	1	16	201	333.33
C14	COLUMN B	400X400	160000	1600	1600	1	16	201	333.33
C14	COLUMN B	400X400	160000	1600	3264	2	16	201	333.33
C15	COLUMN B	400X400	160000	1600	2453	2	16	201	333.33
C15	COLUMN B	400X400	160000	1600	1600	1	16	201	333.33
C15	COLUMN B	400X400	160000	1600	3426	2	16	201	333.33
C16	COLUMN B	400X400	160000	1600	1600	1	16	201	333.33
C16	COLUMN B	400X400	160000	1600	1600	1	16	201	333.33
C16	COLUMN B	400X400	160000	1600	1600	1	16	201	333.33
C17	COLUMN B	400X400	160000	1600	1600	1	16	201	333.33
C17	COLUMN B	400X400	160000	1600	1600	1	16	201	333.33
C17	COLUMN B	400X400	160000	1600	1600	1	16	201	333.33
C18	COLUMN B	400X400	160000	1600	2512	2	16	201	486.01
C18	COLUMN B	400X400	160000	1600	1600	1	16	201	492.82

C18	COLUMN B	400X400	160000	1600	3584	2	16	201	499.63
C19	COLUMN B	400X400	160000	1600	2512	2	16	201	486.01
C19	COLUMN B	400X400	160000	1600	1600	1	16	201	492.82
C19	COLUMN B	400X400	160000	1600	3584	2	16	201	499.63
C20	COLUMN B	400X400	160000	1600	1882	1	16	201	333.33
C20	COLUMN B	400X400	160000	1600	1600	1	16	201	333.33
C20	COLUMN B	400X400	160000	1600	3169	2	16	201	333.33
C21	COLUMN B	400X400	160000	1600	2512	2	16	201	486.01
C21	COLUMN B	400X400	160000	1600	1600	1	16	201	492.82
C21	COLUMN B	400X400	160000	1600	3584	2	16	201	499.63
Story5									
C1	COLUMN B	400X400	160000	1600	2075	1	16	201	333.33
C1	COLUMN B	400X400	160000	1600	1600	1	16	201	333.33
C1	COLUMN B	400X400	160000	1600	1653	1	16	201	333.33
C2	COLUMN B	400X400	160000	1600	3661	2	16	201	333.33
C2	COLUMN B	400X400	160000	1600	1600	1	16	201	333.33
C2	COLUMN B	400X400	160000	1600	2221	1	16	201	333.33
C3	COLUMN B	400X400	160000	1600	3275	2	16	201	333.33
C3	COLUMN B	400X400	160000	1600	1600	1	16	201	333.33
C3	COLUMN B	400X400	160000	1600	2189	1	16	201	333.33
C4	COLUMN B	400X400	160000	1600	3661	2	16	201	333.33
C4	COLUMN B	400X400	160000	1600	1600	1	16	201	333.33
C4	COLUMN B	400X400	160000	1600	2221	1	16	201	333.33
C5	COLUMN B	400X400	160000	1600	2075	1	16	201	333.33
C5	COLUMN B	400X400	160000	1600	1600	1	16	201	333.33

C5	COLUMN B	400X400	160000	1600	1653	1	16	201	333.33
C6	COLUMN B	400X400	160000	1600	3900	2	16	201	333.33
C6	COLUMN B	400X400	160000	1600	1600	1	16	201	333.33
C6	COLUMN B	400X400	160000	1600	2407	2	16	201	333.33
C8	COLUMN B	400X400	160000	1600	2075	1	16	201	333.33
C8	COLUMN B	400X400	160000	1600	1600	1	16	201	333.33
C8	COLUMN B	400X400	160000	1600	1653	1	16	201	333.33
C9	COLUMN B	400X400	160000	1600	3661	2	16	201	333.33
C9	COLUMN B	400X400	160000	1600	1600	1	16	201	333.33
C9	COLUMN B	400X400	160000	1600	2221	1	16	201	333.33
C10	COLUMN B	400X400	160000	1600	1600	1	16	201	333.33
C10	COLUMN B	400X400	160000	1600	1600	1	16	201	333.33
C10	COLUMN B	400X400	160000	1600	2215	1	16	201	333.33
C11	COLUMN B	400X400	160000	1600	1600	1	16	201	333.33
C11	COLUMN B	400X400	160000	1600	1600	1	16	201	333.33
C11	COLUMN B	400X400	160000	1600	2215	1	16	201	333.33
C12	COLUMN B	400X400	160000	1600	1600	1	16	201	333.33
C12	COLUMN B	400X400	160000	1600	1600	1	16	201	333.33
C12	COLUMN B	400X400	160000	1600	2182	1	16	201	333.33
C13	COLUMN B	400X400	160000	1600	1600	1	16	201	333.33
C13	COLUMN B	400X400	160000	1600	1600	1	16	201	333.33
C13	COLUMN B	400X400	160000	1600	2182	1	16	201	333.33
C14	COLUMN B	400X400	160000	1600	3275	2	16	201	333.33
C14	COLUMN B	400X400	160000	1600	1600	1	16	201	333.33

C14	COLUMN B	400X400	160000	1600	2189	1	16	201	333.33
C15	COLUMN B	400X400	160000	1600	3661	2	16	201	333.33
C15	COLUMN B	400X400	160000	1600	1600	1	16	201	333.33
C15	COLUMN B	400X400	160000	1600	2221	1	16	201	333.33
C16	COLUMN B	400X400	160000	1600	1600	1	16	201	333.33
C16	COLUMN B	400X400	160000	1600	1600	1	16	201	333.33
C16	COLUMN B	400X400	160000	1600	2215	1	16	201	333.33
C17	COLUMN B	400X400	160000	1600	1600	1	16	201	333.33
C17	COLUMN B	400X400	160000	1600	1600	1	16	201	333.33
C17	COLUMN B	400X400	160000	1600	2215	1	16	201	333.33
C18	COLUMN B	400X400	160000	1600	3900	2	16	201	333.33
C18	COLUMN B	400X400	160000	1600	1600	1	16	201	333.33
C18	COLUMN B	400X400	160000	1600	2407	2	16	201	333.33
C19	COLUMN B	400X400	160000	1600	3900	2	16	201	333.33
C19	COLUMN B	400X400	160000	1600	1600	1	16	201	333.33
C19	COLUMN B	400X400	160000	1600	2407	2	16	201	333.33
C20	COLUMN B	400X400	160000	1600	2075	1	16	201	333.33
C20	COLUMN B	400X400	160000	1600	1600	1	16	201	333.33
C20	COLUMN B	400X400	160000	1600	1653	1	16	201	333.33
C21	COLUMN B	400X400	160000	1600	3900	2	16	201	333.33
C21	COLUMN B	400X400	160000	1600	1600	1	16	201	333.33
C21	COLUMN B	400X400	160000	1600	2407	2	16	201	333.33
Story4									
C1	COLUMN B	400X400	160000	1600	2332	1	16	201	333.33
C1	COLUMN B	400X400	160000	1600	1600	1	16	201	333.33

C1	COLUMN B	400X400	160000	1600	2620	2	16	201	333.33
C2	COLUMN B	400X400	160000	1600	4520	3	16	201	333.33
C2	COLUMN B	400X400	160000	1600	1600	1	16	201	333.33
C2	COLUMN B	400X400	160000	1600	4445	3	16	201	333.33
C3	COLUMN B	400X400	160000	1600	4211	3	16	201	333.33
C3	COLUMN B	400X400	160000	1600	1600	1	16	201	333.33
C3	COLUMN B	400X400	160000	1600	4366	3	16	201	333.33
C4	COLUMN B	400X400	160000	1600	4520	3	16	201	333.33
C4	COLUMN B	400X400	160000	1600	1600	1	16	201	333.33
C4	COLUMN B	400X400	160000	1600	4445	3	16	201	333.33
C5	COLUMN B	400X400	160000	1600	2332	1	16	201	333.33
C5	COLUMN B	400X400	160000	1600	1600	1	16	201	333.33
C5	COLUMN B	400X400	160000	1600	2620	2	16	201	333.33
C6	COLUMN B	400X400	160000	1600	4674	3	16	201	333.33
C6	COLUMN B	400X400	160000	1600	1600	1	16	201	333.33
C6	COLUMN B	400X400	160000	1600	4654	3	16	201	333.33
C8	COLUMN B	400X400	160000	1600	2332	1	16	201	333.33
C8	COLUMN B	400X400	160000	1600	1600	1	16	201	333.33
C8	COLUMN B	400X400	160000	1600	2620	2	16	201	333.33
C9	COLUMN B	400X400	160000	1600	4520	3	16	201	333.33
C9	COLUMN B	400X400	160000	1600	1600	1	16	201	333.33
C9	COLUMN B	400X400	160000	1600	4445	3	16	201	333.33
C10	COLUMN B	400X400	160000	1600	6041	4	16	201	333.33
C10	COLUMN B	400X400	160000	1600	1600	1	16	201	333.33

C10	COLUMN B	400X400	160000	1600	6616	4	16	201	333.33
C11	COLUMN B	400X400	160000	1600	6041	4	16	201	333.33
C11	COLUMN B	400X400	160000	1600	1600	1	16	201	333.33
C11	COLUMN B	400X400	160000	1600	6616	4	16	201	333.33
C12	COLUMN B	400X400	160000	1600	5881	4	16	201	333.33
C12	COLUMN B	400X400	160000	1600	1600	1	16	201	333.33
C12	COLUMN B	400X400	160000	1600	6472	4	16	201	333.33
C13	COLUMN B	400X400	160000	1600	5881	4	16	201	333.33
C13	COLUMN B	400X400	160000	1600	1600	1	16	201	333.33
C13	COLUMN B	400X400	160000	1600	6472	4	16	201	333.33
C14	COLUMN B	400X400	160000	1600	4211	3	16	201	333.33
C14	COLUMN B	400X400	160000	1600	1600	1	16	201	333.33
C14	COLUMN B	400X400	160000	1600	4366	3	16	201	333.33
C15	COLUMN B	400X400	160000	1600	4520	3	16	201	333.33
C15	COLUMN B	400X400	160000	1600	1600	1	16	201	333.33
C15	COLUMN B	400X400	160000	1600	4445	3	16	201	333.33
C16	COLUMN B	400X400	160000	1600	6041	4	16	201	333.33
C16	COLUMN B	400X400	160000	1600	1600	1	16	201	333.33
C16	COLUMN B	400X400	160000	1600	6616	4	16	201	333.33
C17	COLUMN B	400X400	160000	1600	6041	4	16	201	333.33
C17	COLUMN B	400X400	160000	1600	1600	1	16	201	333.33
C17	COLUMN B	400X400	160000	1600	6616	4	16	201	333.33
C18	COLUMN B	400X400	160000	1600	4674	3	16	201	333.33
C18	COLUMN B	400X400	160000	1600	1600	1	16	201	333.33

C18	COLUMN B	400X400	160000	1600	4654	3	16	201	333.33
C19	COLUMN B	400X400	160000	1600	4674	3	16	201	333.33
C19	COLUMN B	400X400	160000	1600	1600	1	16	201	333.33
C19	COLUMN B	400X400	160000	1600	4654	3	16	201	333.33
C20	COLUMN B	400X400	160000	1600	2332	1	16	201	333.33
C20	COLUMN B	400X400	160000	1600	1600	1	16	201	333.33
C20	COLUMN B	400X400	160000	1600	2620	2	16	201	333.33
C21	COLUMN B	400X400	160000	1600	4674	3	16	201	333.33
C21	COLUMN B	400X400	160000	1600	1600	1	16	201	333.33
C21	COLUMN B	400X400	160000	1600	4654	3	16	201	333.33
Story3									
C1	column A	550X500	275000	2750	2750	1	16	201	416.67
C1	column A	550X500	275000	2750	2750	1	16	201	416.67
C1	column A	550X500	275000	2750	2750	1	16	201	416.67
C2	column A	550X500	275000	2750	2750	1	16	201	416.67
C2	column A	550X500	275000	2750	2750	1	16	201	416.67
C2	column A	550X500	275000	2750	2750	1	16	201	416.67
C3	column A	550X500	275000	2750	2750	1	16	201	416.67
C3	column A	550X500	275000	2750	2750	1	16	201	416.67
C3	column A	550X500	275000	2750	2750	1	16	201	416.67
C4	column A	550X500	275000	2750	2750	1	16	201	416.67
C4	column A	550X500	275000	2750	2750	1	16	201	416.67
C4	column A	550X500	275000	2750	2750	1	16	201	416.67
C5	column A	550X500	275000	2750	2750	1	16	201	416.67
C5	column A	550X500	275000	2750	2750	1	16	201	416.67
C5	column A	550X500	275000	2750	2750	1	16	201	416.67
C6	column A	550X500	275000	2750	2750	1	16	201	416.67
C6	column A	550X500	275000	2750	2750	1	16	201	416.67
C6	column A	550X500	275000	2750	2750	1	16	201	416.67
C8	column A	550X500	275000	2750	2750	1	16	201	416.67
C8	column A	550X500	275000	2750	2750	1	16	201	416.67
C8	column A	550X500	275000	2750	2750	1	16	201	416.67
C9	column A	550X500	275000	2750	2750	1	16	201	416.67
C9	column A	550X500	275000	2750	2750	1	16	201	416.67
C9	column A	550X500	275000	2750	2750	1	16	201	416.67
C10	column A	550X500	275000	2750	2750	1	16	201	416.67
C10	column A	550X500	275000	2750	2750	1	16	201	416.67
C10	column A	550X500	275000	2750	2750	1	16	201	416.67

C11	column A	550X500	275000	2750	2750	1	16	201	416.67
C11	column A	550X500	275000	2750	2750	1	16	201	416.67
C11	column A	550X500	275000	2750	2750	1	16	201	416.67
C12	column A	550X500	275000	2750	2750	1	16	201	416.67
C12	column A	550X500	275000	2750	2750	1	16	201	416.67
C12	column A	550X500	275000	2750	2750	1	16	201	416.67
C13	column A	550X500	275000	2750	2750	1	16	201	416.67
C13	column A	550X500	275000	2750	2750	1	16	201	416.67
C13	column A	550X500	275000	2750	2750	1	16	201	416.67
C14	column A	550X500	275000	2750	2750	1	16	201	416.67
C14	column A	550X500	275000	2750	2750	1	16	201	416.67
C14	column A	550X500	275000	2750	2750	1	16	201	416.67
C15	column A	550X500	275000	2750	2750	1	16	201	416.67
C15	column A	550X500	275000	2750	2750	1	16	201	416.67
C15	column A	550X500	275000	2750	2750	1	16	201	416.67
C16	column A	550X500	275000	2750	2750	1	16	201	416.67
C16	column A	550X500	275000	2750	2750	1	16	201	416.67
C16	column A	550X500	275000	2750	2750	1	16	201	416.67
C17	column A	550X500	275000	2750	2750	1	16	201	416.67
C17	column A	550X500	275000	2750	2750	1	16	201	416.67
C17	column A	550X500	275000	2750	2750	1	16	201	416.67
C18	column A	550X500	275000	2750	2750	1	16	201	416.67
C18	column A	550X500	275000	2750	2750	1	16	201	416.67
C18	column A	550X500	275000	2750	2750	1	16	201	416.67
C19	column A	550X500	275000	2750	2750	1	16	201	416.67
C19	column A	550X500	275000	2750	2750	1	16	201	416.67
C19	column A	550X500	275000	2750	2750	1	16	201	416.67
C20	column A	550X500	275000	2750	2750	1	16	201	416.67
C20	column A	550X500	275000	2750	2750	1	16	201	416.67
C20	column A	550X500	275000	2750	2750	1	16	201	416.67
C21	column A	550X500	275000	2750	2750	1	16	201	416.67
C21	column A	550X500	275000	2750	2750	1	16	201	416.67
C21	column A	550X500	275000	2750	2750	1	16	201	416.67
Story2									
C1	column A	550X500	275000	2750	2750	1	16	201	416.67
C1	column A	550X500	275000	2750	2750	1	16	201	416.67
C1	column A	550X500	275000	2750	2750	1	16	201	416.67
C2	column A	550X500	275000	2750	2750	1	16	201	416.67
C2	column A	550X500	275000	2750	2750	1	16	201	416.67
C2	column A	550X500	275000	2750	2750	1	16	201	416.67
C3	column A	550X500	275000	2750	2750	1	16	201	416.67
C3	column A	550X500	275000	2750	2750	1	16	201	416.67
C3	column A	550X500	275000	2750	2750	1	16	201	416.67
C4	column A	550X500	275000	2750	2750	1	16	201	416.67
C4	column A	550X500	275000	2750	2750	1	16	201	416.67
C4	column A	550X500	275000	2750	2750	1	16	201	416.67
C5	column A	550X500	275000	2750	2750	1	16	201	416.67
C5	column A	550X500	275000	2750	2750	1	16	201	416.67

C5	column A	550X500	275000	2750	2750	1	16	201	416.67
C6	column A	550X500	275000	2750	2750	1	16	201	416.67
C6	column A	550X500	275000	2750	2750	1	16	201	416.67
C6	column A	550X500	275000	2750	2750	1	16	201	416.67
C8	column A	550X500	275000	2750	2750	1	16	201	416.67
C8	column A	550X500	275000	2750	2750	1	16	201	416.67
C8	column A	550X500	275000	2750	2750	1	16	201	416.67
C9	column A	550X500	275000	2750	2750	1	16	201	416.67
C9	column A	550X500	275000	2750	2750	1	16	201	416.67
C9	column A	550X500	275000	2750	2750	1	16	201	416.67
C10	column A	550X500	275000	2750	4132	2	16	201	416.67
C10	column A	550X500	275000	2750	2750	1	16	201	416.67
C10	column A	550X500	275000	2750	6922	3	16	201	416.67
C11	column A	550X500	275000	2750	4132	2	16	201	416.67
C11	column A	550X500	275000	2750	2750	1	16	201	416.67
C11	column A	550X500	275000	2750	6922	3	16	201	416.67
C12	column A	550X500	275000	2750	3811	1	16	201	416.67
C12	column A	550X500	275000	2750	2750	1	16	201	416.67
C12	column A	550X500	275000	2750	6677	2	16	201	416.67
C13	column A	550X500	275000	2750	3811	1	16	201	416.67
C13	column A	550X500	275000	2750	2750	1	16	201	416.67
C13	column A	550X500	275000	2750	6677	2	16	201	416.67
C14	column A	550X500	275000	2750	2750	1	16	201	416.67
C14	column A	550X500	275000	2750	2750	1	16	201	416.67
C14	column A	550X500	275000	2750	2750	1	16	201	416.67
C15	column A	550X500	275000	2750	2750	1	16	201	416.67
C15	column A	550X500	275000	2750	2750	1	16	201	416.67
C15	column A	550X500	275000	2750	2750	1	16	201	416.67
C16	column A	550X500	275000	2750	4132	2	16	201	416.67
C16	column A	550X500	275000	2750	2750	1	16	201	416.67
C16	column A	550X500	275000	2750	6922	3	16	201	416.67
C17	column A	550X500	275000	2750	4132	2	16	201	416.67
C17	column A	550X500	275000	2750	2750	1	16	201	416.67
C17	column A	550X500	275000	2750	6922	3	16	201	416.67
C18	column A	550X500	275000	2750	2750	1	16	201	416.67
C18	column A	550X500	275000	2750	2750	1	16	201	416.67
C18	column A	550X500	275000	2750	2750	1	16	201	416.67
C19	column A	550X500	275000	2750	2750	1	16	201	416.67
C19	column A	550X500	275000	2750	2750	1	16	201	416.67
C19	column A	550X500	275000	2750	2750	1	16	201	416.67
C20	column A	550X500	275000	2750	2750	1	16	201	416.67
C20	column A	550X500	275000	2750	2750	1	16	201	416.67
C20	column A	550X500	275000	2750	2750	1	16	201	416.67
C21	column A	550X500	275000	2750	2750	1	16	201	416.67
C21	column A	550X500	275000	2750	2750	1	16	201	416.67
C21	column A	550X500	275000	2750	2750	1	16	201	416.67
Story1									
C1	column A	550X500	275000	2750	2750	1	16	201	416.67

C1	column A	550X500	275000	2750	2750	1	16	201	416.67
C1	column A	550X500	275000	2750	4200	2	16	201	416.67
C2	column A	550X500	275000	2750	2750	1	16	201	416.67
C2	column A	550X500	275000	2750	2750	1	16	201	416.67
C2	column A	550X500	275000	2750	7280	3	16	201	416.67
C3	column A	550X500	275000	2750	2750	1	16	201	416.67
C3	column A	550X500	275000	2750	2750	1	16	201	416.67
C3	column A	550X500	275000	2750	7151	3	16	201	416.67
C4	column A	550X500	275000	2750	2750	1	16	201	416.67
C4	column A	550X500	275000	2750	2750	1	16	201	416.67
C4	column A	550X500	275000	2750	7280	3	16	201	416.67
C5	column A	550X500	275000	2750	2750	1	16	201	416.67
C5	column A	550X500	275000	2750	2750	1	16	201	416.67
C5	column A	550X500	275000	2750	4200	2	16	201	416.67
C6	column A	550X500	275000	2750	2750	1	16	201	416.67
C6	column A	550X500	275000	2750	2750	1	16	201	416.67
C6	column A	550X500	275000	2750	7436	3	16	201	416.67
C8	column A	550X500	275000	2750	2750	1	16	201	416.67
C8	column A	550X500	275000	2750	2750	1	16	201	416.67
C8	column A	550X500	275000	2750	4200	2	16	201	416.67
C9	column A	550X500	275000	2750	2750	1	16	201	416.67
C9	column A	550X500	275000	2750	2750	1	16	201	416.67
C9	column A	550X500	275000	2750	7280	3	16	201	416.67
C10	column A	550X500	275000	2750	5924	2	16	201	416.67
C10	column A	550X500	275000	2750	7620	3	16	201	416.67
C10	column A	550X500	275000	2750	14178	5	16	201	416.67
C11	column A	550X500	275000	2750	5924	2	16	201	416.67
C11	column A	550X500	275000	2750	7620	3	16	201	416.67
C11	column A	550X500	275000	2750	14178	5	16	201	416.67
C12	column A	550X500	275000	2750	5396	2	16	201	416.67
C12	column A	550X500	275000	2750	7242	3	16	201	416.67
C12	column A	550X500	275000	2750	13851	5	16	201	416.67
C13	column A	550X500	275000	2750	5396	2	16	201	416.67
C13	column A	550X500	275000	2750	7242	3	16	201	416.67
C13	column A	550X500	275000	2750	13851	5	16	201	416.67
C14	column A	550X500	275000	2750	2750	1	16	201	416.67
C14	column A	550X500	275000	2750	2750	1	16	201	416.67
C14	column A	550X500	275000	2750	7151	3	16	201	416.67
C15	column A	550X500	275000	2750	2750	1	16	201	416.67
C15	column A	550X500	275000	2750	2750	1	16	201	416.67
C15	column A	550X500	275000	2750	7280	3	16	201	416.67
C16	column A	550X500	275000	2750	5924	2	16	201	416.67
C16	column A	550X500	275000	2750	7620	3	16	201	416.67
C16	column A	550X500	275000	2750	14178	5	16	201	416.67
C17	column A	550X500	275000	2750	5924	2	16	201	416.67
C17	column A	550X500	275000	2750	7620	3	16	201	416.67
C17	column A	550X500	275000	2750	14178	5	16	201	416.67
C18	column A	550X500	275000	2750	2750	1	16	201	416.67

C18	column A	550X500	275000	2750	2750	1	16	201	416.67
C18	column A	550X500	275000	2750	7436	3	16	201	416.67
C19	column A	550X500	275000	2750	2750	1	16	201	416.67
C19	column A	550X500	275000	2750	2750	1	16	201	416.67
C19	column A	550X500	275000	2750	7436	3	16	201	416.67
C20	column A	550X500	275000	2750	2750	1	16	201	416.67
C20	column A	550X500	275000	2750	2750	1	16	201	416.67
C20	column A	550X500	275000	2750	4200	2	16	201	416.67
C21	column A	550X500	275000	2750	2750	1	16	201	416.67
C21	column A	550X500	275000	2750	2750	1	16	201	416.67
C21	column A	550X500	275000	2750	7436	3	16	201	416.67

These figures clearly illustrate and justify the key **SAP2000** and **Abaqus** input parameters and modeling assumptions adopted to analyze each structural model in this study and to derive the corresponding analytical and numerical results.

SAP2000

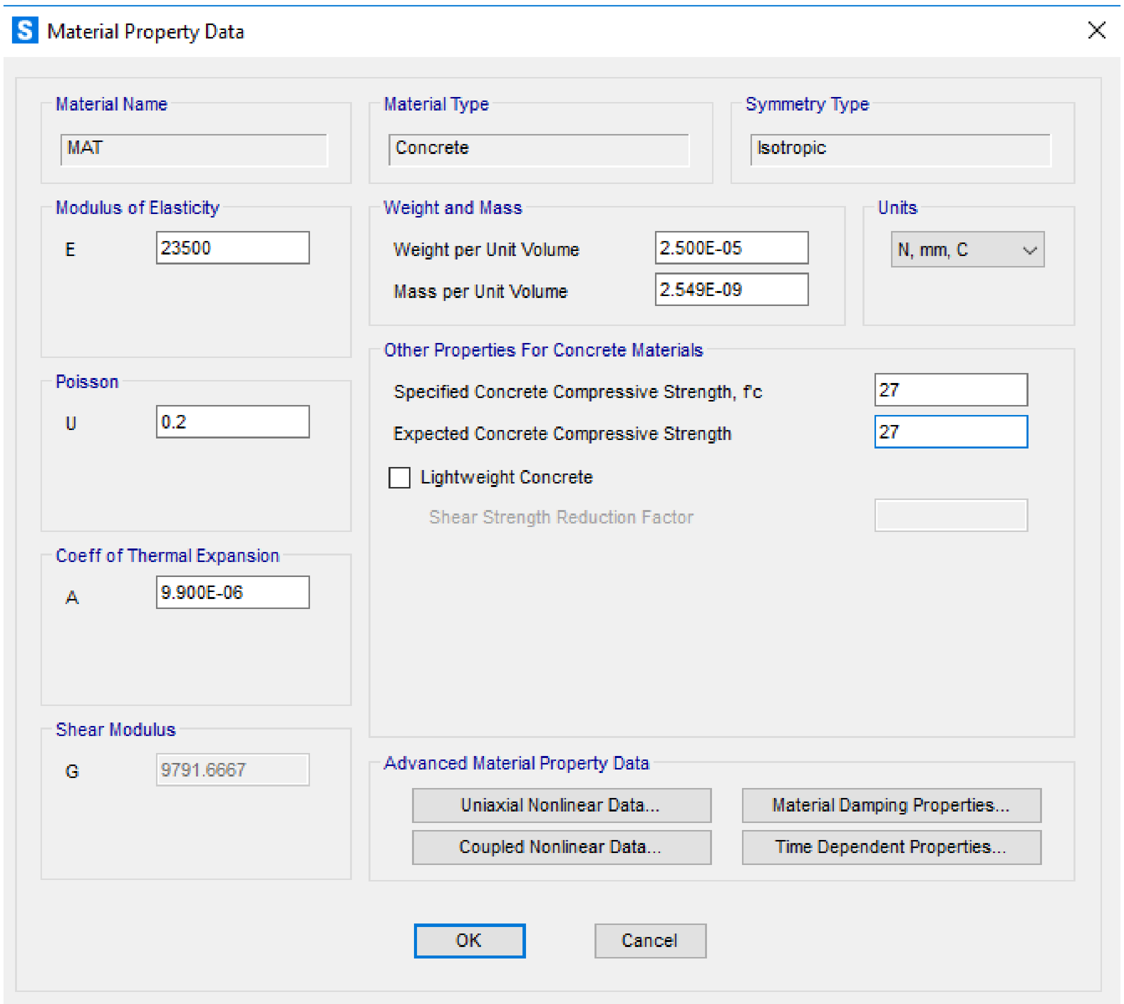

Figure1:Concrete Material Properties in SAP 2000.

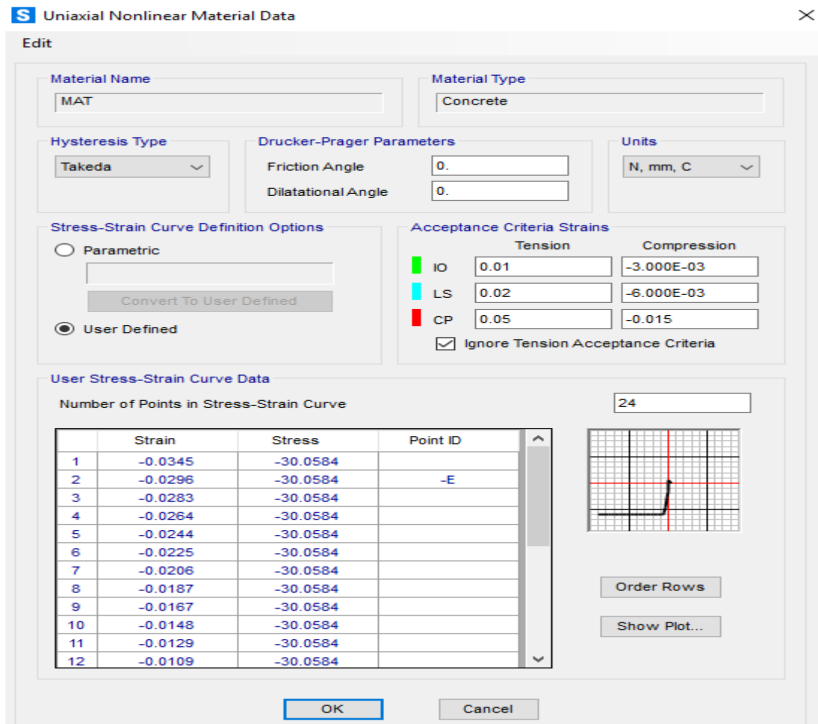

Figure 2:Mander Theory in SAP 2000.

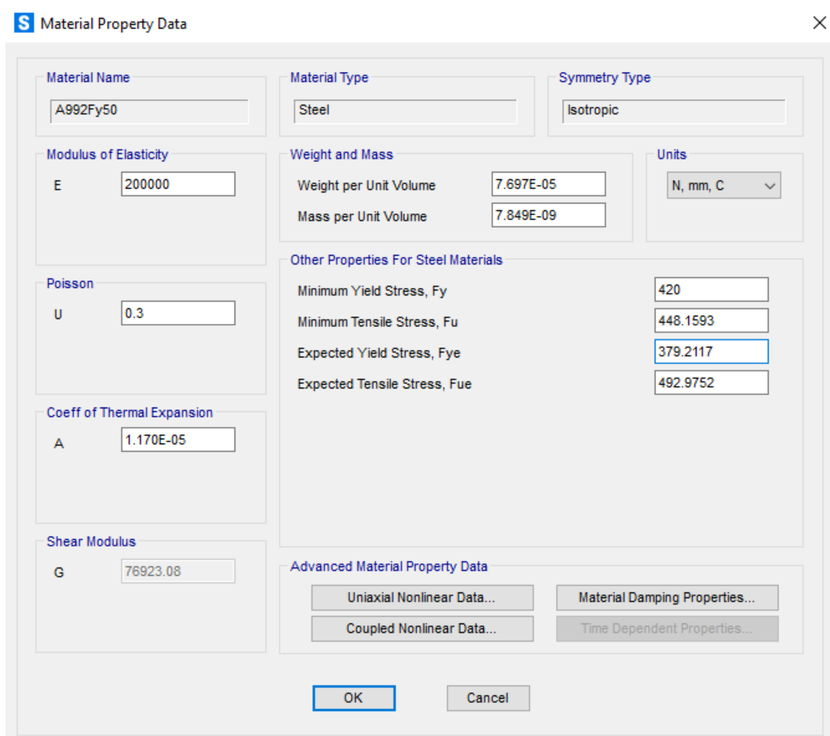

Figure 3: Steel Material Properties in SAP 2000.

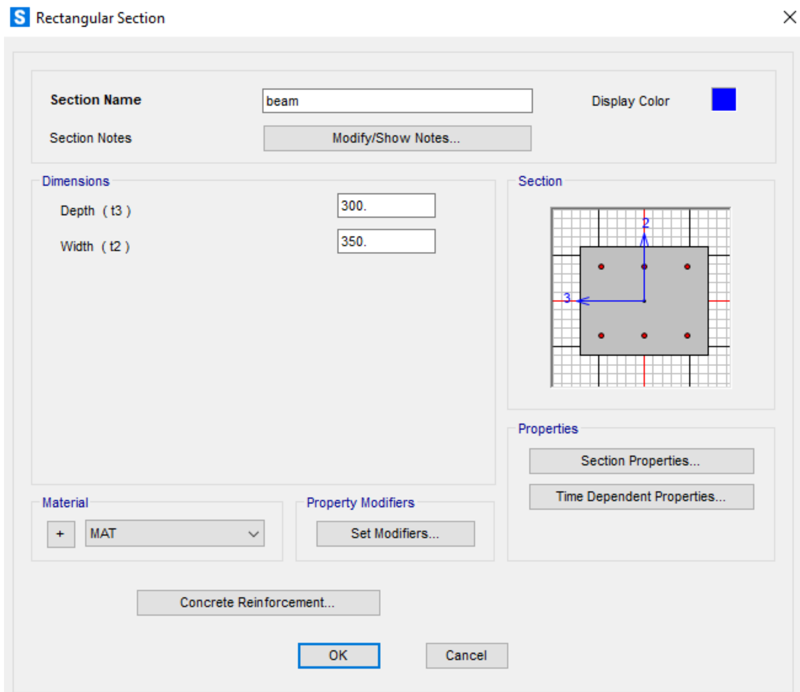

Figure 4:Beams Definition in SAP 2000.

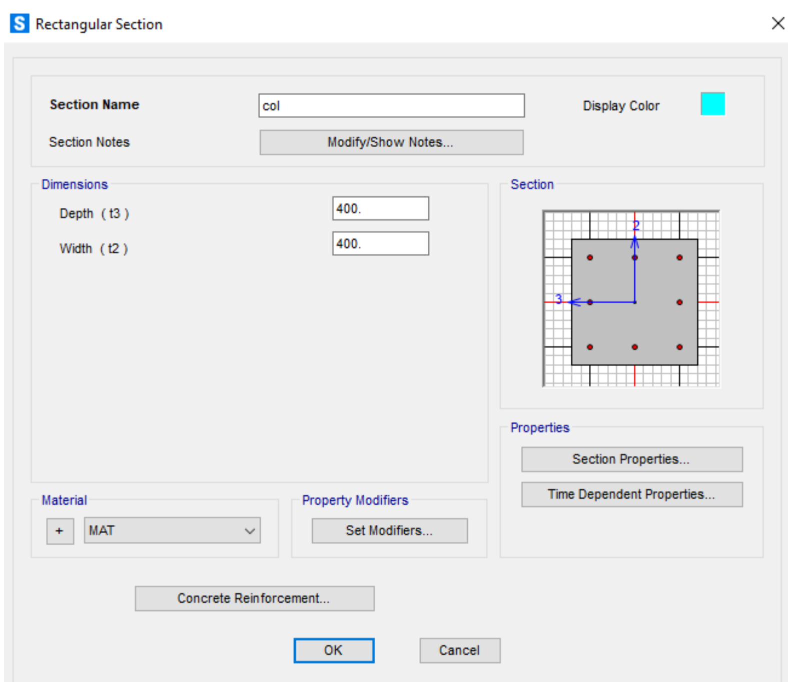

Figure 5:Columns Definition in SAP 2000.

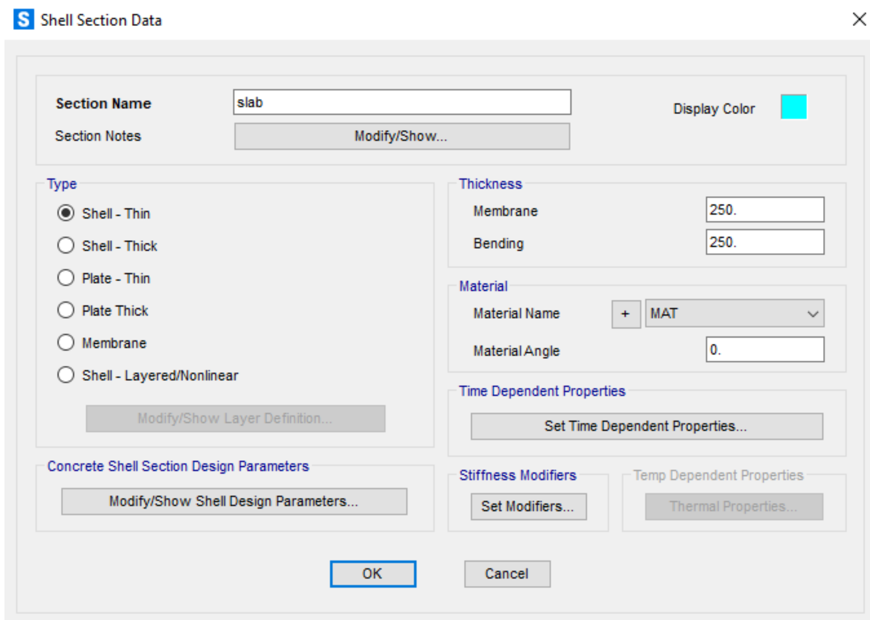

Figure 6:Slab Definition in SAP 2000.

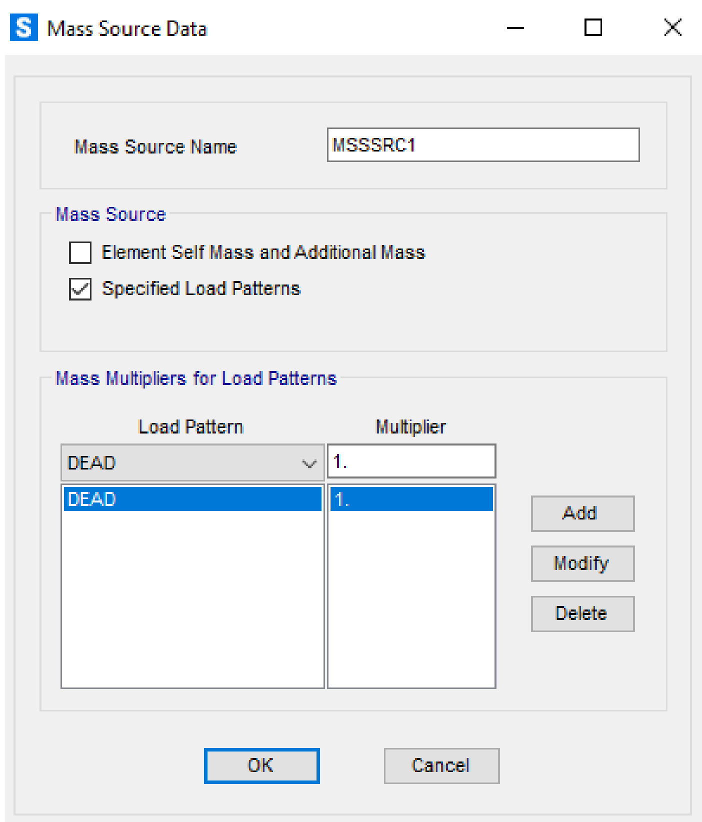

Figure 7:Mass Source Definition in SAP 2000.

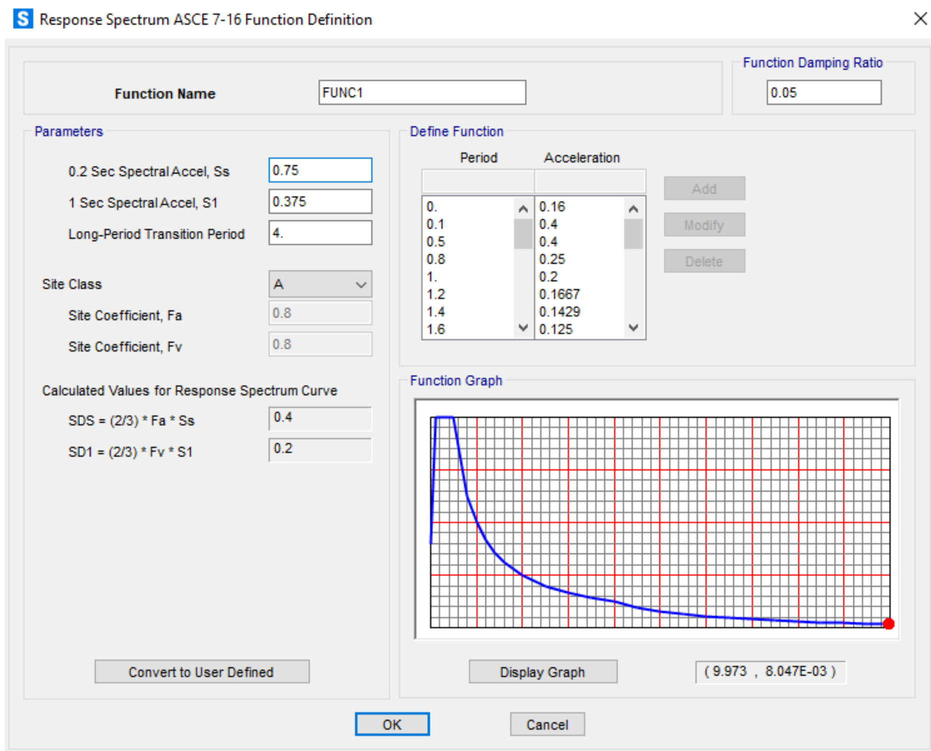

Figure 8:Response Spectrum Definition in SAP 2000.

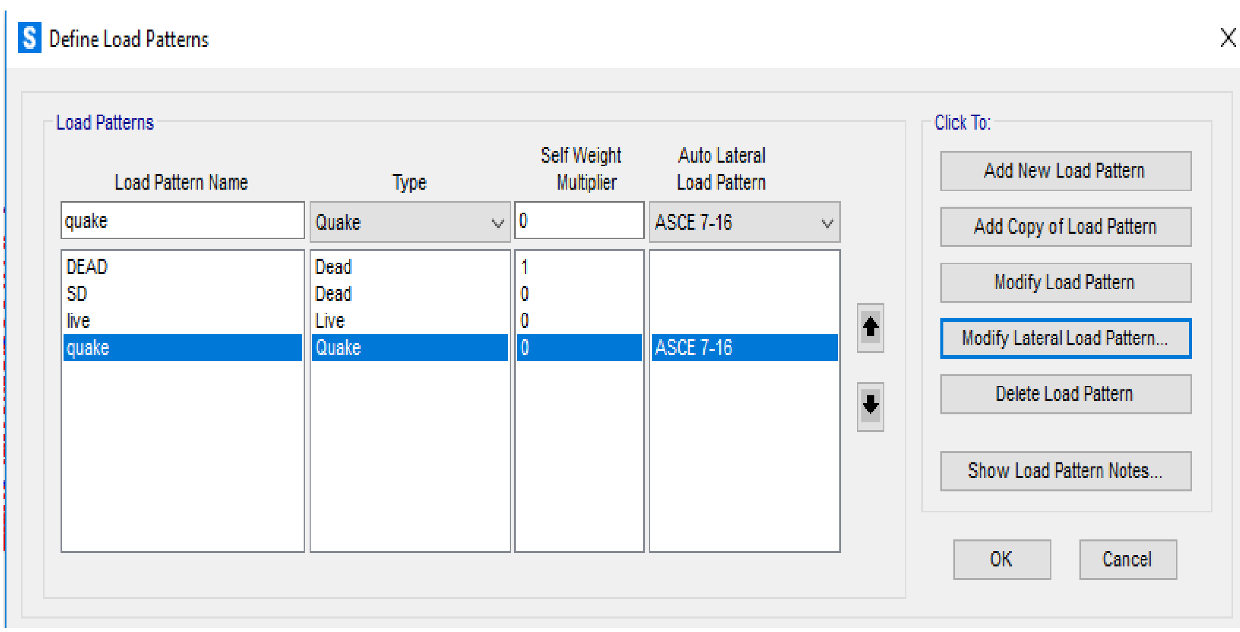

Figure 9: Load Patterns Definition in SAP 2000.

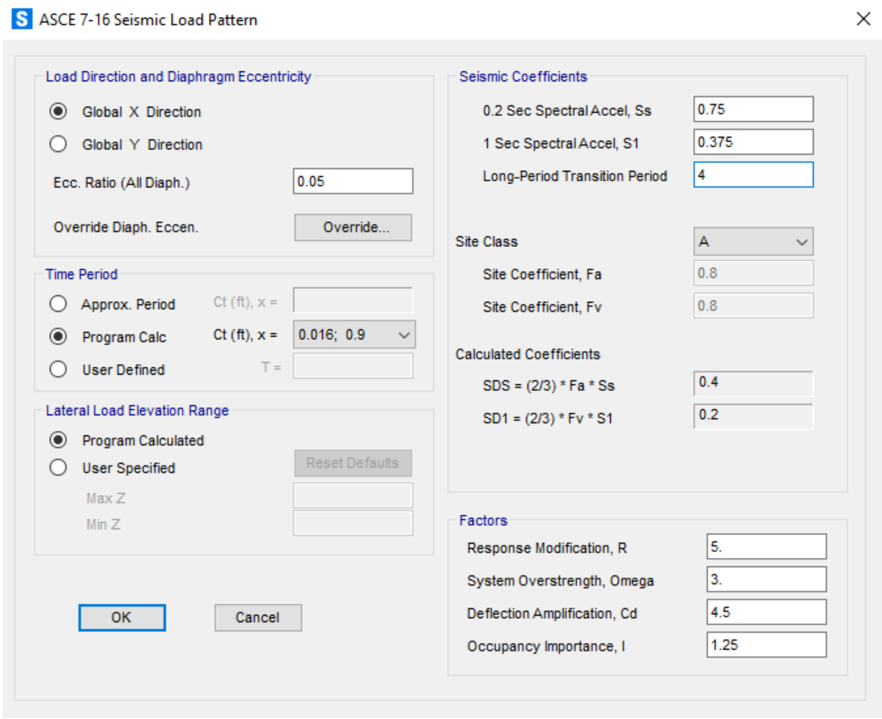

Figure 10: Load Patterns Configuration Setup Definition in SAP 2000.

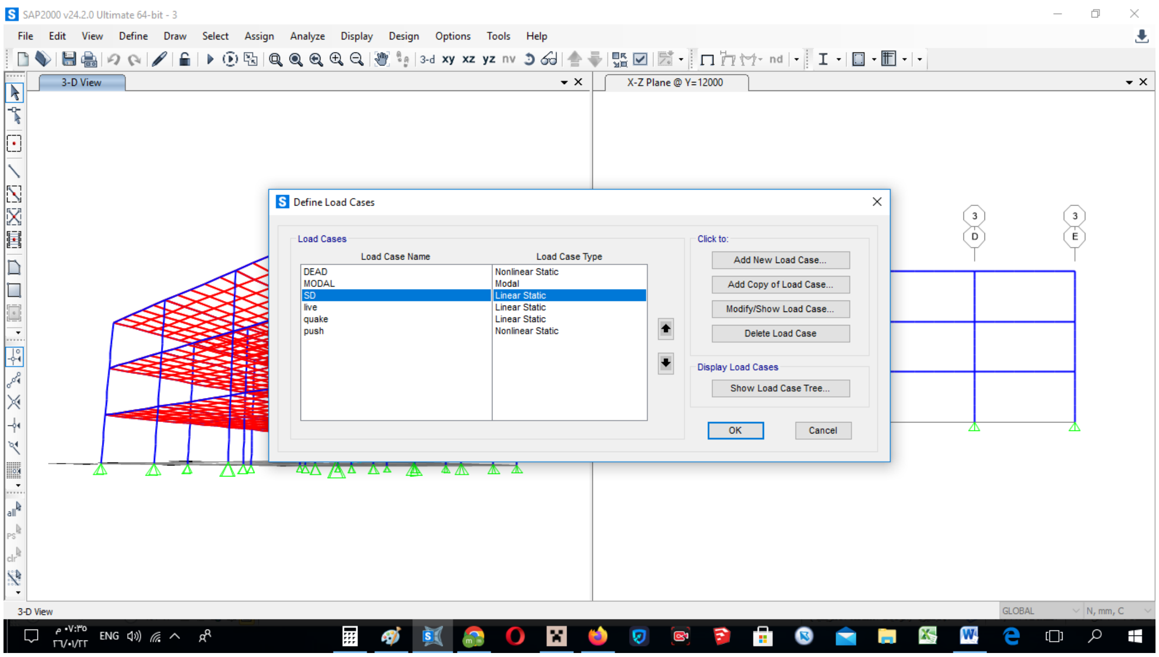

Figure 11: Load Case Configuration Setup Definition in SAP 2000.

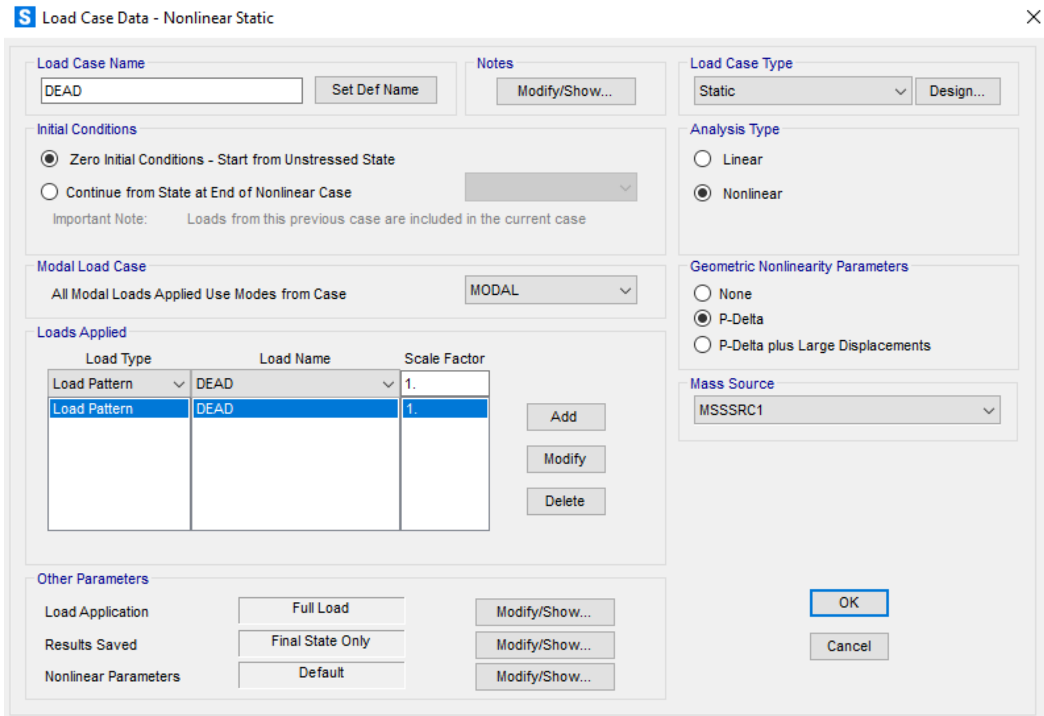

Figure 12: Load Cases Configuration Setup Definition (Dead) in SAP 2000.

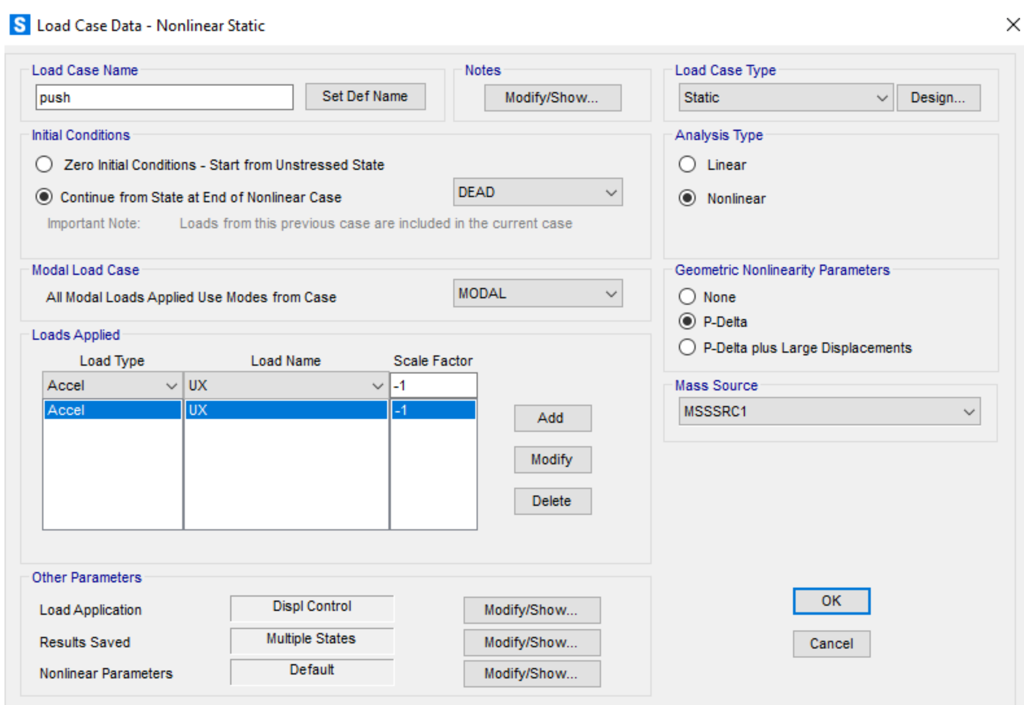

Figure 13: Load Cases Configuration Setup Definition (Push) in SAP 2000.

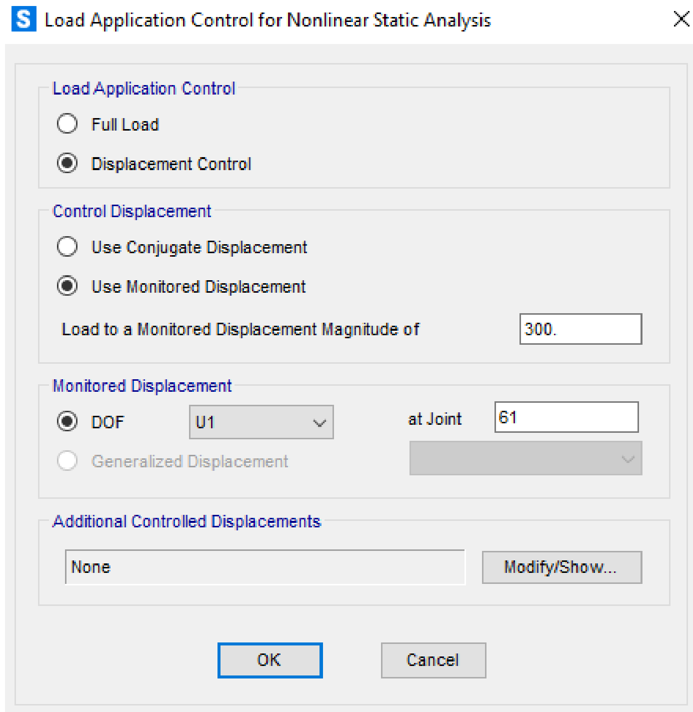

Figure 14: Load Cases Configuration Setup Definition (Push-Load Application) in SAP 2000.

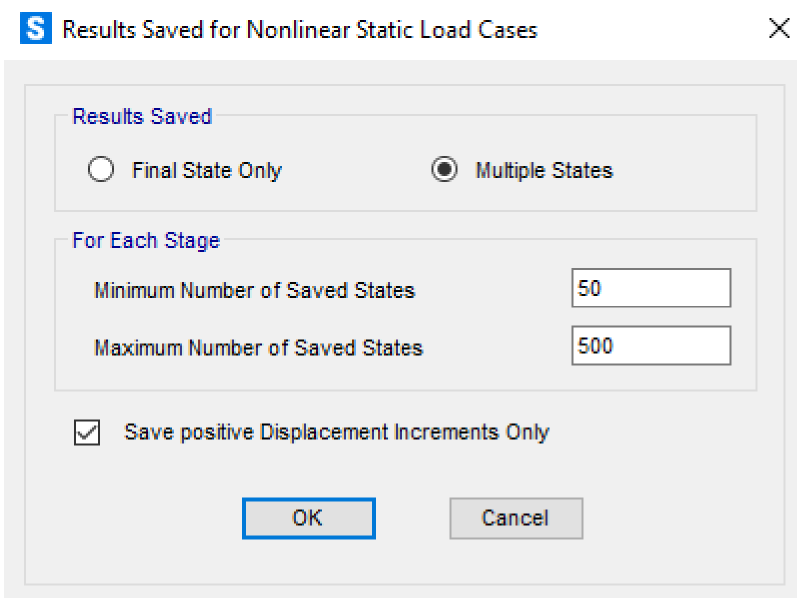

Figure 15: Load Cases Configuration Setup Definition (Push-Result Saved) in SAP 2000.

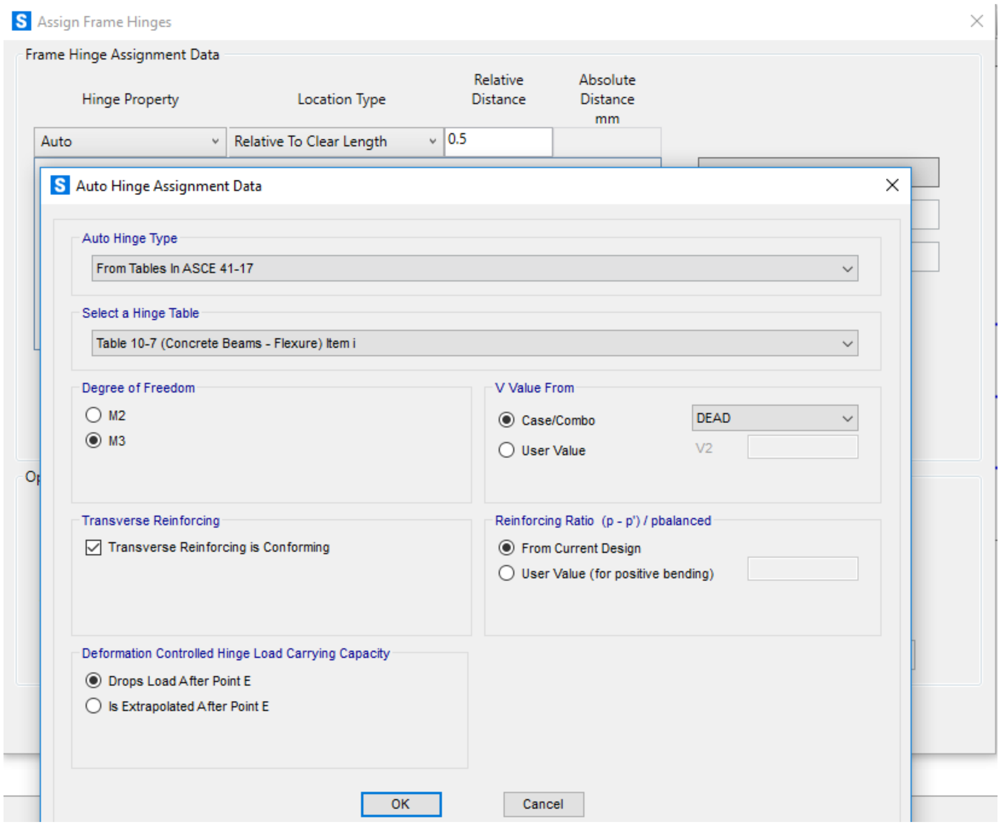

Figure 16: Beam Hinges Definition and Properties Setup in SAP 2000.

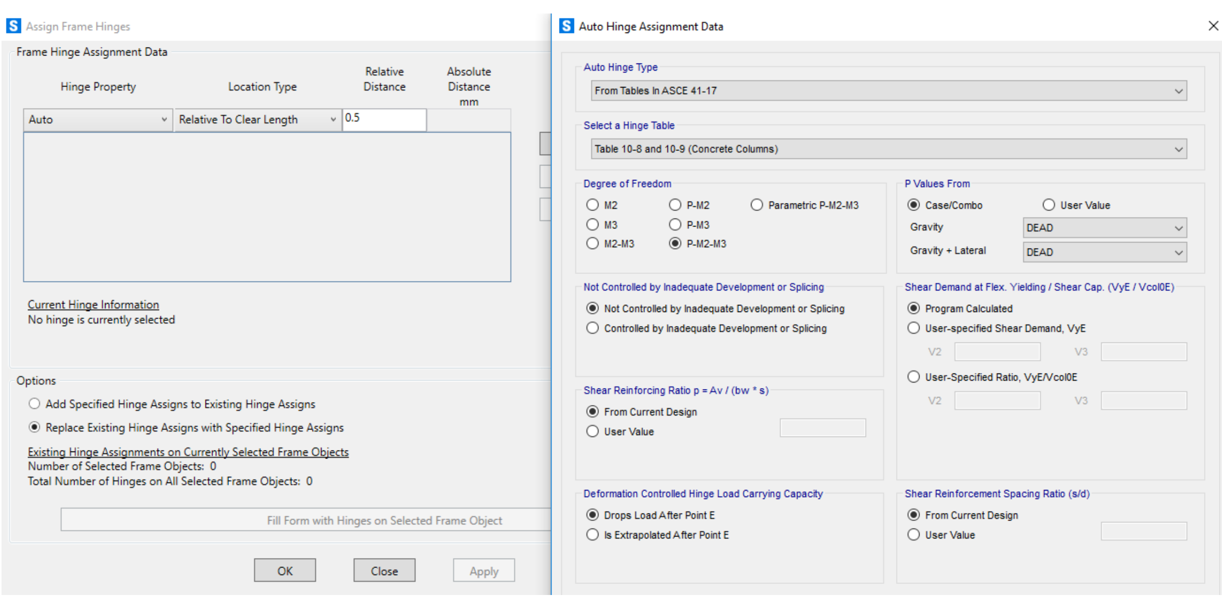

Figure 17: Column Hinges Definition and Properties Setup in SAP 2000.

Abaqus

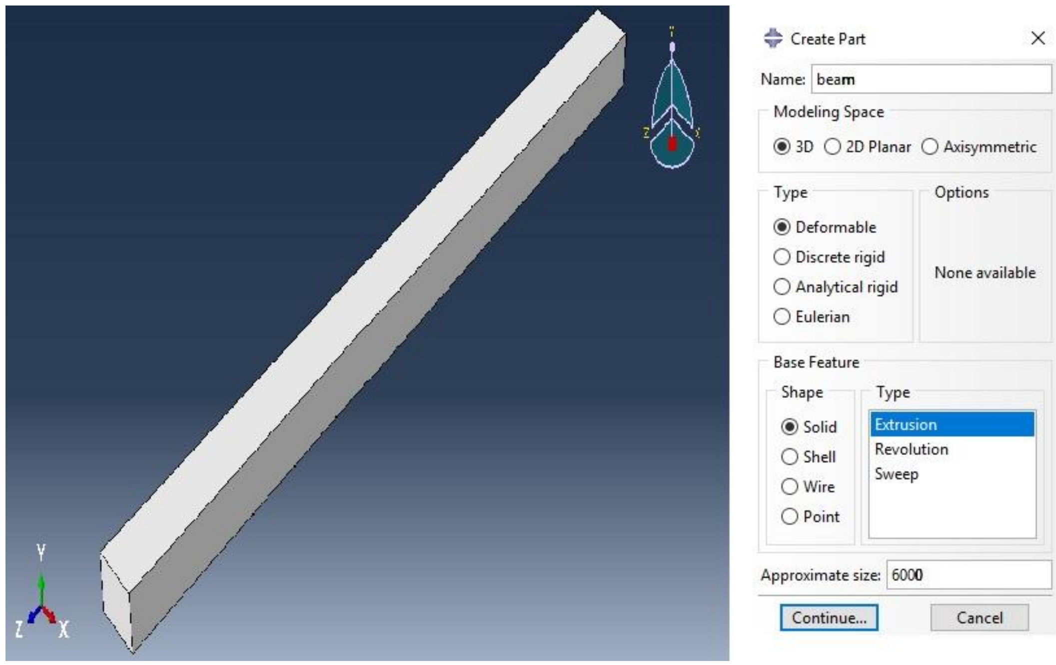

Figure 18:Beams Definition in Abaqus.

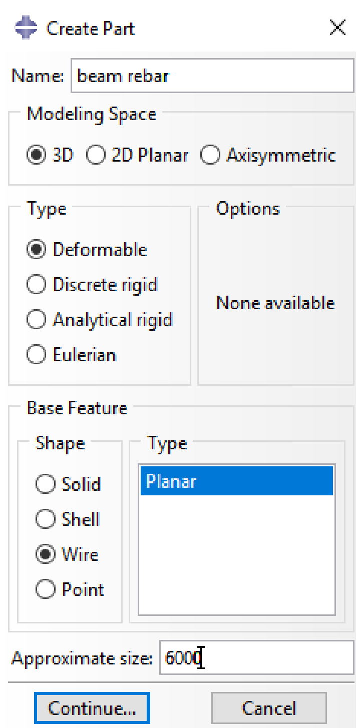

Figure 19:Beam Rebar Definition in Abaqus.

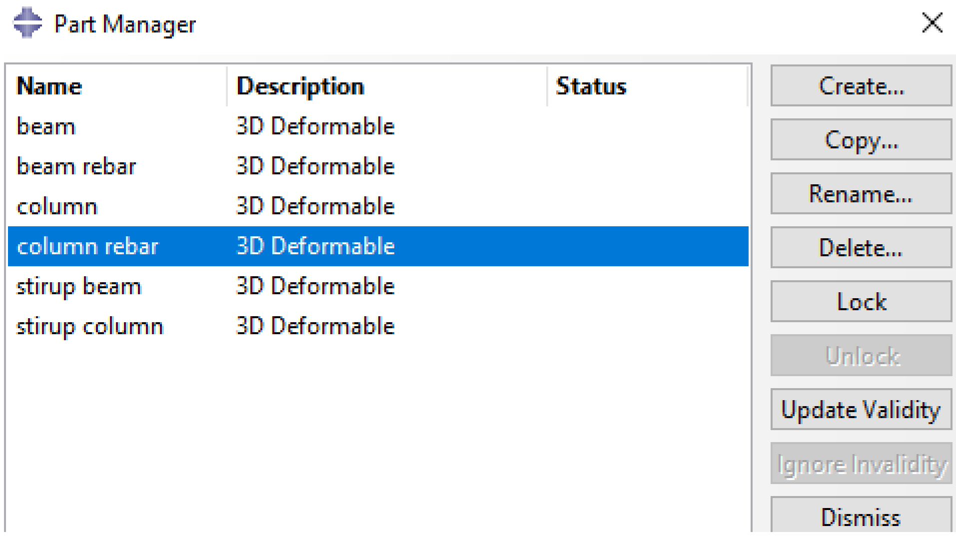

Figure 20:All Part Definition in Abaqus.

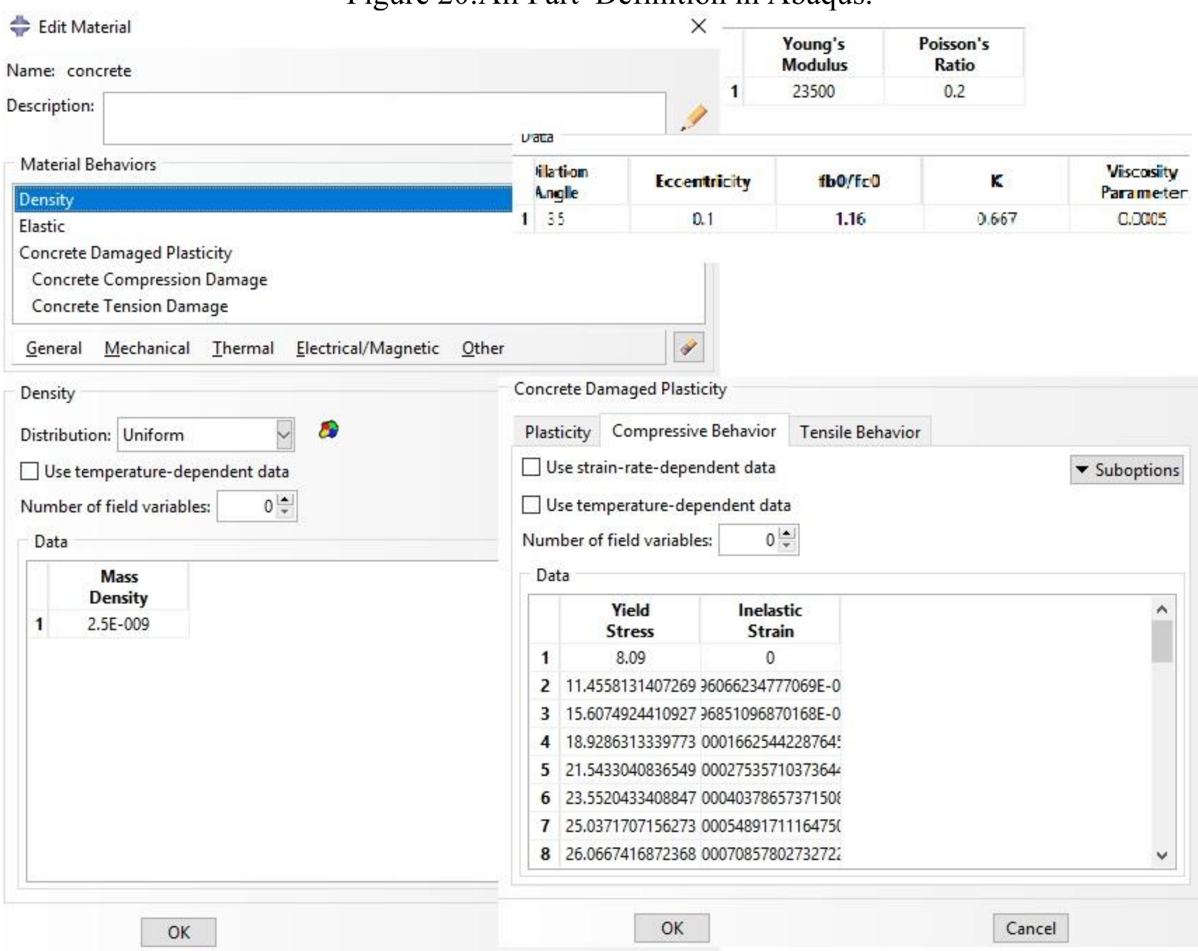

Figure 21: Concrete Material Properties in Abaqus.

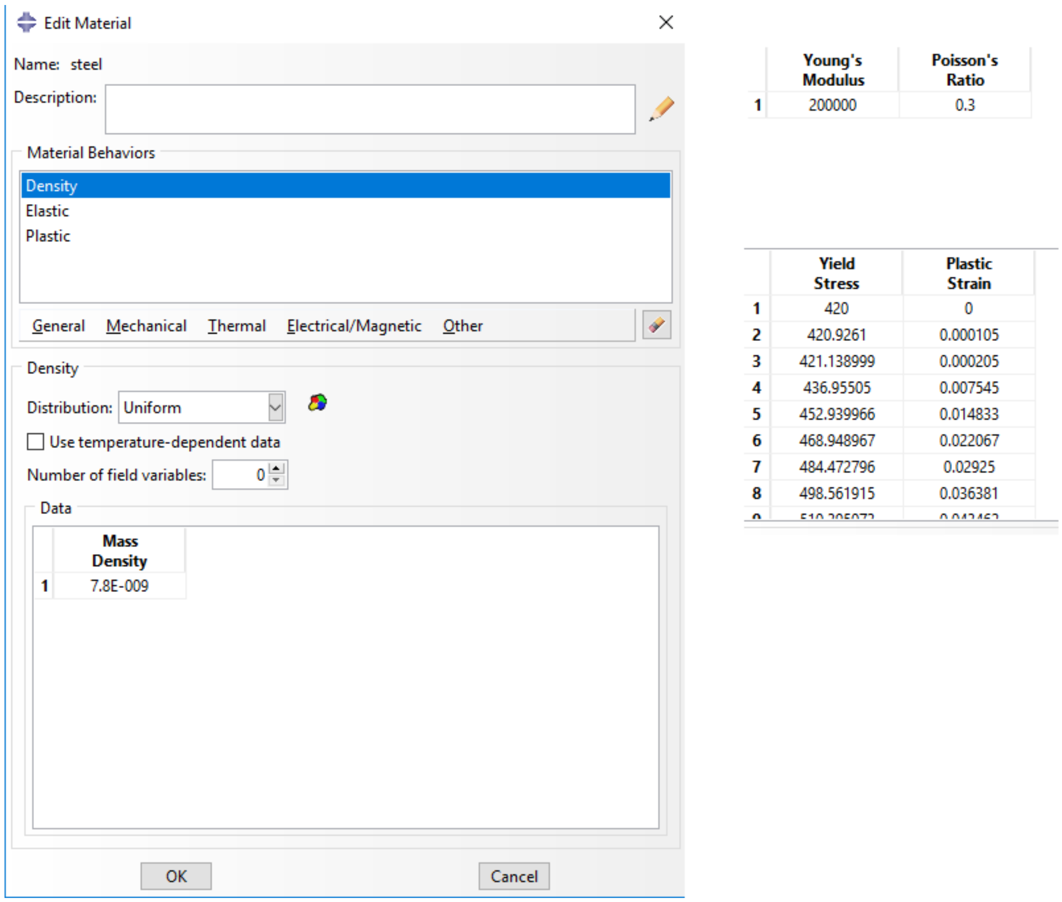

Figure 22: Steel Material Properties in Abaqus.

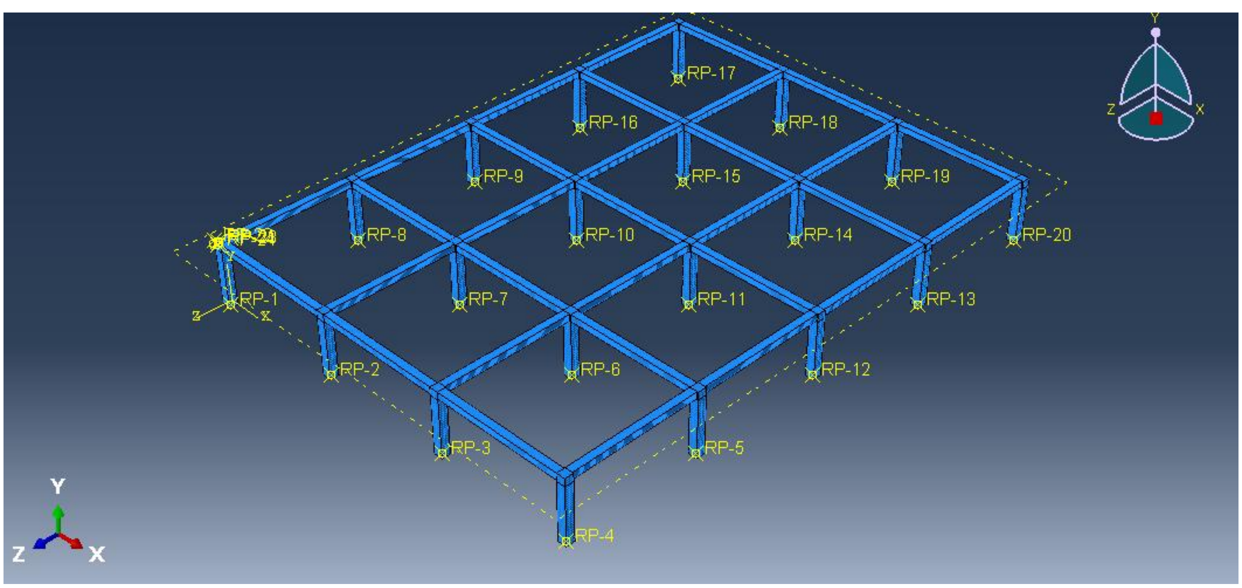

Figure 23:Assembly Definition in Abaqus.

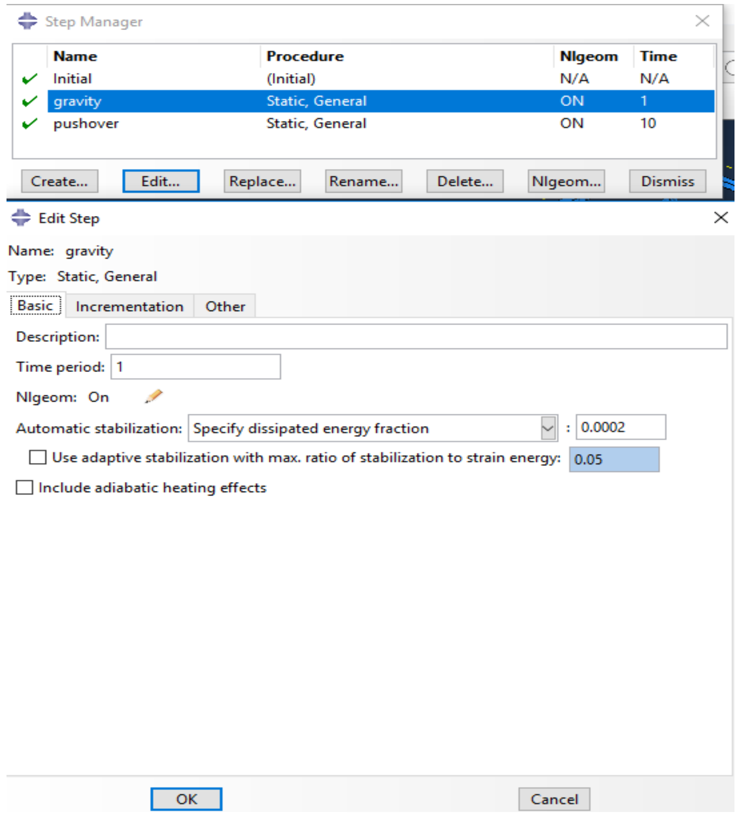

Figure 24:Gravity Step Definition in Abaqus.

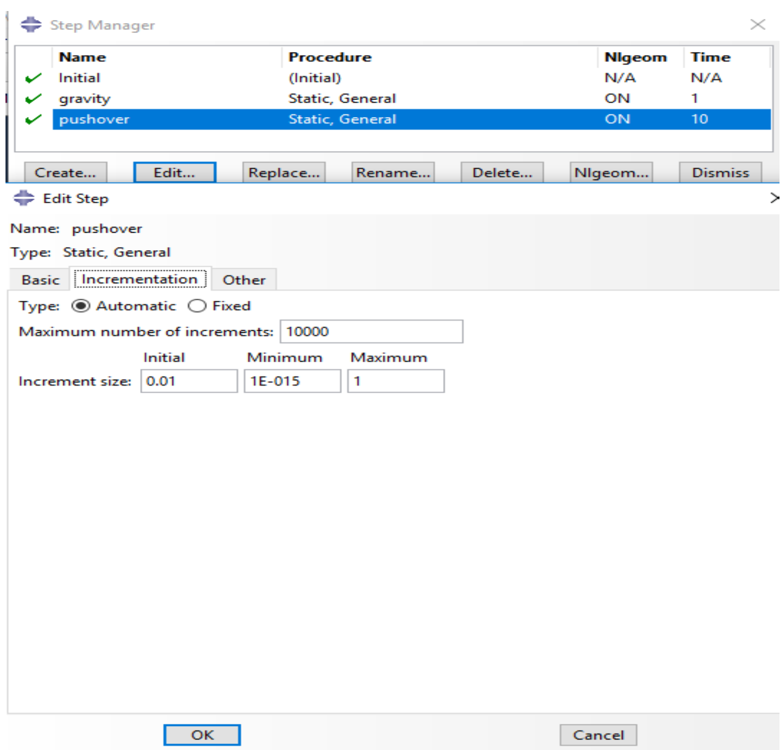

Figure 25:Puwshover Step Definition in Abaqus.

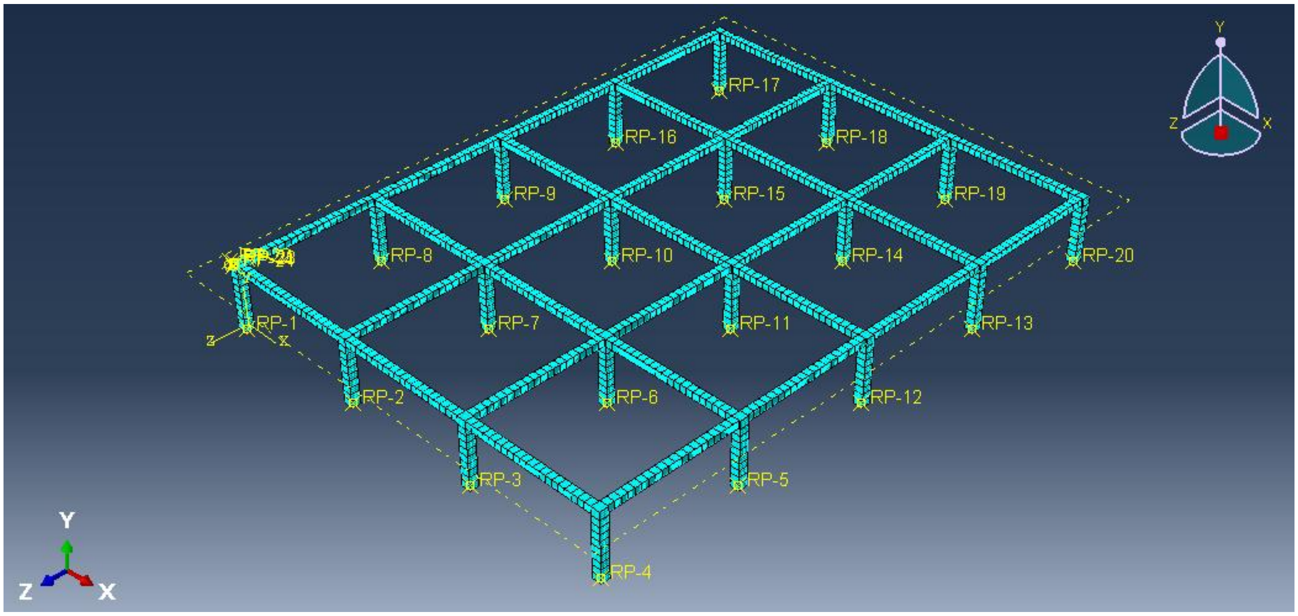

Figure 26:Mesh Definition in Abaqus.

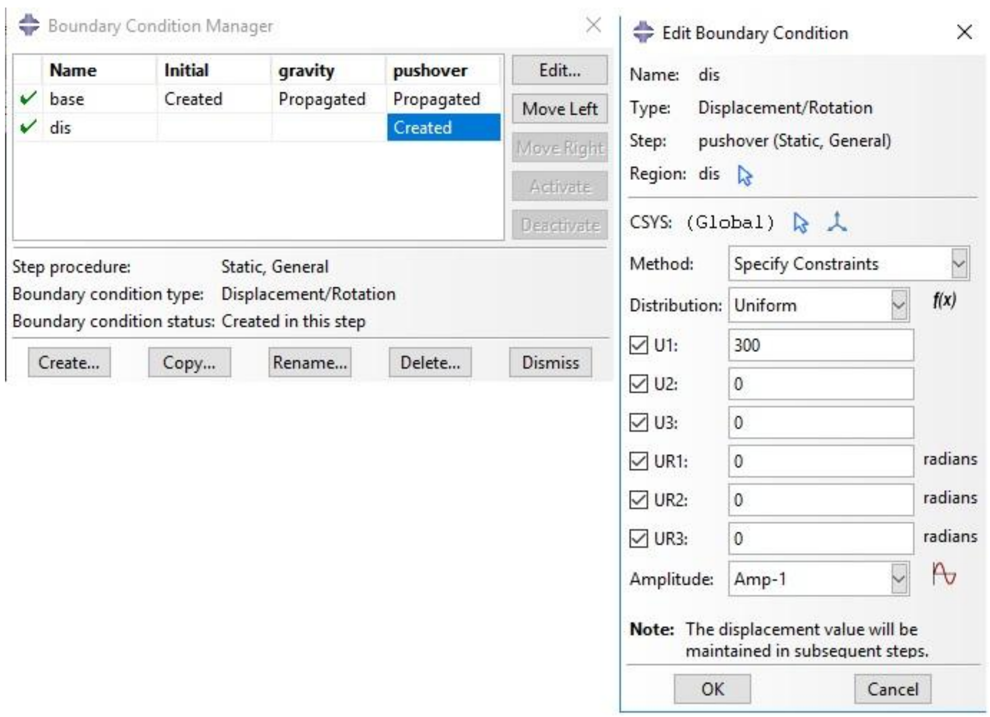

Figure 27:Boundary Condition Definition in Abaqus.